Investigating the molecular mechanisms of recombination-dependent replication in Fission Yeast



DEPARTMENT OF BIOCHEMISTRY
UNIVERSITY OF OXFORD



A thesis presented to the Faculty of Medical Sciences Division, University of Oxford for the degree of Doctor of Philosophy in Biochemistry

Nadiya Ishnazarova

Somerville College,
University of Oxford
Department of Biochemistry

Trinity Term, 2018

DECLARATION

I hereby declare that this dissertation entitled 'Investigating the molecular mechanisms of recombination-dependent replication in Fission Yeast' has been originally carried out by me under the supervision of Professor Matthew Whitby, Department of Biochemistry, University of Oxford. This work has not formed the basis for award of any degree or diploma previously. The particulars given in the report are true to the best of my knowledge.

Nadiya Ishnazarova

Department of Biochemistry
Somerville College,
University of Oxford

ACKNOWLEDGEMENTS

First, I would like to thank my supervisor Professor Matthew Whitby for his patience and support through all four years of my DPhil. He has always managed to find right words to motivate me to break new grounds and he always had answers for all my questions.

I am grateful to all the former and current members of the lab: Dr. Carl Morrow, Dr. Fikret Osman, Andrew Fower, Dr. Manish Jalan, and especially to Dr. Judith Oehler and Dr. Anastasiya Kishkevich for their help and endless optimism and to Sanjeeta Tamang, who became a friend and a comrade on a DPhil road which is scattered with obstacles at least as much as the progression of replication fork. I would like also to thank all the wonderful people from Sherratt and Howarth lab who have provided me with scientific advice and who we had lots of fun with.

I would like to extend my gratitude to the Clarendon Fund Scholarship, Cancer Research UK and Somerville College for giving me the unique opportunity not only to pursue my doctoral degree in Oxford but also to become part of this university and community of extremely bright and fascinating people.

I would like to thank Prof. Christina Redfield and Dr. Ed Lowe for their help with NMR and crystallisation trials.

I want to express my deepest gratitude to my professors. There were excellent teachers, brilliant scientists and simply good people who taught me to think critically, and, what is more important, to be myself but understand others.

I am thankful to friends who I knew before, especially Nina and Sasha for keeping the connection between us and making me feel home no matter where I am, and to all friends I met in Oxford, especially Friederike, for long sense-of-life-talks, Tianyi, for always being on my side, Florence, for following my adventurous ideas, Can, for warm hugs and sense of reality, and Masha, for making me laugh all the time. I would like to thank Dr. Andrey Bolbat, he and his selfless love has been a source of my inspiration and energy for many years and without this I would never be able to start my journey in Oxford.

A special mention to my family for their love, they are always in my heart.

Thank you, Alexis for your patience, support and unconditional love that have been leading me through this year and especially through the period of writing the thesis. There are no words to express my sincere gratitude and love. Without you being there for me every minute and every second physically, mentally and emotionally I would never be where I am now.

Clarendon

Funded by CANCER RESEARCH UK

Somerville College

Investigating the molecular mechanisms of recombination-dependent replication in Fission Yeast

A thesis submitted for the degree of Doctor of Philosophy in Biochemistry by
Nadiya Ishnazarova
Somerville College,
University of Oxford
Department of Biochemistry
Trinity Term, 2018

ABSTRACT

Perturbation of DNA replication is a major cause of cancer and other pathological states causing loss of genome integrity and catastrophic chromosomal rearrangements. To guard against such disaster, mechanisms exist to process and stabilize replication forks (RFs) blocked at barriers, restart collapsed forks and ensure faithful fork merging and termination. Despite recent advances, our understanding of the molecular mechanisms that drive recombination-dependent replication at the replication fork barriers (RFBs) is far from comprehensive, and in particular we know very little about mechanisms used to govern its accuracy.

To characterize factors that are needed for the successful processing and restart of blocked RFs at the site-specific RFB Replication Termination Sequence *RTS1* in *Schizosaccharomyces pombe,* I focused on studying a putative partner protein of the Fml1 DNA helicase called Dbl2; its orthologs can be found from yeast to human. I used a combination of yeast genetics, fluorescent microscopy and live cell imaging to investigate the role of Dbl2. Data from epistasis analysis, with key components of the homologous recombination machinery, highlights differences with a *fml1*Δ mutant and suggest that Dbl2 is involved in destabilizing the Rad51-nucleoprotein filament in conjunction with the Fbh1 DNA helicase. However, this genetic analysis also revealed that Dbl2 has functions that are independent of Fbh1 in the regulation of Rad51-independent Rad52-dependent recombination, spontaneous and induced at *RTS1*. This may include a role in and/or regulating other helicases such as Fml1 and Pfh1. Structure–function studies using a series of truncation and internal deletion mutants of Dbl2 demonstrate that the cooperative action of all regions is required for Dbl2 function to limit recombination induced at RF blocked at *RTS1,* to counteract Rad51 activity in the presence of Rad55 and for its nuclear localization to the multiple sites across the genome. However, only its middle region is important to confer resistance to genotoxins and genetic interaction with most Rad51 mediator proteins. In addition, I have developed expression and purification strategies for full-length Dbl2 and its functional domain and conducted preliminary experiments for the characterization of the conserved N-terminal domain DUF2439 structure.

ABBREVIATIONS

AO RTS1 active orientation
ATP adenosine triphosphate
ATPase adenosine triphosphatase
BIR break-induced replication
BLM Bloom's syndrome helicase
bp base pair
CFP cyan fluorescent protein
Chr Chromosome
CMG Cdc45, Mcm2-7, GINS complex
CO cross-over
CPT camptothecin
DAPI 4',6-diamidino-2-phenylindole
D-loop displacement loop
dHJ double Holliday junction
DNA deoxyribonucleic acid
dNTP deoxynucleoside triphosphate
dsDNA double-stranded DNA
DSB double-strand break
E. coli Escherichia coli
EDTA ethylenediaminetetraacetic acid
EMMG Edinburgh minimal media glutamate
EGTA ethylene glycol-bis(β-aminoethyl ether)-N,N,N',N'-tetraacetic acid
FA Fanconi anaemia
FANCM Fanconi anaemia complementation group M
Fbh1 F-box helicase 1
GFP green fluorescent protein
GST glutathione-S-transferase
HEPES 4-(2-hydroxyethyl)-1-piperazineethanesulfonic acid
HJ Holliday junction
HR homologous recombination
HRP horseradish peroxidase
HU hydroxyurea
IgG Immunoglobulin G
IO RTS1 inactive orientation
iPOND isolation of proteins on nascent DNA
kb kilobases
LA low adenine
LB Luria-Bertani
LOH loss of heterozygosity
MBP maltose binding protein

MCM minichromosome maintenance
MEA malt extract agar
MHF FANCM-associated histone-fold protein
MMS methyl methanesulfonate
MOPS 3-(N-morpholino)propanesulfonic acid
Mph1 mutator phenotype 1
MRN Mre11-Rad50-Nbs1 complex
MRX Mre11-Rad50-Xrs2 complex
MS mass spectrometry
MS-SILAC mass spectrometry and stable isotope labelling in cell culture
NCO non-cross-over
NHEJ non-homologous end-joining
NMR Nuclear magnetic resonance spectroscopy
nmt no message in thiamine
OriC origin of replication
ORF open reading frame
PBS phosphate-buffered saline
PEG polyethylene glycol
Pol DNA Polymerase
PCNA proliferating cell nuclear antigen
PCR polymerase chain reaction
PCV packed cell volume
PI protease inhibitor
PMSF phenylmethylsulphonylfluoride
rDNA ribosomal DNA
RDR recombination-dependent replication
RF replication fork
RFB replication fork barrier
RFC replication factor C
RPA replication protein A
Rtf replication termination factor
RTS1 replication termination sequence 1
Sc *S. cerevisiae Saccharomyces cerevisiae*
SDS-PAGE sodium dodecyl sulphate polyacrylamide gel electrophoresis
SDSA synthesis-dependent strand annealing
SMC structural maintenance of chromosomes
Sp *S. pombe Schizosaccharomyces pombe*
SSA single-strand annealing
SSB single-strand DNA-binding
ssDNA single-stranded DNA
SUMO Small Ubiquitin-like Modifier
TBS tris-buffered saline

TE Tris/EDTA
TLS translesion synthesis
Top topoisomerase
tRNA transfer ribonucleic acid
UV ultraviolet light
WRN Werner syndrome helicase
YE yeast extract
YES yeast extract with supplements
YEP yeast extract peptone
YFP yellow fluorescent protein
1D gel one dimensional gel
2D gel one dimensional gel

TABLE OF CONTENT

ACKNOWLEDGEMENTS..... iii

ABSTRACT..... iv

ABBREVIATIONS..... v

Introduction 1

1.1 Background 2

1.2 Fundamentals of DNA replication 4

1.2.1 Initiation of replication 4

1.2.2 Replisome 5

1.2.3 Termination of replication 7

1.3 Impediments to DNA replication 8

1.3.1 RFBs: DNA damage 8

1.3.2 Unusual DNA structures 10

1.3.3 Transcription-replication conflict 10

1.3.4 Programmed DNA replication perturbations 11

1.3.5 Mating type switching and the *RTS1* replication fork barrier 12

1.3.6 General strategies of cellular defence against RFBs 13

1.4 Overview of homologous recombination: key players and mechanism 14

1.4.1 Pre-synapsis: resection 18

1.4.2 Pre-synapsis to synapsis: Rad51 nucleoprotein filament formation and strand invasion 20

1.4.2.1 Rad52 20

1.4.2.2 Rad55-Rad57 21

1.4.2.3 Swi5-Sfr1 22

1.4.2.4 Rdl1-Rlp1-Sws1/Shu1-Shu2-Psy3-Csm2 23

1.4.3 Homology search and DNA synthesis 24

1.4.4 Post-synapsis: resolution of recombination intermediates 25

1.4.4.1 Srs2 and Fbh1 25

1.4.4.2 The FANCM family of DNA helicases/translocases 28

1.4.5 Double Holliday junction resolution 29

1.4.6 Double Holliday junction dissolution 30

1.5 Response to replication stress and the role of HR in aiding completion of DNA replication 31

1.5.1 Translesion DNA synthesis (TLS) 31

1.5.2 Template switching 31

1.5.3 Stabilization of stalled forks: the role of HR proteins and the fork protection complex 34

1.5.4 The role of accessory DNA helicases 38

1.5.5 Models of DSB-initiated recombination-dependent replication 39

1.5.6 Model of DSB-free recombination-dependent replication 42

1.6 Aims of study 45

2 Materials and Methods 47

2.1 Media 48

2.1.1 *E. coli* media 48
2.1.2 *S. pombe* media 48
2.1.3 *S. cerevisiae* media 49

2.2 Plasmid construction 50
2.2.1 Site-directed mutagenesis 51
2.2.2 *E. coli* transformation 51

2.3 *S. pombe* strain construction 51
2.3.1 *S. pombe* transformation 51
2.3.2 *S. pombe* colony PCR 52
2.3.3 *S. pombe* genomic DNA extraction 53
2.3.4 *S. pombe* crosses 54

2.4 *S. cerevisiae* transformation 54

2.5 Genetic assays 55
2.5.1 Genotoxin sensitivity spot assay 55
2.5.2 Direct repeat recombination assays 55

2.6 Biochemistry techniques 57
2.6.1 Protein expression and purification of His-tagged proteins from *E. coli* 57
2.6.2 Purification and concentration of the N-terminus of Dbl2 58
2.6.3 Protein expression and purification of MBP- and GST-tagged proteins from *E. coli* 59
2.6.4 Protein expression and purification from *S. cerevisiae* 59
2.6.5 SDS-polyacrylamide gel electrophoresis 60
2.6.6 Western blotting 60
2.6.7 Preparation of *S. pombe* protein extracts 61
2.6.7.1 Lysis by bead beating using a FastPrep machine 61
2.6.7.2 French press lysis 62
2.6.7.3 Cryo-grinding lysis 62
2.6.7.4 Alkaline lysis 63
2.6.8 Immunoprecipitation and co-immunoprecipitation of proteins from yeast cell extracts 63
2.6.9 Protein biotinylation 65

2.7 Structure characterization 66
2.7.1 Nuclear magnetic resonance spectroscopy (NMR) 66
2.7.2 X-ray crystallography 66

2.8 Cell biology technics 67
2.8.1 Flow-cytometry analysis 67
2.8.2 Microscopy 67

2.9 Data analysis 69
2.9.1 Image processing and analysis 69

2.10 Statistics 69

3 The identification of factors needed for the replication restart at a site-specific replication fork barrier 90

3.1 Introduction 91

3.2 Results 94
3.2.1 Establishing a system for identifying proteins at the *RTS1* RFB 94
3.2.2 Investigating the interaction between Fml1 and Elg1 99
3.2.3 Investigating the interaction between Fml1 and Smc5 101
3.3 Discussion 103
4 Investigating the role of Dbl2 in the maintenance of genome stability 109
4.1 Introduction 110
4.2 Results 110
4.2.1 The deletion of the *dbl2* gene generates two types of strains 110
4.2.2 The non-suppressed *dbl2*Δ is hypersensitive to genotoxins.. 114
4.2.3 Once acquired *dbl2*Δ suppression is stably inherited 116
4.2.4 Attempts to identify the *dbl2*Δ suppressor 121
4.2.5 A putative prion state of Fml1 is not responsible for the suppression of *dbl2*Δ 124
4.2.6 Dbl2 limits recombination at blocked replication forks 128
4.2.7 Dbl2 is not required for limiting template switching downstream of *RTS1-AO* 131
4.2.8 Dbl2 limits spacer dependent recombination 134
4.2.9 The suppressed *dbl2*Δ strain exhibits reduced levels of *RTS1-AO*-induced recombination 136
4.3 Discussion 138
5 Epistasis analysis of *dbl2* and key components of the homologous recombination machinery 142
5.1 Introduction 143
5.2 Results 144
5.2.1 Genetic interactions between *dbl2*Δ and *fml1*Δ 144
5.2.2 Epistasis analysis between *dbl2*Δ and *fbh1*Δ 150
5.2.3 Evidence that Dbl2 has a role in the repair/tolerance of DNA damage that is independent of both Fml1 and Fbh1 154
5.2.4 Overexpression of Fbh1 improves the growth of a *dbl2*Δ mutant but also sensitizes it to MMS 155
5.2.5 Overexpression of Dbl2 rescues *fbh1*Δ sensitivity to CPT, MMS and UV 159
5.2.6 Dbl2 influences both Rad51-dependent and Rad51-independent recombination 159
5.2.7 Effect of *rad55* deletion on spontaneous and *RTS1-AO*-induced direct repeat recombination in a *dbl2*Δ mutant 164
5.2.8 Dbl2 limits both Rad51-dependent and Rad51-independent recombination induced by the *RTS1* RFB in spacer strains 168
5.2.9 Dbl2 functions in a Rad52-dependent pathway of DNA repair 170

5.2.10 The effect of *dbl2* deletion on Rad51-CFP and Rad52-YFP focus formation at *RTS1* 171
5.2.11 Overexpression of Rad52 does not mimic the *dbl2Δ* phenotype 176
5.2.12 Genetic interactions between *dbl2*/*fbh1* and *Rad51* mediators 178
5.2.12.1 rad55 and rad57 179
5.2.12.2 swi5 and sfr1 179
5.2.12.3 rdl1, rlp1 and sws1 185
5.2.13 Genetic interaction between *dbl2*Δ and *rqh1*Δ....185

5.3 Discussion....190
6 Purification of Dbl2 and analysis of its N-terminal domain....198

6.1 Introduction....199

6.2 Results....200
6.2.1 Bioinformatic analysis of Dbl2 200
6.2.2 Purification of full-length Dbl2 from *E. coli* and *S. cerevisiae* 205
6.2.3 Expression and purification of Dbl2's functional domains 206
6.2.4 Purification of N-terminus Dbl2 from *E. coli*....210
6.2.5 Crystallisation trials of N-terminus Dbl2....214
6.2.6 Analysis of N-terminus Dbl2 by NMR 216

6.3 Discussion....217
7 Structure-function analysis of Dbl2....222

7.1 Introduction....223

7.2 Results....224
7.2.1 Genotoxin sensitivity of truncation and internal deletion mutants of Dbl2 224
7.2.2 The importance of different Dbl2 domains in suppressing spontaneous and *RTS1*-induced direct repeat recombination....228
7.2.3 Genetic interactions between truncation and internal deletion mutants of Dbl2 and key components of the homologous recombination machinery 232
7.2.4 Identifying which of Dbl2's domains is required for it to form nuclear foci....235
7.2.5 Investigating the recruitment of Dbl2 to *RTS1* by fluorescence microscopy....245

7.3 Discussion....246
8 Concluding remarks....252
Appendix....261
Bibliography....266

Chapter 1

Introduction

1.1 Background

Maintaining genetic fidelity is crucial for the normal functioning and survival of all organisms. Indeed, aberrations in the genome can lead to cancer and developmental disorders (Jackson and Bartek, 2009; Magdalou et al., 2014; Menck and Munford, 2014). The key processes of DNA replication and chromosome segregation are arguably the most hazardous stages of the cell cycle, where genomic instability can readily arise (Leman and Noguchi, 2013). During DNA replication, the replication fork (RF) encounters a variety of obstacles including DNA interstrand crosslinks, lesions in the template DNA resulting either from endogenous or exogenous DNA damage, as well as accidental and programmed fork-blocking sites (Labib and Hodgson, 2007; Branzei and Foiani, 2010; Lambert and Carr, 2013; Gadaleta and Noguchi, 2017). These replication fork barriers (RFBs) can cause fork stalling, where the replisome components remain associated with the arrested RF enabling the resumption of DNA synthesis following resolution of the impediment (Hu et al., 2012). Stalled RFs can be protected and stabilised such that either DNA synthesis can resume when the barrier is removed, or so it can merge with the fork coming from the opposing direction. Failure to maintain an arrested fork in a stalled configuration leads to fork 'collapse'. A collapsed RF is a dysfunctional fork that has lost the capacity to perform DNA synthesis (Cortez, 2015), and in such cases the resumption of DNA synthesis is possible only with the help of factors that facilitate the reloading of replisome components (Cobb et al., 2003; Katou et al., 2003; Lucca et al., 2004). RF collapse has been studied mainly under pathological conditions (e.g. in replication

checkpoint mutants following global replication disturbance induced by drugs/genotoxins). Based on such studies, collapse was thought to involve complete replisome disassembly (Lopes et al., 2001; Tercero and Diffley, 2001; Zeman and Cimprich, 2014), however, other work has shown that it may involve only partial replisome loss and/or remodelling (De Piccoli et al., 2012).

Collapsed RFs can be restarted by homologous recombination (HR) (Haber, 2000; Costes and Lambert, 2012; Saada et al., 2018). HR is perhaps best known for its role in repairing DNA double-strand breaks (DSBs), and similarly it can repair collapsed RFs that break to form one-ended DSBs (Mayle et al., 2015). However, not all collapsed forks are broken and it seems that DSB formation is not essential for the recruitment of HR proteins at impaired forks or for their restart (Hashimoto et al., 2010; Lambert et al., 2010; Teixeira-Silva et al., 2017).

The intervention of HR to restart collapsed/broken RFs appears to be vital for promoting genome stability by ensuring the timely completion of DNA replication (McGlynn et al., 2002a; b; Chen et al., 2010; Errico et al., 2012; Jones et al., 2012). However, paradoxically, replication restarted by HR can also cause genome instability as it is associated with a large increase in the rate of mutagenesis (Deem et al., 2011), clustered mutations (Sakofsky et al., 2014), and an increased frequency of template switching (Smith et al., 2007). Moreover, restarting replication HR may inadvertently recombine ectopic homologous sequences, which can lead to changes including deletions, duplications, inversions, and translocations that can ultimately result in the

development of different human pathologies (Chen et al., 2007; Fusco et al., 2012; Guirouilh-Barbat et al., 2014).

In my study, the fission yeast *Schizosaccharomyces pombe (S. pombe)* is used as a model system to study the recombination induced at blocked RFs. In the first chapter, I review fundamentals of DNA replication and highlight what we know about major types of impediments to DNA replication. Most of the cellular strategies to cope with these impediments in order to prevent DNA damage during DNA duplication involve HR, therefore I describe the major stages of HR and the key proteins involved. As HR is an evolutionarily conserved process, I will discuss insights that have been discovered using the bacterium *Escherichia coli* (*E. coli*), the budding yeast *Saccharomyces cerevisiae* (*S. cerevisiae*) and other organisms. Alongside that, I will allude to the wide range of strategies cells employ to overcome impediments during DNA replication.

1.2 Fundamentals of DNA replication

1.2.1 Initiation of replication

DNA replication is initiated at replication origins, specific loci where sister RFs emanate and move bidirectionally away from each other. In *E. coli*, DNA replication of its circular chromosome starts from a single origin of replication (*OriC*) and ends within a defined terminus region (Gao and Zhang, 2007; Leonard and Mechali, 2013; Dimude et al., 2016). This means that, in *E. coli*, the collapse of a single RF prior to termination could result in a failure to

complete DNA replication. However, this fate is avoided because *E. coli* has several replication restart pathways that typically utilise HR proteins to convert a broken or collapsed RF into a substrate on to which replisome components can be reloaded (Michel and Sandler, 2017; Windgassen et al., 2018). In eukaryotes, the multi-subunit Origin Recognition Complex binds to a replication origin and recruits the pre-replication complex, which licenses the origin for firing (Waga and Stillman, 1998; Parker et al., 2017). However, in eukaryotes, efficient replication of the entire genomic DNA content is achieved through the firing of multiple origins along each chromosome. Moreover, there is a set of excess origins that may be activated within active replicon clusters if RF progression is inhibited (Ge et al., 2007; Ibarra et al., 2008). Thus, in eukaryotes, restart of interrupted replication is not as vital as it is for bacteria because the firing of a “backup” origin can compensate for the potential loss of replicative capacity caused by the collapse of a RF. However, this strategy, for ensuring that DNA replication is completed, is not foolproof because there will not always be an origin between converging RFs and, therefore, if both forks fail then restart of at least one of them will be necessary.

1.2.2 Replisome

Each RF proceeds within a multi-component complex, called the ‘replisome’. The replisome is comprised of DNA helicases, including the Mcm2-7 (minichromosome maintenance) replicative helicase complex, replication elongation factors (which include the three regular DNA polymerases: Pol α (alpha), Pol δ (delta), and Pol ε (epsilon)), and accessory proteins, such as

proliferating cell nuclear antigen (PCNA), clamp loader replication factor C (RFC) and other factors required for fork stabilization (Waga and Stillman, 1998; Branzei and Foiani, 2010; Kelly, 2017). RFC, composed of the Rfc1 – Rfc5 subunits, recognizes ss-dsDNA junctions and loads the replicative helicase and the homotrimeric DNA polymerase clamp PCNA, which maintains the speed and processivity of DNA polymerases during replication (Majka and Burgers, 2004). The CMG complex, consisting of the ring-shaped helicase Mcm2–Mcm7, Cdc45 and GINS complex, is the main replicative helicase that drives fork progression and is also a key scaffold for protein-protein interactions within the replisome (Branzei and Foiani, 2010; Ilves et al., 2010). The replicative helicase unwinds the parental dsDNA enabling the RF establishment on two separated strands. Each strand is then copied by replicative polymerases which are Pol1 (α), Pol2 (ε), and Pol3 (δ) in yeast. DNA polymerases are polar and synthesize DNA only in the 5' to 3' direction, thus one strand is replicated continuously (leading strand) in the same direction as the movement of the RF, while the other strand (lagging strand) is replicated discontinuously in the opposite direction as short DNA fragments (Okazaki fragments), which requires repeated initiation from a primer. Following their synthesis, Okazaki fragments are processed by Pol δ-mediated displacement of the RNA primer and cleavage of the resulting flap by Flap endonuclease 1 (FEN1)/Dna2, enabling consecutive fragments to be ligated to each other by DNA ligase I (Adl1 in *S. pombe* and Cdc9 in *S. cerevisiae*) to form a continuous strand (Stewart et al., 2008, 2009). DNA synthesis is initiated by Pol α, which synthesises a short (~ 10 bp) RNA primer. In the

classical model of DNA replication, Pol α is believed to be replaced, following primer synthesis, by Pol δ and Pol ε on the lagging and leading strand, respectively (Miyabe et al., 2011). However, this view of replication has recently been challenged by the finding that Pol δ can copy both template strands and that Pol ε only proofreads errors made by Pol δ during leading-strand replication (Johnson et al., 2015; Garbacz et al., 2018). This idea has garnered some controversy in the field and future studies will be needed to reach a definitive model of polymerase usage during normal DNA replication.

1.2.3 Termination of replication

In *E.coli* RFs move around the chromosome in opposite directions at a rate of ~60 kb/minute and terminate in a specific nucleotide sequence region across from the origin termed *TER* sites (A–J), which can bind the DNA replication terminus site-binding protein (Tus) to form polar RFBs (Dimude et al., 2016; Dewar and Walter, 2017). In contrast, eukaryotic DNA replication generally does not have a defined termination zone with RFBs. Instead replication ends when replisomes emanating from neighbouring replication origins converge. When the two forks converge DNA synthesis is completed, the replication machinery is disassembled and catenated sister chromatids are resolved by DNA topoisomerase II (TopII) as seen in the mammalian DNA tumor virus SV40 (Ishimi et al., 1992) or redundantly by the Sgs1-TopIII-Rmi1 complex in the budding yeast (Mundbjerg et al., 2015). Key components of the replisome are also disassembled in late S phase, including the CMG helicase, which is ubiquitylated on its Mcm7 subunit in a SCF^{Dia2}-dependent manner

that targets it for extraction from the DNA by p97 (Maric et al., 2014; Priego Moreno et al., 2014; Maculins et al., 2015). Active dissociation of CMG occurs without inhibition of DNA synthesis when forks approach each other and only after the final ligation step. In addition, the helicase disassembly is not required for completion of DNA synthesis, strongly suggesting that converging CMGs pass one another before they dissociate from dsDNA (Dewar et al., 2015). Recently, $CRL2^{LRR1}$ (Cullin RING ligase 2 associated with LRR1) was identified as the ubiquitin ligase that promotes MCM7 ubiquitylation and CMG unloading at the end of S phase in worms and frog (Dewar and Walter, 2017; Dewar et al., 2017; Sonneville et al., 2017). Conceivably, the replication termination is a carefully orchestrated process as revealed by the discovery of an active CMG removal pathway albeit by ubiquitylation rather than by the phospho-regulatory mechanisms that are used during replication initiation. If so, it would be important to investigate whether misregulation of termination contributes to genomic instability and human disease (Dewar and Walter, 2017).

1.3 Impediments to DNA replication

1.3.1 RFBs: DNA damage

RFBs can impede the progression of the RF causing fork stalling and even collapse (Mirkin and Mirkin, 2007; Lambert and Carr, 2013; Gadaleta and Noguchi, 2017). At a stalled or collapsed fork, replication can be restarted or the RF structure will be maintained in a configuration capable of converging

with the opposing fork (Lambert and Carr, 2013). Examples of RFBs include damaged DNA templates, unusual DNA structures, transcription-replication collisions, strong RNA-DNA hybrids and DNA-binding proteins.

DNA damage, including strand breaks, pyrimidine dimers, abasic sites, alkylated bases, bulky adducts and interstrand cross-links, which occurs either as a consequence of normal physiological processes (e.g. oxidative metabolism) or through cellular exposure to external genotoxins, can be an obstacle to the replicative DNA polymerases. A number of different genotoxic agents can lead to damage of the DNA template and consequent restriction of fork passage. For example, 3-methyladenine adducts are formed upon exposure to methyl methanesulfonate (MMS) (Wyatt and Pittman, 2006), cyclobutane pyrimidine dimers are induced by ultraviolet light (UV), and DNA strand breakage can be caused by ionizing radiation. Camptothecin (CPT) inhibits the re-ligation step such that the topoisomerase I (Top1)-DNA covalent intermediate is blocked at the 5′ end of the ssDNA nick (Hsiang et al., 1985). A one-ended DSB can be formed as a result of the leading strand polymerase running off the template when it encounters nicks (Kuzminov, 2001).Whereas, a two-ended DSB can be formed when the RF runs into a nick on the lagging strand as the synthesis of the lagging strand is discontinuous (Caldecott, 2008). The depletion of the cellular deoxyribonucleoside triphosphate (dNTP) pool by hydroxyurea (HU) can temporarily pause RFs. The impediments to fork progression caused by the aforementioned agents can induce recombination. However, the induction of recombination is not always the consequence of fork stalling (Calzada et al., 2005). The outcome of

recombination, if induced, varies for different genotoxins: UV-induced dimers promote gene conversion between direct repeats, whereas CPT induces deletions (Ahn et al., 2005).

1.3.2 Unusual DNA structures

Inverted repeats, mirror repeats, and direct tandem repeat DNA sequences can often undergo structural transitions that lead to the formation of secondary DNA structures including hairpins, H-DNA (triplex), G-quartets, Z-DNA and S-DNA (Sinden et al., 1998). Such DNA structures also represent a challenge for RF progression (Mirkin and Mirkin, 2007). Many human diseases and hereditary disorders are believed to be caused by repeat expansions, which in some cases have been attributed to abnormal replication of the repeats associated with RF stalling, especially in the case of trinucleotide repeats (Kremer et al., 1991; Samadashwily et al., 1997; Budworth and McMurray, 2013; Le et al., 2015; Gerhardt et al., 2016; Gadaleta and Noguchi, 2017)

1.3.3 Transcription-replication conflict

Collisions between transcription and replication machineries are mutagenic as shown in prokaryotes and eukaryotes (Gaillard et al., 2013; Hamperl and Cimprich, 2016) and have recently been linked to oncogene-induced DNA damage in cancer cells (Kotsantis et al., 2016). Torsional stress in DNA associated with active concurrent transcription and replication can lead to abundant reversed forks which contribute to slowing replication progression and to the recruitment of nucleases (Helmrich et al., 2013). R-loops, which are

RNA–DNA hybrids with displaced ssDNA that are formed as a result of the nascent RNA hybridizing back to its complementary DNA strand, are also barriers to RF progression that are associated with increased chromosomal fragility (Mirkin and Mirkin, 2007; Gaillard et al., 2013; Helmrich et al., 2013).

1.3.4 Programmed DNA replication perturbations

Interestingly, in a range of cases cells have evolved programmed protein-DNA RFBs to specifically direct DNA replication across certain genomic loci to regulate important biological processes. These barriers are polar which means that progression of forks is blocked only in one direction. One of the most extensively studied programmed barriers is the Tus-*ter* barrier in *E. coli.* The DNA replication terminus site-binding protein (Tus) bound to specific termination sites, *terA-terJ,* blocks RFs, prevents the unwinding of DNA by the replicative helicase DnaB and limits any re-replication after aberrant initiation in the termination zone (Hiasa and Marians, 1994; Rudolph et al., 2013; Wendel et al., 2014; Dewar and Walter, 2017). In eukaryotes polar RFBs are found located between ribosomal DNA repeats (rDNA). For example, in *S. cerevisiae* the Fob1 protein-DNA barrier prevents head-on collisions between transcription and replication machinery by blocking RFs moving in the direction opposite to transcription (Brewer and Fangman, 1988; Choudhury et al., 2015; Gadaleta and Noguchi, 2017). Another example of a programmed RFB is replication termination sequence 1 (*RTS1*) that promotes mating-type switching in *S. pombe* (Dalgaard and Klar, 2001). A detailed description of mating type switching and the *RTS1* RFB is given in the next section.

1.3.5 Mating type switching and the *RTS1* replication fork barrier

Mating-type switching in fission yeast can be considered as a form of cell differentiation where cells can efficiently switch between two distinct cell types by reprogramming their genomic DNA (Egel, 2004). The two mating types are termed P (*p*lus), and M (*m*inus). The functional state is encoded by the actively expressed mating-type 'cassette' (P or M state of the *mat1* locus), which can be exchanged for one of two silent backup copies *mat2-P* and *mat3-M* via HR driven by identical repetitive sequence elements on either end of all three loci (Dalgaard and Klar, 1999). An epigenetic modification of the *mat1*-cassette DNA, referred to as an 'imprint', causes the initial switch-related damage (Vengrova and Dalgaard, 2006; Yamada-Inagawa et al., 2007). In order for the switching to occur, a RF has to move in a telomere-to-centromere direction across *mat1* so that the imprint can be laid down, which then stimulates mating-type switching in the next generation (Dalgaard and Klar, 1999). *RTS1* promotes the establishment of the imprint by preventing replication of the *mat1* locus in the centromere-to-telomere direction (Holmes et al., 2005; Vengrova and Dalgaard, 2006).

RTS1 consists of four repeated 55 bp motifs (region B), whose function is enhanced by a 60 bp purine-rich region (region A) (Codlin and Dalgaard, 2003). The factor Sap1 binds to the enhancer region A, however Sap1 binding does not affect the replication barriers in the mating-type region (Dalgaard and Klar, 2000). The barrier function of *RTS1* depends on the Swi1–Swi3 complex and the replication termination factors Rtf1 and Rtf2. Rtf1 binds to the regions

A and B, and stabilizes the barrier by protecting DNA from unwinding by the replicative helicase through self-interaction with its C-terminus (Eydmann et al., 2008). Rtf1 is a member of the family of factors that includes *S. cerevisiae* Reb1, *S. pombe* Reb1 and human/mouse TTF-I (Eydmann et al., 2008). Rtf2 stabilizes the stalled fork and prevents Srs2-dependent replication restart at *RTS1* so that DNA replication is completed by a converging RF (Inagawa et al., 2009). The Swi1-Swi3 complex is part of the Fork Protection Complex that travels with the RF and serves critical roles in stabilizing and protecting stalled forks and in the activation of the replication checkpoint kinase Cds1 (Dalgaard and Klar, 2000; Noguchi et al., 2004, 2012). Intriguingly RFs arrested at the *RTS1* barrier are prone to collapse, which triggers an HR-dependent replication restart event (Ahn et al., 2005; Lambert et al., 2005; Nguyen et al., 2015). RF blockage at *RTS1* can therefore be resolved either through RF collapse followed by restart or by passive termination involving RF merging at the barrier. Thus, *RTS1* can be used in *S. pombe* as a model for studying how cells cope with strong pRFBs, fork collapse and subsequent repair by HR-dependent mechanisms.

1.3.6 General strategies of cellular defence against RFBs

To ensure the successful passage of a RF through obstacles and sufficient replication fidelity and efficiency, cells employ a range of different strategies, which are collectively termed the DNA damage response. As a first line of defence, cells have evolved mechanisms to counteract RFB activity either before or during replication; e.g. repairing damaged DNA prior to its replication,

avoiding transcription-replication clashes, and using additional helicases to displace RFBs (Helmrich et al., 2013; Brüning et al., 2014; Marteijn et al., 2014). However, if a RF is arrested by a RFB, then a second line of response seems to be the stabilization and maintenance of the RF and its replisome components so that it can either rapidly resume DNA synthesis following resolution of the impediment or be rescued by fork convergence (Errico and Costanzo, 2012). Third, if stabilisation fails, this will result in fork collapse (Lambert and Carr, 2013). The collapsed fork can either be stabilised in a conformation that is capable of merging with a converging fork or restarted by re-setting the replisome capable of continuation of DNA synthesis. These responses are discussed later in this chapter. The HR machinery appears to play a key role in these events (Branzei and Foiani, 2010; Costes and Lambert, 2012; Lambert and Carr, 2013; Wilhelm et al., 2016; Saada et al., 2018).

1.4 Overview of homologous recombination: key players and mechanism

HR is a highly conserved mechanism that promotes genetic diversity during various biological processes, such as antigenic variation in pathogens (Robertson and Meyer, 1992), bacterial conjugation, mating-type switching in budding yeast and fission yeast (Dalgaard and Klar, 1999; Haber, 2012) and meiosis (Champion and Hawley, 2002). HR plays a major role in DNA damage response and the faithful completion of DNA replication when the fork encounters various RFBs, including DSBs and ssDNA gaps and nicks (Costes and Lambert, 2012; Branzei and Szakal, 2016). In addition to this, HR proteins,

such as Rad51, and its mediator partners, stabilize impeded RFs by protecting newly synthesized strands from extensive end-resection (Costanzo, 2011; Errico and Costanzo, 2012).

A key initiating substrate for HR is ssDNA coated with ssDNA-binding protein (SSB in prokaryotes and RPA in eukaryotes). As ssDNA is a common intermediate of many DNA metabolic processes, HR has to be carefully regulated during the cell cycle and in response to DNA damage to avoid potentially detrimental genetic exchanges (Krejci et al., 2012).

HR has been most extensively studied in the context of DSB repair (Ranjha et al., 2018). There are four main models that describe the different ways in which HR can repair DSBs: the DSB repair model, synthesis-dependent strand annealing (SDSA), break-induced replication (BIR) and single-strand annealing (SSA). The HR pathways include three basic stages: pre-synapsis, synapsis and post-synapsis (Fig 1.1). During pre-synapsis, the broken DNA is resected by exonuclease and key recombination proteins are loaded onto the resulting ssDNA. During synapsis a nucleoprotein complex searches for a homologous DNA template through homologous pairing and strand invasion or ssDNA annealing occurs. Lastly, during post-synapsis, the intermediate DNA structures are resolved or dissolved (Ranjha et al., 2018). Below I describe some of the HR proteins that play a crucial role in HR reactions. A list of key HR proteins in fission yeast, as well as their functional homologues in bacteria, budding yeast and mammals, is presented in Table 1.1.

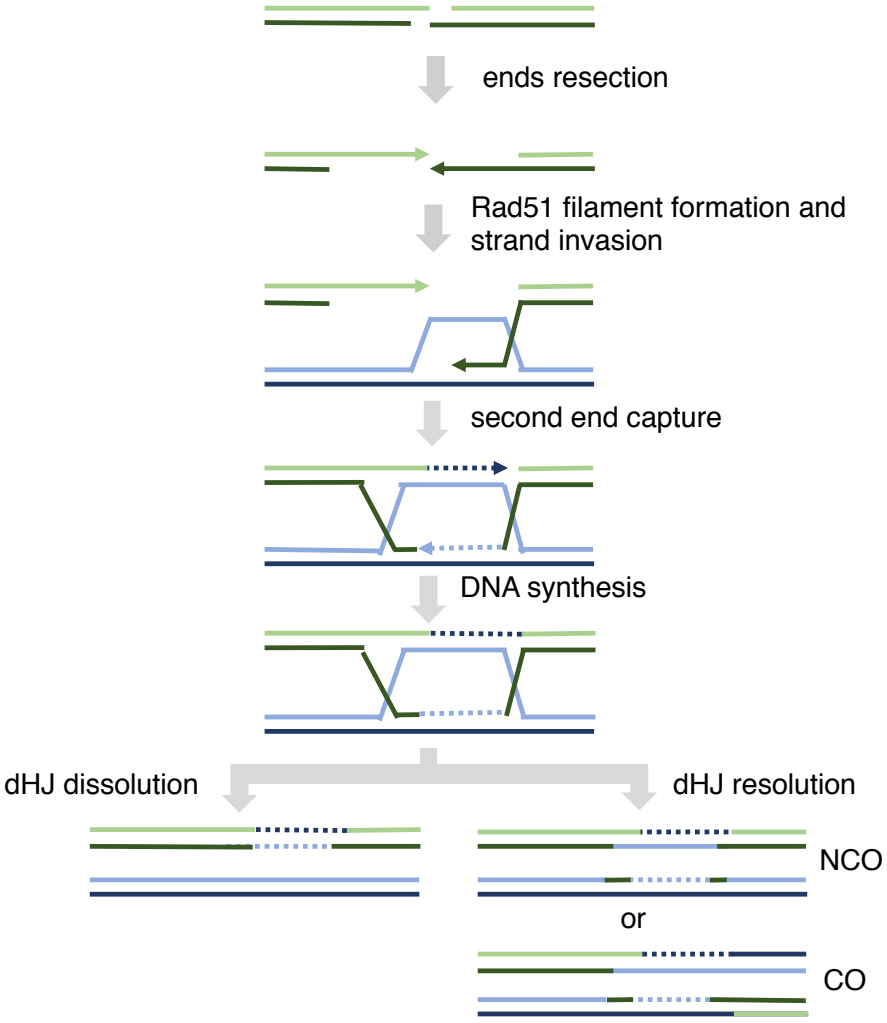


Figure 1.1. The canonical model of DNA DSBs repair.

DSBs are efficiently repaired by HR. In pre-synapsis, 3'-ssDNA tails as substrates for the further reactions are generated by a two-step end resection cascade. In synapsis, after the formation of long patches of 3'-ssDNA ends, the Rad51 nucleoprotein filament is formed and homology search takes place. Once a homologous region is identified, the nucleoprotein filament invades the duplex DNA (sister chromatid or homologous chromosome), and forms a D-loop. The 3′ end of the invading strand primes DNA synthesis. The second broken DNA end can anneal to the displaced ssDNA strand of the D-loop structure to stabilize the D-loop. In post-synapsis, the dHJ structure can be resolved by either endonucleolytic cleavage to generate both crossover (CO) or non-crossover (NCO) outcomes or exclusively NCO by the concerted action of a helicase with topoisomerase III, referred to as dHJ resolution and dHJ dissolution, respectively. Adapted from Mehta et al., 2014.

Table 1.1 Homologous Recombination Proteins

	E. coli	***S. cerevisiae***	***S. pombe***	**Mammals**
Pre-synapsis Processing of broken DNA ends	RecBCD			
	SbcD-SbcC	Mre11-Rad50-Xrs2	Mre11 (Rad32)-Rad50-Nbs1	MRE11-RAD50-NBS1
	-	Sae2	Ctp1	CtIP1
	RecQ	Sgs1	Rqh1	BLM
	-	Dna2	Dna2	DNA2
	RecE, RecJ	Exo1	Exo1	EXO1
	SSB	RPA	RPA	RPA
	-	-	Fbh1	FBH1
	UvrD	Srs2	Srs2	PARI
Synapsis Homologous pairing and DNA strand exchange	RecA	Rad51	Rad51 (Rhp51)	RAD51
	RecO	Rad52	Rad52 (Rad22)	RAD52
	RecF- RecR	Rad55-Rad57	Rad55 (Rhp55)-Rad57 (Rhp57)	RAD51B, RAD51C-XRCC3
	-	Sae3-Mei5	Swi5-Sfr1	SWI5-SFR1
	-	Shu1-Shu2-Psy3-Csm2	Rlp1-Sws1-Rdl1	XRCC2-SWS1-RAD51D-SWSAP1
	-	Rad54	Rad54 (Rhp54)	RAD54
Post-synapsis Resolution of recombination intermediates	TopoIII	Top3	Top3	TopoIIIα
	RecQ	Sgs1	Rqh1	BLM, RECQ1, RECQ4, RECQ5, WRN
	-	Mph1	Fml1	FANCM
	-	-	Fbh1	FBH1
	UvrD	Srs2	Srs2	PARI
	RuvAB			
	-	Mus81-Mms4	Mus81-Eme1	MUS81-EME1
	RuvC	Yen1	-	GEN1
	-	Slx1-Slx4	Slx1-Slx4	SLX1-SLX4

Note: Homologous or functionally equivalent recombination proteins from the different species are arranged in the same row.

1.4.1 Pre-synapsis: resection

The process of HR starts with pre-synapsis, where the 5′-terminated DNA strand is resected in two steps to form an extended region of ssDNA (Mimitou and Symington, 2008; Zhu et al., 2008). The initial step is catalysed in fission yeast by the Mre11-Rad50-Nbs1 (MRN) complex and Ctp1 (Mre11-Rad50-Xrs2 (MRX) complex and Sae2 in budding yeast and MRN complex and CtIP in human cells) (Paull and Gellert, 1998; Sartori et al., 2007; Buis et al., 2008). The nuclease activity of Mre11 and Ctp1 is aided by Rad50. The MRX/MRN complex performs only short-range resection, because the vicinity of the DNA end is required for its activity (Zhu et al., 2008) (Fig. 1.2).

Nbs1 targets the complex to DNA ends through its DNA binding activity (Trujillo et al., 2003). The preliminary resection is most likely initiated by the endonucleolytic cleavage of the 5′-terminated DNA strand away from the DNA end by MRX/N, followed by resection back towards the DNA end mediated by the 3' to 5' exonuclease activity of MRX/MRN (Mimitou and Symington, 2008). Following initial resection by MRX/MRN, further "long range" resection can be catalysed either by the 5'-3' exonuclease Exo1, or by the 3'-5' DNA helicase Sgs1 (the budding yeast orthologue of *S. pombe* Rqh1) working in conjunction with the endonuclease Dna2 (Mimitou and Symington, 2008; Zhu et al., 2008).

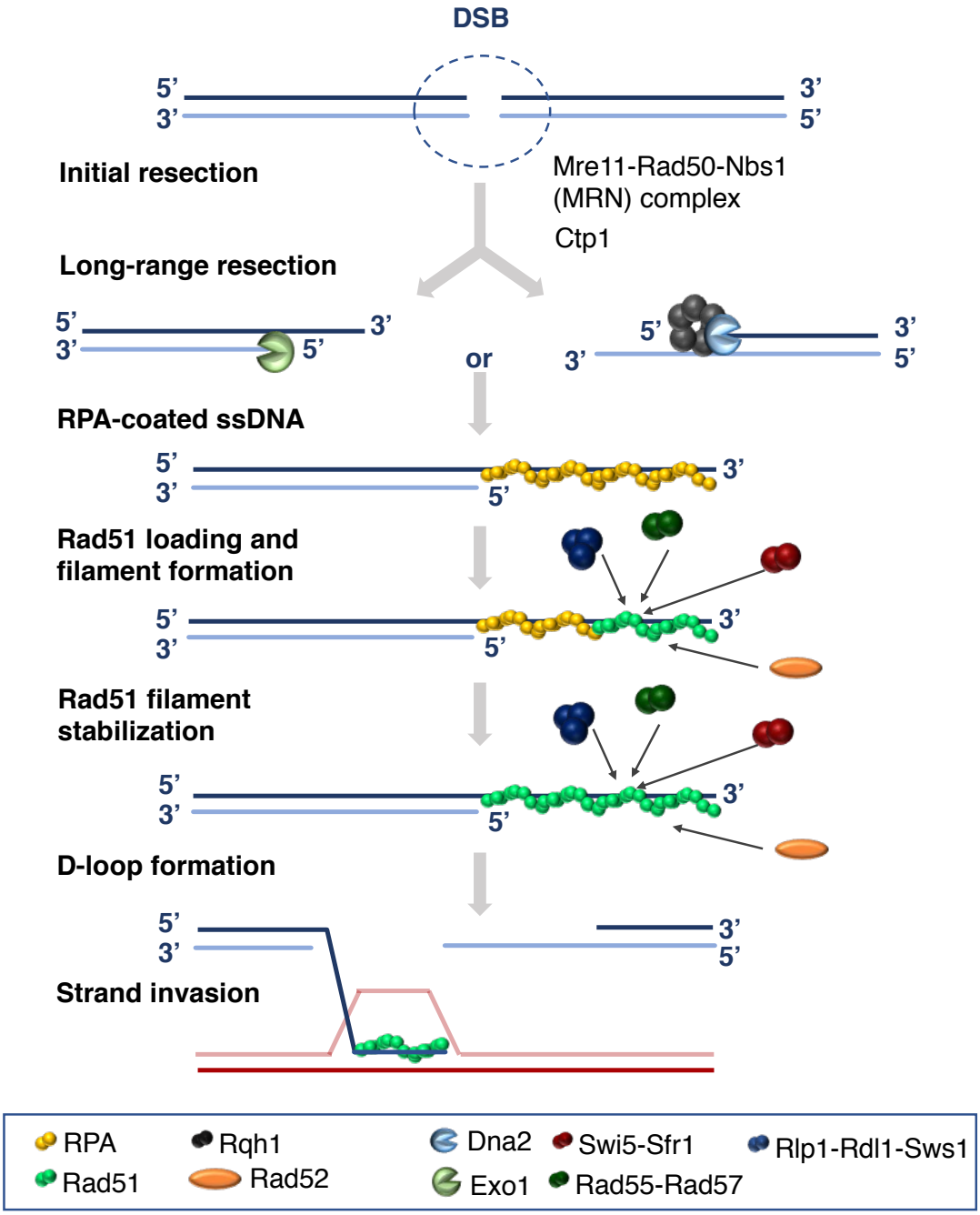


Figure 1.2. The central reaction of homologous recombination.

Following the short- and long-range resection, broken DNA ends are coated with RPA. Rad52 overcomes RPA inhibition and facilitates Rad51 loading and nucleofilament formation. The Rad51 mediator complexes Rad55-Rad57, Swi5-Sfr1, Rdl1-Rlp1-Sws1stabilise and protect the presynaptic filament. The Rad51 filament then performs homology search and once the homologous sequence is found, DNA synthesis starts. Adapted from Godin et al., 2016.

1.4.2 Pre-synapsis to synapsis: Rad51 nucleoprotein filament formation and strand invasion

Following the formation of 3′-overhanged ssDNA, replication protein A (RPA) coats the tail eliminating secondary structures and protecting the DNA from nucleolytic cleavage (Binz et al., 2004). RPA is then replaced by the central recombinase Rad51 (RecA in bacteria). RPA inhibits Rad51 binding to DNA as it has higher affinity toward ssDNA than Rad51 (New et al., 1998; Shinohara and Ogawa, 1998; Wang et al., 2004; Ma et al., 2017). Cells have evolved various recombination mediator proteins to aid Rad51 loading onto ssDNA by displacing RPA in the process and to stabilise the formed nucleoprotein filament (also referred to as a presynaptic filament) (Gaines et al., 2015) (Fig. 1.2). Some of Rad51's key mediators and accessory proteins are highlighted below.

1.4.2.1 Rad52

In fission yeast, the key recombination mediator that displaces RPA from ssDNA is Rad52 (Song and Sung, 2000; Kurokawa et al., 2008). Interestingly, contrary to the current model Rad52-Rad51 association was reported to be essential to protect Rad51 filaments against Srs2 but is not essential for Rad51 filament assembly. However, this hypothesis should be tested further (Ma et al., 2018). Rad52 contains an N-terminal DNA-binding domain and self-association domain, a central RPA interaction domain and a C-terminal Rad51- and secondary DNA-binding domain (Kagawa et al., 2002; Korolev, 2017). Rad52 is essential for all recombination events whether they are

Rad51-dependent or-independent in fission yeast (Doe et al., 2004). Rad52 is highly conserved in eukaryotes but surprisingly its activity in mediating RAD51-dependent homology-directed DNA repair in mammalian cells seems to be functionally redundant between RAD52 and BRCA2 (Rijkers et al., 1998; Liu and Heyer, 2011). Interestingly, in recent studies RAD52 was shown to promote mitotic DNA synthesis following replication stress. This process also involved MUS81 and POLD3 and seemingly acts to repair collapsed RFs during mitosis independently of ATR, BRCA2, and RAD51 (Minocherhomji et al., 2015; Bhowmick et al., 2016; Sotiriou et al., 2016). Another RAD51-independent role of RAD52 is its ability to promote DNA strand annealing between complementary sequences which is a crucial step in the SSA pathway (Mortensen et al., 1996; Grimme et al., 2010; Verma and Greenberg, 2016). Furthermore, Rad52 can catalyse a process termed 'inverse' strand exchange in which a DNA duplex 'invades' a homologous ssDNA or RNA molecule (Kwon and Sung, 2017; Mazina et al., 2017).

1.4.2.2 Rad55-Rad57

The Rad51 nucleofilament is further stabilised by a group of proteins referred to as Rad51 paralogs. In fission and budding yeast, these include Rad55, Rad57, Rdl1 and Rlp1 (Liu et al., 2011a) and, in mammals, RAD51B, RAD51C, RAD51D, XRCC2, and XRCC3 (Masson et al., 2001). A heterodimer of Rad55-Rad57 *in vitro* is able to overcome RPA inhibition of Rad51-mediated strand exchange (Sung, 1997a). Unlike Rad52, Rad55-Rad57 does not interact with RPA directly and, therefore, it does not appear to aid the nucleation of Rad51 onto DNA. Instead it appears to promote the stabilization

of the Rad51 nucleoprotein filament protecting it from the anti-recombinase activity of the Srs2 helicase (Hays et al., 1995; Johnson and Symington, 1995; Liu et al., 2011a).

1.4.2.3 Swi5-Sfr1

Rad51 is also assisted by the conserved Swi5-Sfr1 complex, which appears to function in a parallel pathway to Rad55-Rad57 for promoting Rad51-dependent HR in *S. pombe* (Akamatsu et al., 2007; Argunhan et al., 2017). For example, overexpression of Rad51 rescues *rad57*Δ and *rad55*Δ sensitivity to UV but only partially suppresses sensitivity of a *rad57*Δ *swi5*Δ double mutant (Tsutsui et al., 2000; Akamatsu et al., 2003, 2007). A *swi5*Δ*rad55*Δ double mutant also exhibits a synergistic increase in genotoxin sensitivity compared to its component single mutants (Haruta et al., 2008). However, these are not simple alternatives for promoting Rad51 activity. Unlike Rad55-Rad57, Swi5-Sfr1 it is not essential for formation of crossover products in mitotic recombination (Akamatsu et al., 2007), and overexpression of Sfr1 or Swi5 does not suppress the genotoxin sensitivity of *rad57*Δ mutant nor does overexpression of Rad57 rescue defects observed in *swi5*Δ or *sfr1*Δ mutants (Haruta et al., 2008). In budding yeast, the homolog of Swi5-Sfr1 – Sae3-Mei5 forms a meiosis-specific recombination accessory complex that promotes the activity of Dmc1, but not Rad51 (Hayase et al., 2004). However, deletion of *SWI5* and *SFR1* in human cells does impair mitotic HR, in mice a defect is only seen when HR is already compromised (Yuan and Chen, 2011; Tsai et al., 2012). Unlike its fission yeast homologs, both subunits of the human complex

interact with RAD51 (only Sfr1 interacts with Rad51 in *S. pombe*) (Haruta et al., 2006; Yuan and Chen, 2011).

Experiments involving the *in vitro* reconstitution of the Rad51 strand exchange reaction have led to a model where Rad51 is recruited to DNA by Rad52 which directly interacts with RPA (Argunhan et al., 2017). Swi5-Sfr1 promotes Rad51 nucleoprotein filament formation in an ATP-dependent manner and stabilises the filament by inducing its conformational change (Fornander et al., 2014). Moreover, Swi5-Sfr1 counteracts the presynaptic filament disruption activity of the F-box DNA helicase Fbh1 (Tsutsui et al., 2014).

1.4.2.4 Rdl1-Rlp1-Sws1/Shu1-Shu2-Psy3-Csm2

In budding yeast Rad55-Rad57 physically interacts with Rad51, Rad52 and the Shu complex, comprised of Csm2, Psy3, Shu1 and Shu2 (Godin et al., 2013; Gaines et al., 2015). *In vitro,* the Shu complex stimulates Rad51 nucleation onto DNA ~ 2-3-fold, but only in the presence of Rad52 and Rad55-Rad57 (Godin et al., 2013; Gaines et al., 2015). Its functional equivalents in fission yeast and humans are the Rdl1-Rlp1-Sws1 and XRCC2-SWS1-RAD51D-SWSAP1 complexes, respectively (Martín et al., 2006; Liu et al., 2011b; Ranjha et al., 2018). However, a homolog of the Csm2 subunit, bridging interaction between the Shu complex and Rad55-Rad57, which connects the Shu complex to the Rad51 nucleofilament, has not been discovered in fission yeast (Gaines et al., 2015).

Nevertheless, the Rdl1-Rlp1-Sws1 complex interacts with Rad55-Rad57 according to yeast two-hybrid analysis, and *rad55*Δ and *rlp1*Δ exhibit an

epistatic interaction with respect to sensitivity to MMS and IR (Khasanov et al., 2004).

Interestingly, Sws1 has been shown to interact with Srs2 in yeast two-hybrid screens (Martín et al., 2006), and deletion of the budding yeast Shu1 leads to increased Srs2 recruitment to both induced and spontaneous foci and a corresponding decrease in Rad51 foci (Bernstein et al., 2011). This suggests that the Shu complex may have a conserved and direct role in antagonizing the antirecombinase activity of Srs2 in disassembling Rad51 filaments.

1.4.3 Homology search and DNA synthesis

Once Rad51 is loaded onto ssDNA, and the presynaptic filament is formed, it starts to search for a homologous DNA sequence. However, the mechanism of homology search is not defined in detail, the current hypothesis is that the Rad51 filament scans the nuclear volume and contacts different short DNA duplexes randomly (Renkawitz et al., 2014; Ranjha et al., 2018). Units of microhomology which are more than 7 nt of homology form more stable contacts allowing the Rad51 filament to sample flanking sequences for additional homology (Qi et al., 2015). Once a homologous dsDNA sequence has been identified, the invading strand of the presynaptic filament intertwines with its complementary strand in the donor DNA to form a displacement loop (D-loop) structure (Baumann et al., 1996). Subsequent DNA synthesis is primed by the 3′-terminated strand within the D-loop with the intact homologous sequence being used as the template. Different DNA polymerases are implicated during HR-associated DNA synthesis including

Pol δ, Pol ε and various translesion polymerases (Wang et al., 2004; Hicks et al., 2010; Goodman and Woodgate, 2013; Sakofsky et al., 2015; Mcvey et al., 2016). To facilitate polymerase access to the 3' end of the invading DNA strand, Rad51 is displaced from the heteroduplex dsDNA by the DNA-dependent ATPase/DNA translocase Rad54 (Solinger et al., 2002; Wright and Heyer, 2014). Rad54 is conserved between yeast and humans and has a number of important roles in HR, which also include facilitating Rad51 strand invasion and D-loop formation through remodelling the chromatin in the intact homologous duplex (Alexeev et al., 2003; Ceballos and Heyer, 2011).

1.4.4 Post-synapsis: resolution of recombination intermediates

The D-loop is considered to be a key intermediate of HR, and a variety of enzymes have been identified that can process it and thereby influence the direction of the reaction. In particular, DNA helicases/translocases play key roles in positively and/or negatively regulating synapsis by dissociating D-loops or promoting their formation. Some of these enzymes are described below.

1.4.4.1 Srs2 and Fbh1

Bacterial PcrA and UvrD, budding/fission yeast Srs2, fission yeast and human Fbh1 have all been implicated in RecA/Rad51 nucleoprotein filament disruption and through this activity dissociation of the D-loop if the latter is formed (Krejci et al., 2003; Osman et al., 2005; Ruiz-Maso et al., 2006; Chiolo et al., 2007; Petrova et al., 2015). In the case of Srs2, it translocates in a 3' to 5' direction along DNA until it encounters a Rad51 protomer, with which it then

interacts, and stimulates it to hydrolyse ATP converting it into its low DNA binding affinity form (Krejci et al., 2003; Veaute et al., 2003; Antony et al., 2009; Seong et al., 2009; Sasanuma et al., 2013). In this way Srs2 can progressively dislodge Rad51 from ssDNA. Srs2 is known to play a key role in limiting Rad51 activity at stalled RFs and, at least in budding yeast, is recruited to these sites through its interaction with SUMOylated PCNA. Rad55-Rad57, the SHU complex and Rad52 all play key roles in protecting Rad51 nucleofilaments against the activity of Srs2 (Bernstein et al., 2011; Liu et al., 2011a; Ma et al., 2018).

Like Srs2, the F-box helicase 1 (Fbh1) is related to bacterial UvrD but, although present in fission yeast and mammals, is absent in *S. cerevisiae* (Chiolo et al., 2007). Similar to UvrD and Srs2, Fbh1 has a 3' to 5' DNA translocation activity but unlike all other known DNA helicases it also contains an F-box and can act as part of a SCF (SKP1, CUL1 and F-box) E3 ubiquitin ligase complex (Chu et al., 2015). It was first identified as a key factor in HR as a suppressor of *rad52*Δ (Osman et al., 2005). Genetic studies showed that *fbh1*Δ is synthetically lethal with *srs2Δ* and *rqh1Δ* - an interaction which was suppressed by deletion of *rad51* or *rad57* (Morishita et al., 2005; Osman et al., 2005). Although previously increased CO formation in *srs2Δ* was reported (Wang et al., 2001; Ira et al., 2003; Robert et al., 2006), in the site-specific DSB repair assay used by Tsutsui et al., (2014), Fbh1, but not Rqh1 or Srs2, suppressed Rad55-Rad57 dependent crossover formation induced by a single HO-induced DSB. Fbh1, Srs2 and Rqh1 have overlapping, albeit not completely redundant activities, and resolve HR intermediates formed in a

Rad51 and Rad55-Rad57 dependent pathway to limit CO formation during interchromosomal recombination (Tsutsui et al., 2014).

Fbh1 is proposed to negatively regulate HR by two main pathways. Firstly, it physically disrupts the presynaptic Rad51 nucleofilament and, in doing so, counteracts the stabilisation effect of Rad52 and other Rad51 mediators (Osman et al., 2005; Lorenz et al., 2009; Simandlova et al., 2013). Secondly, as part of the SCF^{Fbh1} complex, it ubiquitinylates Rad51 preventing it from rebinding to ssDNA and targeting it for degradation (Tsutsui et al., 2014; Chu et al., 2015). Interestingly, the Swi5-Sfr1 mediator complex seems to protect Rad51 against both of these inhibitory activities of Fbh1 as shown *in vitro* by disruption of Rad51 nucleofilaments in the absence, but not the presence, of Swi5-Sfr1 and inhibition of ubiquitylation of Rad51 by SCF^{Fbh1} (Tsutsui et al., 2014).

The prevailing hypothesis that Fbh1 acts only as negative regulator of Rad51 was challenged by the finding that it can catalyse fork reversal *in vitro* and *in vivo* and may do so to aid ssDNA formation at blocked RFs to facilitate loading of RPA (Fugger et al., 2009). Fbh1 is also required for checkpoint signalling through stress-activated protein kinases following RF stalling (Boyer and Sørensen, 2015; Fugger et al., 2015). Fork reversal (also termed fork regression) is the process in which the nascent DNA strands at a stalled fork are unwound and anneal to each other resulting in a four-way DNA junction. *In vivo* these DNA structures can be used as substrates for recombination protein loading and HR-mediated replication restart (McGlynn and Lloyd, 2002b).

1.4.4.2 The FANCM family of DNA helicases/translocases

The conserved FANCM-like helicases, including Hef protein in archaea, Mph1 in budding yeast, Fml1 in fission yeast, and FANCM in mammals, have been implicated in crossover suppression during mitotic and meiotic recombination, processing D-loops, DNA branch point migration and fork reversal (Mosedale et al., 2005; Whitby, 2010; Crismani et al., 2012; Lorenz et al., 2012; Nandi and Whitby, 2012; Boyer and Sørensen, 2015). These proteins are members of the superfamily 2 (DEAH-box helicases with significant homology within their helicase domains and in their C-terminal regions (Xue et al., 2015a).

The ability of FANCM family helicases to catalyse RF reversal means that they have the potential to promote HR-mediated replication restart (Gari et al., 2008a; b; Sun et al., 2008; Zheng et al., 2011; Xue et al., 2014). In contrast to this pro-recombinogenic activity, their D-loop dissociation activity can be used to abort recombination or channel it into the SDSA pathway which generates noncrossover recombinants (Gari et al., 2008a; b; Sun et al., 2008; Prakash et al., 2009). The ability of FANCM family helicases to work on a wide range of different DNA substrates means that its activity in the cell has to be strictly regulated, and studies in budding yeast have shown that at least part of this regulation depends on the Smc5-Smc6 complex (Chen et al., 2009; Xue et al., 2015a). Additional factors that influence the FANCM/Mph1/Fml1 activity include the Histone-fold-containing protein complex Mhf1-Mhf2 (MHF), which forms a DNA-processing complex with FANCM family members (Singh et al., 2010; Yan et al., 2010; Fox et al., 2014; Zhao et al., 2014). MHF promotes FANCM stability and its recruitment to DNA in mammals (Singh et al., 2010;

Yan et al., 2010; Fox et al., 2014; Zhao et al., 2014), although the same does not appear to be true in budding yeast (Xue et al., 2015b).

1.4.5 Double Holliday junction resolution

D-loop stability determines the particular HR pathway used and thus the steps and key factors required to resolve the heteroduplex structure. If the D-loop is stabilized and “captures” the second resected dsDNA end, DNA synthesis and ligation results in a double Holliday junction (dHJ) (Szostak et al., 1983; Hunter and Kleckner, 2001; McIlwraith and West, 2008; Bzymek et al., 2010). In addition, a dHJ can be formed as a consequence of strand invasion events at both ends of the DSB, followed by DNA synthesis and annealing (Hunter and Kleckner, 2001). dHJs can be resolved or dissolved by several different mechanisms giving rise to either non-crossover (NCO) or crossover (CO) products (Ranjha et al., 2018).

HJ resolution is achieved by nuclease cleavage and, depending on the orientation with which they cleave, each junction can give rise to either CO or NCO products (Dehé and Gaillard, 2017). HJ resolvases RuvC in *E. coli* and Yen1/GEN1 introduce symmetrical incisions across the junction (Dunderdale et al., 1991; Ip et al., 2008; Rass et al., 2010; Shah Punatar et al., 2017). Mus81-Eme1, and Slx1-Slx4 provide a second and genetically distinct pathway of HJ resolution in eukaryotes (Gaillard et al., 2003; Wyatt et al., 2013).The nuclease pathways are tightly controlled and are not activated until G2/M phase, which suggests that dHJs may primarily be dissolved and nucleolytic resolution is a backup mechanism to ensure that all joint molecule

DNA intermediates are resolved in time for chromosome segregation (Matos et al., 2011; Dehé et al., 2013).

1.4.6 Double Holliday junction dissolution

dHJ dissolution is catalysed by a collaboration between a RecQ family helicase and Topoisomerase III (Top3) leading to only NCOs (Cejka et al., 2010; Xue et al., 2013). RecQ family helicases RecQ (*E. coli*), WRN, BLM, RecQ1, RecQ4 and RecQ5 (*H. sapiens*), Sgs1 (*S. cerevisiae*) and Rqh1 (*S. pombe*) have D-loop unwinding activity which is shown to prevent excessive HR. In yeast, dissolution is mediated by the Sgs1-Top3-Rmi1 complex (Cejka et al., 2010), while in human cells the BLM helicase-TOPOIIIα complex, in conjugation with the RMI1-RMI2 complex, dissolves HJs preventing formation of CO products (Wu and Hickson, 2003; Singh et al., 2008; Xue et al., 2013). In this mechanism two HJs migrate toward each other, then Top3/TOPOIIIα transiently creates a nick in ssDNA to relax torsional stress, and finally RMI1/Rmi1 promotes the processing of a hemicatenane assisted by RPA (Cejka et al., 2010; Xue et al., 2013; Ranjha et al., 2018). BLM-deficient cells are characterised by the elevated levels of inter-sister chromatid and, as a consequence, genome rearrangements that might contribute to cancer predisposition of Bloom syndrome patients (Yamanishi et al., 2013).

1.5 Response to replication stress and the role of HR in aiding completion of DNA replication

In this section I discuss some of the mechanisms that are employed by cells to promote replication in the face of RFBs, highlighting the key roles that HR plays in these processes. These mechanisms include bypassing RFBs, stabilisation of the RF and replication restart when the fork collapses.

1.5.1 Translesion DNA synthesis (TLS)

TLS is a specialized bypass mechanism that enables cells to tolerate certain types of RF blocking DNA lesions (Jackson and Bartek, 2009; Waters et al., 2009; Branzei and Szakal, 2016). Whilst TLS enables replication past a lesion, it actually does not repair the DNA damage and, therefore, other repair pathways (e.g. nucleotide excision repair) have to operate after TLS has occurred. TLS depends on specialized DNA polymerases that are able to accommodate distorted/damaged DNA within their active site. However, these polymerases tend to be error-prone and, therefore, TLS is more mutagenic than regular DNA replication (Waters et al., 2009; Branzei and Szakal, 2016).

1.5.2 Template switching

Another way in which cells tolerate fork-blocking lesions is by employing template switching to bypass the RFB. Unlike TLS, template switching is considered to be error-free and involves recombination to a homologous template (usually the sister chromatid) either during or after DNA replication

(Smith and Rothstein, 1995; Zhang and Lawrence, 2005; Branzei, 2011). So-called post-replicative template switching occurs following the “skipping” of a DNA lesion by the RF, which leaves a lesion-containing daughter strand gap behind in the DNA. HR initiated from this gap enables the nascent DNA strand of the sister chromatid to be used as a template for DNA synthesis (Mourón et al., 2013; Branzei and Szakal, 2016). The D-loop structure that is formed during this process is extended to form a dHJ-like structure which in budding yeast is dissolved by the Sgs1-Top3-Rmi1 complex (McGlynn and Lloyd, 2002b; Branzei and Szakal, 2016) (Fig. 1.3A).

If the lesion is on the leading strand, following the transient uncoupling of leading and lagging strand polymerases, the lagging strand polymerase proceeds beyond the position at which the leading strand polymerase is blocked (Pages and Fuchs, 2003). Subsequent fork regression allows usage of the extended lagging strand as a template for the prematurely terminated leading strand (Daigaku et al., 2010; Branzei and Szakal, 2016). The regressed fork can subsequently be re-set so that DNA replication can continue.

In budding yeast the choice between TLS and template switching is governed by the ubiquitination of PCNA, with the E2 ubiquitin conjugating enzyme Rad6 and E3 ubiquitin ligase Rad18 acting to mono-ubiquitinate PCNA on lysine 164 (Branzei, 2011; Branzei and Szakal, 2016). Monoubiquitinated PCNA promotes TLS, whereas the addition of further ubiquitin molecules by

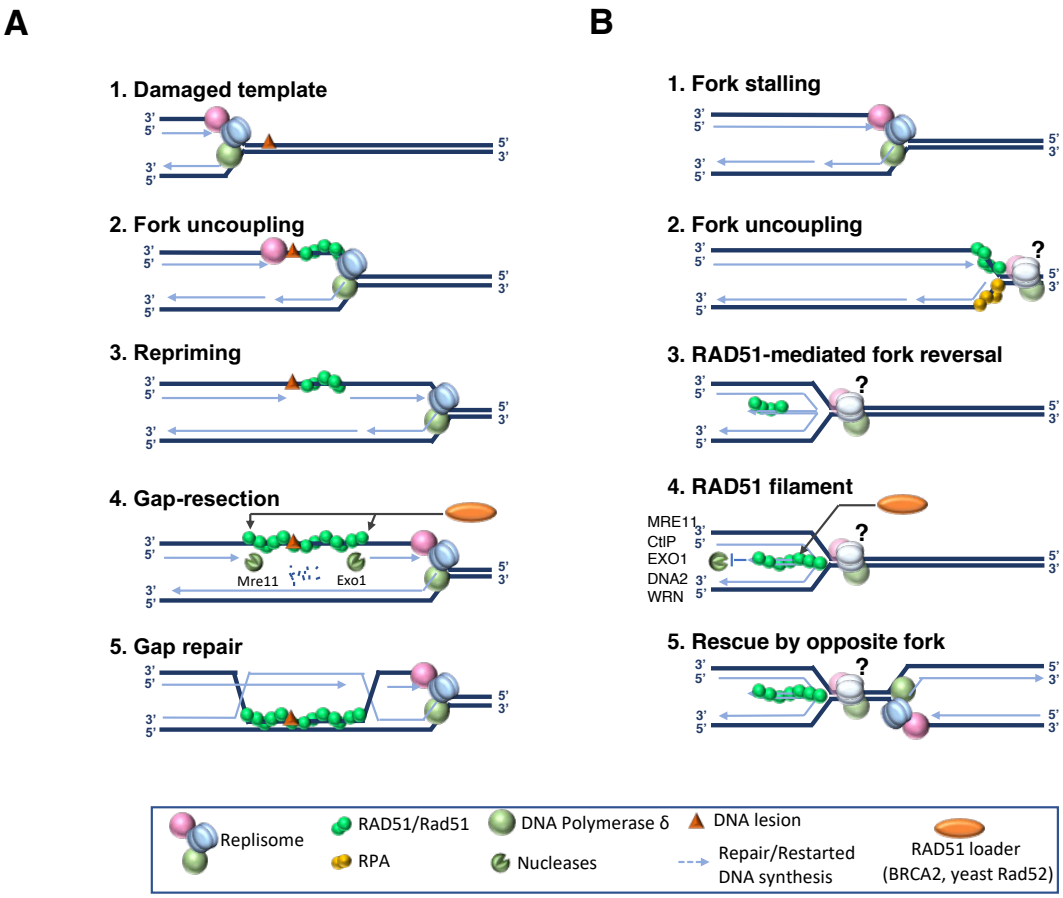


Figure 1.3. Models of post-replicative gap filling and fork-protection by Rad51.

(**A**) When the replisome runs into a DNA lesion, the replicative polymerases can be transiently uncoupled, the lagging strand polymerase proceeds beyond the position at which the leading strand polymerase is blocked, exposing a ssDNA gap, which is subsequently coated by Rad51. The fork can be reversed, to allow synthesis using the newly synthesised lagging strand as a template, or DNA synthesis can be resumed via re-priming downstream of the DNA lesion. The gap region, left behind the fork, anneals to the homologous sequence, which gives rise to a dHJ-like intermediate. This is subsequently dissolved to hemicatenanes by the Sgs1-Top3-Rmi1 complex, further dissolved most likely by Top3 in G2 phase. (**B**) Protection of stalled RFs by the Rad51 fork-reversal function. See text for details. Figure is taken from Ait Saada et al., 2018, colour code and order of mechanisms presentation is changed. doi.org/10.1016/j.dnarep.2018.08.017 is used under a Creative Commons license https://creativecommons.org/licenses/by/4.0/legalcode.

Rad5–Mms2–Ubc13 to generate polyubiquitinated PCNA, promotes the error-free template switching pathway (Johnson et al., 1994; Hoege et al., 2002; Branzei, 2011).

1.5.3 Stabilization of stalled forks: the role of HR proteins and the fork protection complex

The intra-S phase checkpoint plays a major role in stabilising stalled RFs so that they can resume DNA synthesis upon barrier dissolution or terminate in a non-pathological manner with a converging fork (Lindsay et al., 1998; Lopes et al., 2001; Tercero and Diffley, 2001). Two major kinases, a phosphoinositol-3 kinase-like kinase (PIKK) (ATR in metazoans), that senses RPA (Zou and Elledge, 2003), and a downstream checkpoint kinase, activated by ATR through the mediator protein Claspin, phosphorylate replisome components and DNA repair proteins (Errico and Costanzo, 2012). In *S. pombe*, Rad3 (the ATR homologue) and Cds1 are similarly required for protecting stalled RFs from collapse (Lindsay et al., 1998).

HR proteins also play important roles in protecting stalled RFs through their 'recombination-independent' functions (Hashimoto et al., 2010; Kolinjivadi et al., 2017). Fission yeast Rad51 was shown to preserve arrested forks from becoming dysfunctional through Rad51-mediated fork reversal and to prevent their excessive degradation through its DNA binding but not strand exchange activity (Quinet et al., 2017; Saada et al., 2017) (Fig. 1.3B). The non-homologous end joining heterodimer Ku70-Ku80 binds to the dsDNA end exposed as a result of RF regression (Teixeira-Silva et al., 2017). The MRN

complex and Ctp1 then remove Ku through initial fork-resection, which generates a short ssDNA gap for Rad51 to load on to. Exo1 can then extend the ssDNA gap, which would promote further Rad51 loading on to DNA. However, Rad51 appears to limit the amount of Exo1-mediated degradation, which maintains the fork in a configuration that merges well with the oncoming RF (see Section 1.4.6) (Saada et al., 2017, 2018).

Fork reversal frequently occurs in mammalian cells as a response to different types of genotoxic stress (Fig. 1.4). Protection of the reversed fork from the activity of nucleases is a crucial process to prevent increased chromosomal breakage and preserve genome stability (Quinet et al., 2017; Taglialatela et al., 2017). In human cells there are few enzymes that have been implicated in fork regression. FBH1 promotes fork regression *in vivo*, however the molecular mechanism of further stabilisation is not fully understood (Fugger et al., 2015). Translocases of the SWI/SNF protein family ZRANB3 and SMARCAL1 also can reverse a RF (Kolinjivadi et al., 2017; Taglialatela et al., 2017; Vujanovic et al., 2017) which is then protected by BRCA1 and BRCA2 (Kolinjivadi et al., 2017; Lemaçon et al., 2017; Mijic et al., 2017; Taglialatela et al., 2017). However, it is not well understood whether the two factors act together, their activity is redundant or different remodelers are needed for particular structures of replication intermediates. In addition to that, other DNA translocases/helicases, including RAD54 (Bugreev et al., 2011) and FANCM (Gari et al., 2008b) are known to promote fork regression *in vitro*.

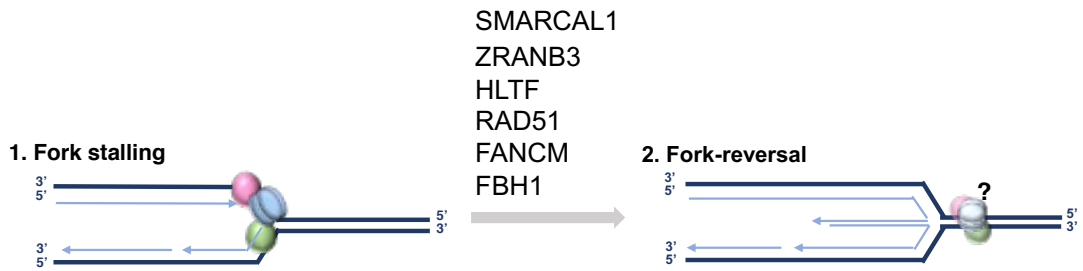


Figure 1.4. Reversed RF formation.

The blockage of RF can mediate fork reversal through the coordinated annealing of the two newly synthesized strands and the re-annealing of the parental strands, resulting in four-way junction. RF reversal by various fork remodelers can facilitate the restart of DNA synthesis or stabilize the blocked fork. Figure is adapted from Ait Saada et al., 2018. doi.org/10.1016/j.dnarep.2018.08.017 is used under a Creative Commons license https://creativecommons.org/licenses/by/4.0/legalcode.

Reversed forks can be restarted in a process mediated by helicases such as RECQ1 (Berti et al., 2013) or by Dna2 assisted by the WRN helicase (Thangavel et al., 2015; Berti and Vindigni, 2016).

However, it remains unclear whether the fork reversal is an obligatory intermediate for the RF stabilisation/restart and what changes occur in replisome composition and structure during the fork regression.

The Fork Protection Complex (Timeless and Tipin in metazoans, Swi1 and Swi3 in *S. pombe*, and Tof1 and Csm3 in *S. cerevisiae*) also plays an important role in preserving RF integrity.

Unlike replication stress-induced guardian mechanisms, the Fork Protection Complex appears to be a constitutive component of the RF and loss of Swi1 leads to the degradation of replicative DNA polymerases and helicases (Noguchi et al., 2004; Leman and Noguchi, 2012; Roseaulin et al., 2013). The Fork Protection Complex is vital during replication in vegetative cells, aids in replicating difficult-to-replicate parts of the genome and maintains the RF under conditions of replication stress (Leman and Noguchi, 2012). The Fork Protection Complex is crucial for activating the replication and DNA damage checkpoints and for the coupling of the replicative helicase with the DNA polymerases, to avoid ssDNA accumulation which can trigger deleterious rearrangements (Noguchi et al., 2003; Unsal-Kaçmaz et al., 2007).

1.5.4 The role of accessory DNA helicases

Proteins associated with the DNA (such as transcription machinery proteins) are a common problem for the progression of the RF. In addition to the main replicative helicase, the replisome comprises additional “accessory” helicases that can help in actively displacing proteins bound to DNA, which would otherwise impede the passage of the RF. These include bacterial Rep and UvrD, the budding yeast helicases Rrm3 and Pif1, fission yeast Pfh1 and human PIF1 (Ivessa et al., 2003; Guy et al., 2009; Gupta et al., 2013; Brüning et al., 2014; Byrd and Raney, 2017). It is not well understood whether these helicases are associated with the replisome during the whole process of replication or are only recruited when the fork is paused. Pif1 family helicases also facilitate replication across difficult-to-replicate sites including rDNA, tRNA genes, centromeres, telomeres, inactive replication origins, and transcriptional silencers (Geronimo and Zakian, 2016; Mendoza et al., 2016; Byrd and Raney, 2017; Sabouri, 2017). By reducing RF pausing at such sites, Pif1 family helicases help prevent RF collapse and the consequent recruitment of HR proteins. Pif1 in *S. cerevisiae* not only facilitates replication through hard-to-replicate sites but also plays a key role during BIR by promoting DNA Pol δ-mediated DNA synthesis and D-loop migration (Sabouri et al., 2012; Wilson et al., 2013; Vasianovich et al., 2014).

1.5.5 Models of DSB-initiated recombination-dependent replication

If a blocked fork is not successfully stabilised due to a failure to quickly activate the intra-S phase checkpoint (note that blockage at some RFBs does not result in rapid ssDNA production), and is not rescued by a converging fork, then it most likely collapses. In such cases the collapsed fork is restarted through DSB-dependent or -independent replication restart pathways (Hashimoto and Costanzo, 2011).

A DSB can be formed as a consequence of the RF encountering a nick during DNA synthesis or if the Mus81-Eme1 endonuclease cleaves the stalled or collapsed RF (Doe et al., 2002; Froget et al., 2008; Harper et al., 2010; Forment et al., 2011). Replication events that are induced by DSBs are referred to as BIR and have been predominantly studied in budding yeast using systems in which a non-replication associated DSB is repaired using a template DNA that shares homology with only one end of the break (Anand et al., 2013; Sakofsky and Malkova, 2017) (Fig. 1.5A, B).

As with most HR-mediated mechanisms, BIR starts with the generation of a 3' ssDNA overhang by the DNA end-resection machinery, onto which RPA, Rad52 and Rad51 are subsequently loaded with the help of other Rad51 mediators to form a Rad51 nucleofilament (Anand et al., 2013). A homology search then ensues leading to strand invasion and the formation of a D-loop from which DNA synthesis can be primed. BIR appears to depend on most of the key replisome components including the CMG helicase, PCNA and clamp loader (Lydeard et al., 2010).

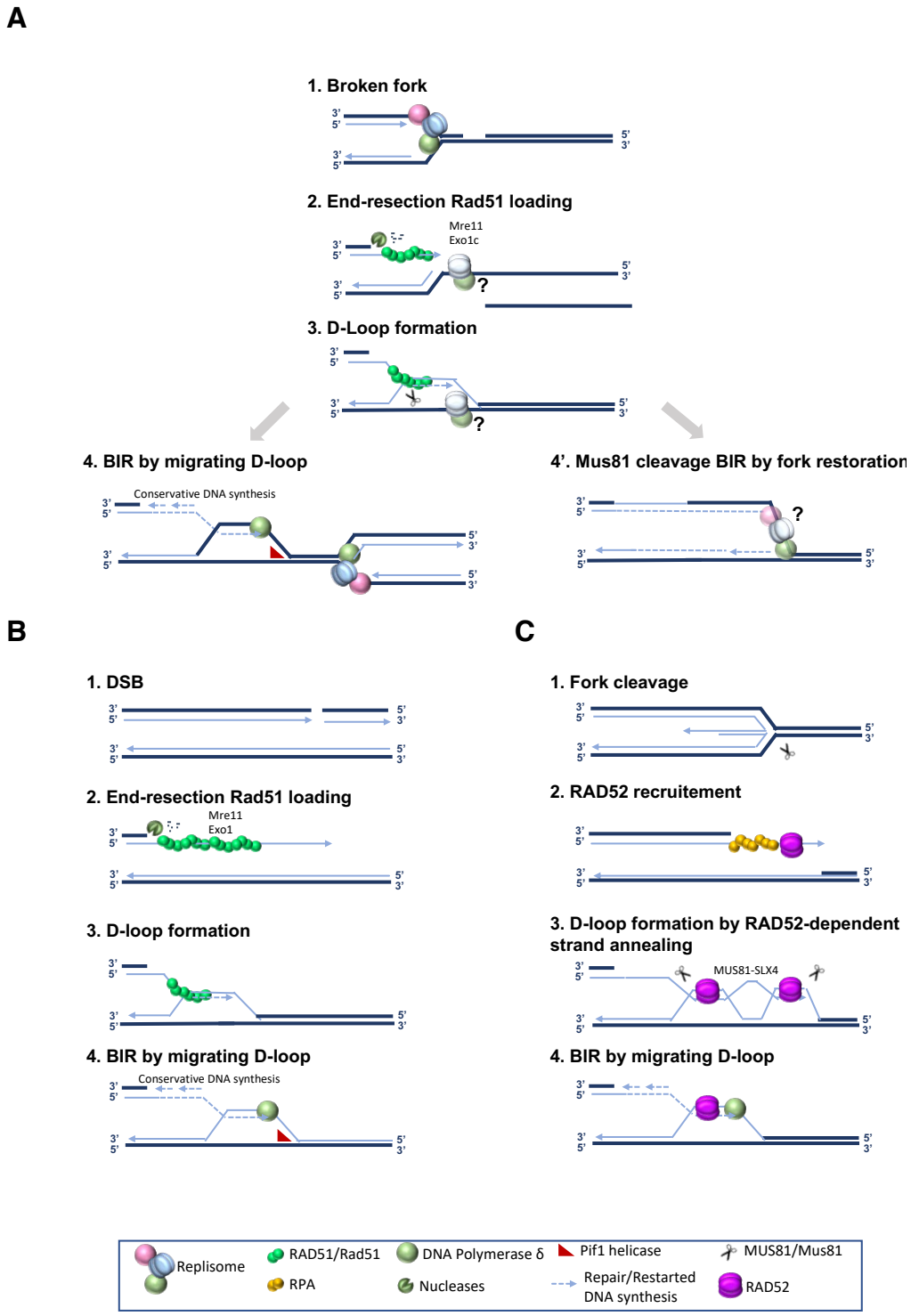


Figure 1.5. Models of DSB-initiated recombination-dependent replication.

(**A**) Fork repair by BIR in S phase. (**B**) DSB repair by BIR in G2 phase. (**C**) Fork repair by mitosis-specific DNA synthesis in G2/M. See text for details. Figure is taken from Ait Saada et al., 2018, colour code and order of mechanisms presentation is changed. doi.org/10.1016/j.dnarep.2018.08.017 is used under a Creative Commons license https://creativecommons.org/licenses/by/4.0/legalcode.

However, unlike canonical DNA replication, BIR is conservative, leading and lagging strand synthesis is not coupled, and it depends on Pif1 and the non-essential Pol32 subunit of DNA polymerase delta (Morrow et al., 1997; Donnianni and Symington, 2013; Saini et al., 2013; Wilson et al., 2013; Sakofsky and Malkova, 2017). Moreover, BIR is considerably less accurate than regular DNA replication being prone to template exchange events and increased rates of mutagenesis including an association with clustered mutations, which may result from damage of the extensive amount of ssDNA that is exposed due to uncoupled DNA synthesis (Smith et al., 2007, 2009; Deem et al., 2011; Saini et al., 2013; Elango et al., 2017). As BIR has mainly been studied outside of the context of S phase, it was unclear how closely this mechanism reflected what happens during the repair of a broken RF. However, using a system in budding yeast where RF breakage was induced by a site-specific single strand nick, Mayle and co-workers found that broken RFs are repaired by BIR (Mayle et al., 2015).

However, they did find some differences with “non-S phase” BIR including a much faster restart of replication, which occurred without the usual 2 hour delay seen in other BIR studies, and a role for Mus81 and fork convergence in limiting the region downstream of the broken fork that is susceptible to template switching (Deem et al., 2011; Mayle et al., 2015) (Fig. 1.5A).

In human cells, it is thought that BIR only operates during S phase to restart DNA replication at fragile sites or when crucial HR factors are impaired (Minocherhomji et al., 2015; Bhowmick et al., 2016; Lemaçon et al., 2017). Conservative, Rad51-independent but Rad52 dependent mitosis-specific DNA

synthesis has recently been discovered in human cells (Bergoglio et al., 2013; Minocherhomji et al., 2015; Bhowmick et al., 2016; Sotiriou et al., 2016) (Fig. 1.5C). Mitosis-specific DNA synthesis occurs at common fragile sites and at telomeres in cancer cells using alternative lengthening of telomeres (Dilley et al., 2016; Min et al., 2017). In mitosis-specific DNA synthesis, unresolved RFs appear to be cleaved in a MUS81 and SLX4-dependent manner in late G2 and mitosis leading to a restart process that depends on the strand annealing activity of RAD52 (Bhowmick et al., 2016; Duda et al., 2016).

1.5.6 Model of DSB-free recombination-dependent replication

Recombination-dependent replication (RDR) of a collapsed fork can occur without the RF being broken, however it remains unclear whether this RDR pathway is widely used in human cells (Fig. 1.6). The most extensively studied model of DSB-free RDR in eukaryotes is based on systems that use *RTS1* to induce site-specific RF collapse in fission yeast (Section 1.2.5) (Ahn et al., 2005; Lambert et al., 2005). At *RTS1*, forks collapse without breakage and the sister chromatids are physically attached during the restart event (Tsang et al., 2014; Saada et al., 2017; Teixeira-Silva et al., 2017). Rad51/Rad52-dependent recombination is induced by fork collapse at *RTS1*, which can lead to replication restart as well as various genomic rearrangements if ectopic DNA sequences are recombined (Ahn et al., 2005; Lambert et al., 2005, 2010; Mizuno et al., 2009).

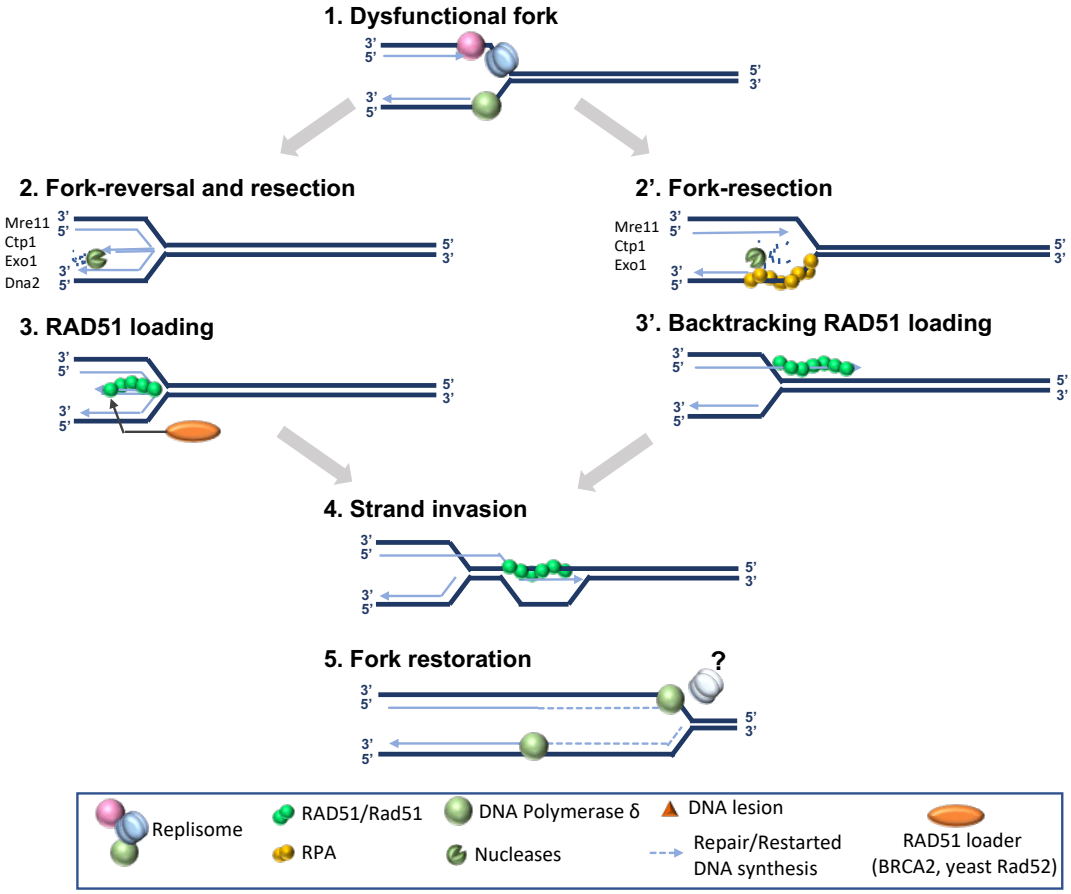


Figure 1.6. Model of DSB-free recombination-dependent replication.

Restart of RFs that have lost replication competence can happen without fork breakage. See text for details. Figure is taken from Ait Saada et al., 2018, colour code and order of mechanisms presentation is changed. doi.org/10.1016/j.dnarep.2018.08.017 is used under a Creative Commons license https://creativecommons.org/licenses/by/4.0/legalcode.

The recruitment of Rad52 and Rad51 to *RTS1* was determined by ChIP analysis (Lambert et al., 2005). Furthermore, single-cell resolution time-lapse microscopy revealed that Rad52 is recruited to *RTS1* in the majority of cells after 10-20 minutes of fork blockage (Nguyen et al., 2015). Similar to BIR, the restarted fork is mutagenic, prone to replication slippage at micro-homology and is associated with a high frequency of template switching (Iraqui et al., 2012; Mizuno et al., 2012; Nguyen et al., 2015).

However, unlike BIR, template switching is not constrained to a 10 kb region downstream of the barrier and the DNA synthesis is semi-conservative with the synthesis in both strands being catalysed by Pol δ (Miyabe et al., 2015; Nguyen et al., 2015).

RF reversal at *RTS1* appears to provide the necessary dsDNA end for the production of a 3' ssDNA tail by the MRN complex/Ctp1 and Exo1 with the Ku70-Ku80 limiting the initial resection step (Teixeira-Silva et al., 2017).

In fission yeast there are several DNA helicases/translocases, including Fml1, Rqh1, Fbh1 and Rad54, that have known or putative fork regression activity *in vitro*, which, in theory, could promote recombination at *RTS1* (Gari et al., 2008a; Sun et al., 2008; Whitby, 2010; Zheng et al., 2011; Fugger et al., 2015; Quinet et al., 2017). However, from this list only Fml1 and Rad54 seem to be needed to promote recombination at *RTS1*, whereas Rqh1 and Fbh1 appear to constrain it (Ahn et al., 2005; Sun et al., 2008; Lorenz et al., 2009).

1.6 Aims of study

The main aim of my project was to identify and characterize factors that are needed for successful RDR after restart of blocked replication forks at *RTS1*. I have addressed this aim using two different approaches.

In the first approach I attempted to develop a novel proteomic method, incorporating mass spectrometry and stable isotope labelling in cell culture (MS-SILAC), to define changes in replisome composition during replication fork collapse at *RTS1* (Chapter 3).

In my second approach, I focused on studying a putative partner protein of the Fml1 DNA helicase called Dbl2, which appears to be conserved from yeast to human. In Chapter 4, I characterise the mitotic phenotype of a *dbl2*Δ mutant and describe my attempts to identify a putative suppressor of its mutant phenotype. In Chapter 5, I present further characterisation of *dbl2* including epistasis analysis with key HR factors such as *rad51*, *rad52*, *fml1* and *fbh1*. In addition, I compared a *dbl2*Δ mutant to a *fbh1*Δ mutant in the context of their role in recombination induced by RFs blocked at the *RTS1* barrier and their genetic interactions with Rad51 mediator proteins.

In Chapter 6, I present bioinformatical, biochemical and structural experiments on full-length Dbl2 and truncation mutants of Dbl2, including analysis of its conserved DUF2439 domain, and the predicted structured regions in its middle segment and at its C-terminus. Lastly (Chapter 7), I present a structure-function analysis of Dbl2 using a series of truncation and internal deletion mutants of Dbl2, which were analysed using several genetic assays.

Fluorescence microscopy was also used to determine subcellular localization of full-length and mutant proteins, including their recruitment to the *RTS1* barrier.

Chapter 2

2 Materials and Methods

2.1 Media

2.1.1 *E. coli* media

All *E. coli* cultures were grown in Luria-Bertani broth (LB) (10 g/l Tryptone, 5 g/l yeast extract (YE), 5 g/l NaCl) or on LB-agar (15 g/l agar) at 37 °C, unless otherwise stated. Media were supplemented with antibiotics where appropriate, namely ampicillin (final concentration 50 µg/ml), carbenicillin (final concentration 50 µg/ml) and chloramphenicol (final concentration 34 µg/ml) (Sambrook, 2001). Antibiotics were filtered (0.2 µm Milipore syringe filters) and stored as 1000 X stocks at +4 and -20 °C (Sambrook, 2001). The *E.coli* strain expressing N-terminal Dbl2 domain was grown in M9 minimal media (12.8 g/l, $Na_2HPO_4 \bullet 7H_2O$, 3 g/l, KH_2PO_4, 0.5 g/l, NaCl, 1.0 g/l, NH_4Cl, 0.2 % (v/v) final volume glucose, 1mM $MgSO_4$, 100 µM $CaCl_2$) (Elbing and Brent, 2002).

2.1.2 *S. pombe* media

YE (30 g D-Glucose and 5 g Yeast Extract in 1 l water) and YE supplemented with 225 mg/l uracil, leucine, lysine, histidine and adenine each (referred as YES) were used as complete medium. Edinburgh Minimal Media with 3.7 mg/ml L-glutamic acid monosodium salt (EMMG) (3 g potassium hydrogen phthalate, 2.2 g anhydrous Na2HPO4, 3.7 g sodium glutamate, 30 g D-glucose, 20 ml 50 X salts, 1 ml 1,000 X vitamins, 0.1 ml 10,000 X minerals in 1 l water) was used as minimal media and supplemented with amino acids as appropriate (Sabatinos and Forsburg, 2010). When necessary, 18 g/l Difco

agar (FisherScientific) was added to the media. *S. pombe* were grown at 30 °C.

Strains that are auxotrophic for one or more of the following: adenine, arginine, histidine, leucine, and/or uracil, require the respective supplements at 225 mg/l for growth on minimal media. For selection of strains carrying antibiotic resistance, media were supplemented with geneticin (G418, final concentration 100 mg/l), nourseothricin (clonNat, final concentration 100 mg/l) or hygromycin B (final concentration 200 mg/l).

To repress expression from the *nmt* promoter, thiamine was added to a final concentration 4 µM to EMMG in genotoxin sensitivity assays, and to a final concentration 1 µM to grow *S. pombe* cultures for microscopy experiments

To differentiate between *ade*$^{+}$ and *ade*$^{-}$ colonies, cells were plated onto low adenine (LA) medium containing 10 mg/l adenine, which allows *ade*$^{+}$ colonies to appear white and *ade*$^{-}$ colonies red. In the recombination assays, *ade*$^{+}$ recombinants were selected for on YE media lacking adenine and supplemented with 200 mg/l guanine, dissolved in 1 M NaOH, to prevent uptake of residual adenine (Osman and Whitby, 2009).

2.1.3 *S. cerevisiae* media

All *S. cerevisiae* strains were grown in YEP broth with 2 % Raffinose (11 g/l yeast extract, 22 g/l peptone, 55 mg/l adenine), on YEP-agar (11 g/l agar) or –HIS agar (8 g/l yeast nitrogen base without amino acids, 55 mg/l tyrosine, 55 mg/l uracil, 55 mg/l adenine, 22 g/l agar, 20 mg/l arginine, 10 mg/l histidine, 60

mg/l isoleucine, 60 mg/l leucine, 40 mg/l lysine HCl, 10 mg/l methionine, 60 mg/l phenylalanine, 50 mg/l threonine, 40 mg/l tryptophan) (Louis, 2016).

2.2 Plasmid construction

All restriction enzymes used in this study were supplied by New England Biolabs. Oligonucleotides for colony polymerase chain reaction (PCR) amplification were custom made, supplied by Sigma-Genosys or Eurogentec, and are listed in Table 2.1. PCR reactions were performed using either a Hybaid (OmniGene) or Biometra thermocycler.

For plasmid construction, the appropriate DNA fragment was PCR- amplified with Q5 High-Fidelity DNA Polymerase (New England Biolabs) from the appropriate parental plasmid construct or *S. pombe* genomic DNA. DNA fragments were purified by 0.8-1.6 % agarose gel eletrophoresis, followed by extraction from the gel using a QIAquick Gel Extraction Kit (Qiagen)nor Monarch® DNA Gel Extraction Kit (New England Biolabs). Fragments were ligated with appropriately digested plasmid DNA using T4 DNA ligase (New England Biolabs), incubating at 16 °C overnight. Correctly constructed plasmids were verified by restriction digests and sequencing.

The plasmids used in this study and a brief description of their construction are presented in Table 2.2. All restriction digests, ligation, site-directed mutagenesis, PCR reactions, mini and midi-scale plasmid preps were performed according to the manufacturer's instructions.

2.2.1 Site-directed mutagenesis

Site-directed mutagenesis was performed using the the QuikChange® Site-Directed Mutagenesis Kit (Stratagene) and the Q5® Site-Directed Mutagenesis Kit (New England Biolabs) following the manufacturer's manual. PCR reactions were performed using a Biometra thermocycler.

2.2.2 *E. coli* transformation

Competent *E. coli* DH5α, Bl21(DE3), RIPL(DE3), Rosetta (DE3) cells were transformed with 10 to 200 ng plasmid DNA using the standard 42 °C heat shock bacterial transformation (Sambrook and Russell, 2001). Cells were plated on LB medium containing appropriate selective antibiotic(s) and grown at 37 °C overnight. For mini and midi-scale plasmid preps, the QIAScreen Miniprep protocol and QIAprep Spin Midiprep Kits (Qiagen) were used, respectively.

2.3 *S. pombe* strain construction

Molecular genetic techniques for *S. pombe* are based on established protocols (Sabatinos and Forsburg, 2010). The brief annotations of the *S. pombe* strains constructed and described in this study are presented in Table 2.3.

2.3.1 *S. pombe* transformation

To integrate linear DNA constructs or expression plasmids, *S. pombe* was transformed using the standard lithium acetate transformation protocol

(Okazaki et al., 1990). Cells were grown in 100 ml complete media in 500 ml glass flasks overnight. The cells were harvested by centrifugation, washed thoroughly with sterile Milli-Q water and resuspended in an equal volume of 0.1 mM lithium acetate (pH 7.5) in TE (10 mM Tris-HCl (pH 7.5), 1 mM EDTA (ethylenediaminetetraacetic acid)). At least 10 µg of linearized DNA fragment or 1 µg of plasmid DNA and 20 µg of carrier DNA (sonicated salmon sperm DNA) are added to 100 µl of cells suspension and incubated at room temperature (RT) for 10 minutes. 240 µl of 0.1 mM lithium acetate-TE and 40 % polyethylene glycol (PEG) were then added to the mixture, which was then incubated at 30 °C for 2 hours. 43 µl of dimethylsulfoxide (DMSO) was added before the cells were heat-shocked at 42 °C for 5 minutes. Finally, the transformed cells were washed thoroughly, resuspended in 200 µl sterile Milli-Q water and were plated in 1:1, 1:10 and 1:100 dilutions, either directly onto selective media (for auxotrophic markers) or plated onto complete media without antibiotics and incubated at 30 °C for 48 hours before replica plating the transformants onto selective media (for geneticin, hygromycin B and nourseothricin selection).

2.3.2 *S. pombe* colony PCR

S. pombe colony PCR was used to screen for the colonies with a correct integration of the DNA construct. To release chromosomal DNA from yeast cells a yeast colony was boiled at 100 °C for 5 minutes. Subsequent amplification of specific DNA fragments that would result from correct integration of the DNA construct was performed using *Taq* DNA polymerase

(New England BioLabs) and an Hybaid (OmniGene) thermocycler. PCR primers were designed such that at least one primer anneals to the parental chromosomal sequence that flanks the targeted site while the second primer anneals within the inserted DNA fragment. Where appropriate genomic DNA was extracted, and the fragment of interest was PCR-amplified by Q5 High-Fidelity DNA Polymerase (New England Biolabs) and sequenced to confirm the presence or absence of point mutations. At least 6 independent transformants were subsequently tested for growth and genotoxin sensitivity to determine the reproducibility of the phenotype.

2.3.3 *S. pombe* genomic DNA extraction

Small-scale preparations for PCR were made from 10 ml overnight cultures of *S. pombe*. Harvested cells were spheroplasted by incubating in 1 ml of Citrate Phosphate buffer (40 mM EDTA, 50 mM Na_2HPO_4, 55 mM citric acid and 1.2 M sorbitol) containing 2.5 mg of Zymolyase 20T (MP Biomedical) for 1 hour at 37 °C. The efficiency of spheroplasting was assessed by microscopic examination of cells mounted in 2 % sodium dodecyl sulphate (SDS). Spheroplasts were resuspended in 550 µl TE (10 mM Tris-HCl (pH 8.0, 1 mM EDTA) with 1 % SDS and incubated at 65 °C for 1 hour. 175 µl of 5 M potassium acetate was then added and the sample was centrifuged at 4 °C for 15 minutes at 16,000 g. The supernatant was retained, and an equal volume of isopropanol was added to precipitate the DNA. After pelleting the DNA by centrifugation, the DNA was washed in 70 % ice-cold ethanol, resuspended in

50 µl of TE containing 20 µg/ml RNaseA and incubated at 65 °C for 10 minutes. The DNA was stored at -20 °C.

2.3.4 *S. pombe* crosses

Cells with opposite mating types (h^+ and h^-) were mixed and grown on Malt Extract Agar (MEA) (30 g/l malt extract, 20 g/l agar (pH > 5.5)) at 25 °C for 2-5 days until ascus formation was observed. The spores were released by overnight Glusulase (PerkinElmer) digestion at 30 °C. Released spores were then washed with sterile Milli-Q water and plated either directly onto selective media (for auxotrophic markers) or plated onto complete media without antibiotics and incubated at 30 °C for 72 hours before replica plating the transformants onto selective media (for geneticin, hygromycin B and nourseothricin selection). Progeny were screened for appropriate genetic markers and genotoxin sensitivities.

2.4 *S. cerevisiae* transformation

S. cerevisiae were grown shaking in 100 ml of YEP medium at 30 ° C. At the mid-log phase, the cells were harvest by centrifugation, washed thoroughly with sterile water and with TE (10 mM Tris-HCl (pH 8.0) and 1.0 mM EDTA) and were suspended in equal volume of 0.2 mM lithium acetate-TE. After 1 h at 30 °C with shaking at 140 g, 100 µl of the cells were incubated statically with 15 μg of a linearized DNA fragment at 30 °C for 30 min. Equal volume of filter-sterilized 70 % PEG 4,000 was added and the suspension was mixed thoroughly on a vortex mixer. After 1 h incubation at 30 °C, cells were heat-

shocked at 42 °C for 5 min. Cells were cooled on ice, washed and then plated on selective solid medium (Ito et al., 1983; Kawai et al., 2010).

2.5 Genetic assays

2.5.1 Genotoxin sensitivity spot assay

The spot assays are used to reveal and show relative differences in survival and growth following a single exposure to UV or prolonged exposure to CPT, HU and MMS, which generate DNA lesions that can variously cause RF stalling, blockage and breakage. Exponentially growing cells from liquid cultures were harvested, washed, and diluted to 1 x 10^7 cells/ml. In each spot assay, the spot referred as 1 is undiluted and represents 1 x 10^7 cells, whereas 0.1, 0.01, and 0.001 spots represent subsequent 10-times dilutions down to 1 x 10^4 cells. Aliquots (10 µl) of the cell suspensions were spotted onto YES or EMMG plates containing various concentrations of chemical genotoxins (CPT, HU, MMS) or irradiated with various doses of UV light using a Stratalinker (Stratagene) as specified. Plates were incubated at 30 °C for up to 6 days. EMMG plates containing 4 µM thiamine were used to repress expression from *nmt* promoter.

2.5.2 Direct repeat recombination assays

Strains were initially grown on minimal media without histidine and containing only low levels of adenine (EMMG-his/LA) at 30 °C for 5 days. One colony with the intact (red colonies) ade6$^-$-duplication from each strain was then

resuspended in 1 ml sterile Milli-Q water and serially diluted in 10-fold steps. 100 µl of the 10^{-3} suspension was plated onto YELA plates and 100 µl of the neat suspension was plated on YE-ade+guanine plates to assess whether substrate was intact; 100 µl of the 10^{-3} suspension (10^{-2} suspension for the strains with poor viability) were plated onto YES-5S plates (YES with additional supplements added 225 mg/l uracil, leucine, lysine, histidine and adenine each) and incubated at 30 °C for 5 to 6 days.

Single colonies from each strain to be assayed were picked from YES+5S plates then resuspended in sterile Milli-Q water. 100 µl of the 10^{-3} suspension was plated onto YELA plates to assess cell viability. 100 µl of the neat or 10^{-1} cell suspension was plated onto YE-ade+guanine plates, to score for Ade^+ recombinants. The frequency of recombinants was calculated by counting the colonies on the plates typically after 5 to 6 days of incubation at 30 °C. Plates with Ade^+ recombinants were then replica-plated onto minimal media without adenine and histidine (EMMG-ade-his) to estimate the proportion of conversion-type recombinants (Ade^+His^+). After 2 days of incubation at 30 °C, the frequency of conversion-type recombinants was calculated by counting colonies. In strains with the direct-repeat reporter at Site II (12.4 kb away from the endogenous *ade6* locus), expression of adenine in recombinants with a gene deletion is poor, therefore YE plates lacking adenine were incubated for 8 to 10 days at 30 °C before *ade*$^+$ colonies are counted. Direct repeat recombination was assayed by measuring the frequency of Ade^+ recombinants as described (Osman and Whitby, 2009).

2.6 Biochemistry techniques

2.6.1 Protein expression and purification of His-tagged proteins from *E. coli*

A culture of *E.coli* BL21(DE3) or Rosetta(DE3) (Novagen) (volume varied in different experiments from 1 to 10 litres) was grown in LB containing 50 µg/mL ampicillin and 34 µg/ml chloramphenicol at 37 °C at 200 rpm to OD_{600} 0.5-0.6, and induced with 0.4 mM sopropyl-1-thio-D-galactopyranoside IPTG at 22 °C at 200 rpm overnight (for 4 hours at 30 °C for the expression of SpyCatcher and BirA-GST). The cells were then harvested by centrifugation, resuspended in the lysis buffer (50 mM HEPES pH 7.5, 300 mM NaCl, 5 % glycerol, 10 mM imidazole with addition of EDTA-free protease inhibitor cocktail tablets (Roche) and 1mM phenylmethylsulfonyl fluoride (PMSF)). The resuspended mixture was sonicated 4-times for 30 s, with a minimum of 1 min between each pulse placed in an ice-salt water bath. The lysates were spun and 400 µl per 1 l of initial culture of packed pre-equilibrated Ni-NTA agarose (Qiagen) was added to the pre-cleared lysate. The purification of His-tagged protein was further conducted according to the Ni-NTA agarose (Qiagen) manufacturer's instructions. The final elution fractions were cleared over a mini polyprep column (Bio-Rad) to remove any agarose resin. The flow-through in 1.5 mL centrifuge tubes was spun for 10 min at 4 °C at 16,000 g, pipetted into a 3 kDa MWCO cellulose ester dialysis tubing (SpectrumLabs) and dialyzed overnight at 4 °C against appropriate buffer.

2.6.2 Purification and concentration of the N-terminus of Dbl2

Protein expression and the efficiency of the first purification step were analysed by SDS-polyacrylamide gel electrophoresis (SDS-PAGE). The fractions containing the protein of interest were mixed and loaded on a cation exchanger HiTrap SP FF 1 ml using 50 ml superloop (GE Healthcare). Buffer IEC (50 mM HEPES, pH 8, 5 % glycerol) with NaCl concentration ranging from 0 to 1 mM was used to load and elute the sample from the column. The fractions of the peak containing N-terminal-Dbl2 as determined by SDS-polyacrylamide gel electrophoresis (SDS-PAGE) were then mixed and loaded onto HiLoad 16/60 Superdex 75 pg gel filtration column (GE Healthcare). The SEC buffer (25 mM Tris-HCl, pH 7.5, 0.1 mM EDTA, 2 mM dithiothreitol, 10 % glycerol, 0.1 mM PMSF) and 150 mM NaCl was used for the gel-filtration step. The fractions of the peak that were confirmed to contain N-terminal-Dbl2 by SDS-polyacrylamide gel electrophoresis (SDS-PAGE) were again loaded on HiTrap SP FF 1 ml. For the second attempt of crystallization trials 6His-tag was cleaved by thrombin for 2 h at 16 °C and overnight at 4 °C after the first Ni-NTA resin purification. The flow-through of the subsequent Ni-NTA resin purification was used for further purification according to the described protocol.

2.6.3 Protein expression and purification of MBP- and GST-tagged proteins from *E. coli*

The MBP- and GST-tagged proteins from *E. coli* were purified similar to the protocol described in 2.6.1 but using amylose resin (New England Biolabs) for MBP-tagged and Glutathione Sepharose 4B resin (GE Healthcare) for GST-tagged proteins following the manufacturer's instructions.

2.6.4 Protein expression and purification from *S. cerevisiae*

Four litres of a *S. cerevisiae* strain expressing *S. pombe* Dbl2 tagged with GST at its N-terminus were grown in YEP with 2 % raffinose to OD_{600} 1.8-2. Protein expression was induced by adding galactose (2 %) and incubating the cultures at 30 °C for 4 hours. The cells were harvested by centrifugation, washed with MQ water, and re-suspended in 1 ml/g of 1 X lysis buffer (50 mM Phosphate buffer (pH 8.0), 0.5 M NaCl, 1 mM EDTA, 10 % Glycerol, 10 mM dithiothreitol, 1 mM PMSF and 1 tablet of Roche PI cocktail per 25 ml of the buffer). The suspension was then pipetted into liquid nitrogen. Cells were grinded manually for 40 min, cell breakage was inspected visually under a microscope. Lysates were cleared by centrifugation at 4 °C for 19,000 g for 1 hour. Preequilibrated Glutathione Sepharose 4B resin (GE Healthcare) (100 µl of 50 % slurry per 1 ml of lysate) was added and purification was performed following the manufacturer's instructions. Protein expression was analysed by SDS-PAGE or western blot when needed.

2.6.5 SDS-polyacrylamide gel electrophoresis

Resolving gels containing 12 % (29:1) acrylamide (375 mM Tris-Cl (pH 8.8), 0.1 % w/v SDS) and stacking gels containing 5 % (29:1) acrylamide (125 mM Tris-Cl (pH 6.8), 0.1 % w/v SDS) were used for SDS-PAGE. Protein samples were mixed with 4 X Laemmli sample buffer (250 mM Tris-HCl (pH 6.8), 10 % v/v β-mercaptoethanol, 8 % SDS, 0.1 % Bromophenol Blue, and 40 % v/v glycerol) and boiled at 98 °C for 7 minutes prior to loading alongside a protein marker (either Prestained protein Marker, Broad Range, New England Biolabs; or Fermentas PageRuler Unstained protein ladder, Fermentas). Gels were run at 40 mA for approximately 2 h and subsequently either stained with InstantBlue (Expedeon) or processed for western blotting. Stained gels were imaged using a ChemiDoc XRS imager and ImageLab (version 6.0.0) software (Bio-Rad).

2.6.6 Western blotting

Protein gels were electroblotted onto Hybond enhanced chemiluminescence nitrocellulose membranes (GE Healthcare) using the Bio-Rad mini trans blot system with magnetic stirrer (Mini-PROTEAN 3 Cell) at 100 V for 2 hours in an ice bath. Blots were stained with Ponceau S (Sigma) to stain total protein, blocked at room temperature for 1 hour in TBST-blocking buffer (5 % milk powder, 2.5 % Bovine Serum Albumin, 1.8 % lysine in Tris-buffered saline with 1 % Tween 20 (TBST)) before incubating with the primary (anti-Halo, Promega G9211 (1:1,000); anti-c-myc (1:1,000), anti-HA (1:2,500), Abcam ab9132,

9110; anti-CFP, anti-YFP Clontech 632380 (1:1,000); antiGFP, Sigma G6539 (1:1,000); anti-CBP, Milipore 07482 (1:1,000); anti-pk, Serotec (1:1,000); anti-Mhf1,anti-Mhf2, Genscript custom made (1:1,000)) and secondary (anti-Mouse (1:10,000), anti-Rabbit (1:5,000), anti-Goat (1:5,000), Sigma A9044, A6154, F9887, respectively) antibodies. For the 3 times 15 minutes washing before and after incubation with secondary antibodies TBST buffer was used. Blots were visualized by enhanced chemiluminescence according to the manufacturer's instructions (enhanced chemiluminescence WBting Detection Reagents, GE Healthcare) and exposed to X-ray film (Sigma).

2.6.7 Preparation of *S. pombe* protein extracts

All procedures of the extract preparation described below use extracts that were prepared from yeast cells grown to late log phase (OD_{600} 1.8-2). Cell pellets were harvested by centrifugation, washed once with water, once with stop buffer (150 mM NaCl, 50 mM NaF, 10 mM EDTA, and 1 mM NaN_3) and pelleted again. The packed cell volume (PCV) was measured and the tube was frozen with liquid nitrogen. Before lysis the sample was rapidly thawed and kept at 4 °C. All subsequent steps were performed at 4 °C with precooled buffer and equipment. The yield of the lysis was estimated by microscopy.

2.6.7.1 Lysis by bead beating using a FastPrep machine

Extracts were prepared from 50 ml of yeast culture. 0.75 ml of nuclear isolation buffer (NIB) (50 mM MOPS (pH 7.2), 150 mM CH_3COOK, 2 mM $MgCl_2$, 0.5 mM Spermidine, 0.15 mM Spermine, 17 % glycerol) and 0.75 ml of acid washed beads were added to the processed earlier pellet from -80 °C. Cells

then were burst with the FastPrep-24 tissue and cell homogenizer (MPBiomedicals) trough 12 cycles of 20 sec run at the speed 5 m/sec with 2 min incubation on ice between runs. The extract containing cytoplasm fraction was carefully removed, beads were washed with 1 ml of NIB and 100 µl of RIPA buffer (10 mM KH_2PO_4, pH 7, 1 % Triton X-100, 0.1 % SDS, 2 mM EDTA, 150 mM NaC1, 50 mM NaF, 0.1 mM sodium vanadate, 4 µg/ml leupeptin, 1 mM PMSF) was added. The extract is carefully transferred from beads after centrifugation.

2.6.7.2 French press lysis

Extracts were prepared from 0.5 l of yeast cells. One PCV of Buffer HB (25 mM MOPS (pH 7.2) 60 mM p-glycerophosphate, 15 mM $MgCl_2$, 15 mM EGTA (ethylene glycol-bis(β-aminoethyl ether)-N,N,N',N'-tetraacetic acid), 1 mM dithiothreitol, 0.1 mM sodium vanadate, 1 % Triton X-100, 1 mM PMSF, 20 µg/ml leupeptin, 40 µg/ml aprotinin, 100 µM benzamidine, 10 µM bestatin, 5 µM pepstatin A, Benzonase Nuclease (Sigma) 400 U/ml) was added to the processed earlier pellet from -80 °C. Cells were broken by passing them three times through a French press (Sim-Aminco) at a pressure of 8.27 MPa (1,200 psi). The extract is carefully transferred from chromatin pellet after centrifugation at 100,000 g for 1h.

2.6.7.3 Cryo-grinding lysis

Extracts were prepared from 1 l of yeast cells. One PCV of Buffer HB (25 mM MOPS, pH 7.2, 60 mM p-glycerophosphate, 15 mM $MgCl_2$, 15 mM EGTA, 1 mM dithiothreitol, 0.1 mM sodium vanadate, 1 % Triton X-100, 1 mM PMSF, 20 µg/ml leupeptin, 40 µg/ml aprotinin, 100 µM benzamidine, 10 µM bestatin,

5 µM pepstatin A) was added to the processed earlier pellet from -80 °C. Cells again were frozen in liquid nitrogen and grinded for 40 minutes (continuously kept frozen). Cells were pelleted and resuspended in one PCV of HB buffer in glass tubes, equal amounts of acid washed beads were added. Cells were vortexed 5 times for 1 min with 2 min incubation on ice in between vortexing. The extract was transferred from beads after centrifugation.

2.6.7.4 Alkaline lysis

Extracts were prepared from 10 ml of yeast cells. Following centrifugation at 3,000 g for 3 minutes, the thawed cells were resuspended in 0.3 ml sterile water plus 0.3 ml 0.6 M NaOH and incubated at room temperature for 10 minutes (Matsuo et al., 2006). The cells were then pelleted and washed with sterile water. The cells were then resuspended in SDS-PAGE loading buffer (60 mM Tris-HCl (pH 6.8), 4 % β-Mercaptoethenol, 4 % Sodium Dodecyl Sulphate (SDS), 0.01 % Bromophenol Blue and 5 % Glycerol), lysed by boiling at 100 °C for 3 minutes and processed for loading onto a SDS-PAGE gel for further analysis as previously described.

2.6.8 Immunoprecipitation and co-immunoprecipitation of proteins from yeast cell extracts

Pull-down using TAP-tagged proteins is performed with IgG Sepharose 6 Fast Flow (GE Healthcare Life Sciences) according to the protocol (Puig et al., 2001) except the elution step is conducted following the manufacturer's protocol without TEV-protease cleavage.

Pull-down using Halo-tagged protein is performed with Halo-tag resin (Promega) according to the manufacturer's instructions.

Immunoprecipitation using Myc-tag was performed with Pierce Protein G Agarose covalently conjugated to the primary anti-c-myc antibodies (Abcam ab9132). The lysates were precleared by incubation with protein G at 4 °C with rotation. The antibodies were incubated with protein G for 2 hours at 4 °C, and then centrifuged to remove unbound antibodies. Beads were washed, re-suspended and incubated with end-over-end shaking at room temperature in 0.1 M sodium borate (pH 9, 1 ml of borate buffer per 0.1 ml beads). Beads were spun and resuspended in 1 ml fresh dimethyl pimelimidate/borate solution. The buffer was removed, and beads were washed two times with 1ml of 50 mM Glycine, pH 2.5 and several times in HB buffer. The precleared lysate was added and incubated at 4 °C overnight. Beads were then washed with PBS three times and re-suspended in 100 µl Soft elution Buffer (0.2 % (w/V) SDS, 0.1 % (V/V) Tween-20, 50 mM Tris-HCl (pH 8.0)). The elution step was repeated. All elution fractions were combined, acetone precipitated, resuspended in HB buffer and processed for loading onto a SDS-PAGE gel for further analysis as described in 2.6.5.

For affinity purification of SpyTagged protein using SpyCatcher-Biotin (Veggiani et al., 2016) 1 ml of the lysate was incubated with 100 µl of 8 µM SpyCatcher-Biotin for 5 hours at 4 °C with end-to-end rotation. 20 X excess of MPB-SpyTag was added to remove the non-bound SpyCatcher. The solution was incubated for 4 hours at 4 °C with end-to-end rotation. MBP-SpyTag and MBP-SpyTag – SpyCatcher-Biotin were removed using amylose resin (New

England Biolabs) column. The flow-through from the column was collected and Rtf1-SpyTag – SpyCatcher-Biotin was biotinylated using BirA as described in the section 2.6.9 (Fairhead and Howarth, 2015) and purified using monomeric Avidin Resin (Pierce) following the manufacturer's instructions. All elution fractions were combined, acetone precipitated, resuspended in HB buffer and processed for loading onto a SDS-PAGE gel for further analysis as described in 2.6.5.

For affinity purification of SpyTagged protein using SpyCatcher-Cysteine (Zakeri et al., 2012), firstly SpyCatcher-Cysteine was reduced by 250 mM tris(2-carboxyethyl) phosphine (TCEP) solution. SpyCatcher-Cysteine was coupled to SulfoLink™ Coupling Resin (ThermoFisher) following the manufacturer's instructions. *S. pombe* protein extracts were loaded onto the resin with SpyCatcher-Cysteine, washed by PBS and TEV cleavage buffer. Rtf1 was TEV cleaved using TEV protease (Sigma-Aldrich) according to the manufacturer's instructions. All elution fractions were combined, acetone precipitated, resuspended in HB buffer and processed for loading onto a SDS-PAGE gel for further analysis as described in 2.6.5.

2.6.9 Protein biotinylation

Site-specific biotinylation by BirA (Fairhead and Howarth, 2015) and subsequent surface immobilization of SpyCatcher for Rtf1-SpyTag pull-down was performed following a published protocol (O'Callaghan et al., 1999; Fairhead and Howarth, 2015). To 100 µM AviTag-fused protein in 952 µl of PBS, 5 µl 1 M magnesium chloride, 20 µl 100 mM ATP, 20 µl 50 µM GST-BirA

and 3 µl 50 mM D-Biotin were added. The samples were incubated for 1 hour at 30 °C with gentle mixing. The same amount of fresh biotin and GST-BirA were added and incubated for a further hour. GST-BirA was removed with Glutathione Sepharose 4B resin (GE Healthcare). Sample was dialyzed into suitable buffer, for storage and to remove the excess biotin.

2.7 Structure characterization

2.7.1 Nuclear magnetic resonance spectroscopy (NMR)

For NMR analysis protein samples were exchanged into phosphate buffer (pH 8.0), 100 mM NaCl. NMR experiments were carried out using spectrometers operating at ^{1}H frequency 500 MHz. NMR data were acquired using either GE/Omega software with in-house pulse sequences, or Topspin software and pulse sequences in the Topspin libraries from Bruker Biospin.

2.7.2 X-ray crystallography

N-terminus Dbl2 was concentrated to 18 mg/ml using protein concentrators (ThermoFisher) (5,000 Da molecular weight cutoff, 20 ml). Crystallisation trials were performed in 96-well 3-drop Swissci plates (Molecular Dimensions). In screens Morpheus, Midas, PACT and JCSG+ crystals appeared as triangles, squares or needles after few weeks incubation at 18 °C. Although the quality of these crystals did not allow data collection, they were used to generate seeds. A few crystals were crushed with micro-tools and sonicated for 1 min in an ultrasonic water bath. A crystal was formed in

0.2 M ammonium nitrate and 20 w/v polyethylene glycol 3,350 after 72 days at 18 °C (JCSG+, Molecular Dimensions). Crystals were cryoprotected by increasing the PEG 3350 concentration to 35 % (w/v) and data were collected at the Diamond Light Source beamline I03 (Harwell, United Kingdom) using a Pilatus 6 M detector (DECTRIS).

2.8 Cell biology technics

2.8.1 Flow-cytometry analysis

Cells were fixed with ice-cold 70 % ethanol, pelleted and then washed with 1 ml sterile Milli-Q water and once with sterilised 50 mM Na citrate buffer. The pellet was then resuspended in 0.5 ml of 50 mM Na citrate. 0.1 mg/ml RNaseA was added and cells were incubated at 37 °C for 2 hours. 0.5 ml 50 mM Na citrate containing 4 µg/ml propidium iodide (Sigma P4107) was then added to the samples. Samples were sonicated for 10 minutes using a Decon FS300b sonicator. Samples were analysed using a FACS Calibur and Cell Quest Pro software (BD Bioscience).

2.8.2 Microscopy

Cells from an exponentially growing culture in EMMG lacking leucine were harvested and fixed with 70 % ethanol for subsequent microscopy. The fixed cells were stained with 3 µM DAPI (4',6-diamidino-2-phenylindole).

Microscopic analysis with cells fixed in 70 % ethanol was done using a 100x/1.30 UPlanFl objective of an Olympus BX50 epifluorescence microscope

equipped with the appropriate filter sets to detect blue and yellow fluorescence (Chroma Technology Corp., Bellows Falls, VT). Black-and-white images were taken with a CoolSNAP HQ^2 CCD camera (Photometrics) controlled by MetaMorph v7.7.3.0 software (Molecular Devices Inc.). Single channel pictures were pseudo-coloured and overlaid using Fiji-ImageJ (Schindelin et al., 2012; Rueden et al., 2017)

For the live-cell snapshot imaging, the cells were grown at 30 °C in filter-sterilised EMMG lacking histidine with 1 µM thiamine for a minimum of 36 hours to ensure de-repression of the *nmt* promoter. Live cells were imaged on an inverted Olympus IX71 microscope controlled by a DV Elite Core using DeltaVision softWoRx 5.6.1 softwear (Applied Precision Inc.). Images were taken using either the CFP/YFP/mCherry or YFP/mCherry filters with an Evolve™ 512 EMCCD camera (Photometrics) using an oil-immersed Olympus 100X UPlanSApo objective with a NA of 1.40. A stack of 16 focal planes at a step-size of 0.3 µm was taken. Brightfield images of the cells and LacI-tdKatushka2 were imaged with a 100 ms exposure time and 10 % neutral density filter. Rad52-YFP and Dbl2-YFP were imaged with a 100 ms exposure time and 10 % neutral density filter. Rad51-CFP, 100 ms exposure time and 5 % neutral density filter.

2.9 Data analysis

2.9.1 Image processing and analysis

To quantify speckling of fluorescence levels in cells, a single in-focus plane was acquired. Using ImageJ (v1.48, NIH)(Rueden et al., 2017), an outline was drawn around each nucleus. Area and mean fluorescence were measured, along with several adjacent background readings. The total corrected nuclear fluorescence = integrated density – (area of selected nucleus × mean fluorescence of background readings), was calculated (McCloy et al., 2014).

Raw images collected on the DV Elite Core were subsequently denoised with Priism with the dimensionality set to “3D: xyz” for three iterations (Kervrann and Boulanger, 2006). Denoised images were then deconvolved with softWoRx 5.5.0 software with the “additive” method for 12 cycles (Applied Precision). Foci were scored manually and separately for each of the fluorescent channels. Foci were distinguished from background as being at least three to five times brighter in intensity and having a minimum volume of 2X2 pixels. Perfect co-localisation was manually assessed and scored as foci in separate channels overlapping in xyz by a minimum of 2 pixels.

2.10 Statistics

Data were tested for normal distribution by the Shapiro-Wilk normality test and official outliers were eliminated using the Thompson tau technique, both analyses were performed in Microsoft Office Excel compatible software for statistical analysis XLSTAT (ADDINSOFT). In accordance with the distribution

of data, means were compared by the appropriate independent-sample two-tailed T-test using Microsoft Office Excel 2016. *P* values below 0.05 were considered significant (5 % significance interval), and *P* values below 0.01 were considered highly significant (1 % significance interval).

Table 2.1. List of primers used in this study

Oligo name	Oligo sequence (5'→3')
oMW805	AAGGATCCATGGGTAAGGAAAAGACTC
oMW848	GGACGAGGCAAGCTAAAC
oMW1427	ATAGTCGACGAACGCTGATCCTGGATTTCC
oMW1428	ACTTAATTAATGTTGTACTGTTTTCTTTC
oMW1669	ATATTAATTAACCTCGAGCCAACCACTGAGG
oMW1670	TTAGGCGCGCCTTAACCGGAAATCTCCAGAG
oMW1671	ATAGTCGACCGGATACAGAGGACAATG
oMW1672	ATATTAATTAACGCATAAATCATCGGCGTTAGT
oMW1673	ATAGAATTCTACATGAACAAATTTATTTT
oMW1674	GGAGATATCCCTATTTTGAAAAGC
oMW1717	ATACAGCTGGCTCTCAAAAACCATCAC
oMW1718	TTAGTCGACCTAATCAGTATAGCAAGGGAC
oMW1719	ATAGTCGACCTCGAGCCAACCAC
oMW1720	ATATTAATTAACACCGGAAATCTCCAGAGTAG
oMW1722	TTAGGCGCGCCACTAGCATAAATCATC
oMW1732	ATATTAATTAACATGCAAGGAAAAAACAATTTA
oMW1733	ATACATATGATGCAAGGAAAAAACAATTTAAG
oMW1734	TTAGGATCCCTAGCATAAATCATCGGC
oMW1735	ATAGGATCCGCATAAATCATCGGCGTTAG
oMW1736	ATAGGATCCATGAAGCGACGATGGAAA
oMW1737	TTATACGTATTATTCTTTGTTGAATTTGTTATCCG
oMW1781	ATATTAATTAACATGGGTATTCCTAACCC
oMW1782	ATACTCGAGATCAAGACCAAGCAAAG
oMW1787	ATAGAAGTTGCCTGCGCTATTTGG
oMW1790	TTAATTAACATGGGTATTCCTAAC
oMW1791	GCATAAATCATCGGCGTTAG
oNI1	GGCGCGCCCTATTTAGTAGGTTTATAAGCATCAACCATAACAATATG AGCACCGGATCC
oNI2	GGATCCGGTGCTCATATTGTTATGGTTGATGCTTATAAACCTACTAAA TAGGGCGCGCC
oMW1831	AAATACATATGGATACAAGTTCCAATG
oMW1832	ATAGGATCCTCAAATAAAGTCACCATC
oMW1833	GTCAGAAGCTATGTCGTCTTC
oMW1834	AAAGCCTTTCAACCCGTGAAG
oMW1835	ATAGTCGACTGTAAACAAGTACCTCATATC
oMW1836	ATAGGATCCTTTAAAGCCTGTAAAGGCAG
oMW1837	ATAGAGCTCTTCGTACGTTGAAACTTC
oMW1838	ATAGAATTCAGACACTATTTAGTGCTG
oMW1839	ATAGTCGACATGGATACAAGTTCCAATG
oMW1840	ATAGGATCCCAATAAAGTCACCATCTTCG
oMW1841	CGCTCTAGCTTTTCCATCAGTCA
oMW1842	AGGCATTAGAAAATGGAAATGAAG
oMW1843	ATAGATATCAGACACTATTTAGTGCTG
oMW1844	ATAGCGGCCGCGCTCAAATAAAGTCAC

Oligo name	Oligo sequence (5'→3')
oMW805	AAGGATCCATGGGTAAGGAAAAGACTC
oMW848	GGACGAGGCAAGCTAAAC
oMW1845	ATACCCGGGAATGGATACAAGTTCCAATG
oMW1862	ATAGGATCCTCACCTCTTCCCTGTC
oMW1863	AAACATATGTCACCCAGCAAAAACCA
oMW1864	ATAGGATCCTCAACCAAACGAGGACGAA
oMW1865	AAACATATGCCTTCCAACAAAAACGATG
oMW1866	ATAGGATCCTCATAGCGAAGGAATGTG
oMW1867	ATAGGATCCCCTCTTCCCTGTCTCA
oMW1868	ATAGGATCCGGCGGCAGCGGCGGCGGCAGCGGCGGCTCACCCAG CAAAAACCAAAAG
oMW1869	ATAGCTGAGCTCAAATAAAGTCACCATCTTC
oMW1876	CAACAATATTAAGCTTTTCGTAAGC
oMW1877	TGAATTTATTCTACATTAAACCCTA
oMW1878	ATACCATGGGCAGCAGCCATCAT
oMW1879	ATACATATGACCACTACCAGACCCACCGCT
oMW1892	AGAAACGTTAGAGCTCAC
oMW1893	AATGGGACTGTGTAAGTG
oMW1894	TGGGCAAGATTTTGACTC
oMW1895	ATGGTATCTCGATCTGAG
oMW1896	AGCACTAAATAGTGTCTG
oMW1897	AGAACGAGATGCAAATGATATG
oMW1898	TTAATGGAAATGGCTCAAACTG
oMW1899	TCTCTTCATTCCATACATGGTC
oMW1900	TAAGGTGTCTGTCGAGAG
oMW1901	AAGTACATATTTTCGACG
oMW1902	ATCGACCAATTCAACGATGG
oMW1903	ATCATCTCTACAGAACTGTC

Table 2.2. List of plasmids used in this study

Name	Vector	*E. coli* marker	*S. pombe* marker	Description
pRA3	pFA6a	Amp	kanMX6	PCR amplified (oMW1673, oMW1674) from F0656 gDNA; cloned as EcoRI-EcoRV into pRA2, resulting in the plasmid to replace Rtf1 at its endogenous locus by Rtf1-Halo
pRA4	pREP41	Amp	LEU2	NdeI/BamHI Rtf1-Halo from pRA3 cloned into pREP41
pAG25	pFA6a	Amp	natMX4	General vector for deletions, cause resistance to CLONNAT (Nourseothricin).
pAG32	pFA6a	Amp	hphMX	General vector for deletions, cause resistance to Hygromycin B
pMW637	pREP41	Amp	LEU2	Genomic *fbh1* amplified with oMW645 + 646 from pMW627 using pfu.
pMW613	pREP41	Amp	LEU2	Vector for the overexpression of Rad52 from *nmt41* promoter
pIN42	pRS303	Amp	HIS3	3.3-kb GST-Rad54 SgrAI/NotI fragment from pIN41 to replace the cdt1 fragment inside the pJF2 to construct pRS303-Gal4-GST-Rad54. Budding yeast strain is MCW8108 (yJF1 MATa,(Frigola et al., 2013))
pGEX-GST-BirA	pGEX	Amp	NA	Vector for the bacterial expression of BirA-GST was kindly provided by Howarth's lab, University of Oxford (O'Callaghan et al., 1999).
pDEST14-Cys-SpyCatcher002	pDEST14 Gateway	Amp	NA	Vector for the bacterial expression of modified SpyCatcher allowing reaction with thiol coupling reagents was kindly provided by Howarth's lab, University of Oxford (Keeble et al., 2017).
AviTag-SpyCatcher	pDEST14 Gateway	Amp	NA	Vector for the bacterial expression of SpyCatcher with a peptide tag enabling site-specific biotinylation was kindly provided by Howarth's lab, University of Oxford (Veggiani et al., 2016).

Name	**Vector**	***E. coli* marker**	***S. pombe* marker**	**Description**
pMBP-SpyTag	pGEX	Amp	NA	Vector for the bacterial expression of MBP-SpyTag enabling binding to SpyCatcher was kindly provided by Howarth's lab, University of Oxford (Veggiani et al., 2016).
pKB235	pET-21b(+)	Amp	NA	Plasmid for the bacterial expression 6xHIS-THR-MBPx-TEV-Benzonase, which after TEV cleavage of the N-terminal part transforms into fully functional benzonase and used in cell lysis was kindly provided by Dr. K. Brune.
pNI1	pFA6a	Amp	kanMX6	PCR amplified (oMW1673, oMW1674) 3'UTR rtf1 from F0652 gDNA; cloned as EcoRI-EcoRV fragment into pFA6-kanMX66.
pNI2	pFA6a	Amp	kanMX6	PCR amplified (oMW1717, oMW1718) 5'UTR rtf1 from F0652 gDNA; cloned as PvuII-SalI fragment into pNI1.
pNI3	pFA6a	Amp	kanMX6	PCR amplified (oMW1719, oMW1720) Halo-tag from MCW1743 gDNA; cloned as SalI-PacI fragment into pNI2.
pNI4	pFA6a	Amp	kanMX6	PacI-PmeI fragment from pmw2674 into pmw 907.
pNI5	pFA6a	Amp	kanMX6	PCR amplified (oMW1732, oMW1722) rtf1 from F0652 gDNA; cloned as PacI-AscI fragment into pNI3.
pNI6	pREP41	Amp	LEU2	PCR amplified (oMW1733, oMW1734) rtf1 from F0652 gDNA; cloned as a NdeI-BamHI fragment into pREP41-NTAP.
pNI7	pREP41	Amp	LEU2	PCR amplified (oMW1736, oMW1737) CTAP-tag from pmw1853; cloned as a BamHI-SnaBI fragment into pNI8.
pNI8	pREP41	Amp	LEU2	PCR amplified (oMW1733, oMW1735) rtf1 from F0652 gDNA; cloned as a NdeI-BamHI fragment into pREP41-GFPC.
pNI9	pREP41	Amp	LEU2	PCR amplified (oMW1733, oMW1734) rtf1 from F0652 gDNA; cloned as a NdeI-BamHI fragment into pREP41-GFPN.

Name	**Vector**	***E. coli* marker**	***S. pombe* marker**	**Description**
pNI10	pREP41	Amp	LEU2	PCR amplified (oMW1733, oMW1734) rtf1 from F0652 gDNA; cloned as a NdeI-BamHI fragment into pREP42-3HAN.
pNI11	pREP41	Amp	LEU2	PCR amplified (oMW1733, oMW1735) rtf1 from F0652 gDNA; cloned as a NdeI-BamHI fragment into pREP41-pkC.
pNI12	pFA6a	Amp	kanMX6	PCR amplified (oMW1781, oMW1782) 3pk tag from pNI11; cloned as PacI/XhoI into MW2674 (resulting in Rtf1-3pk-Halo in pFa6a-KanMX). Then plasmid was mutated using primers oMW1790, oMW1791 and NEB Q5 Kit to delete extra-nucleotide (1671 C) that caused frame shift and introduced stop codon after Rtf1 before Halo-tag.
pNI13	pREP81	Amp	LEU2	1,2 kb BstAPI/FspI fragment from pNI12 subcloned into 10,3 kb BstAPI/SmaI fragment of MW747 resulting in pREP81 based Rtf1-3pk-Halo.
pNI14	pREP1	Amp	LEU2	3 kb NdeI/PmlI fragment from pNI13 subcloned in 8,5 kb bachbone of pREP1 resulting in pREP1 based Rtf1-3pk-Halo.
pNI15	pREP41	Amp	LEU2	3 kb NdeI/PmlI fragment from pNI13 subcloned in 8,5 kb bachbone of pREP41 resulting in pREP41 based Rtf1-3pk-Halo.
pNI16	pREP1	Amp	LEU2	PCR amplified Spy-tag with codons optimized for *S. pombe* as BamHI-Asc fragment subcloned in pNI14 resulting in pREP1 expressed Rtf1-3pk-Spy.
pNI17	pREP81	Amp	LEU2	PCR amplified Spy-tag with codons optimized for *S. pombe* as BamHI-Asc fragment subcloned in pNI13 resulting in pREP81 expressed Rtf1-3pk-Spy.

Name	**Vector**	***E. coli* marker**	***S. pombe* marker**	**Description**
pNI18	pFA6a	Amp	kanMX6	PCR amplified 5'UTR Dbl2 (OMW1835, OMW1836) (382 bp) as SalI/BamHI fragment subcloned in pFA6a-kanMX66.
pNI19	pET14b	Amp	NA	PCR amplified Dbl2 (OMW1831, OMW1832) (2157 bp) as NdeI/BamHI fragment subcloned in pET-14b.
pNI20	pFA6a	Amp	kanMX6	PCR amplified Dbl2 (OMW1839, OMW1840) (2157 bp) as SalI/BamHI fragment subcloned in pFA6a-13Myc-kanMX66.
pNI21	pFA6a	Amp	kanMX6	PCR amplified Dbl2 (OMW1839, OMW1840) (2157 bp) as SalI/BamHI fragment subcloned in pFA6a-3HA-kanMX66.
pNI21	pFA6a	Amp	kanMX6	PCR amplified Dbl2 (OMW1839, OMW1840) (2157 bp) as SalI/BamHI fragment subcloned in pFA6a-GFP-kanMX66.
pNI23	pFA6a	Amp	kanMX6	PCR amplified Dbl2 (OMW1839, OMW1840) (2157 bp) as SalI/BamHI fragment subcloned in pFA6a-GST-kanMX66.
pNI24	pFA6a	Amp	kanMX6	PCR amplified 3'UTR Dbl2 (OMW1837, OMW1838) (475 bp) as SacI/EcoRI fragment subcloned in pNI18 resulting in construct for making ΔDbl2 strain.
pNI25	pFA6a	Amp	kanMX6	PCR amplified 3'UTR Dbl2 (OMW1837, OMW1843) (475 bp) as SacI/EcoRV fragment subcloned in pNI20 resulting in construct for making Dbl2-13Myc strain.
pNI26	pFA6a	Amp	kanMX66	PCR amplified 3'UTR Dbl2 (OMW1837, OMW1843) (475 bp) as SacI/EcoRV fragment subcloned in pNI21 resulting in construct for making Dbl2-3HA strain.

Name	**Vector**	***E. coli* marker**	***S. pombe* marker**	**Description**
pNI27	pFA6a	Amp	kanMX6	PCR amplified 3'UTR Dbl2 (OMW1837, OMW1843) (475 bp) as SacI/EcoRV fragment subcloned in pNI22 resulting in construct for making Dbl2-GFP strain.
pNI28	pFA6a	Amp	kanMX6	PCR amplified 3'UTR Dbl2 (oMW1837, oMW1843) (475 bp) as SacI/EcoRV fragment subcloned in pNI23 resulting in construct for making Dbl2-GST strain.
pNI29	pJF2	Amp	*S. cerevisiae* HIS	PCR amplified Dbl2 (oMW1844, oMW1845) (2,1 kb) as XmaI/NotI fragment subcloned in pIN42 resulting in construct for making budding yeast strain expressing GST-Dbl2 under the GAL4-promoter.
pNI30	pREP41	Amp	LEU2	2.1 kb NdeI/BamHI fragment from pNI1 subcloned in 8,5 kb bachbone of pREP41 resulting in the plasmid for overexpression of Dbl2 under nmt41 promoter.
pNI31	pET14b	Amp	NA	PCR amplified N-terminus of Dbl2 (0.3 kb) (oMW1831, oMW1862) subcloned as NdeI/BamHI in pET14b resulting in the plasmid to express N-terminally 6-His-THR tagged 1-100 aa fragment of Dbl2.
pNI32	pET14b	Amp	NA	PCR amplified C-terminus of Dbl2 (0.3 kb) (oMW1832, oMW1863) subcloned as NdeI/BamHI in pET14b resulting in the plasmid to express N-terminally 6-His-THR tagged 621-715 aa fragment of Dbl2.

Name	**Vector**	***E. coli* marker**	***S. pombe* marker**	**Description**
pNI33	pET14b	Amp	NA	PCR amplified N-terminus of Dbl2 (1.4 kb) (oMW1831, oMW1864) subcloned as NdeI/BamHI in pET14b resulting in the plasmid to express N-terminally 6-His-THR tagged 1-467 aa fragment of Dbl2.
pNI34	pET14b	Amp	NA	PCR amplified middle region of Dbl2 (0.3 kb) (oMW1865, oMW1866) subcloned as NdeI/BamHI in pET14b resulting in the plasmid to express N-terminally 6-His-THR tagged 1321-426 aa fragment of Dbl2.
pNI35	pET14b	Amp	NA	PCR amplified 6-His-Avi-GSGGSGSG (oMW1878, oMW1879) subcloned as NdeI/NcoI in pNI31 resulting in the plasmid to express N-terminally 6-Hi-Avi-THR tagged 1-100 aa fragment of Dbl2.
pNI36	pREP41	Amp	LEU2	PCR amplified N-terminus of Dbl2 (0.3 kb) (oMW1831, oMW1862) subcloned as NdeI/BamHI in 8,5 kb bachbone of pREP41 resulting in the plasmid for overexpression of Dbl2 under nmt41 promoter.

Table 2.3. List of *S. pombe* strains used in this study

Name	Description	Method of construction
FO652	*ura4-D18 leu1-32 his3-D1 arg3-D4*	Lab strain
FO656	*ura4-D18 leu1-32 his3-D1 arg3-D4*	Lab strain
FO1814	*fbh1Δ::KanMX6 ura4-D18 leu1-32 his3-D1 arg3-D4 ade6-M375 int::pUC8/his3+/RTS1 IO/ade6-L469*	Lab strain
FO1816	*fbh1Δ::KanMX6 ura4-D18 leu1-32 his3-D1 arg3-D4 ade6-M375 int::pUC8/his3+/RTS1 AO/ade6-L469*	Lab strain
FO1831	*fbh1 D::arg3+ rad52 D::ura4+ ura4-D18 leu1-32 his3-D1 arg3-D4 ade6-M375 int::pUC8/his3+/RTS1 IO /ade6-L469*	Lab strain
FO1833	*fbh1 D::arg3+ r ad22 D::ura4+ ura4-D18 leu1-32 his3-D1 arg3-D4 ade6-M375 int::pUC8/his3+/RTS1 AO/ade6-L469*	Lab strain
MCW1088	*rad51Δ::arg3+ ura4-D18 leu1-32 his3-D1 arg3- D4*	Lab strain
MCW1231	*rad55Δ::arg3+ ura4-D18 leu1-32 his3-D1 arg3-D4*	Lab strain
MCW1242	*rhp57Δ::LEU2+ ura4-D18 leu1-32 his3-D1*	Lab strain
MCW1285	*rad52Δ::ura4+ ura4D-18 leu1-32 his3-D1 arg3-D4*	Lab strain
MCW1481	*swi5Δ::ura4+ ura4-D18 leu1-32 his3-D1 arg3-D4*	Lab strain
MCW1566	*rad55Δ::arg3+ fbh1Δ: kanMX6 ura4-D18 leu1-32 his3-D1 arg3-D4*	Lab strain
MCW1687	*rad52Δ::ura4+ ura4-D18 leu1-32 his3-D1 arg3-D4 - ade6 - L469/pUC8/RTS1-IO/ade6-M375)*	Lab strain
MCW1688	*rad52Δ::ura4+ ura4-D18 leu1-32 his3-D1 arg3-D4 - ade6 L469/pUC8/RTS1-AO/ade6-M375)*	Lab strain
MCW1691	*rad51Δ::arg3+ ura4-D18 leu1-32 his3-D1 arg3-D4 - ade6 -L469/pUC8/his3+/RTS1-IO ade6-M375*	Lab strain
MCW1692	*rad51Δ::arg3+ ura4-D18 leu1-32 his3-D1 arg3-D4 - ade6 -L469/pUC8/his3+/RTS1-AO ade6-M375*	Lab strain
MCW1773	*fbh1Δ::arg3+ ura4-D18 leu1-32 his3-D1 arg3-D4*	Lab strain
MCW1884	*fbh1Δ::arg3+ ura4-D18 leu1-32 his3-D1 arg3-D4*	Lab strain
MCW2080	*fml1Δ::natMX4 his3-D1 ura4-D18 leu1-32 arg3-D4*	Lab strain
MCW2544	*fbh1Δ::kanMX6 fml1Δ::natMX4 ura4-D18 his3-D1 leu1-32 arg3-D4*	Lab strain
MCW3058	*fml1Δ::natMX4 ura4-D18 leu1-32 his3-D1 arg3-D4 ade6-L469/pUC/his3+/RTS1-IO/ade6-M375*	Lab strain
MCW3060	*fml1Δ::natMX4 ura4-D18 leu1-32 his3-D1 arg3-D4 ade6-L469/pUC/his3+/RTS1-AO/ade6-M375*	Lab strain
MCW3263	*sfr1Δ::natMX4 ura4-D18 leu1-32 his3-D1 arg3-D4*	Lab strain
MCW4712	*ura4-D8 leu1-32 his3-D1 arg3-D4 ade6-L469/pUC/his3+/RTS1-IO/ade6-M375*	Lab strain
MCW4713	*ura4-D8 leu1-32 his3-D1 arg3-D4 ade6-L469/pUC/his3+/RTS1-AO/ade6-M375*	Lab strain
MCW4971	*fbh1Δ::arg3+ rdl1Δ::kanMX6 ura4-D18 leu1-32 his3-D1 arg3-D4*	Lab strain
MCW4979	*fbh1Δ::arg3+ sws1Δ::kanMX6 ura4-D18 leu1-32 arg3-D4*	Lab strain
MCW4982	*fbh1Δ::arg3+ rlp1Δ::kanMX6 ura4-D18 leu1-32 his3-D1 arg3-D4*	Lab strain
MCW4985	*fbh1Δ::arg3+ swi5Δ::his3+ ura4-D18 leu1-32 his3-D1 arg3-D4*	Lab strain
MCW5864	*fbh1Δ::kanMX6 sfr1Δ::natMX4 his3+-aim ade6-469 ura4-D18 his3-D1 arg3-D4*	Lab strain

Name	Description	Method of construction
MCW6119	*rdl1Δ::natMX4 ura4-D18 leu1-32 his3-D1 arg3-D4*	Lab strain
MCW6120	*rlp1Δ::natMX4 ura4-D18 leu1-32 his3-D1 arg3-D4*	Lab strain
MCW6342	*sws1Δ::kanMX6 ura4-D18 leu1-32 his3-D1 arg3-D4*	Lab strain
MCW7258	*ade6::RTS1-IO-hphMX4 ade6-L469/pUC8/his3+/ade6-M375-KanMX-aim1 ura4-D18 leu1-32 his3-D1 arg3-D4 ade6-D1*	Lab strain
MCW7260	*ade6::RTS1-AO-hphMX4 ade6-L469/pUC8/his3+/ade6-M375-KanMX-aim1 ura4-D18 leu1-32 his3-D1 arg3-D4 ade6-D*	Lab strain
MCW7812	*rad51Δ::arg3+ ade6::RTS1-IO-hphMX4 ade6-L469/pUC8/his3+/ade6-M375-KanMX-aim1 ura4-D18 leu1-32 his3-D1 arg3-D4*	Lab strain
MCW7814	*rad51Δ::arg3+ ade6::RTS1-AO-hphMX4 ade6-L469/pUC8/his3+/ade6-M375-KanMX-aim1 ura4-D18 leu1-32 his3-D1 arg3-D4*	Lab strain
MCW7852	FO652 + pREP41-*rtf1-Halo* pRA4	Transformation of the plasmid
MCW7853	FO652 + pREP41-*CFP-rtf1* pmw746	Transformation of the plasmid
MCW7936	*mhf1Δ::mhf1-HaloTag-kanMX6 ura4-D18 leu1-32 his3-D1 arg3-D4*	Integration into the genome
MCW7937	*mhf1Δ::mhf1-HaloTag-kanMX6 ura4-D18 leu1-32 his3-D1 arg3-4*	Integration into the genome
MCW7938	*rtf1Δ::HaloTag-rtf1-kanMX6 ura4-D18 leu1-32 his3-D1 arg3-D4*	Integration into the genome
MCW7939	FO652 + pREP41-*TAP-rtf1* pNI6	Transformation of the plasmid
MCW7940	FO652 + pREP41-*rtf1-TAP* pNI7	Transformation of the plasmid
MCW7941	FO652 + pREP41-*GFP-rtf1* pNI9	Transformation of the plasmid
MCW7942	FO652 + pREP41-*rtf1-GFP* pNI8	Transformation of the plasmid
MCW7943	FO652 + pREP41-*3HA-rtf1* pNI10	Transformation of the plasmid
MCW7944	FO652 + pREP41-*rtf1-3PkC* pNI11	Transformation of the plasmid
MCW7945	FO652 + pREP41-*NTAP*	Transformation of the plasmid
MCW7946	FO652 + pREP41-*CFPN*	Transformation of the plasmid
MCW7947	FO652 + pREP41-*GFPC*	Transformation of the plasmid
MCW7948	FO652 + pREP41-3*HAN*	Transformation of the plasmid
MCW7949	FO652 + pREP41-*MHN*	Transformation of the plasmid
MCW7950	FO652 + pREP41-*3PkC*	Transformation of the plasmid
MCW7951	FO652 + pREP41-*3PkN*	Transformation of the plasmid
MCW7952	*sms6Δ::smc6-13myc-arg+ ura4-D18 leu1-32 arg3-D4 his3-D1* (MCW1705 + pCB37)	Integration into the genome

Name	Description	Method of construction
MCW7953	*sms6Δ::smc6x-13myc-arg+ ura4-D18 leu1-32 arg3-D4 his3-D1* (MCW1712 + pCB37)	Integration into the genome
MCW7991	*elg1-TAP-natMX6 ura4-D18 leu1-32 his3-D1 arg3-D4*	Lab strain
MCW7993	*elg1-TAP-natMX6 mhf1Δ:: mhf1-HaloTag-kanMX ura4-D18 leu1-32 his3-D1 arg3-D4*	Lab strain
MCW8023	*ura4-D18 leu1-32 his3-D1 arg3-D4 ade6-L469/pUC/5kb spacer/his3+/RTS1-AO/ade6-M375*	Lab strain
MCW8059	*mhf1Δ::mhf1-HaloTag-kanMX6 ura4-D18 leu1-32 his3-D1arg3-D4 fml1+::13myc-hphMX4 ade6-M210*	Cross MCW7936 and MCW4406
MCW8060	*mhf1Δ::mhf1-HaloTag-kanMX6 smc6Δ::smc6-13myc-arg+ ura4-D18 leu1-32 his3-D1arg3-D4*	Cross MCW7936 and MCW1705
MCW8063	*mhf1Δ::mhf1-HaloTag-kanMX6 fml1Δ::fml1-4XTAP-natMX4 ura4-D18 leu1-32 his3-D1 arg3-D4*	Cross MCW7936 and MCW4629
MCW8064	*mhf1Δ::mhf1-HaloTag-kanMX6 fml1Δ::fml1-3HA-natMX4 ura4-D18 leu1-32 his3-D1 arg3-D4*	Cross MCW7936 and MCW4650
MCW8077	*fml1Δ::fml1-13myc-hphMX4 sms6Δ::smc6-13myc-arg+ ura4-D18 leu1-32 arg3-D4 his3-D1ade6-M210*	Cross MCW5423 and MCW8066
MCW8078	*fml1Δ::fml1-4Xtap-natMX4 sms6Δ::smc6-13myc-arg+ ura4-D18 leu1-32 arg3-D4 his3-D1*	Cross MCW8070 and MCW7952
MCW8079	*fml1Δ::fml1-4Xtap-natMX4 sms6Δ::smc6X-13myc-arg+ ura4-D18 leu1-32 arg3-D4 his3-D1*	Cross MCW8070 and MCW7953
MCW8080	*mhf1Δ::mhf1-HaloTag-kanMX6 sms5Δ::smc5-3HA-ura+ ura4-D18 his3-D1 leu1-32 arg3-D4*	Cross MCW7936 and MCW8069
MCW8081	*fml1Δ::fml1-13myc-natMX4 sms5Δ::smc5-HA-ura+ ura4-D18 his3-D1 leu1-32 arg3-D4 ade6-M216*	Cross MCW4608 and MCW8069
MCW8082	*fml1Δ::fml1-4Xtap-natMX4 sms5Δ::smc5-3HA-ura+ ura4-D18 leu1-32 his3-D1 arg3-D4*	Cross MCW8070 and MCW8069
MCW8083	*elg1Δ::elg1-TAP-natMX4 fml1Δ::fml1-13myc-hphMX4 ura4-D18 leu1-32 his3-D1 arg3-D4 ade6-M210*	Cross MCW7991 and MCW5423
MCW8087	*elg1D::elg1-TAP-natMX4 mhf1Δ::mhf1-HaloTag-kanMX6 fml1Δ::fml1-13myc-hphMX4 ura4-D18 leu1-32 his3-D1 arg3-D4*	Cross MCW7993 and MCW5423
MCW8136	*rad51Δ::arg3+ ade6-L469/pUC8/5kb λ spacer/his3+/RTS1-AO/Ade6-M375 ura4-D18 leu1-32 his3-D1 arg3-D4*	Lab strain
MCW8265	*rtf1Δ:: rtf1-3xPk-HaloTag-kanMX ura4-D18 leu1-32 his3-D1 ade6-D1 arg3-D4*	Integration into the genome
MCW8266	*rtf1Δ:: rtf1-3xPk-HaloTag-kanMX ura4-D8 leu1-32 his3-D1 arg3-D4 ade6-L469/pUC/his3+/RTS1-IO/ade6-M375 (MCW8265 X MCW 4712)*	Cross MCW4712 and MCW8265
MCW8267	*rtf1Δ:: rtf1-3xPk-HaloTag-kanMX ura4-D8 leu1-32 his3-D1 arg3-D4 ade6-L469/pUC/his3+/RTS1-AO/ade6-M375 (MCW8265 X MCW 4713)*	Cross MCW4713 and MCW8265
MCW8268	FO652 + pREP41-*rtf1-3Pk-Halo* pNI15	Transformation of the plasmid
MCW8269	FO652 + pREP81-*rtf1-3Pk-Halo* pNI13	Transformation of the plasmid
MCW8270	FO652 + pREP1-*rtf1-3Pk-Halo* pNI14	Transformation of the plasmid
MCW8271	MCW8265 + pREP1-*RTS1* pBZ142	Transformation of the plasmid
MCW8561	FO656 x pNI17 Rtf1-3Pk-SpyTag under *nmt81* promoter	Transformation of the plasmid

Name	Description	Method of construction
MCW8562	FO656 x pNI16 Rtf1-3Pk-SpyTag under *nmt1* promoter	Transformation of the plasmid
MCW8563	*dbl2Δ::kanMX6 ura4-D18 leu1-32 his3-D1 ade6-D1 arg3-D4 (FO656+pNI24)*	Integration into the genome
MCW8564	*dbl2Δ::kanMX6 ura4-D18 leu1-32 his3-D1 ade6-D1 arg3-D4 (FO656+pNI24)*	Integration into the genome
MCW8565	*dbl2Δ::dbl2-13myc-kanMX6 ura4-D18 leu1-32 his3-D1 ade6-D1 arg3-D4 (FO656+pNI25)*	Integration into the genome
MCW8566	*dbl2Δ::dbl2-3HA-kanMX6 ura4-D18 leu1-32 his3-D1 ade6-D1 arg3-D4 (FO656+pNI26)*	Integration into the genome
MCW8567	*dbl2Δ::dbl2-GFP-kanMX6 ura4-D18 leu1-32 his3-D1 ade6-D1 arg3-D4 (FO656+pNI27)*	Integration into the genome
MCW8568	*dbl2Δ::dbl2-GST-kanMX6 ura4-D18 leu1-32 his3-D1 ade6-D1 arg3-D4 (FO656+pNI28)*	Integration into the genome
MCW8607	*dbl2Δ::kanMX6 ura4-D18 leu1-32 his3-D1 ade6-D1 arg3-D4*	Cross FO656 and MCW8564
MCW8608	*dbl2Δ::natMX4 ura4-D18 leu1-32 his3-D1 ade6-D1 arg3-D4 (MCW8564+pAG25)*	Integration into the genome
MCW8609	*dbl2Δ::hphMX4 ura4-D18 leu1-32 his3-D1 ade6-D1 arg3-D4 (MCW8564+pAG32)*	Integration into the genome
MCW8610	*dbl2Δ::natMX4 ura4-D18 leu1-32 his3-D1 ade6-D1 arg3-D4*	Cross FO656 and MCW8608
MCW8611	*dbl2Δ::hphMX4ura4-D18 leu1-32 his3-D1 ade6-D1 arg3-D4*	Cross FO656 and MCW8609
MCW8622	*dbl2Δ::KanMX6 fml1Δ::natMX4 ura4-D18 leu1-32 his3-D1 arg3-D4 ade6-L469/pUC/his3⁺/RTS1-IO/ade6-M375*	Cross MCW8564 and MCW3058
MCW8623	*dbl2Δ::KanMX6 fml1Δ::natMX4 ura4-D18 leu1-32 his3-D1 arg3-D4 ade6-L469/pUC/his3⁺/RTS1-AO/ade6-M375*	Cross MCW8564 and MCW3060
MCW8627	*dbl2Δ::KanMX6 ura4-D8 leu1-32 his3-D1 arg3-D4 ade6-L469/pUC/his3⁺/RTS1-IO/ade6-M375*	Cross MCW8607 and MCW4712
MCW8628	*dbl2Δ::KanMX6 ura4-D8 leu1-32 his3-D1 arg3-D4 ade6-L469/pUC/his3⁺/RTS1-AO/ade6-M375*	Cross MCW8607 and MCW4713
MCW8645	*dbl2Δ::kanMX6 rad55Δ::arg3⁺ ura4-D18 leu1-32 his3-D1 arg3-D4 ade6-L469/pUC/his3⁺/RTS1-IO/ade6-M375*	Cross MCW2649 and MCW8564
MCW8646	*dbl2Δ::kanMX6 rad55Δ::arg3⁺ ura4-D18 leu1-32 his3-D1 arg3-D4 ade6-L469/pUC/his3⁺/RTS1-AO/ade6-M375*	Cross MCW2654 and MCW8564
MCW8647	*rad52Δura4⁺ dbl2Δ::kanMX6 ura4-D18 leu1-32 his3-D1 arg3-D4 - ade6 -L469/pUC8/his3⁺/RTS1IO ade6-M375*	Cross MCW1687 and MCW8607
MCW8648	*rad52Δura4⁺ dbl2Δ::kanMX6 ura4-D18 leu1-32 his3-D1 arg3-D4 - ade6 -L469/pUC8/his3⁺/RTS1AO ade6-M375*	Cross MCW1688 and MCW8607
MCW8650	FO656 + pREP41-*dbl2*	Transformation of the plasmid
MCW8651	FO656 + pREP41	Transformation of the plasmid
MCW8652	MCW8564 + pREP41-*dbl2* (pNI30)	Transformation of the plasmid
MCW8653	MCW8564 + pREP41	Transformation of the plasmid

Name	Description	Method of construction
MCW8654	MCW8607 + pREP41-*dbl2* (pNI30)	Transformation of the plasmid
MCW8655	MCW8607 + pREP41	Transformation of the plasmid
MCW8671	*MATa/ade2-1/ura3-1/his3-11,15::HIS3pNI29/trp1-1/leu2-3,112/can1-100/bar1::Hyg/pep4::kanMX6*	Integration into the genome
MCW8685	*dbl2Δ::dbl2-13myc-hphMX4 ura4-D18 leu1-32 his3-D1 ade6-D1 arg3-D4*	Integration into the genome
MCW8686	*dbl2Δ::dbl2-3HA-hphMX4 ura4-D18 leu1-32 his3-D1 ade6-D1 arg3-D4*	Integration into the genome
MCW8687	*dbl2Δ::dbl2-GFP-hphMX4 ura4-D18 leu1-32 his3-D1 ade6-D1 arg3-D4*	Integration into the genome
MCW8688	*dbl2Δ::dbl2-GST-hphMX4 ura4-D18 leu1-32 his3-D1 ade6-D1 arg3-D4*	Integration into the genome
MCW8709	FO656+ pREP41-*Fbh1* pMW637	Transformation of the plasmid
MCW8711	MCW8564 + pREP41-*Fbh1* pMW637	Transformation of the plasmid
MCW8712	MCW1773 + pREP41-*Fbh1* pMW637	Transformation of the plasmid
MCW8713	MCW1773 + pREP41-*dbl2* pNI30	Transformation of the plasmid
MCW8714	MCW1773 + pREP41	Transformation of the plasmid
MCW8715	*rad57Δ::LEU2⁺ dbl2Δ::kanMX6 ura4-D18 leu1-32 his3-D1*	Cross MCW1242 and MCW8607
MCW8717	*swi5Δ::ura4⁺ dbl2Δ::kanMX6 ura4-D18 leu1-32 his3-D1 arg3-D4*	Cross MCW1481 and MCW8607
MCW8718	*rdl1Δ::natMX4 dbl2Δ::kanMX6 ura4-D18 leu1-32 his3-D1 arg3-D4*	Cross MCW6119 and MCW8607
MCW8719	*sws1Δ::kanMX6 dbl2Δ::natMX4 ura4-D18 leu1-32 arg3-D4*	Cross MCW6342 and MCW8610
MCW8720	*rlp1Δ::natMX4 dbl2Δ::kanMX6 ura4-D18 leu1-32 his3-D1 arg3-D4*	Cross MCW6120 and MCW8607
MCW8739	*fbh1Δ::arg3⁺ dbl2Δ::kanMX6 ura4-D18 leu1-32 his3-D1 arg3-D4 ade6-M375 int::pUC8/his3⁺/RTS1 IO/ade6-L469*	Cross FO1814 and MCW8607
MCW8740	*fbh1Δ::arg3⁺ dbl2Δ::kanMX6 ura4-D18 leu1-32 his3-D1 arg3-D4 ade6-M375 int::pUC8/his3⁺/RTS1 AO/ade6-L469*	Cross FO1816 and MCW8607
MCW8747	*fml1Δ:: natMX4 dbl2Δ::kanMX6 ura4-D18 leu1-32 his3-D1 ade6-D1 arg3-DMCW*	Cross MCW2080 and MCW8607
MCW8748	*fbh1Δ::arg3⁺ dbl2Δ::kanMX6 ura4-D18 leu1-32 his3-D1 ade6-D1 arg3-D*	Cross MCW1884 and MCW8564
MCW8749	*mus81Δ::arg3⁺ dbl2Δ::kanMX6 ura4-D18 leu1-32 his3-D1 arg3-D4*	Cross MCW1779 and MCW8607
MCW8750	*fml1Δ::fml1-13myc-natMX4 dbl2Δ::dbl2-GST-kanMX6 ura4-D18 leu1-32 his3-D1 ade6-D1 arg3-D4*	Cross MCW4574 and MCW8568
MCW8752	*fbh1Δ::fbh1-13myc- kanMX6 dbl2Δ::dbl2-GST-natMX4 ura4-D18 leu1-32 his3-D1 ade6-D1 arg3-D4*	Cross MCW1754 and MCW8708
MCW8754	*rqh1Δ::ura4⁺ dbl2Δ::kanMX6 ura4-D18 leu1-32 his3-D1 ade6-D1 arg3-D4*	Cross MCW831 and MCW8607
MCW8755	*rad52Δ::ura4⁺ dbl2Δ::kanMX6 ura4-D18 leu1-32 his3-D1 ade6-D1 arg3-D4*	Cross MCW8607 and MCW1285

Name	Description	Method of construction
MCW8756	*rad51Δ::arg3⁺ dbl2Δ::kanMX6 ura4-D18 leu1-32 his3-D1 ade6-D1 arg3-D4*	Cross MCW8607 and MCW1088
MCW8757	*rad52Δ::ura4⁺ rad51::Δarg3 dbl2Δ::kanMX6 ura4-D18 leu1-32 his3-D1 ade6-D1 arg3-D4*	Cross MCW8607 and MCW1285
MCW8759	*sfr1Δ::natMX4 dbl2Δ::kanMX6 ura4-D18 leu1-32 his3-D1 ade6-D1 arg3-D4*	Cross MCW3263 and MCW8607
MCW8760	*rad55Δ::arg3⁺ dbl2Δ::kanMX6 ura4-D18 leu1-32 his3-D1 ade6-D1 arg3-D4*	Cross MCW1231 and MCW8607
MCW8767	*rad55Δ::arg3⁺ rad57Δ::LEU2+ dbl2Δ::kanMX6 ura4-D18 leu1-32 his3-D1 ade6-D1 arg3-D4*	Cross MCW1242 and MCW8760
MCW8768	*fml1Δ::natMX4 fbh1Δ::arg3⁺ dbl2Δ::kanMX6 ura4-D18 leu1-32 his3-D1 ade6-D1 arg3-D*	Cross MCW2080 and MCW8748
DY11448	*his3-D1 ura4-294 or ura4-D18 arg3Δ::HOsite-natMX ars1::P41nmt1-HO(his3+) lys1-131::Pdis1-mCherry-LacI(lys1+) erg7ter::lacOrepeat(ura4+) rad52-2xCFP::hphMX4 dbl2 Δ::kanMX6 leu1-32::Pdbl2-dbl2(full length)(leu1+)*	*Li-Lin Du lab*
DY11449	*his3-D1 ura4-294 or ura4-D18 arg3Δ::HOsite-natMX ars1::P41nmt1-HO(his3+) lys1-131::Pdis1-mCherry-LacI(lys1+) erg7ter::lacOrepeat(ura4+) rad52-2xCFP::hphMX4 dbl2Δ::kanMX6 leu1-32::Pdbl2-dbl2(Δ6-103)(leu1+)*	*Li-Lin Du lab* (Yu et al., 2013)
DY11450	*his3-D1 ura4-294 or ura4-D18 arg3Δ::HOsite-natMX ars1::P41nmt1-HO(his3+) lys1-131::Pdis1-mCherry-LacI(lys1+) erg7ter::lacOrepeat(ura4+) rad52-2xCFP::hphMX4 dbl2Δ::kanMX6 leu1-32::Pdbl2-dbl2(Δ321-430)(leu1+)*	*Li-Lin Du lab* (Yu et al., 2013)
DY11451	*his3-D1 ura4-294 or ura4-D18 arg3Δ::HOsite-natMX ars1::P41nmt1-HO(his3+) lys1-131::Pdis1-mCherry-LacI(lys1+) erg7ter::lacOrepeat(ura4+) rad52-2xCFP::hphMX4 dbl2Δ::kanMX6 leu1-32::Pdbl2-dbl2(Δ621-715)(leu1+)*	*Li-Lin Du lab* (Yu et al., 2013)
DY11452	*his3-D1 ura4-294 or ura4-D18 arg3Δ::HOsite-natMX ars1::P41nmt1-HO(his3+) lys1-131::Pdis1-mCherry-LacI(lys1+) erg7ter::lacOrepeat(ura4+) rad52-2xCFP::hphMX4 dbl2Δ::kanMX6 leu1-32::Pdbl2-dbl2(Δ6-50)(leu1+)*	*Li-Lin Du lab* (Yu et al., 2013)
DY11453	*his3-D1 ura4-294 or ura4-D18 arg3Δ::HOsite-natMX ars1::P41nmt1-HO(his3+) lys1-131::Pdis1-mCherry-LacI(lys1+) erg7ter::lacOrepeat(ura4+) rad52-2xCFP::hphMX4 dbl2Δ::kanMX6 leu1-32::Pdbl2-dbl2(Δ104-210)(leu1+)*	*Li-Lin Du lab* (Yu et al., 2013)
DY11454	*his3-D1 ura4-294 or ura4-D18 arg3Δ::HOsite-natMX ars1::P41nmt1-HO(his3+) lys1-131::Pdis1-mCherry-LacI(lys1+) erg7ter::lacOrepeat(ura4+) rad52-2xCFP::hphMX4 dbl2Δ::kanMX6 leu1-32::Pdbl2-dbl2(Δ211-320)(leu1+)*	*Li-Lin Du lab* (Yu et al., 2013)
DY11455	*his3-D1 ura4-294 or ura4-D18 arg3Δ::HOsite-natMX ars1::P41nmt1-HO(his3+) lys1-131::Pdis1-mCherry-LacI(lys1+) erg7ter::lacOrepeat(ura4+) rad52-2xCFP::hphMX4 dbl2Δ::kanMX6 leu1-32::Pdbl2-dbl2(Δ431-520)(leu1+)*	*Li-Lin Du lab* (Yu et al., 2013)

Name	Description	Method of construction
DY11456	*his3-D1 ura4-294 or ura4-D18 arg3Δ::HOsite-natMX ars1::P41nmt1-HO(his3+) lys1-131::Pdis1-mCherry-LacI(lys1+) erg7ter::lacOrepeat(ura4+) rad52-2xCFP::hphMX4 dbl2Δ::kanMX6 leu1-32::Pdbl2-dbl2(Δ521-620)(leu1+)*	*Li-Lin Du lab* (Yu et al., 2013)
DY11457	*his3-D1 ura4-294 or ura4-D18 arg3Δ::HOsite-natMX ars1::P41nmt1-HO(his3+) lys1-131::Pdis1-mCherry-LacI(lys1+) erg7ter::lacOrepeat(ura4+) rad52-2xCFP::hphMX4 dbl2Δ::kanMX6 leu1-32::Pdbl2-dbl2(Δ621-715)(leu1+)*	*Li-Lin Du lab* (Yu et al., 2013)
DY11459	*his3-D1 ura4-294 or ura4-D18 arg3Δ::HOsite-natMX ars1::P41nmt1-HO(his3+) lys1-131::Pdis1-mCherry-LacI(lys1+) erg7ter::lacOrepeat(ura4+) rad52-2xCFP::hphMX4 dbl2Δ::kanMX6 leu1-32::Pdbl2-dbl2(621-715)(leu1+)*	*Li-Lin Du lab* (Yu et al., 2013)
DY11462	*his3-D1 ura4-294 or ura4-D18 arg3Δ::HOsite-natMX ars1::P41nmt1-HO(his3+) lys1-131::Pdis1-mCherry-LacI(lys1+) erg7ter::lacOrepeat(ura4+) rad52-2xCFP::hphMX4 dbl2Δ::kanMX6 leu1-32::Pdbl2-dbl2(321-430)(leu1+)*	*Li-Lin Du lab* (Yu et al., 2013)
DY11464	*his3-D1 ura4-294 or ura4-D18 arg3Δ::HOsite-natMX ars1::P41nmt1-HO(his3+) lys1-131::Pdis1-mCherry-LacI(lys1+) erg7ter::lacOrepeat(ura4+) rad52-2xCFP::hphMX4 dbl2Δ::kanMX6 leu1-32::Pdbl2-dbl2(Δ321-350)(leu1+)*	*Li-Lin Du lab* (Yu et al., 2013)
DY11466	*his3-D1 ura4-294 or ura4-D18 arg3Δ::HOsite-natMX ars1::P41nmt1-HO(his3+) lys1-131::Pdis1-mCherry-LacI(lys1+) erg7ter::lacOrepeat(ura4+) rad52-2xCFP::hphMX4 dbl2Δ::kanMX6 leu1-32::Pdbl2-dbl2(Δ351-370)(leu1+)*	*Li-Lin Du lab* (Yu et al., 2013)
DY11468	*his3-D1 ura4-294 or ura4-D18 arg3Δ::HOsite-natMX ars1::P41nmt1-HO(his3+) lys1-131::Pdis1-mCherry-LacI(lys1+) erg7ter::lacOrepeat(ura4+) rad52-2xCFP::hphMX4 dbl2Δ::kanMX6 leu1-32::Pdbl2-dbl2(Δ371-396)(leu1+)*	*Li-Lin Du lab* (Yu et al., 2013)
DY11470	*his3-D1 ura4-294 or ura4-D18 arg3Δ::HOsite-natMX ars1::P41nmt1-HO(his3+) lys1-131::Pdis1-mCherry-LacI(lys1+) erg7ter::lacOrepeat(ura4+) rad52-2xCFP::hphMX4 dbl2Δ::kanMX6 leu1-32::Pdbl2-dbl2(Δ397-420)(leu1+)*	*Li-Lin Du lab* (Yu et al., 2013)
DY11472	*his3-D1 ura4-294 or ura4-D18 arg3Δ::HOsite-natMX ars1::P41nmt1-HO(his3+) lys1-131::Pdis1-mCherry-LacI(lys1+) erg7ter::lacOrepeat(ura4+) rad52-2xCFP::hphMX4 dbl2Δ::kanMX6 leu1-32::Pdbl2-dbl2(Δ421-430)(leu1+)*	*Li-Lin Du lab* (Yu et al., 2013)
MCW8869	*dbl2Δ::kanMX6 leu1-32::Pdbl2-dbl2 (Δ6-103)(leu1⁺) ura4-D18 leu1-32 his3-D1 ade6-D1 arg3-D4*	Cross FO656 and DY11449
MCW8870	*dbl2Δ::kanMX6 leu1-32::Pdbl2-dbl2(full length) (leu1⁺) ura4-D18 leu1-32 his3-D1 ade6-D1 arg3-D4*	Cross FO656 and DY11448
MCW8871	*dbl2Δ::kanMX6 leu1-32::Pdbl2-dbl2(Δ321-430)(leu1⁺) ura4-D18 leu1-32 his3-D1 ade6-D1 arg3-D4*	Cross FO656 and DY11450
MCW8872	*dbl2Δ::kanMX6 leu1-32::Pdbl2-dbl2(Δ321-430)(leu1⁺) ura4-D18 leu1-32 his3-D1 ade6-D1 arg3-D4*	Cross FO656 and DY11450

Name	Description	Method of construction
MCW8873	*dbl2Δ::kanMX6 leu1-32::Pdbl2-dbl2(Δ621-715)(leu1+) ura4-D18 leu1-32 his3-D1 ade6-D1 arg3-D4*	Cross FO656 and DY11451
MCW8874	*dbl2Δ::kanMX6 leu1-32::Pdbl2-dbl2(Δ6-50)(leu1+) ura4-D18 leu1-32 his3-D1 ade6-D1 arg3-D4*	Cross FO656 and DY11452
MCW8875	*dbl2Δ::kanMX6 leu1-32::Pdbl2-dbl2(Δ104-210)(leu1+) ura4-D18 leu1-32 his3-D1 ade6-D1 arg3-D4*	Cross FO656 and DY11453
MCW8876	*dbl2Δ::kanMX6 leu1-32::Pdbl2-dbl2(Δ211-320)(leu1+) ura4-D18 leu1-32 his3-D1 ade6-D1 arg3-D4*	Cross FO656 and DY11454
MCW8877	*dbl2Δ::kanMX6 leu1-32::Pdbl2-dbl2(Δ431-520)(leu1+) ura4-D18 leu1-32 his3-D1 ade6-D1 arg3-D4*	Cross FO656 and DY11455
MCW8878	*dbl2Δ::kanMX6 leu1-32::Pdbl2-dbl2(Δ521-620)(leu1+) ura4-D18 leu1-32 his3-D1 ade6-D1 arg3-D4*	Cross FO656 and DY11456
MCW8879	*dbl2Δ::kanMX6 leu1-32::Pdbl2-dbl2(Δ621-715)(leu1+) ura4-D18 leu1-32 his3-D1 ade6-D1 arg3-D4 DY11457*	Cross FO656 and DY11457
MCW8880	*dbl2Δ::kanMX6 leu1-32::Pdbl2-dbl2(621-715)(leu1+) ura4-D18 leu1-32 his3-D1 ade6-D1 arg3-D4*	Cross FO656 and DY11459
MCW8881	*dbl2Δ::kanMX6 leu1-32::Pdbl2-dbl2(321-430)(leu1+) ura4-D18 leu1-32 his3-D1 ade6-D1 arg3-D4 is2*	Cross FO656 and DY11462
MCW8882	*dbl2Δ::kanMX6 leu1-32::Pdbl2-dbl2(Δ321-350)(leu1+) ura4-D18 leu1-32 his3-D1 ade6-D1 arg3-D4*	Cross FO656 and DY11464
MCW8883	*dbl2Δ::kanMX6 leu1-32::Pdbl2-dbl2(Δ351-370)(leu1+) ura4-D18 leu1-32 his3-D1 ade6-D1 arg3-D4*	Cross FO656 and DY11466
MCW8884	*dbl2Δ::kanMX6 leu1-32::Pdbl2-dbl2(Δ371-396)(leu1+) ura4-D18 leu1-32 his3-D1 ade6-D1 arg3-D4 is3*	Cross FO656 and DY11468
MCW8885	*dbl2Δ::kanMX6 leu1-32::Pdbl2-dbl2(Δ397-420)(leu1+) ura4-D18 leu1-32 his3-D1 ade6-D1 arg3-D4*	Cross FO656 and DY11470
MCW8887	*dbl2Δ::kanMX6 leu1-32::Pdbl2-dbl2(Δ421-430)(leu1+) ura4-D18 leu1-32 his3-D1 ade6-D1 arg3-D4*	Cross FO656 and DY11472
MCW8890	*dbl2 Δ::kanMX6 leu1-32::Pdbl2-dbl2(Δ6-103)(leu1+) ura4-D18 his3-D1 ade6-D1 arg3-D4 ade6-L469/pUC/his3+/RTS1-IO/ade6-M375*	Cross MCW4712 and MCW8869
MCW8891	*dbl2 Δ::kanMX6 leu1-32::Pdbl2-dbl2(Δ6-103)(leu1+) ura4-D18 his3-D1 ade6-D1 arg3-D4 ade6-L469/pUC/his3+/RTS1-AO/ade6-M375*	Cross MCW4713 and MCW8869
MCW8892	*dbl2Δ::kanMX6 leu1-32::Pdbl2-dbl2(full length)(leu1+) ura4-D18 leu1-32 his3-D1 ade6-D1 arg3-D4 ade6-L469/pUC/his3+/RTS1-IO/ade6-M375*	Cross MCW4712 and MCW8870
MCW8893	*dbl2Δ::kanMX6 leu1-32::Pdbl2-dbl2(full length)(leu1+) ura4-D18 leu1-32 his3-D1 ade6-D1 arg3-D4 ade6-L469/pUC/his3+/RTS1-AO/ade6-M375*	Cross MCW4713 and MCW8870
MCW8894	*dbl2Δ::kanMX6 leu1-32::Pdbl2-dbl2(Δ321-430)(leu1+) ura4-D18 leu1-32 his3-D1 ade6-D1 arg3-D4 ade6-L469/pUC/his3+/RTS1-IO/ade6-M375*	Cross MCW4712 and MCW8872

Name	Description	Method of construction
MCW8895	*dbl2Δ::kanMX6 leu1-32::Pdbl2-dbl2(Δ321-430)(leu1+) ura4-D18 leu1-32 his3-D1 ade6-D1 arg3-D4 ade6-L469/pUC/his3+/RTS1-AO/ade6-M375*	Cross MCW4713 and MCW8872
MCW8896	*dbl2Δ::kanMX6 leu1-32::Pdbl2-dbl2(Δ621-715)(leu1+) ura4-D18 leu1-32 his3-D1 ade6-D1 arg3-D4 ade6-L469/pUC/his3+/RTS1-IO/ade6-M375 DY11451derivative*	Cross MCW4712 and MCW8873
MCW8897	*dbl2Δ::kanMX6 leu1-32::Pdbl2-dbl2(Δ621-715)(leu1+) ura4-D18 leu1-32 his3-D1 ade6-D1 arg3-D4 ade6-L469/pUC/his3+/RTS1-AO/ade6-M375 DY11451derivative*	Cross MCW4713 and MCW8873
MCW8898	*dbl2Δ::kanMX6 leu1-32::Pdbl2-dbl2(Δ6-50)(leu1+) ura4-D18 leu1-32 his3-D1 ade6-D1 arg3-D4 ade6-L469/pUC/his3+/RTS1-IO/ade6-M375*	Cross MCW4712 and MCW8874
MCW8899	*dbl2Δ::kanMX6 leu1-32::Pdbl2-dbl2(Δ6-50)(leu1+) ura4-D18 leu1-32 his3-D1 ade6-D1 arg3-D4 ade6-L469/pUC/his3+/RTS1-AO/ade6-M375*	Cross MCW4713 and MCW8874
MCW8902	*dbl2Δ::kanMX6 leu1-32::Pdbl2-dbl2(621-715)(leu1+) ura4-D18 leu1-32 his3-D1 ade6-D1 arg3-D4 ade6-L469/pUC/his3+/RTS1-IO/ade6-M375*	Cross MCW4712 and MCW8880
MCW8903	*dbl2Δ::kanMX6 leu1-32::Pdbl2-dbl2(621-715)(leu1+) ura4-D18 leu1-32 his3-D1 ade6-D1 arg3-D4 ade6-L469/pUC/his3+/RTS1-AO/ade6-M375*	Cross MCW4713 and MCW8880
MCW8904	*dbl2Δ::kanMX6 leu1-32::Pdbl2-dbl2(321-430)(leu1+) ura4-D18 leu1-32 his3-D1 ade6-D1 arg3-D4 ade6-L469/pUC/his3+/RTS1-IO/ade6-M375*	Cross MCW4712 and MCW8881
MCW8905	*dbl2Δ::kanMX6 leu1-32::Pdbl2-dbl2(321-430)(leu1+) ura4-D18 leu1-32 his3-D1 ade6-D1 arg3-D4 ade6-L469/pUC/his3+/RTS1-AO/ade6-M375*	Cross MCW4713 and MCW8881
MCW8955	*dbl2Δ::KanMX6 ura4-D8 leu1-32 his3-D1 arg3-D4 ade6-L469/pUC/his3+/RTS1-IO/ade6-M375*	Cross MCW8563 and MCW6504
MCW8960	*dbl2Δ::KanMX6 ura4-D8 leu1-32 his3-D1 arg3-D4 ade6-L469/pUC/his3+/RTS1-AO/ade6-M375*	Cross MCW8563 and MCW6506
MCW8968	*swi5Δ::ura4+ dbl2Δ::kanMX6 leu1-32::Pdbl2-dbl2(321-430)(leu1+) ura4-D18 leu1-32 his3-D1 ade6-D1 arg3-D4*	Cross MCW1481 and MCW8881
MCW8969	*swi5Δ::ura4+ dbl2Δ::kanMX6 leu1-32::Pdbl2-dbl2(Δ621-715)(leu1+) ura4-D18 leu1-32 his3-D1 ade6-D1 arg3-D4 DY11451derivative*	Cross MCW1481 and MCW8873
MCW8970	*swi5Δ::ura4+ dbl2Δ::kanMX6 leu1-32::Pdbl2-dbl2(621-715)(leu1+) ura4-D18 leu1-32 his3-D1 ade6-D1 arg3-D4*	Cross MCW1481 and MCW8880
MCW8971	*swi5Δ::ura4+ dbl2Δ::kanMX6 leu1-32::Pdbl2-dbl2(full length)(leu1+) ura4-D18 leu1-32 his3-D1 ade6-D1 arg3-D4*	Cross MCW1481 and MCW8870
MCW8972	*swi5Δ::ura4+ dbl2 Δ::kanMX6 leu1-32::Pdbl2-dbl2(Δ6-103)(leu1+) ura4-D18 leu1-32 his3-D1 ade6-D1 arg3-D4*	Cross MCW1481 and MCW8869
MCW8973	*swi5Δ::ura4+ dbl2Δ::kanMX6 leu1-32::Pdbl2-dbl2(Δ321-430)(leu1+) ura4-D18 leu1-32 his3-D1 ade6-D1 arg3-D4*	Cross MCW1481 and MCW8871
MCW8974	*rad55Δ::arg3+ dbl2Δ::kanMX6 leu1-32::Pdbl2-dbl2(321-430)(leu1+) ura4-D18 leu1-32 his3-D1 ade6-D1 arg3-D4 is2*	Cross MCW1231 and MCW8881

Name	Description	Method of construction
MCW8977	*rad55Δ::arg3⁺ dbl2Δ::kanMX6 leu1-32::Pdbl2-dbl2(full length)(leu1⁺) ura4-D18 leu1-32 his3-D1 ade6-D1 arg3-D4*	Cross MCW1231 and MCW8870
MCW8978	*rad55Δ::arg3⁺ dbl2Δ::kanMX6 leu1-32::Pdbl2-dbl2(621-715)(leu1⁺) ura4-D18 leu1-32 his3-D1 ade6-D1 arg3-D4*	Cross MCW1231 and MCW8880
MCW8979	*rad55Δ::arg3⁺ dbl2 Δ::kanMX6 leu1-32::Pdbl2-dbl2(Δ6-103)(leu1⁺) ura4-D18 leu1-32 his3-D1 ade6-D1 arg3-D4*	Cross MCW1231 and MCW8869
MCW8980	*rad55Δ::arg3⁺ dbl2Δ::kanMX6 leu1-32::Pdbl2-dbl2(Δ621-715)(leu1⁺) ura4-D18 leu1-32 his3-D1 ade6-D1 arg3-D4*	Cross MCW1231 and MCW8873
MCW8981	*rdl1Δ::natMX4 dbl2Δ::kanMX6 leu1-32::Pdbl2-dbl2(621-715)(leu1⁺) ura4-D18 leu1-32 his3-D1 ade6-D1 arg3-D4*	Cross 6119 and MCW8880
MCW8982	*rdl1Δ::natMX4 dbl2 Δ::kanMX6 leu1-32::Pdbl2-dbl2(Δ6-103)(leu1⁺) ura4-D18 leu1-32 his3-D1 ade6-D1 arg3-D4*	Cross 6119 and MCW8869
MCW8983	*rdl1Δ::natMX4 dbl2Δ::kanMX6 leu1-32::Pdbl2-dbl2(321-430)(leu1⁺) ura4-D18 leu1-32 his3-D1 ade6-D1 arg3-D4*	Cross 6119 and MCW8881
MCW8984	*rdl1Δ::natMX4 dbl2Δ::kanMX6 leu1-32::Pdbl2-dbl2(Δ621-715)(leu1⁺) ura4-D18 leu1-32 his3-D1 ade6-D1 arg3-D4*	Cross 6119 and MCW8873
MCW8985	*rdl1Δ::natMX4 dbl2Δ::kanMX6 leu1-32::Pdbl2-dbl2(full length)(leu1⁺) ura4-D18 leu1-32 his3-D1 ade6-D1 arg3-D4*	Cross 6119 and MCW8870
MCW8986	FO656 + pREP41-Nterm*dbl2(100aa)* pNI36	Transformation of the plasmid
MCW8987	MCW8564 + pREP41-Nterm*dbl2(100aa)* pNI36	Transformation of the plasmid
MCW9010	*rad55Δ::arg3⁺ dbl2Δ::kanMX6 leu1-32::Pdbl2-dbl2(Δ321-430)(leu1⁺) ura4-D18 leu1-32 his3-D1 ade6-D1 arg3-D4*	Cross MCW1231 and MCW8872
MCW9012	*rdl1Δ::natMX4 dbl2Δ::kanMX6 leu1-32::Pdbl2-dbl2(Δ321-430)(leu1⁺) ura4-D18 leu1-32 his3-D1 ade6-D1 arg3-D4*	Cross MCW6119 and MCW8872
MCW9016	*dbl2Δ::kanMX6 rad51::Δarg3⁺ ura4-D18 leu1-32 his3-D1 arg3-D4 - ade6 -L469/pUC8/his3⁺/RTS1IO ade6-M375*	Cross MCW1691 and MCW8607
MCW9017	*dbl2Δ::kanMX6 rad51Δ::arg3⁺ ura4-D18 leu1-32 his3-D1 arg3-D4 - ade6 -L469/pUC8/his3⁺/RTS1AO ade6-M375*	Cross MCW1692 and MCW8607
MCW9018	*dbl2 Δ::kanMX6 leu1-32::Pdbl2-dbl2(Δ6-103)(leu1⁺) ade6-L469/pUC8/4.5Kb lacO/his3⁺/RTS1-IO/ade6-M375 lys1-::Pnmt41-NLS-lacI-tdKatushka2-hphMX4 ura4-D18 leu1-32 his3-D1 arg3-D4*	Cross MCW6351 and MCW8869
MCW9019	*dbl2 Δ::kanMX6 leu1-32::Pdbl2-dbl2(Δ6-103)(leu1⁺) ade6-L469/pUC8/4.5Kb lacO/his3⁺/RTS1-AO/ade6-M375 lys1-::Pnmt41-NLS-lacI-tdKatushka2-hphMX4 ura4-D18 leu1-32 his3-D1 arg3-D4*	Cross MCW6536 and MCW8869
MCW9020	*dbl2Δ::kanMX6 leu1-32::Pdbl2-dbl2(full length)(leu1⁺) ade6-L469/pUC8/4.5Kb lacO/his3⁺/RTS1-IO/ade6-M375 lys1-::Pnmt41-NLS-lacI-tdKatushka2-hphMX4 ura4-D18 leu1-32 his3-D1 arg3-D4*	Cross MCW6351 and MCW8870

Name	Description	Method of construction
MCW9021	*dbl2Δ::kanMX6 leu1-32::Pdbl2-dbl2(full length)(leu1+)ade6-L469/pUC8/4.5Kb lacO/his3+/RTS1-AO/ade6-M375 lys1-::Pnmt41-NLS-lacI-tdKatushka2-hphMX4 ura4-D18 leu1-32 his3-D1 arg3-D4*	Cross MCW6536 and MCW8870
MCW9022	*dbl2Δ::kanMX6 leu1-32::Pdbl2-dbl2(Δmid) ade6-L469/pUC8/4.5Kb lacO/his3+/RTS1-IO/ade6-M375 lys1-::Pnmt41-NLS-lacI-tdKatushka2-hphMX4 ura4-D18 leu1-32 his3-D1 arg3-D4*	Cross MCW6351 and MCW8872
MCW9023	*dbl2Δ::kanMX6 leu1-32::Pdbl2-dbl2(Δmid) ade6-L469/pUC8/4.5Kb lacO/his3+/RTS1-AO/ade6-M375 lys1-::Pnmt41-NLS-lacI-tdKatushka2-hphMX4 ura4-D18 leu1-32 his3-D1 arg3-D4*	Cross MCW6536 and MCW8872
MCW9095	*dbl2Δ::natMX4 ade6::RTS1-IO-hphMX4 ade6-L469/pUC8/his3+/ade6-M375-KanMX-aim1 ura4-D18 leu1-32 his3-D1 arg3-D4 ade6-D1*	Cross MCW7258 and MCW8608
MCW9096	*dbl2Δ::natMX4 ade6::RTS1-AO-hphMX4 ade6-L469/pUC8/his3+/ade6-M375-KanMX-aim1 ura4-D18 leu1-32 his3-D1 arg3-D4 ade6-D1*	Cross MCW7260 and MCW8608
MCW9124	*dbl2Δ::natMX4 ade6-L469/pUC/5000bp spacer/his3+/RTS1-AO/ade6-M375 ura4-D18 leu1-32 his3-D1 arg3-D4*	Cross MCW8023 and MCW8610
MCW9125	*rad51Δ::arg3+ dbl2Δ::natMX4 Ade6-L469/pUC8/5kb λ spacer/his3+/RTS1-AO/Ade6-M375 Ura4-D18 Leu1-32 His3-D1 Arg3-D4*	Cross MCW8136 and MCW8610
MCW9126	*dbl2 Δ::hphMX4 leu1-32::Pdbl2-dbl2(Δ6-103)(leu1+) ura4-D18 leu1-32 his3-D1 ade6-D1 arg3-D4*	Cross MCW8869 and MCW8608
MCW9127	*dbl2Δ::hphMX4 leu1-32::Pdbl2-dbl2(full length)(leu1+) ura4-D18 leu1-32 his3-D1 ade6-D1 arg3-D4*	Cross MCW8609 and MCW8870
MCW9128	*dbl2 Δ::natMX4 leu1-32::Pdbl2-dbl2(Δ6-103)(leu1+) ura4-D18 leu1-32 his3-D1 ade6-D1 arg3-D4*	Cross MCW8869 and MCW8608
MCW9129	*dbl2Δ::natMX4 leu1-32::Pdbl2-dbl2(full length)(leu1+) ura4-D18 leu1-32 his3-D1 ade6-D1 arg3-D4*	Cross MCW8608 and MCW8870
MCW9154	FO656+ pREP41-*Rad52* pMW613	Transformation of the plasmid
MCW9155	MCW4713+ pREP41-*Rad52* pMW613	Transformation of the plasmid
MCW9156	MCW4713+ pREP41	Transformation of the plasmid
MCW9176	*dbl2Δ::natMX4 ade6-M375 int::pUC8/lacO115/his3+ /RTS1-IO/ade6-L469 lys1-::Pnmt41-NLS-lacI-tdKatushka2-hphMX4 rad52+::YFP-kanMX6 rad51+::ECFP-rad51+-arg3+ ura4-::rad51+his3-D1 leu1-32 arg3-D4ade6-M375*	Cross MCW7640 and MCW8610
MCW9177	*dbl2Δ::natMX4 ade6-M375 int::pUC8/lacO115/his3+ /RTS1-AO/ade6-L469 lys1-::Pnmt41-NLS-lacI-tdKatushka2-hphMX4 rad52+::YFP-kanMX6 rad51+::ECFP-rad51+-arg3+ ura4-::rad51+his3-D1 leu1-32 arg3-D4ade6-M375*	Cross MCW7638 and MCW8610

Chapter 3

3 The identification of factors needed for the replication restart at a site-specific replication fork barrier

3.1 Introduction

RF blockage at *RTS1* can be resolved either through collapse of the fork followed by recombination-dependent restart or by passive termination involving forks merging at the barrier (Nguyen et al., 2015). To investigate the mechanism of fork collapse at the site-specific RFB *RTS1*, and to define key interactions between the *RTS1* barrier protein Rtf1 and replisome components, which likely trigger fork collapse, a variety of different approaches could be applied. Immunofluorescence imaging can be used to detect proteins recruited to damaged forks (Bekker-Jensen et al., 2006; Bennett et al., 2009). However, immunofluorescence has limitations including a requirement for highly specific antibodies and sufficient amounts of a target protein in the cell for it to be detected. Another approach is co-immunoprecipitation followed by protein identification by mass spectrometry (MS) (Gambus et al., 2006, 2009), but this only allows detection of proteins that are directly or indirectly associated with the replication factor that is being immunoprecipitated and does not specifically detect proteins that are present at RFs during collapse/termination. To overcome these drawbacks iPOND (isolation of proteins on nascent DNA) coupled with MS was developed (Sirbu et al., 2011). However, iPOND provides a picture of an average RF and cannot distinguish the significant heterogeneity between forks within different genomic regions (Sirbu et al., 2012).

Mass spectrometry has become a widespread technology for relative quantitation between experimental conditions (active, stalled and collapsed

replication in different genetic backgrounds) (Sirbu et al., 2011). A number of methods that use introduction of heavy isotopes into a sample have been developed, one of the most powerful is SILAC (stable-isotope labelling by amino acids in cell culture). SILAC was shown to be useful for the quantitative analysis of post translational modifications (Cuomo et al., 2017). Proteins of interest are enriched from SILAC-labelled cells and analysed for changes in processing or for other modifications. SILAC allows incorporating kinetics into site-specific proteomics. For example, three different cell populations were labelled, treated with an inhibitor of transcription and harvested at three different time points (Andersen et al., 2005). To interrogate changes in the proteasome composition of the particular fork during collapse at *RTS1*, proteins at the barrier would be retrieved by purification of Rtf1. Crosslinking prior to pull-down would allow the entire set of proteins that are present at *RTS1* to be enriched and then identified.

To interrogate protein composition at the blocked fork during RF collapse and termination, I have positioned *RTS1* on a multi-copy plasmid and would be able to capture proteins crosslinked to the barrier by pull-down of Rtf1-Halo (Fig. 3.1). Further strategy implied usage of LC-MS SILAC to identify proteins, including their post-translational modifications. By harvesting samples from synchronised cells, I would be able to track changes that occur in the replisome during collapse and termination (NB: RF termination on a plasmid occurs before RDR can initiate).

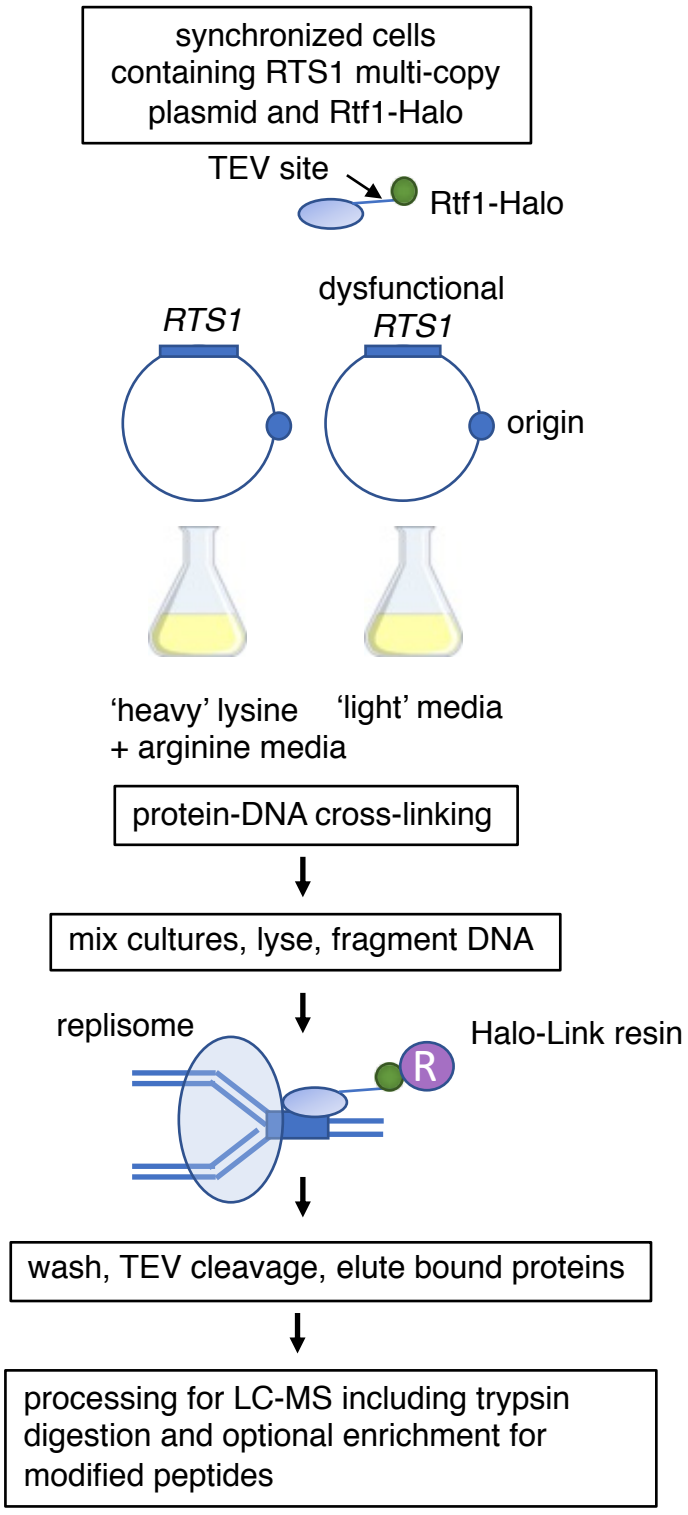


Figure 3.1. Quantitative proteomics strategy to analyse replisome composition at *RTS1*.

Specific residues that are modified will be mutated and their impact on RF collapse, restart and termination assessed.

To characterize factors that are needed for the successful processing and restart of blocked RFs at *RTS1* a candidate-based approach can also be taken. As discussed in Chapter 1, Fml1 has been identified as key factor in the processing of forks that have collapsed at *RTS1* (Sun et al., 2008) and, therefore, identifying proteins that interact with Fml1, using Co-IP of tagged Fml1, might reveal new factors that are important for processing collapsed RFs.

In this chapter I present my preliminary work to establish an experimental approach to interrogate protein composition at *RTS1* during fork collapse and replication restart. I also present additional work focusing on investigating a putative interaction between Fml1-Mhf1 and the PCNA unloader Elg1; Fml1 and the structural maintenance of chromosomes complex Smc5-Smc6.

3.2 Results

3.2.1 Establishing a system for identifying proteins at the *RTS1* RFB

I wanted to suitably tag the barrier protein Rtf1 so that I could use it to isolate the entire complex of proteins present at *RTS1* during different time points in S and G2 phase. The Halo-tag has important advantages over many other standard affinity tags because it forms a covalent and very high affinity interaction with Halo resin (Los et al., 2008). This allows the use of high stringency washes during purification without the concern of removing the

immobilized proteins. In addition, the level of non-specific interaction is decreased due to the high affinity interaction of the Halo-tag and its ligand. Thus, usage of the Halo-tag potentially helps to diminish background signal in MS.

When I joined the lab, a *S. pombe* strain that expresses C-terminal Halo-tagged Rtf1 from its normal chromosomal locus had already been constructed. From the targeting construct used to create this strain I also derived a plasmid for the overexpression of Halo-tagged Rtf1 from the inducible *nmt41* promoter. However, neither construct generated detectable levels of Halo-tagged Rtf1 in soluble cell extracts when analysed on a Western blot using an anti-Halo monoclonal antibody. One potential explanation for this was that the protein was stuck in the insoluble chromatin fraction. I tried various methods of extraction, including alkaline lysis, bead beating, and homogenization followed by extraction of nuclei. However, despite trying various extraction procedures and lysis buffers no Halo-tagged Rtf1 was detected.

It was possible that the tag was proteolyzed during the initial lysis or even earlier in the living cell. Therefore, to determine whether Rtf1 is detectable with alternative epitope tags, I constructed a series of plasmids for the overexpression of Rtf1. In each case I was able to detect the tagged Rtf1 by WB analysis using an antibody directed against the tag (Fig. 3.2). Having found that Rtf1 is readily detected when fused to other epitope tags, I designed a tandem 3xPk-Halo tag with a TEV-cleavage site between the two tags. The addition of a Pk tag allows me to detect Rtf1 following its removal from HaloLink resin by TEV cleavage. I constructed the strains with Rtf1-3xPk-TEV-

Halo expressed from the endogenous *rtf1* promoter and overexpressed from *nmt 1, nmt 41, nmt 81* promoters on a series of plasmids (Fig. 3.3). The tag did not seem to disrupt Rtf1 function as was shown by a genotoxin sensitivity and recombination assay (data not shown). However, attempts to pull-down Rtf1 using Halo-tag-Halo-resin interaction with subsequent TEV cleavage and identification of Rtf1 using 3Pk-tag were not successful. WB analysis revealed that Rtf1-3xPk-Halo binds to the resin with very low efficiency (Fig. 3.4A). Optimization of incubation conditions did not result in improvement of the binding efficiency.

The alternative to using Halo-tag is exploiting other tags that form a covalent bond with an appropriate resin. SpyTag/SpyCatcher is a convenient system in which a short peptide (SpyTag) forms spontaneously an irreversible amide bond with SpyCatcher. SpyCatcher can be immobilized on avidin resin if SpyCatcher-Biotin is used or sulfhydryl coupling resin if SpyCatcher-Cysteine is used.

To investigate whether the SpyTag/SpyCatcher system would prove useful for the purification of Rtf1, I constructed strains with Rtf1-3xPk-TEV-SpyTag overexpressed from the thiamine-repressible *nmt* promoter in plasmids pREP81 and pREP1. However, attempts to pull-down Rtf1-Spytag by formation of SpyTag-SpyCatcher in solution, followed by immobilization of the complex on avidin or sulfhydryl resin and subsequent TEV cleavage, were unsuccessful. WB analysis revealed that Rtf1-3xPk-TEV-SpyTag binds to the resin with very low efficiency (Fig. 3.4B).

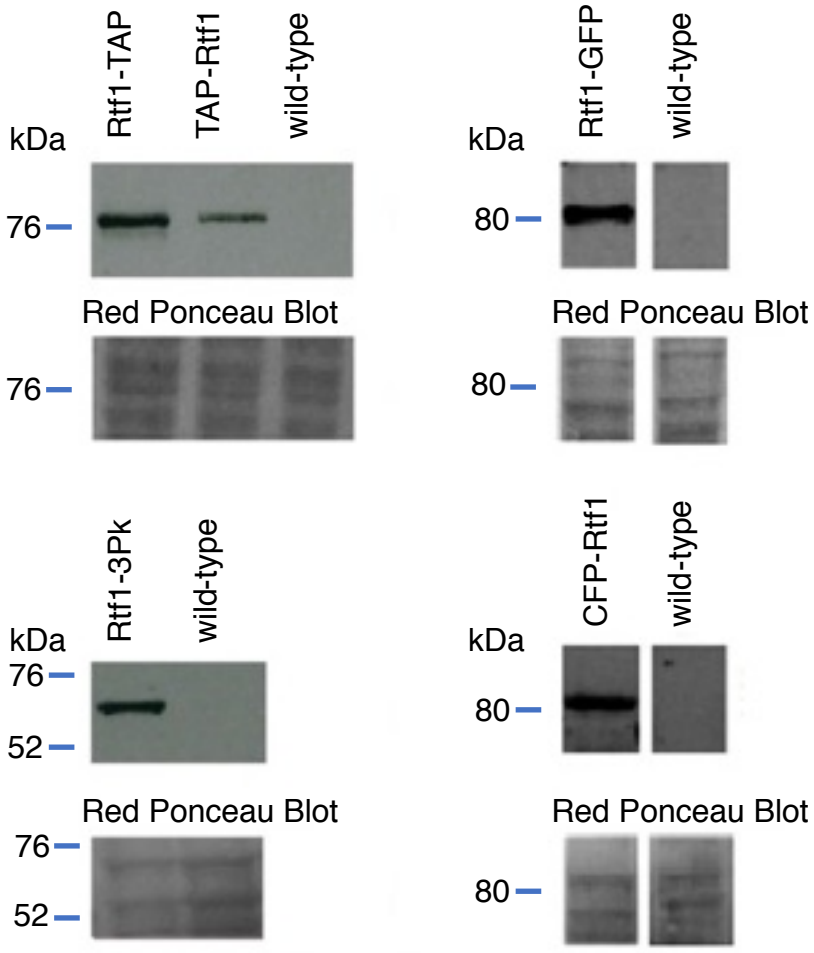


Figure 3.2. Detection of Rtf1 that has been epitope tagged at either N- or C-terminus.

From left to right: WB analysis of expression of Rtf1 tagged with TAP (C- and N-terminus), GFP (C-terminus) (upper row); 3Pk (C-terminus), and CFP (N-terminus) from (bottom row) MCW7940, MCW7939, MCW7942, MCW7944, MCW7946. Cells were lysed by bead beating using a FastPrep machine with cells suspended in RIPA buffer. The blots were probed with suitable primary and secondary antibodies (Section 2.6.6).

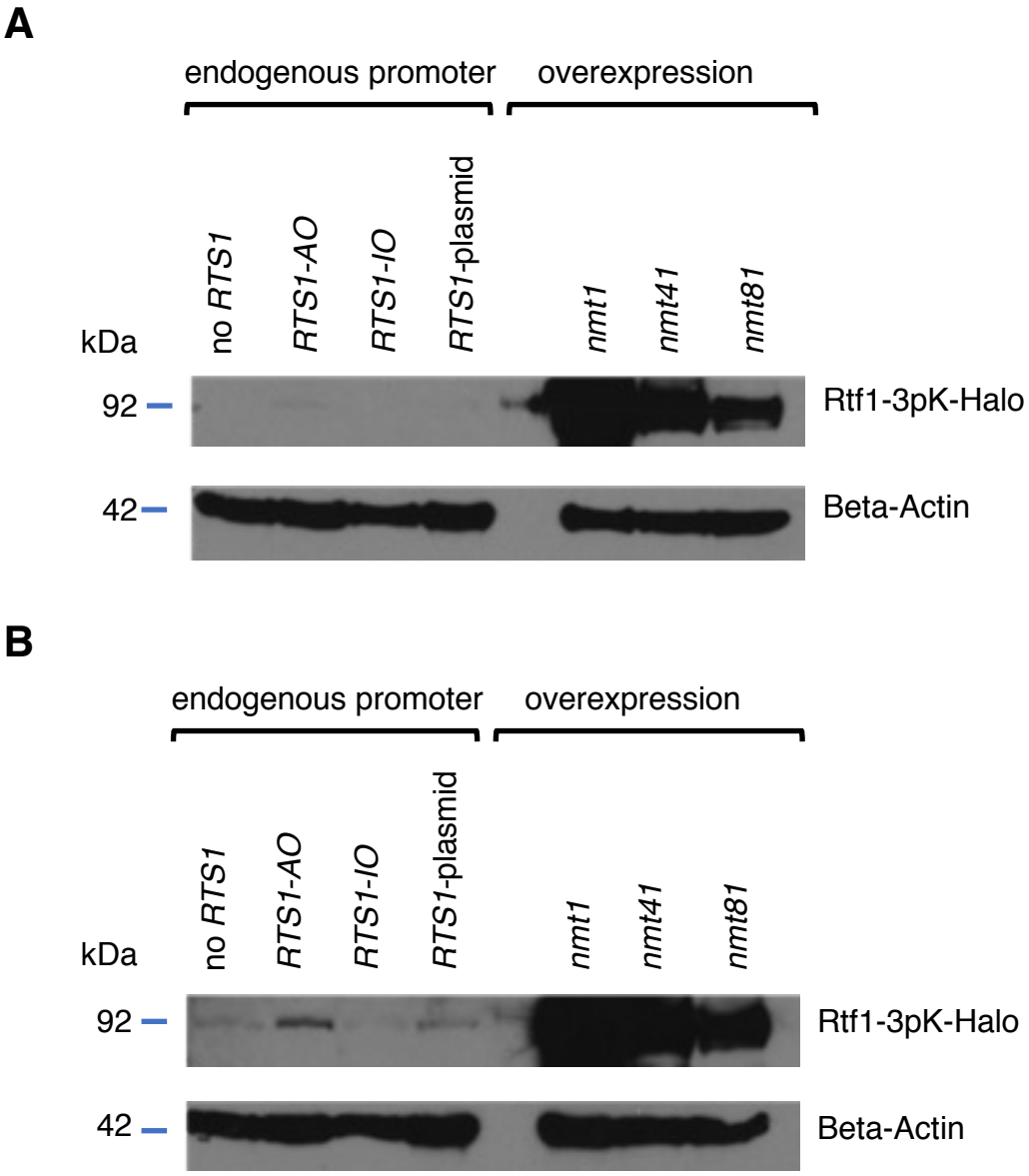


Figure 3.3. Detection of Rtf1 tagged with 3Pk-Halo.

Western blot analysis of expression of Rtf1 tagged with 3Pk-Halo from endogenous and *nmt* promoters in MCW8265, MCW8267, MCW8266, MCW8271, MCW8270, MCW8268, and MCW8269. Cells were lysed by alkaline lysis. The blots were probed with anti-Halo (**A**) and anti-Pk (**B**) primary antibodies (Section 2.6.6).

Altogether these data indicate that neither Halo tag nor SpyTag are suitable for the efficient purification of Rtf1 from lysates of *S. pombe* using their cognate affinity resins. It is possible that further optimization could achieve improved results, however due to time constraints I focused on a more targeted co-immunoprecipitation approach to identify factors needed for replication restart at *RTS1*.

3.2.2 Investigating the interaction between Fml1 and Elg1

The DNA helicase Fml1, together with its accessory proteins Mhf1 and Mhf2, is thought to play an important role in remodelling stalled RFs to promote Rad51-dependent replication restart (Sun et al., 2008) (Chapter 1). However, it is not known how the Fml1-MHF complex is recruited to stalled RFs. Yeast two-hybrid analysis revealed an interaction between Elg1 and both Fml1 and Mhf1 in budding yeast (Singh et al., 2013). Elg1 is part of one of the three alternative clamp loaders (RFC-like complexes or RLCs) identified in eukaryotes (Kupiec, 2016).

The Elg1 RLC is thought to be the principal factor responsible for unloading PCNA from DNA, including during general DNA replication when PCNA is unloaded following the ligation of each Okazaki fragment (Parnas et al., 2010; Kubota et al 2015). To see if the interaction between Mph1 and Elg1 is conserved in fission yeast, I constructed a strain in which Fml1-13myc, Elg1-TAP and Mhf1-Halo are each expressed from their respective endogenous promoters.

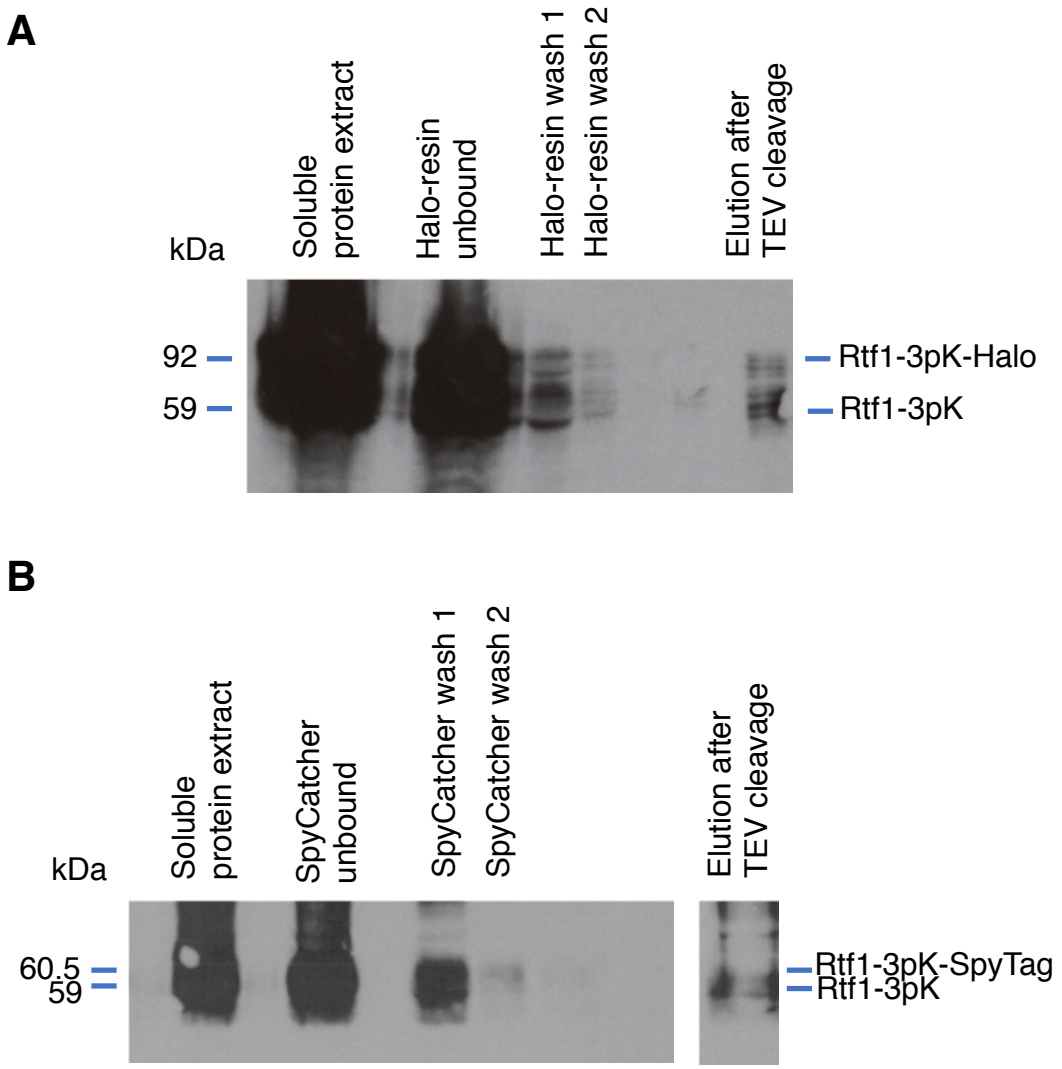


Figure 3.4. Halo- and SpyTagged Rtf1 does not bind efficiently to the suitable resin.

Western blot analysis of the pull-down of Rtf1 tagged with 3Pk-Halo (strain MCW8270) using Halo-resin (**A**) and 3Pk-SpyTag (strain MCW8562) using SpyCatcher-Biotin immobilised on avidin resin (**B**). Cells were lysed by cryogrinding. The protein was cleaved from the resin by TEV protease. The blots were probed with anti-Pk primary and mouse secondary antibodies (Section 2.6.6).

Elg1-Tap precipitates with Fml1-13Myc (Fig. 3.5A) in the presence of anti-myc antibodies. I next tested whether Mhf1-Halo would co-purify with Elg1-TAP on IgG sepharose. As a positive control I also tested the co-purification of Mhf1-Halo with Fml1-TAP in parallel. Initial attempts using bead beating methods of cell disruption with native buffers were inconclusive as little or no protein was detected (data not shown). I therefore scaled-up the number of cells and performed cell disruption under native buffer conditions using either a French Press or cryo-grinding. With the former method I also included Benzonase to digest DNA and thereby help release chromatin-bound proteins. With both methods it was possible to detect Mhf1-Halo, Fml1-TAP and Elg1-TAP in the cell extracts (data not shown and Fig. 3.5). Using an anti-Halo monoclonal antibody Mhf1-Halo was detected in the IgG bead unbound fraction for both Fml1-TAP and Elg1-TAP purifications, however it was only detected in the bound fraction with Fml1-TAP but not Elg1-TAP (Fig. 3.5B). These data confirm that Mhf1 and Fml1 interact *in vivo*, but do not provide evidence that the same is true for Mhf1 and Elg1.

When attempting to purify Mhf1-Halo, I found that Elg1-TAP non-specifically binds the Halo-resin and, therefore, this approach cannot be used for studying whether Elg1-TAP interacts with Halo-tag proteins (Fig. 3.5C).

3.2.3 Investigating the interaction between Fml1 and Smc5

Mph1 interacts with the structural maintenance of chromosome complex Smc5/6 by directly binding to Smc5 (Chen et al., 2009).

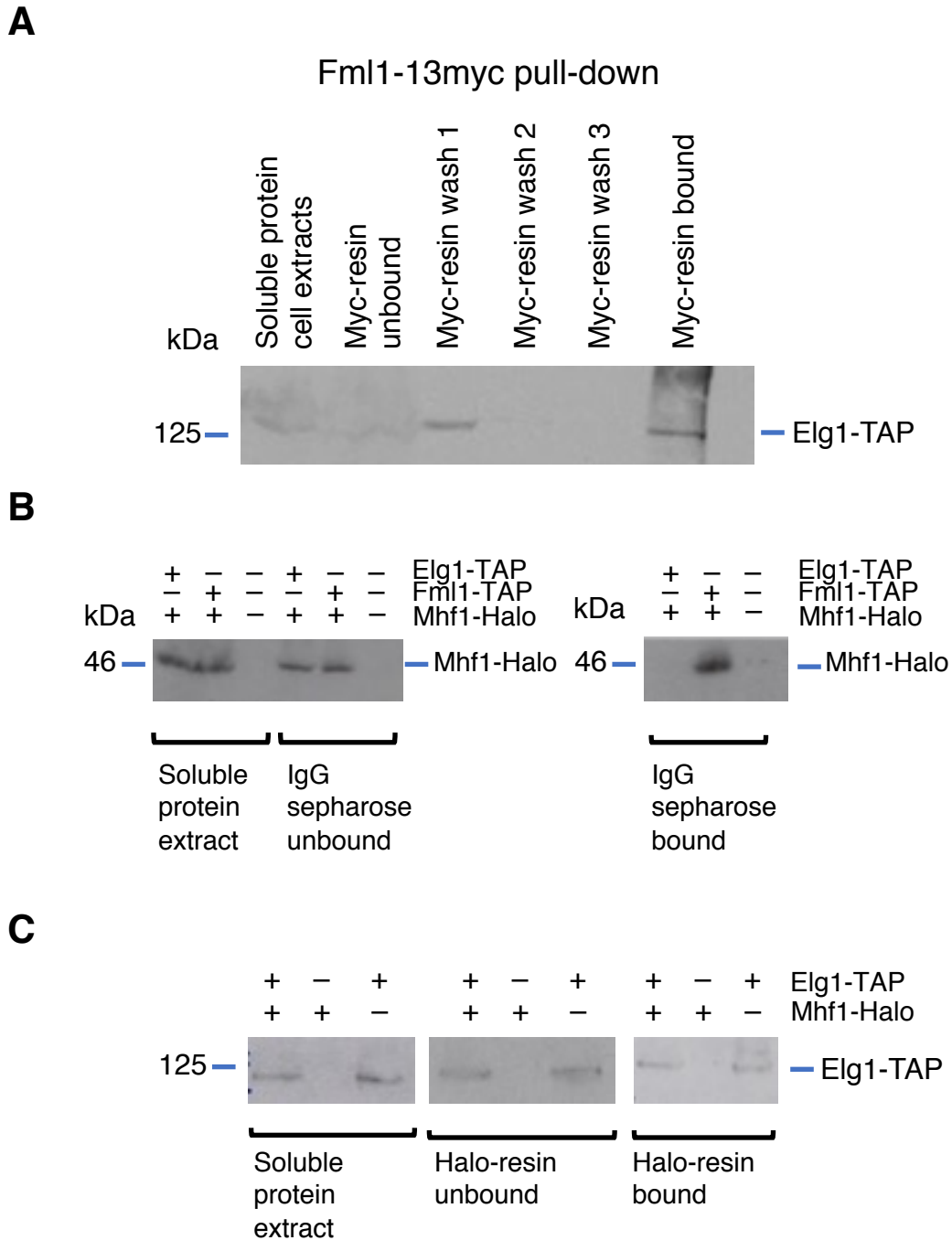


Figure 3.5. Analysis of interaction between Fml1, Elg1 and Mhf1.

(**A**) Elg1-TAP was precipitated by anti-myc antibody resin in the presence of Fml1-13myc (MCW8087). (**B**) Mhf1-Halo bound to IgG sepharose in the presence of Fml1-TAP but not Elg1-TAP (MCW8063 and MCW7993, respectively). (**C**) Elg1-TAP binds non-specifically to Halo-resin (MCW7993 and MCW7991). Cells were lysed by cryogrinding. Soluble protein extracts (input), unbound protein fraction (resin flow-through) and immunoprecipitated proteins were analysed by western blotting using suitable primary and secondary antibodies (Section 2.6.6).

The Smc5/6 complex limits the RF regression but not D-loop dissociation activity of Mph1 (Xue et al., 2014) and restrains Mph1 ability to counter accumulation of RNA-DNA hybrids (Lafuente-Barquero et al., 2017). In fission yeast the Smc5/6 complex is essential and is recruited to DSB sites and stalled RFs. Smc5/6 complex plays a role in homologous recombination-mediated DNA repair and is thought to stabilise stalled replication forks holding them in a conformation that facilitates RPA and Rad52 loading (Ampatzidou et al., 2006; Miyabe et al., 2006; Irmisch et al., 2009). To see if the interaction between Mph1 and Smc5 is conserved in *S. pombe*, I constructed a strain expressing Fml1-13myc and Smc5-3HA. Smc5 co-immunoprecipitates with Fml-13myc suggesting that Fml1 binds Smc5 *in vivo* (Fig. 3.6).

3.3 Discussion

To find out what changes occur in protein composition (including post-translational modifications) at the RF during its collapse or termination at *RTS1*, Rtf1 was used to pull down *RTS1* DNA, which in turn would be a platform for pulling down all the proteins that associate at the RFB. To this end, a system allowing the robust pull-down of Rtf1 is needed

The tag of choice should bind covalently to the resin enabling the efficient purification of the protein with interaction partners while minimizing the non-specific binding and thus facilitating further MS analysis. An epitope tag that should fulfil these requirements is Halo.

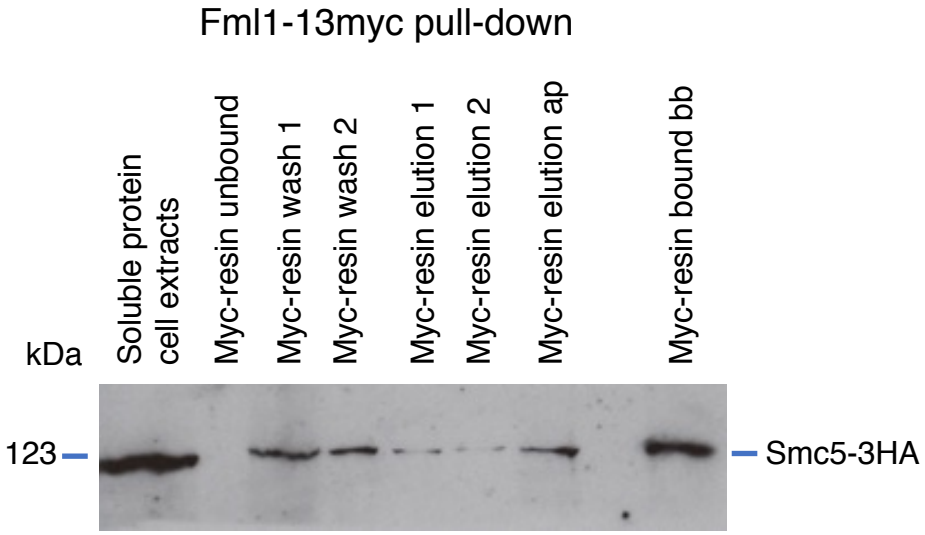


Figure 3.6. Smc5-3HA co-immunoprecipitates with Fml1-13Myc.

Cells (MCW8081) were lysed by cryogrinding. Soluble protein extracts (input), unbound protein fraction (resin flow-through) and immunoprecipitated proteins were analysed by western blotting using suitable primary and secondary antibodies (Section 2.6.6). 'Ap' refers to acetone precipitated fraction and 'bb' to boiled beads' fraction.

Although Rtf1 can be expressed and detected with Halo-tag, Halo-Rtf1 bound very poorly to HaloLink resin (Fig. 3.4A). Therefore, this system appears to be unsuitable for the purpose of pulling down proteins that associate with Rtf1 and/or the *RTS1* DNA that it is bound to. There are two main explanations for this. Firstly, the interaction between Halo-tag and Halo resin requires proper-folding of Halo-tag (34 kDa) (Promega Corporation, 2015), thus if the protein folding is altered in *S. pombe* cells, or partial unfolding/proteolysis occurs in the process of cell lysis, the ability of the Halo-tagged protein to bind the resin will be dramatically reduced or lost completely. To try and counter this potential problem, I attempted to optimize the cell lysis procedure using a variety of cell disruption techniques, including bead beating using a FastPrep machine, French pressing and cryogrinding. However, none of these techniques gave any improvement in the binding of Halo-Rtf1 to HaloLink resin.

The second explanation that could account for the poor binding of Halo-Rtf1 to HaloLink resin is that the interaction between tag and resin may be inhibited by some of the components of *S. pombe* that are released during cell lysis. Interestingly, there have been no reports of Halo tag being used for the purification of proteins from yeast extracts. It has, however, been used in both budding and fission yeast for labelling cells using Halo compatible fluorescent ligands (Kitamura et al., 2011; Stagge et al., 2013). In support of the idea that there may be factors present in yeast extracts that inhibit the interaction between Halo tag and HaloLink resin, Halo-tagged proteins in crude extracts from *S. cerevisiae* did not bind to HaloLink resin, whereas His-tagged affinity-purified *S. cerevisiae* proteins did (personal communication, Dr. Johanna

Scheinost, Nasmyth laboratory). These findings suggest that the Halo-tag cannot be used for pulling down Rtf1, and associated proteins and DNA, and, therefore, alternatives should be found. To this end I tested whether SpyTagged Rtf1 could be used, but under the conditions that I tested the binding between SpyTag and SpyCatcher was inefficient resin (Fig. 3.4B). Due to time constraints, I did not proceed further with the optimisation of Rtf1 pull-down. However, future work should include optimisation of SpyTagged Rtf1 pull-down using its interaction with SpyCatcher in solution followed by immobilisation of the complex. Additional tags, which covalently bind to their cognate resin, such as SNAP and CLIP tags, should also be tested for their utility in purifying Rtf1 from *S. pombe* extracts.

The utility of the Co-IP method is restricted due to difficulties in obtaining native protein extracts from *S. pombe* where weak protein-protein interactions are preserved. The protocol for native lysis therefore has to be optimized for each protein, depending on its abundance in the cell, its stability and solubility, its localization and ability to bind to DNA. I found that cell disruption by bead beating was insufficient for extraction of Mhf1 or Fml1 probably because this method is not particularly efficient in releasing chromatin-bound proteins. In contrast, both cryo-grinding and lysis using a French press in the presence of Benzonase produced extracts with detectable amounts of Mhf1-Halo, Elg1-TAP, Fml1-13myc and Fml1-TAP. Both methods are likely to provide better shearing of DNA and, together with Benzonase, these methods should efficiently solubilize the chromatin fraction.

My data for the Co-IP of Mhf1 and Elg1 suggests that there is no direct interaction between Mhf1 and Elg1 resin (Fig. 3.5B). However, the protein extract came from an asynchronously growing culture of cells and, therefore, if the interaction between Mhf1 and Elg1 is cell cycle dependent it may be under-represented in the sample that was analysed. Further studies should test if an interaction between Elg1 and Mhf1 can be detected specifically in S-phase cells or in cells that have been exposed to agents that cause replication stress.

Elg1 was precipitated by anti-Myc antibody in the presence of Fml1-13Myc resin (Fig. 3.5A), which suggests that Elg1 and Fml1 might interact *in vivo.* Fml1 was previously shown to play a key role in promoting recombination following RF blockage at *RTS1*, and recent unpublished work from the Whitby laboratory has also shown that Elg1 is needed for the timely recruitment of Rad52 to the barrier. Elg1 may be needed for efficient RF collapse at *RTS1*, and at the same time help recruit Fml1-MHF to remodel the RF and kick-start recombination. The interaction should be confirmed by the reciprocal immunoprecipitation of Fml1 by Elg1, and by testing additionally whether Elg1-TAP binds non-specifically the Myc-resin as it binds non-specifically Halo-tag resin. If the interaction is confirmed the future work should be focused on mapping and mutating the residues needed for this interaction to study their importance for recombination at *RTS1*.

S. pombe and *S. cerevisiae* are only distant relatives, being about as divergent from each other as each is to animals (Heckman et al., 2001; Sipiczki, 2000). This means that any conservation of molecular function that is found between

them is a strong indicator that that molecular function is likely to be conserved in humans as well. Therefore, my finding that Smc5 immunoprecipitated with Fml1 resin (Fig. 3.6), together with the previous finding that Mph1 interacts with Smc5 in *S. cerevisiae* (Xue et al., 2014) suggests that this interaction may be conserved in higher eukaryotes, including humans. However, it will be important that the interaction in *S. pombe* is confirmed by reciprocal IP using HA-antibodies. If confirmed, the molecular mechanism of this interaction and regulation of Fml1 activity by Smc5-Smc6 should be addressed in future studies.

Chapter 4

4 Investigating the role of Dbl2 in the maintenance of genome stability

4.1 Introduction

Dbl2 was first identified in a screen for *S. pombe* mutants defective in chromosome segregation during meiosis (Gregan et al., 2005) and later in a proteome-wide visual screen for proteins localizing to HO endonuclease-induced DSB (Yu et al., 2013). Dbl2 is conserved in fungi, animals and plants. Dbl2 is required for normal DSB targeting of the DNA-repair helicase Fml1 (Yu et al., 2013) and for proper segregation of chromosomes during meiosis conceivably by recruitment of the helicase Fbh1 to the sites of DSB repair to dissociate a minor class of joint molecules (Polakova et al., 2016). Furthermore, there have been recent reports of a role for Mte1 (the budding yeast orthologue of Dbl2) in regulating the anti-crossover and RF regression activities of Mph1 (the budding yeast ortholog of Fml1) (Silva et al., 2016; Xue et al., 2016). I was intrigued to know whether Dbl2 also plays an important role in mitotic recombination and wanted to further investigate its role in DNA repair. In this chapter I will describe a series of genetic experiments in which I characterise the mitotic phenotype of a *dbl2*Δ mutant.

4.2 Results

4.2.1 The deletion of the *dbl2* gene generates two types of strains

To investigate the role of Dbl2 in mitotic cells, I replaced the entire Dbl2 gene in a wild-type strain by homologous integration of a linear DNA fragment harbouring a geneticin resistance marker cassette flanked by the 5' and 3' untranslated regions (UTR) of the *dbl2* genomic locus (Fig. 4.1A). Stable,

geneticin resistant transformants can arise by homologous recombination with the target locus (desired outcome) or by non-homologous integration of the cassette elsewhere in the genome. Transformants were screened for correct integration of the DNA construct by colony PCR (Fig. 4.1B). Surprisingly, cytological examination revealed that all transformants with confirmed correct integration could be divided into two classes based on their different morphological phenotypes. The first class contained a high proportion of elongated cells (26 % of cells were longer than normal haploid cell division length (~ 14 μm)), whereas, the second class were similar in length to the parental wild-type strain (Fig. 4.2A and Fig. 4.2B). Staining with the DNA-specific dye DAPI showed that 17% of cells in the first class were either anucleate or contained fragmented DNA, and 57 % of the septated cells contained DNA segregating unevenly between the two daughters (Fig. 4.2A and Fig. 4.2C). Intriguingly, 10 % of cells exhibited a characteristic “figure-eight” nuclear region, in which all DAPI-stained DNA material is distributed between two closely associated or connected compartments: one circular domain with the majority of DNA and a less stained second circular domain (Fig. 4.2B). In contrast, the second class of *dbl2*Δ transformants again did not show any obvious differences, in DNA segregation or nuclear morphology, with wild-type. The isolation of two classes of strains suggests that *dbl2*Δ cells may readily acquire a suppressor mutation(s) and, henceforth, I will refer to Class 1 *dbl2*Δ strains as *dbl2*Δ or *dbl2*Δns when compared to the suppressed class, and Class 2 as *dbl2*Δs.

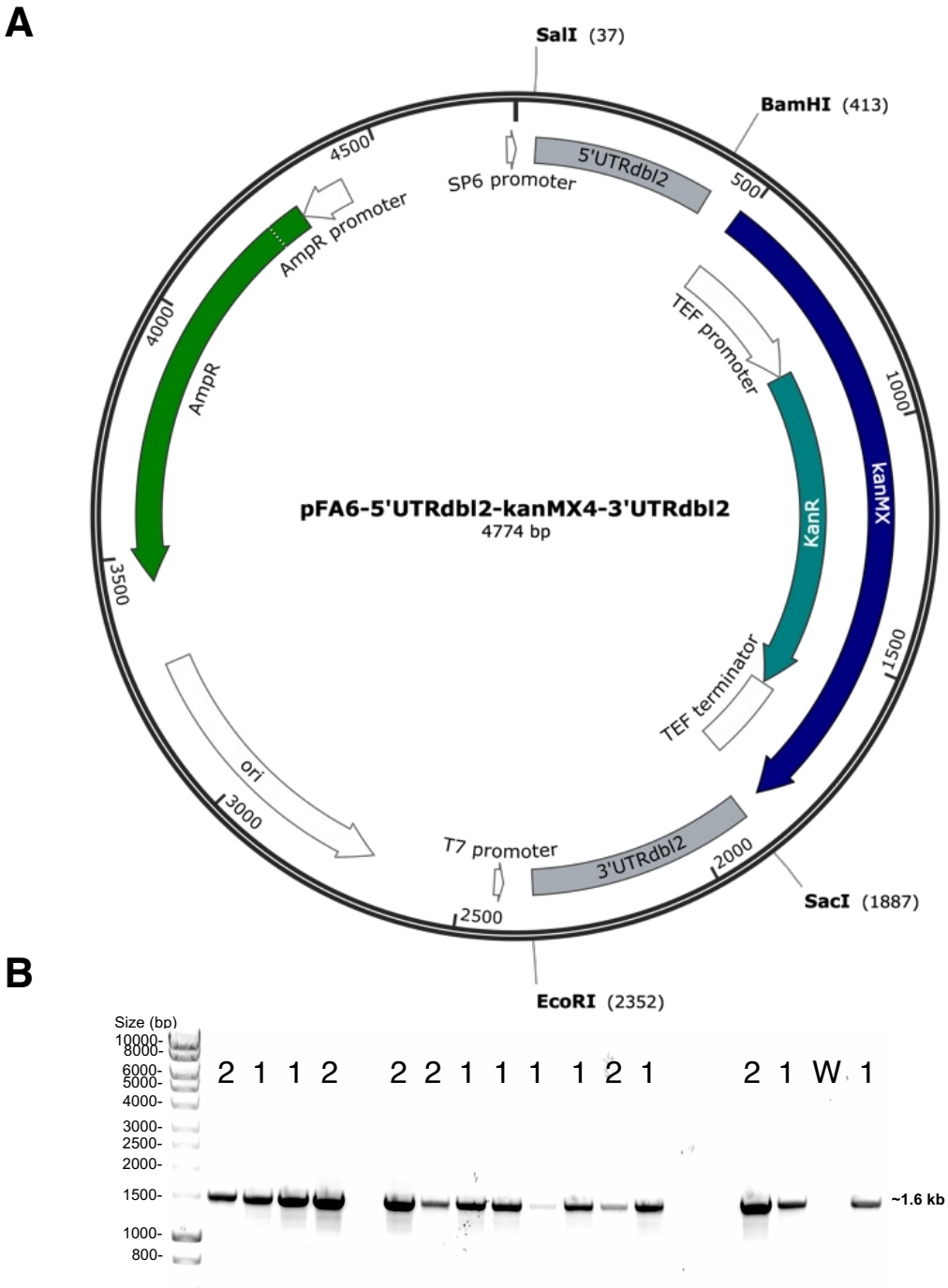
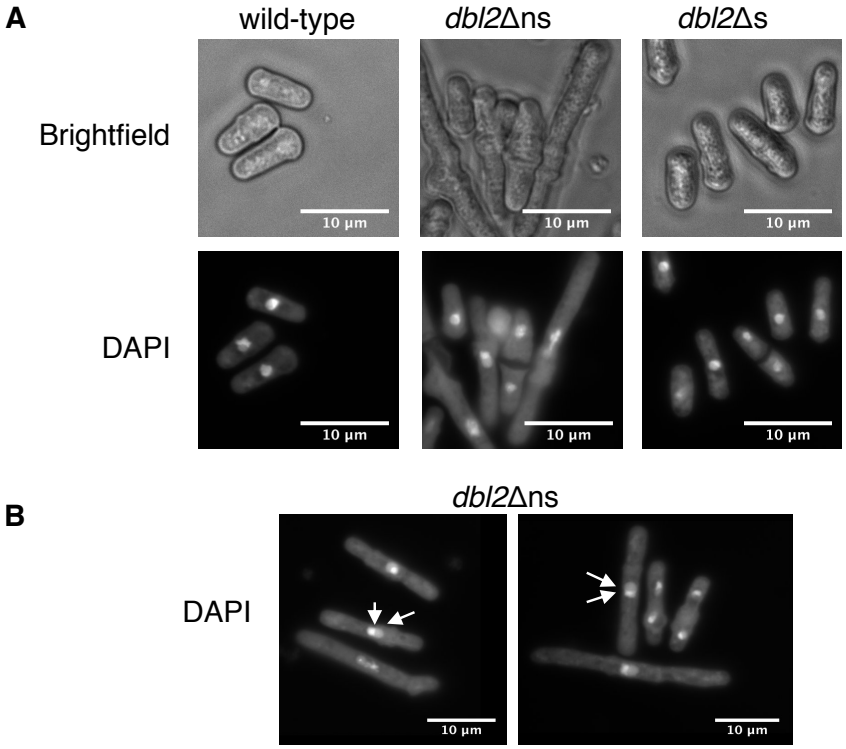


Figure 4.1. Constructing a *dbl2*Δ strain.

(**A**) Schematic showing the plasmid used to generate linearized fragment for the replacement of *dbl2* gene. (**B**) Colony PCR with primers oMW805, oMW1841 amplifying part of *kanMX6*, 3'UTR of *dbl2* and ~ 100bp region downstream 3'UTR of *dbl2.* A 1.6 kb fragment was amplified, corresponding to the construct integrated at the right locus. From left to right different transformants with Class 1 (1) (non-suppressed) or Class 2 (2) (suppressed) phenotypes were screened. W corresponds to a wild-type used as a negative control. Isolate 1 has suppressed phenotype and was saved as MCW8563. Isolate 2 has non-suppressed phenotype and was saved as MCW8564.



C

	wild-type	dbl2Δns	dbl2Δs
% long cells	<0.1	24.7	<0.1
% very long cells	<0.1	3	<0.1
% anucleate cells	1	5	2.5
% not septated binucleate cells	1	5.5	1.9
% cells with fragmented DNA	0.8	11.2	1.1
%cells septated cells with aberrant chromosome generation	<0.1	56	14.2
% cells with figure-of-eight nucleus	0.8	11.5	3.6

Figure 4.2. The deletion of the *dbl2* generates two types of strain with mutant (Class 1 – non-suppressed) and wild-type (Class 2 – suppressed) cell morphology and chromosome segregation phenotypes.

(**A**) Examples of phase-contrast and fluorescence microscopic images of wild-type and DAPI stained *dbl2*Δ cells taken from asynchronously growing cultures. (**B**) Fluorescence microscopic images of DAPI-stained *dbl2*Δ cells with a figure-eight nucleus. The arrows indicate the two circular nuclear domains. (**C**) Comparison of cell morphology and DNA segregation in *dbl2*Δns and *dbl2*Δs mutant growing at 30 °C in minimal medium. Long cells are 14 to 28 µm in length, and very long cells are >28 µm. Septated cells were scored as having aberrant chromosome segregation if they displayed an unequal distribution of DNA between the two daughter cells or if the DNA was fragmented or bisected by the septum. For each strain at least 600 cells were assessed.

The aberrant cell morphology and defects in chromosome segregation observed in the *dbl2*Δns strains is reminiscent of the *fbh1*Δ mutant which exhibits an increased number of anucleated and elongated cells and cells with 'figure-eight' nuclei (Osman et al., 2005). Moreover, like *dbl2*Δ, *fbh1*Δ strains readily acquire suppressor mutations. Altogether, these findings suggest that Dbl2 might act in the same pathway as Fbh1 – a possibility that will be investigated in Chapter 5.

4.2.2 The non-suppressed *dbl2*Δ is hypersensitive to genotoxins

To further examine the non-suppressed and suppressed *dbl2*Δ strains, I tested their sensitivity to a range of different genotoxins (Fig. 4.3). Both mutants exhibited similar growth to a wild-type strain on the YES control plate. However, non-suppressed *dbl2*Δ exhibited hypersensitivity to the topoisomerase I (TopI) inhibitor camptothecin (CPT) and, to a lesser extent, to the alkylating agent Methyl methanesulfonate (MMS), whereas, the suppressed *dbl2*Δ strain was as resistant as the wild-type. Neither mutant exhibited hypersensitivity to the ribonucleotide reductase inhibitor hydroxyurea (HU) or ultraviolet light (UV). To demonstrate that the *dbl2*Δ phenotype is indeed caused by the deletion of the gene, I overexpressed the *dbl2* gene from the thiamine-repressible *nmt* promoter in plasmid pREP41. In the presence of thiamine, the *nmt* promoter is repressed, and under these conditions the pREP41-*dbl2* plasmid has little or no effect on the wild-type strain genotoxin sensitivity but complements the MMS and CPT hypersensitivity of the *dbl2*Δ mutant (Fig. 4.4).

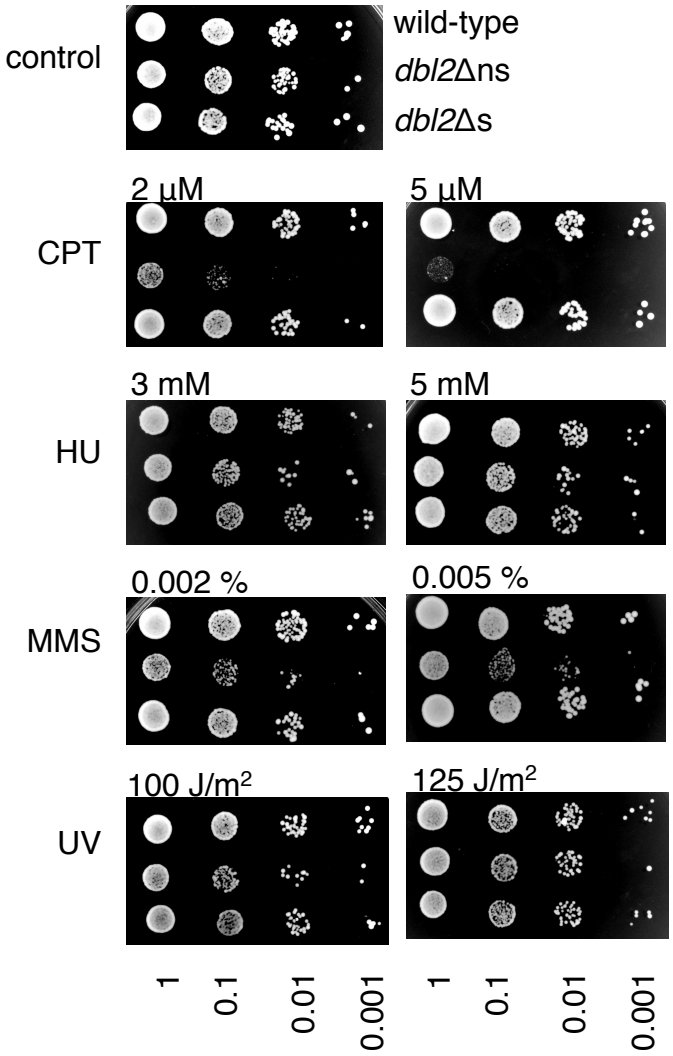


Figure 4.3. Genotoxin sensitivity of non-suppressed and suppressed *dbl2*Δ strains.

Spot assay comparing the growth and genotoxin sensitivity of wild-type (FO656), *dbl2*Δ non-suppressed (MCW8564) and *dbl2*Δ suppressed (MCW8563) strains. The plates were photographed after 4 days of incubation at 30°C.

The *nmt41* promoter is leaky and, therefore, still drives some expression even in the presence of thiamine (Forsburg, 1993). Presumably the low levels of Dbl2 produced from pREP41-*dbl2* in the presence of thiamine are sufficient to rescue *dbl2*Δ sensitivity to MMS and CPT. In the absence of thiamine, when the *nmt41* promoter is de-repressed, the induced expression of *dbl2* causes slower growth and hypersensitivity to CPT, HU, MMS and UV in the wild-type strain compared to the same strain carrying the empty pREP41 plasmid.

These toxic effects of *dbl2* overexpression largely mask the positive effects of restoring Dbl2 to the *dbl2*Δ mutant. However, even under these conditions partial rescue of MMS hypersensitivity is observed.

Altogether, these data show that the genotoxin hypersensitivity of the non-suppressed *dbl2*Δ strain can be rescued by expressing *dbl2* from a plasmid, which strongly indicates that this phenotype is due to the loss of *dbl2* rather than the strain acquiring some additional mutation in another gene. Therefore, unless otherwise stated, the genetic characterization of Dbl2 described in this thesis will focus on non-suppressed *dbl2*Δ strains.

4.2.3 Once acquired *dbl2*Δ suppression is stably inherited

One explanation for the difference between suppressed and non-suppressed *dbl2*Δ strains is that the former is in fact a heterozygous diploid strain, which still carries a copy of *dbl2*. Even a homozygous *dbl2*Δ diploid strain might exhibit a different phenotype to a *dbl2*Δ haploid strain; for example, it is known that diploid yeast strains are more resistant to genotoxins than haploids (Gangloff et al., 2000; Barbour et al., 2006).

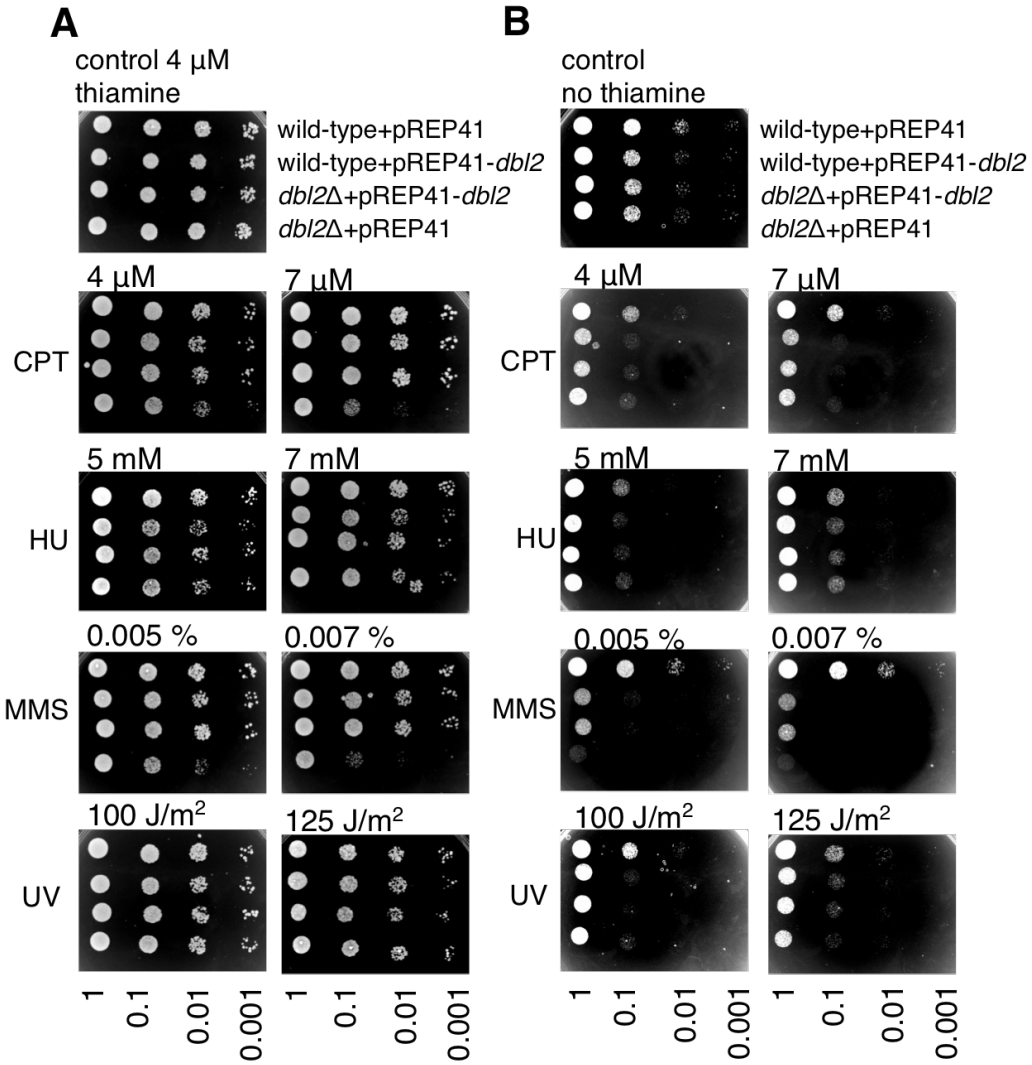


Figure 4.4. Overexpression of Dbl2 at *nmt41* levels sensitizes wild-type cells to genotoxins and partially complements *dbl2*Δ hypersensitivity to MMS.

Spot assay comparing the growth and genotoxin sensitivities of wild-type (FO656) and *dbl2*Δ (MCW8564) carrying the indicated plasmids. The plates were photographed after 4 days of incubation at 30°C.

To rule out the possibility that a difference in ploidy underlies the difference between suppressed and non-suppressed *dbl2*Δ strains, I examined the DNA content of both strains by flow cytometry. Both strains were haploid (data not shown).

Having ruled out ploidy as a cause of the difference between suppressed and non-suppressed *dbl2*Δ strains, it was increasingly likely that suppressed *dbl2*Δ had indeed acquired a suppressor mutation during its creation. It is known that sick strains readily acquire suppressor mutations that restore near normal levels of growth and viability (Hawthorne and Leupold, 1974), for instance both the poor growth and genotoxin sensitivity of a *fbh1*Δ mutant can be suppressed by the deletion of *rad52* (Osman et al., 2005).

To determine whether the suppressed *dbl2*Δ strain (MCW8563) carries a suppressor mutation, I backcrossed it to a wild-type strain to see if it is possible to derive *dbl2*Δ segregants that would be as sensitive to genotoxins as the non-suppressed *dbl2*Δ strain. 30 isolates from the cross were examined microscopically to see if they exhibited the characteristic elongated cell phenotype of the non-suppressed *dbl2*Δ strain, and 10 were also tested for genotoxin sensitivity (Fig. 4.5). However, all isolates that were tested exhibited wild-type cell morphology and sensitivity to genotoxins. In parallel the non-suppressed strain (MCW8564) was backcrossed to see if the suppressor can be acquired. 30 isolates from this cross were also examined microscopically and 10 were tested for genotoxin sensitivity. Indeed, the *dbl2*Δ non-suppressed strain readily acquires suppressors with 6 out of 10 tested isolates

being resistant to genotoxins (Fig. 4.5) and 17 out of 30 displaying no elongated cells.

Having established that a non-suppressed *dbl2*Δ strain can acquire a suppressed status by backcrossing to wild-type (i.e. during meiosis), I next determined whether the suppressor could also be acquired during vegetative growth. Non-suppressed *dbl2*Δ cells were streaked from glycerol stock onto YES plates and grown at 30°C for 5 days followed by a further 5 days at 25 °C. One colony from the plate was then restreaked onto a YES plate and incubated in the same way as the first plate. This cycle of restreaking was repeated a total of 5 times. Colonies from the initial and restreaked plates were tested for genotoxin sensitivity (data not shown) and examined cytologically. Out of 12 colonies that were examined, none had acquired a suppressed status (data not shown). Moreover, in my time working with *dbl2* mutant strains I never observed one becoming suppressed under vegetative growth conditions. These data suggest that *dbl2*Δ mutant strains can only acquire suppressor mutations during transformation or meiotic crosses but never during vegetative growth. Furthermore, once acquired, the suppressed status appears to be stably inherited.

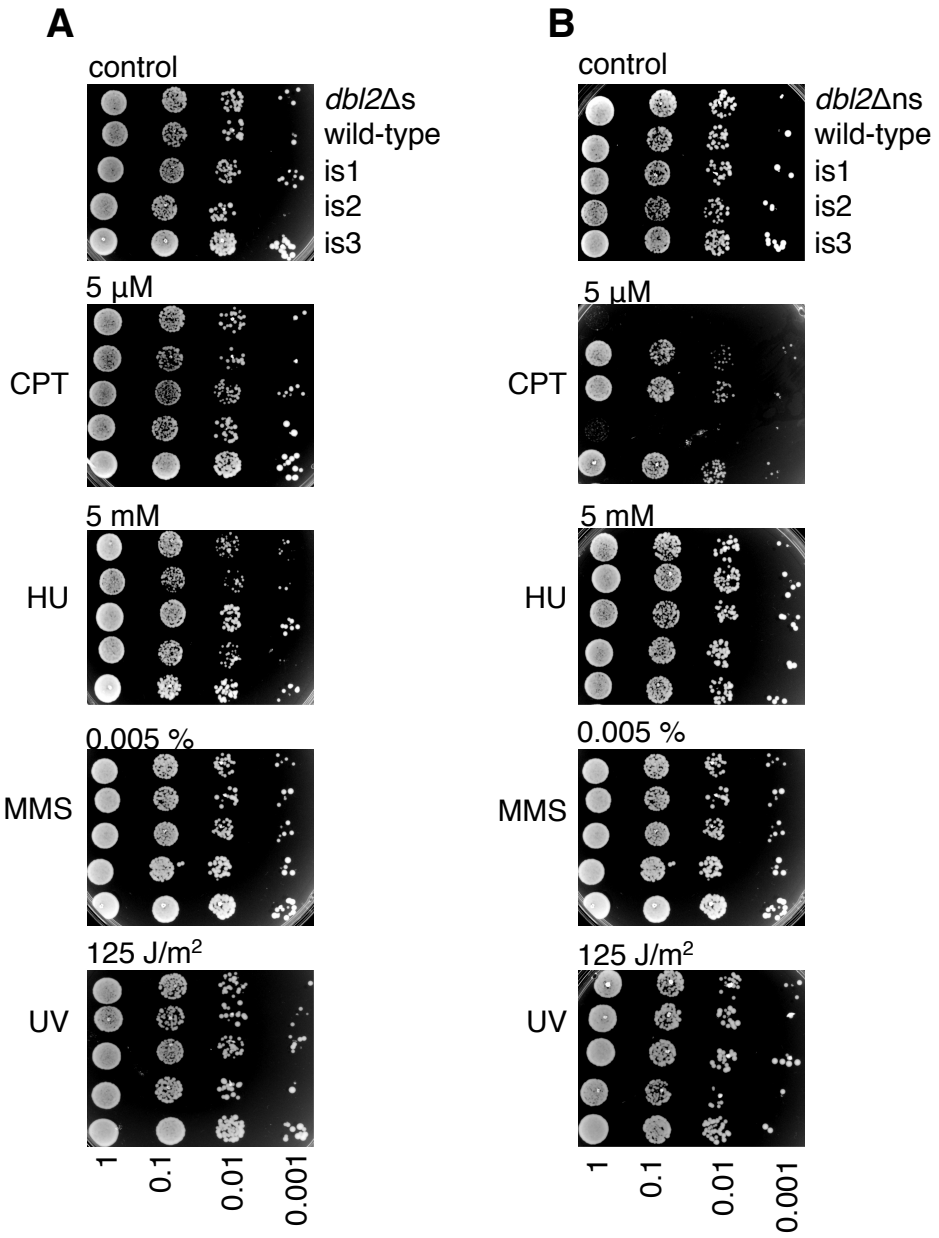


Figure 4.5. Backcrossing to wild-type does not restore genotoxin hypersensitivity to a suppressed *dbl2*Δ strain but does lead to genotoxin resistance amongst non-suppressed *dbl2*Δ progeny

(**A**) Example spot assay comparing the growth and genotoxin sensitivities of *dbl2*Δ suppressed (MCW8563) and segregants obtained in its backcross to a wild-type strain (FO652). (**B**) Example spot assay comparing the growth and genotoxin sensitivities of *dbl2*Δ non-suppressed (MCW8564) and segregants obtained in its backcross to a wild-type strain (FO652). The plates were photographed after 4 days of incubation at 30 °C.

4.2.4 Attempts to identify the *dbl2*Δ suppressor

One possible explanation for the apparent inability to backcross the putative suppressor mutation away from *dbl2*Δ is that they are genetically linked. Genetic linkage is the notable exception to Gregor Mendel's Law of Independent Assortment when the probability for the two genetic markers to be separated onto different chromatids by meiotic recombination is very low due to their physical proximity. The *dbl2* gene is located on Chromosome III with coordinates 310,158312,895 (including UTRs), I therefore scrutinised the genes located nearby (from 210,000 – 410,000 bp) (Fig. 4.6) to see if I could identify candidate suppressors. I reasoned that in order to be a suppressor the gene should fulfil at least one of the following criteria: have known functions in DNA repair or homologous recombination or in processing DNA intermediates; encode a protein that has genetic/physical interactions with DNA repair or homologous recombination proteins; have phenotypes that include genotoxin sensitivity and/or abnormal chromosome segregation. Four genes satisfied at least one of the above criteria:

tfx1 – protein product TRAX (330,444 – 329,749 bp, ~ 16.9 kb away from the *dbl2*). TRAX is a Translin paralog that associates with Translin. Translin and Trax proteins are highly conserved nucleic acid binding proteins that have been implicated in a range of biological processes including tRNA processing (Gomez-Escobar et al., 2016) and DNA repair (Wang et al., 2016).

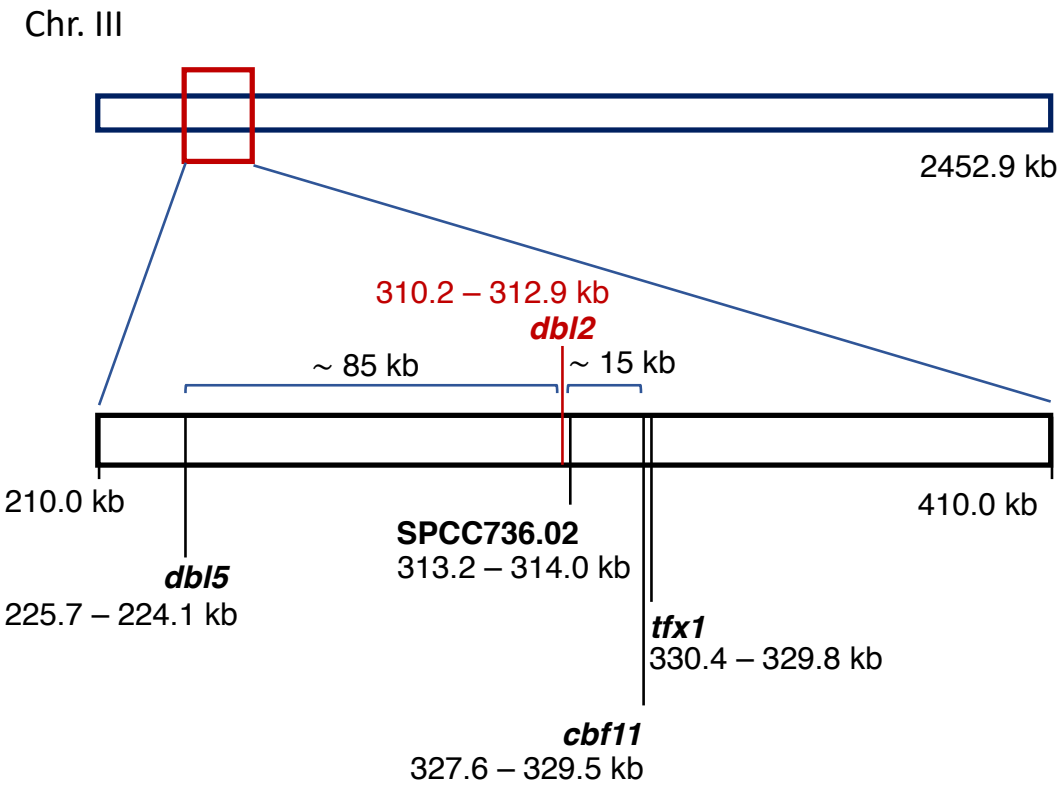


Figure 4.6. Schematic showing the relative position on *S. pombe* chromosome III of candidate *dbl2* suppressor genes.

cbf11 (327,542 – 329,461 bp, ~14.7 kb from the *dbl2* gene) encodes a conserved eukaryotic transcription factor. Vegetative cells with deleted *cbf11* are abnormally shaped (Hayles et al., 2013), elongated and multiseptated (Převorovský et al., 2015). *cbf11*Δ mutants exhibit an abnormal meiotic chromosome segregation phenotype (Blyth et al., 2018). Furthermore, Cbf11 is affinity captured by Fml1 (Pancaldi et al., 2012).

SPCC736.02 (313,183 – 314,043 bp, ~0.3 kb) encodes an uncharacterized *Schizosaccharomyces* specific protein. Deletion of this gene confers hypersensitivity to CPT (Han et al., 2010), an abnormal meiotic chromosome segregation phenotype (Blyth et al., 2018) and a negative genetic interaction with *rad57*Δ (Ryan et al., 2012).

dbl5 (225,643 – 224,087 bp, 84.5 kb from the *dbl2* gene) – encodes a conserved E3 ubiquitin ligase and was identified in a genome-wide screen for proteins localizing to HO-induced DSBs (Yu et al., 2013).

To identify if any of the aforementioned genes were mutated in the suppressed *dbl2*Δ strain, I amplified them from genomic DNA and then sequenced them. The sequences were identical to those obtained from a wild-type and suppressed *dbl2*Δ strain indicating that the suppression of *dbl2*Δ is not caused by a mutation in any of the selected candidate genes.

4.2.5 A putative prion state of Fml1 is not responsible for the suppression of *dbl2*Δ

Another possible explanation for the observed non-Mendelian segregation of the *dbl2*Δs phenotype in genetic crosses is prion-like patterns of inheritance. Prions are an alternative to the traditional inheritance by nucleic acids mechanism in which inheritance of the phenotype is directed by self-replicating protein conformations (Chakrabortee et al., 2016). The prion proteins can exist in a stable self-perpetuating conformational state that allows it to self-template from mother to daughters cells (McGlinchey et al., 2011; Jarosz et al., 2014). The [PRION^{+}] nomenclature reflects prion specific pattern of inheritance: square brackets denote a non-Mendelian meiotic segregation and capital letters indicate that the phenotype of the self-templating state of the protein is dominant (Chakrabortee et al., 2016). A recent study reported that Mph1 can adopt a prion state (Byers et al., 2017). [MPH1^{+}] is a gain-of-function trait, which exhibits resistance to DNA damage. Strikingly, the [MPH1^{+}] gain-of-function phenotypes and its ability to successfully propagate require its helicase-activity as well as its interaction partners – components of the yeast Fanconi anemia pathway. Because of the range of phenotypes observed as a result of one gain-of-function trait, Byers et al. (2017) suggested that [MPH1^{+}] drives various heritable changes not only in one specific protein but in DNA repair networks. The acquisition of [MPH1^{+}] occurred more frequently upon nucleotide starvation. It is known that some of the prions can have adaptive function (Suzuki et al., 2012), therefore the gain of function of [MPH1^{+}] provides survivability advantages and promotes diversification of the next

generation. Mph1 does not have structural features which are characteristic of prion proteins and unlike other known prion proteins, its intrinsically disordered regions are not enriched in glutamine/asparagine (Q/N) residues. However, the C-terminus of Mph1 encompasses long disordered region next to its helicase domains (Jones and Cozzetto, 2015) (Fig. 4.7). This pattern of disorder is conserved in the human ortholog FANCM (Fig. 4.7) as well as in fission yeast Fml1. Considering known interactions between Mph1 and Mte1 (Silva et al., 2016; Xue et al., 2016), and that Dbl2 is required for normal DSB targeting of Fml1 (Yu et al., 2013), the gain-of-function phenotype driven by putative [FML1^{+}] could be the phenotype that is observed in the suppressed *dbl2*Δ mutant.

To test this hypothesis, I performed, in parallel, genetic crosses of *dbl2*Δ suppressed and non-suppressed strains to *fml1*Δ to remove Fml1 protein from the strains. I hypothesized that, if Fml1 is responsible for the suppression of *dbl2*Δ, removing it should “re-set” the strain so that when backcrossed to wild-type to re-introduce *fml1* the former suppressed *dbl2*Δ strain would give rise to suppressed and non-suppressed progeny similar to a non-suppressed *dbl2*Δ strain. A total of 10 *dbl2*Δ*fml1*Δ progeny from each cross were isolated and then backcrossed to wild-type to restore *fml1*. A total of 200 *dbl2*Δ isolates from each of these crosses were then chosen at random and analysed microscopically and 10 of these were also screened for genotoxin sensitivity (Fig. 4.8).

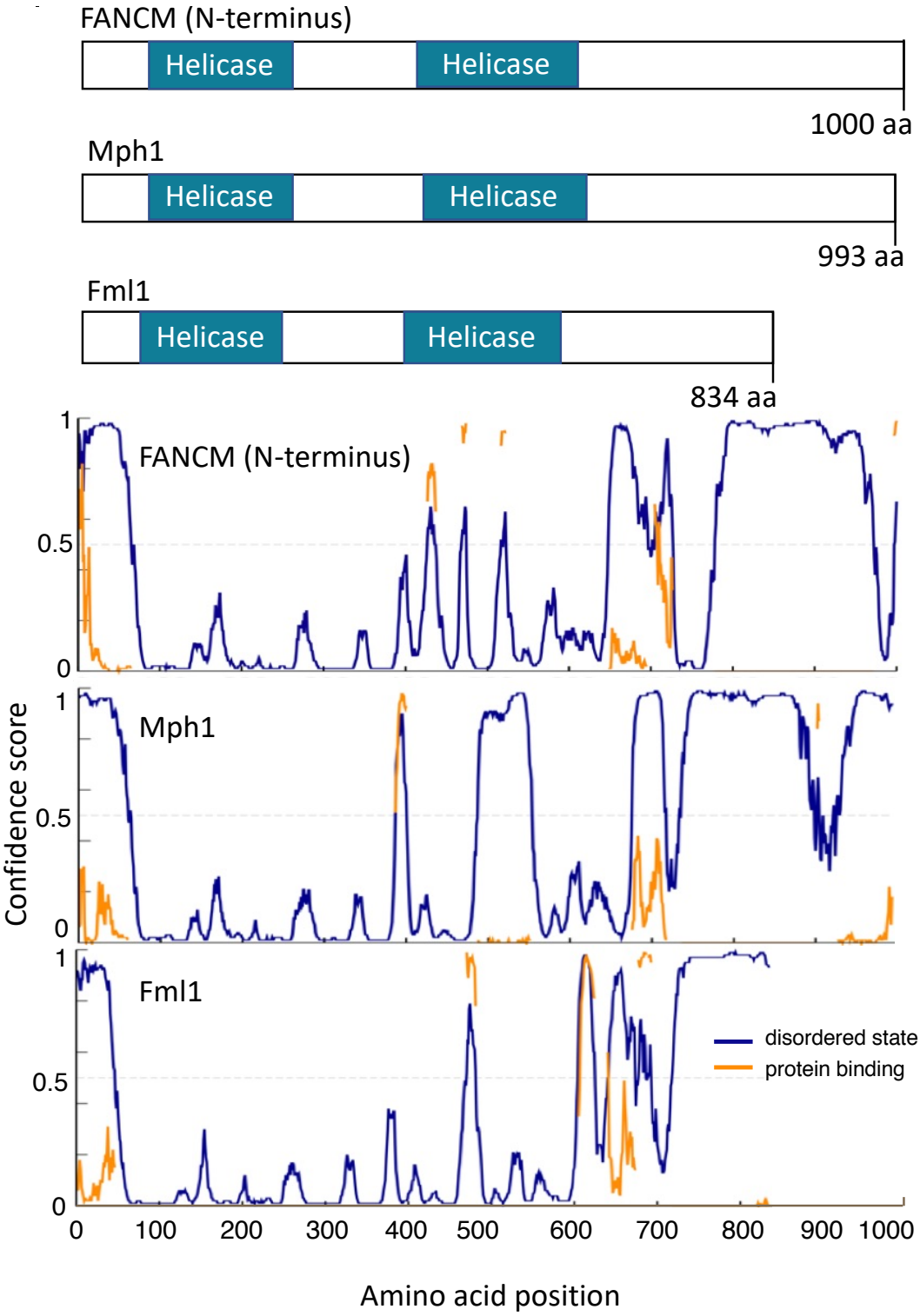


Figure 4.7. Patterns of intrinsic disorder are conserved in human FANCM, *S. cerevisiae* Mph1 and *S. pombe* Fml1.

Top: Graphical view of helicase domain location in human FANCM, *S. cerevisiae* Mph1, *S. pombe* Fml1. Bottom: Intrinsic disorder predictions (Disopred3; (Jones and Cozzetto, 2015)) for N-terminus of FANCM, Mph1, Fml1.

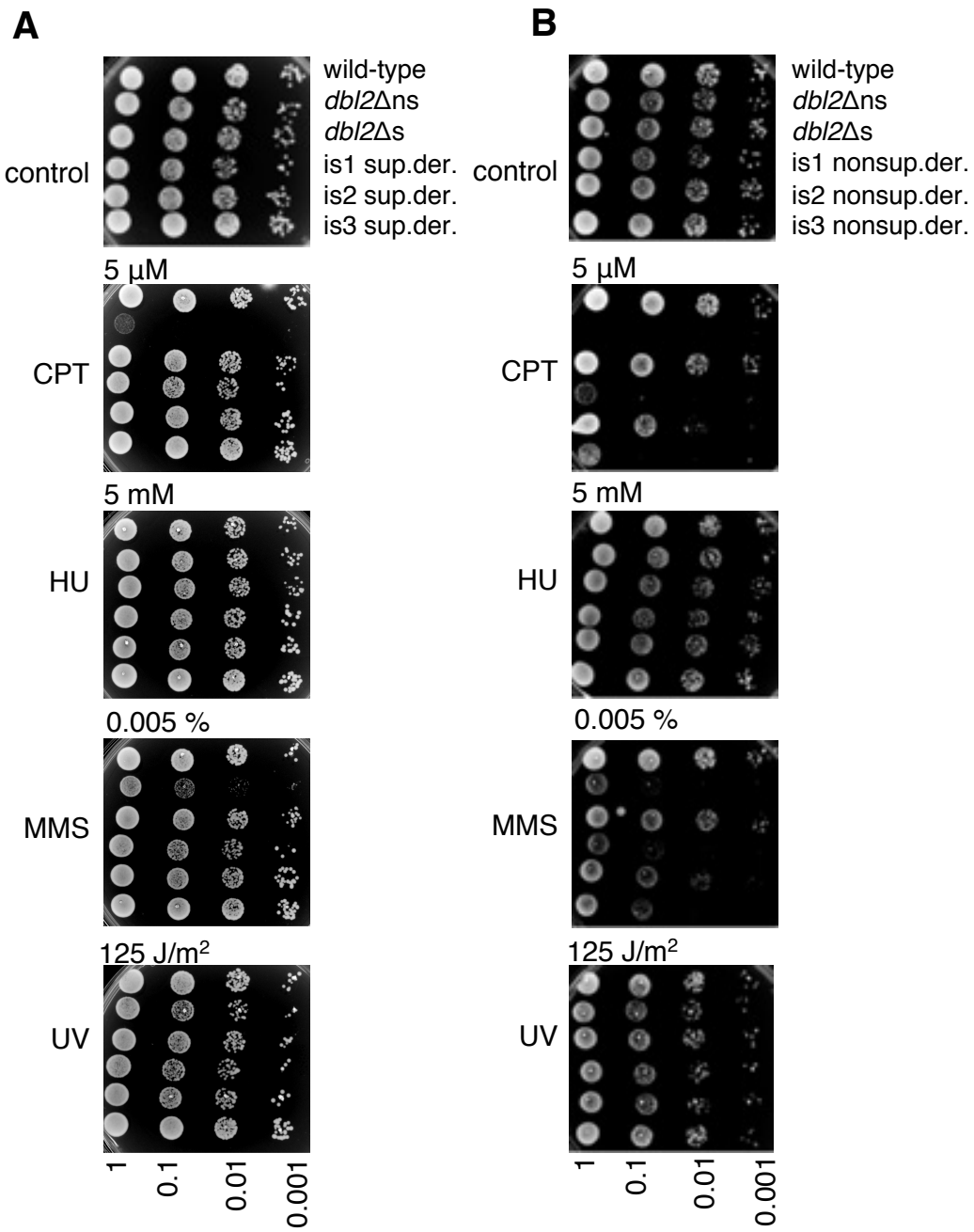


Figure 4.8. Removing and then restoring *fml1* does not affect the stable inheritance of the *dbl2*Δ suppressor.

Example spot assays comparing the growth and genotoxin sensitivities of *dbl2*Δ suppressed (MCW8563), *dbl2*Δ non-suppressed (MCW8564) and segregants obtained from the backcross of *dbl2*Δ *fml1*Δ derived from suppressed *dbl2*Δ (**A**) and from non-suppressed *dbl2*Δ (**B**) to a wild-type strain (FO652). The plates were photographed after 4 days of incubation at 30 °C.

As expected for the non-suppressed strain both suppressed and non-suppressed isolates were obtained (~ 24 % were suppressed as analysed microscopically and ~ 44 % when tested in the genotoxin sensitivity assay) whereas, for the suppressed strain only isolates with a suppressed phenotype were observed (Fig. 4.8A). These data indicate that the *dbl2*Δ suppressor is unlikely to be [FML1^{+}].

4.2.6 Dbl2 limits recombination at blocked replication forks

To measure inter/intra-chromosomal recombination caused by RF collapse at a site-specific RFB our laboratory employs the well-characterised site-specific *RTS1* barrier (Dalgaard et al., 2001). The *RTS1* sequence together with a *his3*$^{+}$ marker is placed between a direct repeat of *ade6*$^{-}$ heteroalleles at the endogenous *ade6* locus on chromosome III (Fig. 4.9A). *RTS1* is a polar RFB: it induces RF blockage at this site for the forks coming from one direction and is permissive to the uninterrupted passage of RFs from the opposite direction (Eydmann et al., 2008). At the direct repeat recombination reporter, replication is essentially unidirectional in the telomere-to-centromere direction due to the presence of a cluster of early firing strong replication origins located on the telomere proximal side of the reporter (Heichinger et al., 2006). Thus, the orientation of *RTS1* that blocks forks moving toward the centromere will be referred as the 'active orientation' (*RTS1-AO*), whereas the opposite orientation of *RTS1* that does not block forks moving toward the centromere will be referred as the inactive orientation (*RTS1-IO*) (Ahn et al., 2005). An Ade^{+} cell can only arise if recombination between the two different loss-of-

function *ade6*$^{-}$ alleles (*ade6-L469* and *ade6-M375*) restores the wild-type *ade6*$^{+}$ gene. This means the frequency at which an Ade^{+} cell is generated allows quantification of the recombination at this site. Ade^{+} recombinants can be divided into two classes: those that retain the *his3*$^{+}$ marker are conversion-types (Ade^{+}His^{+}); whereas those that lose it are deletion-types (Ade^{+}His^{-}) (Fig. 4.9A). Since only Ade^{+} recombinants are scored, this assay measures only ectopic recombination that restores a functional *ade*$^{+}$ allele and it is not representative of the total recombination occurring at the site. Nevertheless, it provides a robust readout for a subclass of recombination events occurring at the site (Osman et al., 2009). Previous studies have shown that *RTS1-AO* strongly induces Ade^{+} recombinants, whereas only spontaneous levels of recombinants are observed with *RTS1-IO* (Ahn et al., 2005; Lorenz et al., 2009; Nguyen et al., 2015).

To determine the role of Dbl2 in spontaneous and *RTS1*-induced recombination, I assessed the effect of *dbl2*Δ on the frequency of direct repeat recombination (Fig. 4.9B). In the wild-type strain the frequency of spontaneous Ade^{+} recombinants is approximately 4.57 x 10^{-4}. Approximately 31 % of these recombinants are conversion types. When *RTS1-AO* is positioned between the direct repeats (Site I) there is ~ 98-fold stimulation in gene conversions and ~ 33-fold increase in deletions as compared to *RTS1-IO* ($P < 0.001$) (Fig. 4.9B). Deletion of *dbl2* has no effect on spontaneous direct repeat recombination as measured by this assay (Fig. 4.9B).

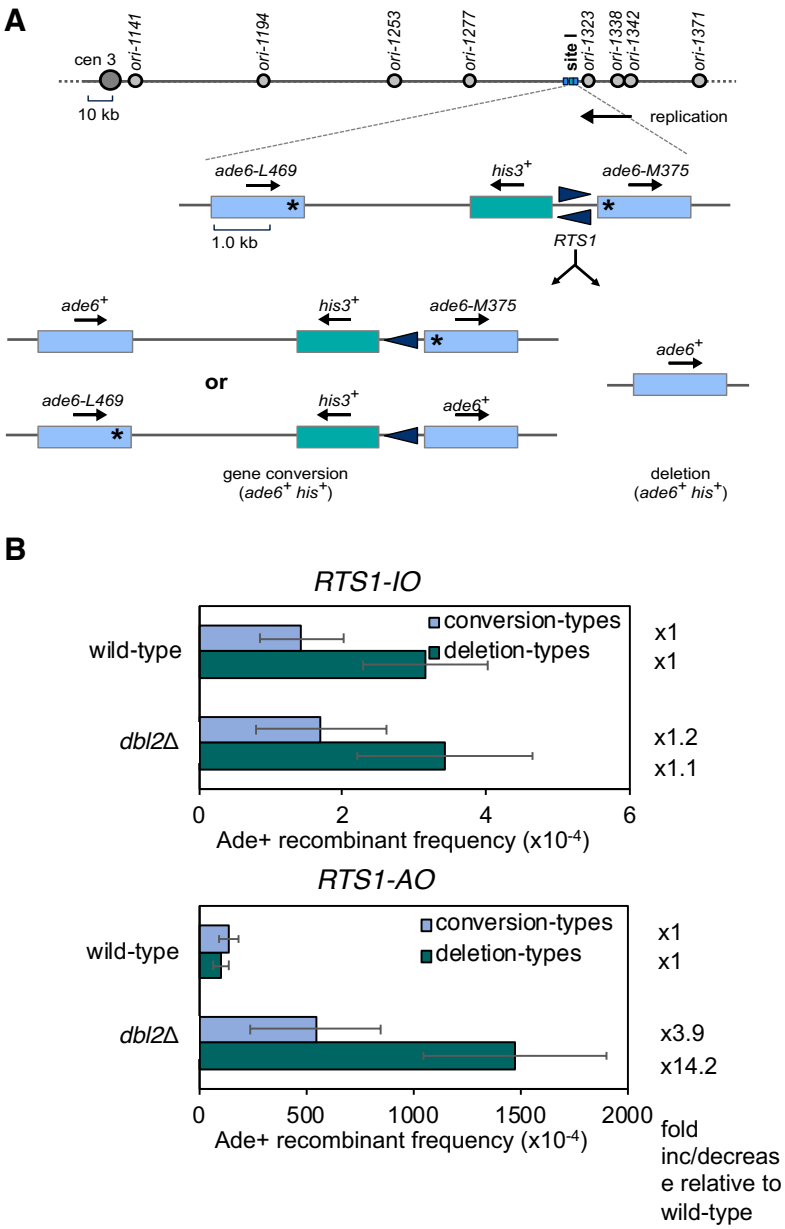


Figure 4.9. Dbl2 has a role in suppressing direct repeat recombination during replication fork block-induced recombination.

(**A**) Schematic showing the position of *RTS1* sequence together with an intervening *his3+* marker placed within a direct repeat of *ade6-* heteroalleles at the endogenous *ade6* locus on chromosome III. Replication is essentially unidirectional in the telomere to centromere (cen) direction. The *RTS1* barrier can be orientated such that forks emanating from the centromere-proximal direction are not impeded – *RTS1-IO* or blocked by the barrier – *RTS1-AO.* Possible *ade6+* recombinant products that may arise spontaneously, or be induced by blockage of the RF, are either gene conversions or deletions. Asterisks indicate the positions of the point mutations in *ade6-L469* and *ade6-M375*. (**B**) Bar chart showing the mean frequency of conversion- and deletion-type Ade+ recombinants in wild-type and *dbl2*Δ with either *RTS1-IO* or *RTS1-AO.* Error bars represent ± one standard deviation. In order of presentation, the strains are MCW4712, MCW8627, MCW4713, and MCW8628.

In contrast, when *dbl2* is deleted in the *RTS1-AO* strain the overall frequency of recombination is significantly increased (~ 8-fold relative to wild-type) ($P < 0.001$). Fork blockage at *RTS1* typically results in almost equal proportions of conversion and deletion types; however, in the *dbl2*Δ strain the majority of induced recombinants are deletion types. There is a ~ 14-fold increase in the frequency of deletions in *RTS1-AO* cells compared to wild-type but only ~ 4-fold increase in the frequency of conversions relative to wild-type. Taken together, these data suggest that Dbl2, similar to Fbh1, has a minor role in controlling recombinational repair of spontaneous lesions that occur during normal growth but has a more important role in limiting recombination associated with a RF that has collapsed at *RTS1*.

4.2.7 Dbl2 is not required for limiting template switching downstream of *RTS1-AO*

Native 2D gel electrophoresis analysis of replication intermediates containing *RTS1* confirms that *RTS1-AO* strongly blocks the passage of RFs. Approximately half the forks blocked at *RTS1* restart before fork converge according to estimations by Nguyen et al., (2015). *RTS1*-induced recombination-dependent replication (RDR) has been shown to be error-prone (Mizuno et al., 2013). To investigate whether the restarted from *RTS1* forks remain prone to recombination as they progress further from the RFB, and which factors are important for this property, the *ade6*$^{-}$ direct repeat was inserted 12.4 kb downstream of *RTS1* (Site II) and the frequency of Ade^{+} recombinants was measured (Fig. 4.10) (Nguyen et al., 2015). At site II, while

the frequency of recombination with *RTS1-IO* was similar to the spontaneous level, with *RTS1-AO* there was an increase of ~ 21-fold over the spontaneous level ($P < 0.001$) (Fig. 4.10B). The majority of recombinants were deletions although there was a noticeable increase (~ 6-fold) in gene conversions leading to the conclusion that at least some recombination is Rad51-dependent. The increase in Ade^+ recombinants can be attributed to frequent template switching associated with restarted replication. Restarted replication is thought to proceed by a migrating D-loop that is prone to dissociation, which results in recurrent recruitment of HR proteins such as Rad51 that can catalyse ectopic recombination (Iraqui et al., 2012; Mizuno et al., 2013). To determine whether Dbl2 affects template switching that is associated with restarted replication downstream of the barrier, I measured direct repeat recombination at site II downstream of *RTS1* in a *dbl2*Δ mutant (Fig. 4.10B). Like at site I, *dbl2*Δ had little or no effect on the frequency of spontaneous recombination, albeit deletions were slightly higher than in the wild-type. Surprisingly, *dbl2*Δ also had relatively little impact on the frequency of *RTS1-AO*-induced recombinants at site II, with no significant change in gene conversions and only a ~ 1.6-fold increase in deletions ($P \leq 0.015$). These data indicate that Dbl2 is not required for controlling template switch recombination associated with restarted replication.

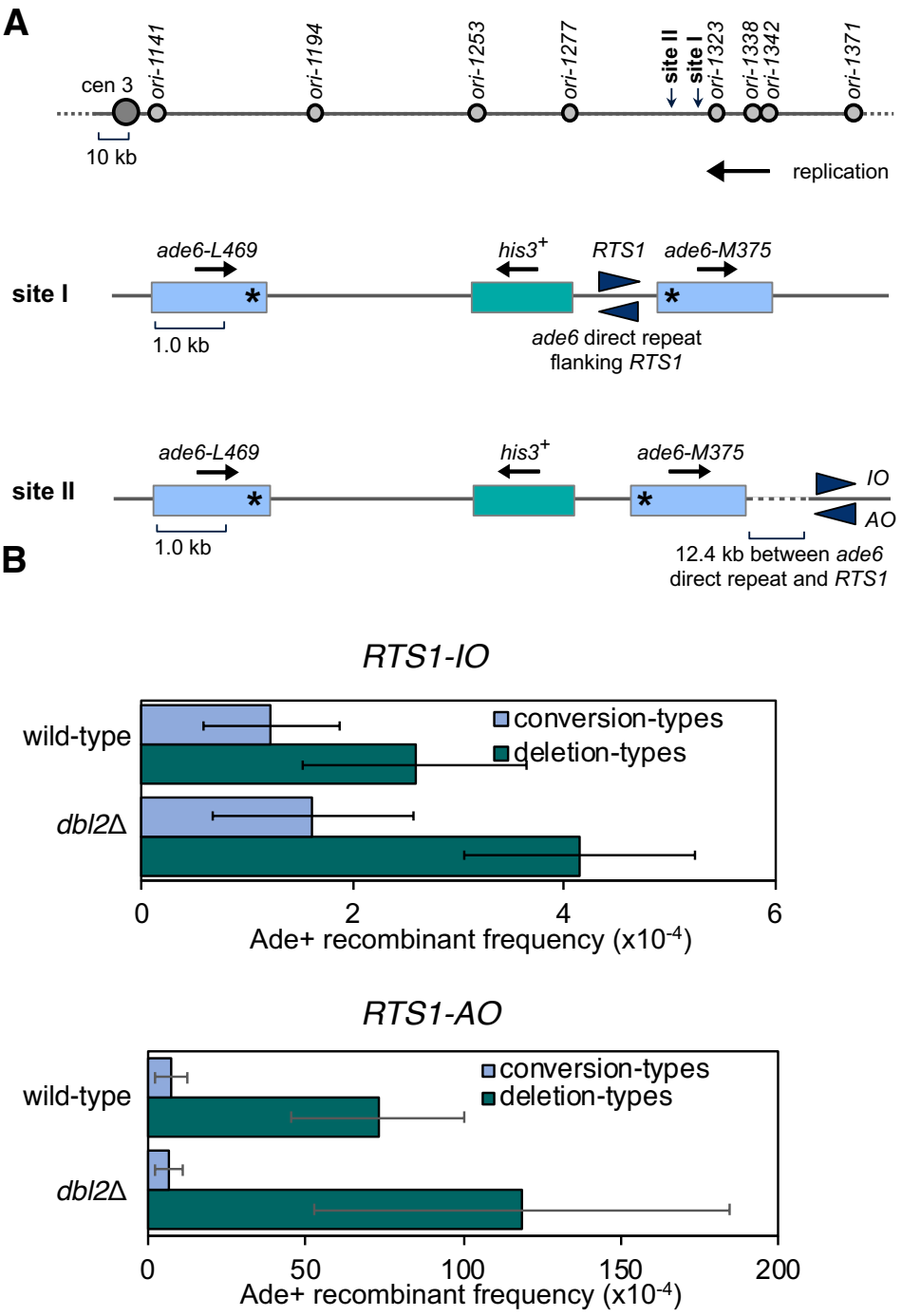


Figure 4.10. Template switching downstream of *RTS1* in wild-type and *dbl2*Δ strains

(**A**) Schematic showing the position of the *ade6*$^{-}$ direct repeat reporter positioned 12.4 kb downstream of *RTS1* on chromosome III. Note that the endogenous *ade6* gene has been replaced by *RTS1*. (**B**) Bar chart showing the mean frequency of conversion- and deletion-type Ade^{+} recombinants in wild-type and *dbl2*Δ with either *RTS1-IO* or *RTS1-AO* at Site II. Error bars represent ± one standard deviation. In order of presentation, the strains are MCW7258, MCW 9095, MCW7260, and MCW9096.

4.2.8 Dbl2 limits spacer dependent recombination

To investigate how the proximity of DNA repeats to the site of RF collapse influences inter-repeat recombination, the DNA spacer of 5 kb was added on either side of *RTS1* to expand the distance between the *ade6*$^{-}$ heteroalleles (Fig. 4.11A) (Morrow et al., 2017). The addition of DNA spacers on the centromere-proximal side of *RTS1-AO* leads to a dramatic increase in inter-repeat recombination, whereas no increase in spontaneous inter-repeat recombination is observed. Crucially, most of the extra recombinants (~ 90 %) are Rad51-independent but Rad52-dependent deletions (Morrow et al., 2017). RF convergence at *RTS1-AO* was shown to be needed to promote these extra deletions, which were dubbed “spacer-dependent deletions”. It was proposed that these deletions formed by a process termed Inter-Fork Strand Annealing, which would occur during non-canonical fork convergence (Morrow et al., 2017). Importantly, Fml1 was shown to limit spacer-dependent deletions. To determine if Dbl2 also has a role in either promoting or preventing deletion formation during RF convergence, I assessed the impact of *dbl2*Δ on Ade^{+} recombinant formation in strains containing the site I recombination reporter with an additional 5 kb DNA spacer between the *ade6*$^{-}$ repeats. As expected, the frequency of the deletions increased by ~ 7-fold with the addition of the 5 kb spacer in the wild-type strain ($P < 0.001$) (Fig. 4.11B). Similar, to the deletion of *fml1*, loss of *dbl2* lead to an increased frequency of deletions (~ 4-fold increase relative to wild-type with 5kb spacer strain, $P < 0.001$).

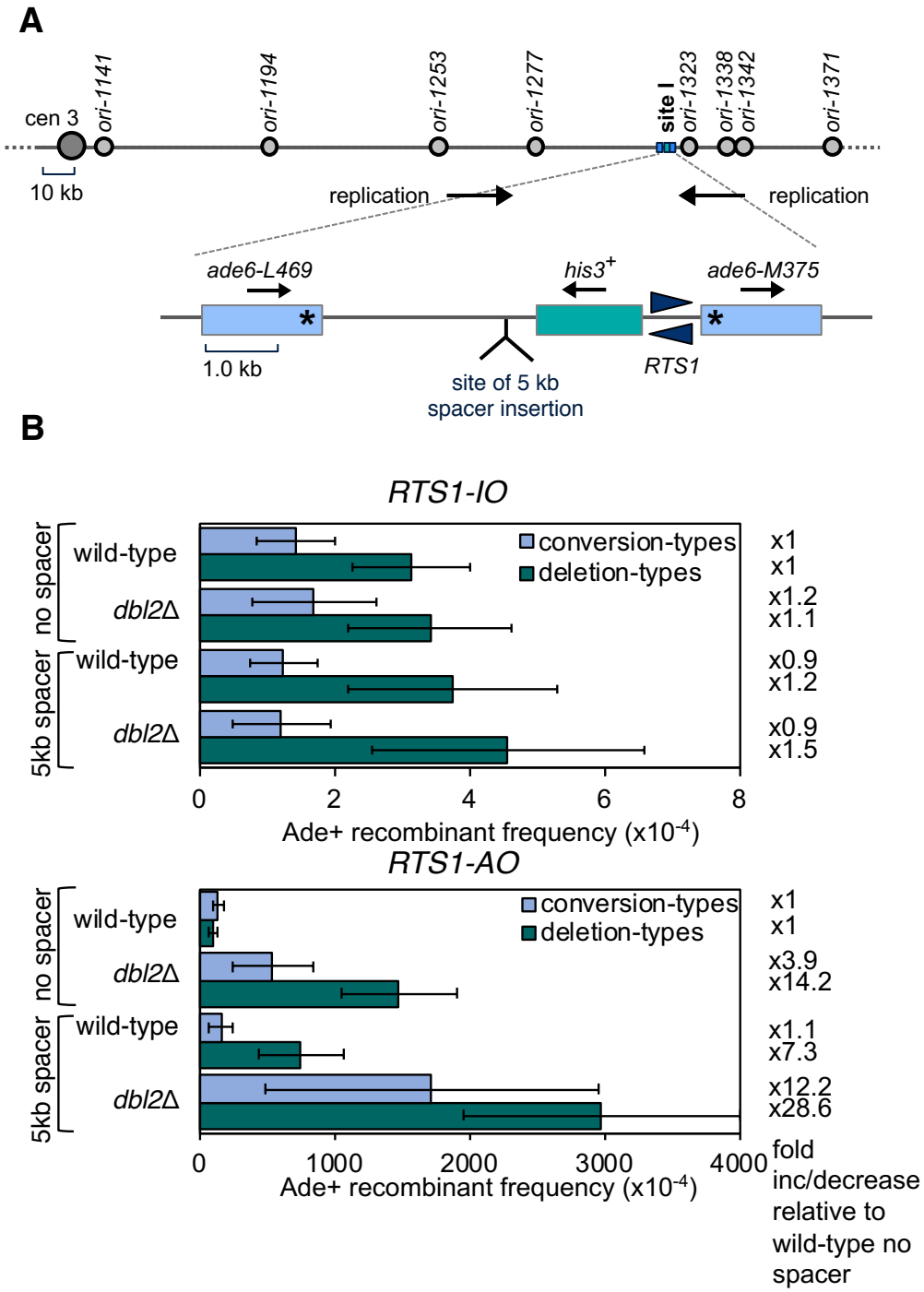


Figure 4.11. Dbl2 limits spacer dependent recombination

(**A**) Schematic showing the position of the *ade6*- direct repeat reporter on chromosome III and the site at which the 5 kb DNA spacer is inserted on the centromere-proximal side of *RTS1*. (**B**) Bar chart showing the mean frequency of conversion- and deletion-type Ade+ recombinants in wild-type and *dbl2*Δ with and without spacer. Error bars represent ± one standard deviation. In order of presentation, the strains are MCW4712, MCW8627, MCW8362, MCW8636, MCW4713, MCW8628, MCW 8023, and MCW9124.

However, unlike *fml1*Δ, *dbl2*Δ also caused a ~ 11-fold increase in gene conversions relative to the wild-type 5kb spacer strain ($P < 0.001$) (Fig. 4.11B). These data indicate that Dbl2 plays a role in suppressing SDDs and spacer-dependent gene conversions.

4.2.9 The suppressed *dbl2*Δ strain exhibits reduced levels of *RTS1-AO*-induced recombination

To see whether suppressed *dbl2*Δ has the same effect on *RTS1-AO*-induced recombination as non-suppressed *dbl2*Δ, I crossed the suppressed *dbl2*Δ strain with the site I reporter strains carrying either *RTS1-IO* or *RTS1-AO* and measured the Ade^+ recombinant frequencies in the resulting strains (Fig. 4.12). Similar to non-suppressed *dbl2*Δ, suppressed *dbl2*Δ had no effect on spontaneous recombination. However, in stark contrast to non-suppressed *dbl2*Δ, suppressed *dbl2*Δ exhibits a reduction in *RTS1-AO*-induced recombination compared to wild-type. Specifically, there is ~ 5-fold decrease in the frequency of gene conversions ($P < 0.001$) and ~ 2-fold decrease in the frequency of deletions ($P < 0.001$). These data indicate that the suppressor of *dbl2*Δ not only compensates for the lack of Dbl2 in tolerating and/or repairing DNA damage, but also inhibits recombination induced by *RTS1-AO*.

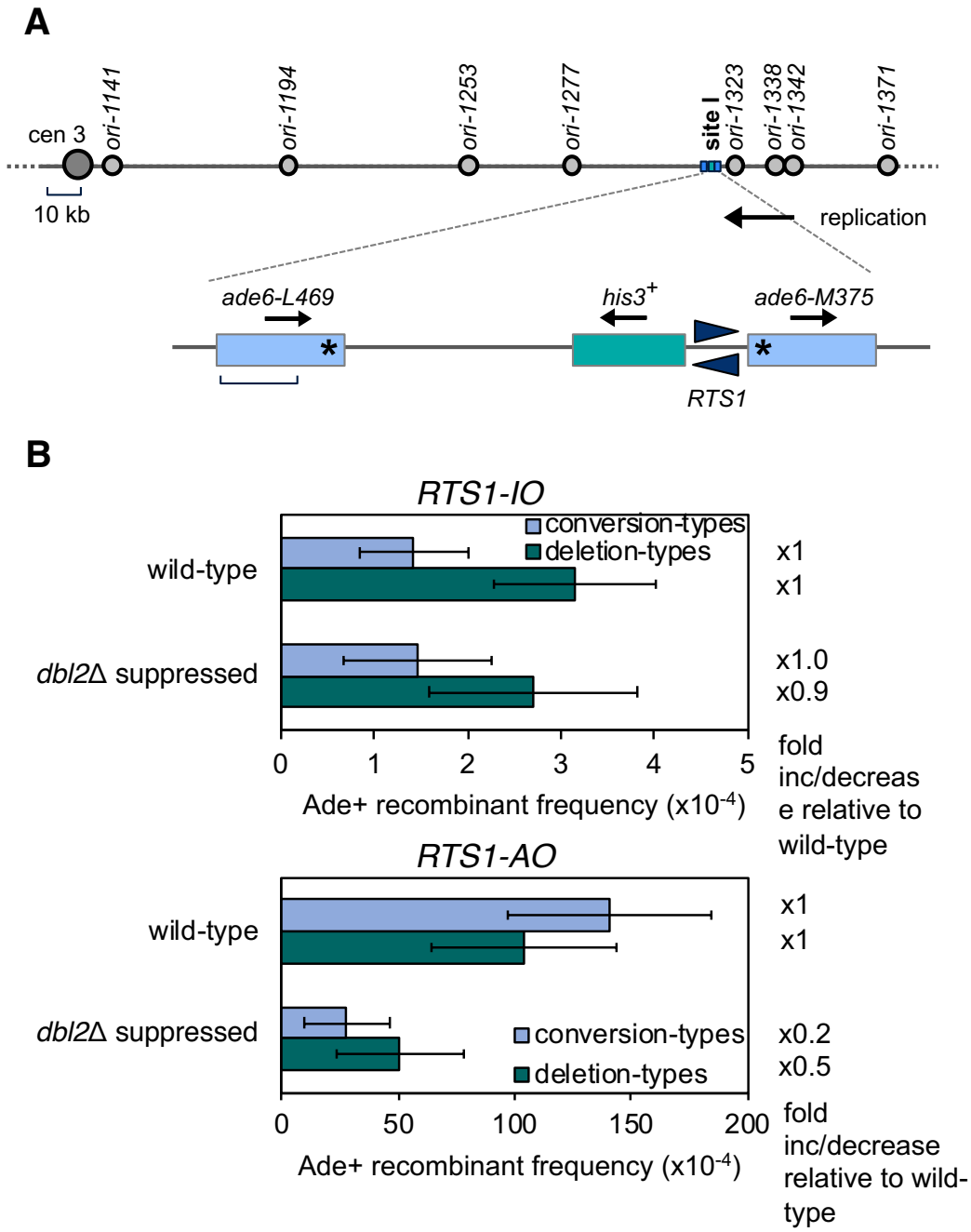


Figure 4.12. *dbl2*Δ suppressor limits recombination at *RTS1*

Bar chart showing the mean frequency of conversion- and deletion-type Ade+ recombinants in wild-type and suppressed *dbl2*Δ. Error bars represent ± one standard deviation. In order of presentation, the strains are MCW4712, MCW8955, MCW4713, and MCW8960.

4.3 Discussion

In this chapter, I have provided evidence that Dbl2 is needed for: efficient DNA repair (Fig. 4.3); correct chromosome segregation during mitosis (Fig. 4.2); normal nuclear morphology (Fig. 4.2); and for limiting recombination that is induced by RF blockage at *RTS1* (Fig. 4.9). In the process of constructing a *dbl2*Δ strain, I also discovered that it readily acquires a suppressed state during meiotic crosses or transformations. Interestingly, suppressed *dbl2*Δ exhibits wild-type chromosome segregation (Fig. 4.2), genotoxin sensitivity and nuclear morphology but is hypo-recombinogenic for *RTS1-AO*-induced recombination (Figs. 4.2, 4.3 and 4.12). It is worth noting that previous studies have not reported that *dbl2*Δ can become suppressed or that the non-suppressed strain exhibits aberrant mitotic chromosome segregation and nuclear morphology (Yu et al., 2013; Polakova et al., 2016).

The hyperrecombination at *RTS1-AO* and other mutant phenotypes of *dbl2*Δ, including hypersensitivity to genotoxins, abnormal cell morphology and aberrant chromosome segregation, and tendency to readily acquire suppressors, are reminiscent of a *fbh1*Δ mutant. Also, like overexpression of Fbh1 (Lorenz et al., 2009), over-expressing Dbl2 has a toxic effect (Fig. 4.4). During the course of my investigation it was reported that Dbl2 is required for efficient formation of Fbh1 foci induce by CPT (Polakova et al., 2016). Moreover, it was shown that Dbl2 is needed for proper meiotic chromosome segregation seemingly by promoting the efficient dismantling of Rad51 nucleofilaments by Fbh1. It is possible that Dbl2's role in suppressing

recombination at the *RTS1* RFB is to promote/direct Fbh1 activity. In Chapter 5, I will explore further the similarities and differences of *dbl2*Δ and *fbh1*Δ mutant phenotypes, as well as investigate the genetic interaction between these two genes.

Despite Dbl2 being needed to suppress recombination at *RTS1*, it seemingly is not required for limiting template switch recombination downstream of the RFB (Fig. 4.10). However, it should be noted that any increase in recombination could be offset by a decrease in replication restart efficiency. Further studies will be needed to "calibrate" my template switch recombination data to account for any changes in restart efficiency. Intriguingly, in unpublished work from Whitby laboratory, it was shown that the Pif1 DNA helicase, Pfh1, promotes template switch recombination downstream of *RTS1*, whilst acting to constrain recombination at the barrier. This apparent incongruity can be explained by the fact that Pfh1 is needed for promoting efficient replication restart and, if one factors in the reduction in restart in a *pfh1* mutant, then it becomes apparent that it actually suppresses template switch recombination rather than promotes it. Interestingly a recent proteomic analysis of Pfh1 interaction partners, found that Pfh1 interacts with Dbl2 during S phase (McDonald et al., 2016). Therefore, it is conceivable that Dbl2 acts with Pfh1 to promote efficient replication restart; for example, by acting as an accessory protein for Pfh1 facilitating its recruitment or activity. This idea is consistent with the observation that the efficiency of restart and/or progression of the restarted fork can be influenced by the amount of Pfh1 that is available (unpublished data from Dr. Manisha Jalan, Whitby laboratory), and with the

fact that *dbl2*Δ does not cause a drop in template switch recombination downstream of *RTS1-AO*, whereas loss of Pfh1 does. Further studies will be needed to explore the relevance of the interaction between Dbl2 and Pfh1.

Recent work from our laboratory showed that the introduction of 5 kb DNA spacer between the *ade6*$^{-}$ repeats on the centromere proximal side of *RTS1-AO* increases the frequency of deletions by ~ 10-fold (Morrow et al., 2017). Importantly, little or no increase in gene conversions was observed. These and other data suggested that spacer-dependent deletions are formed by a Rad51-independent process. Indeed, the frequency of these deletions was very similar in wild-type and *rad51*Δ strains (Morrow et al., 2017). However, my finding that the 5 kb spacer can also lead to an increase in gene conversions in a *dbl2*Δ mutant (Fig. 4.11), suggests that Rad51-dependent recombination can also be enhanced when the distance between the *ade6*$^{-}$ heteroalleles is increased. Presumably the addition of the spacer DNA allows the two copies of *ade6* to come closer in three-dimensional space thereby favouring ectopic strand invasion events catalysed by Rad51. Dbl2's role in suppressing Rad51-dependent and Rad51-independent recombination will be explored further in the next Chapter.

My finding that *dbl2*Δ can acquire a suppressor, which specifically conveys a hypo-recombination phenotype for *RTS1-AO* induced recombination, is reminiscent of the suppression of *fbh1*Δ by *rad52*Δ (Osman et al., 2005; Lorenz et al., 2009). However, unlike suppressed *dbl2*Δ, a *fbh1*Δ*rad52*Δ double mutant is hypo-recombinogenic for gene conversions (Osman et al., 2005; Lorenz et al., 2009). Nevertheless, a mutation that affects the expression or

activity of one of the Rad51 paralogues or mediators would be a candidate for the *dbl2*Δ suppressor. Indeed, in Chapter 5 I will show that suppression can be achieved by the deletion of most mediator proteins but not Rad52. However, the genes for all of the known Rad51 mediators/paralogues reside either on chromosomes I or II, whereas *dbl2* is on chromosome III. Therefore, any mutation in a known Rad51 mediator/paralogue gene should readily be crossed away from *dbl2*Δ. My finding that the suppressed state of *dbl2*Δ is stably inherited suggests, therefore, that the suppressor is not a mutation in one of the known Rad51 mediator/paralogue genes. However, it is conceivable that the suppressor mutation affects the expression of one of the known Rad51 mediator/paralogue genes. Analysis of the DNA sequences of candidate genes near to *dbl2* did not reveal a difference between suppressed and non-suppressed *dbl2*Δ. However, it will be necessary to sequence the entire genomic region surrounding the *dbl2* locus to determine whether there any potential suppressor mutations.

Chapter 5

5 Epistasis analysis of *dbl2* and key components of the homologous recombination machinery

5.1 Introduction

Several DNA helicases are known to strongly suppress inter-repeat recombination induced by replication fork collapse at *RTS1* (Osman et al., 2005; Lorenz et al., 2009; Steinacher et al., 2012). My finding that Dbl2 also plays a role in suppressing *RTS1-AO*-induced recombination, suggested that it might function together with one or more of these helicases. Indeed, it has been reported that Fml1 foci at an HO-induced DSB are dramatically weaker in a *dbl2*Δ mutant compared to wild-type, whereas Dbl2 foci appear to be unaffected by deletion of *fml1* (Yu et al., 2013). Based on these observations, it was suggested that Dbl2 might be needed for the efficient recruitment of Fml1 to sites of DNA damage. Such a role in supporting Fml1 would be consistent with data from budding yeast showing that the Dbl2 homologue, Mte1, physically interacts with Mph1 and is required for the formation of phleomycin-induced Mph1 foci (Yimit et al., 2015; Silva et al., 2016; Xue et al., 2016). Moreover, the number of Mte1 and Mph1 foci that colocalize significantly increases upon MMS treatment (Silva et al., 2016), and *mte1*Δ and *mph1*Δ mutants exhibit an epistatic relationship for genotoxin sensitivity. However, unlike in *S. pombe,* Mte1 foci and enrichment at DSBs was found to be dependent on Mph1 (Yimit et al., 2015; Silva et al., 2016). *In vitro*, Mte1 was shown to enhance fork regression catalysed by Mph1 but also inhibit its D-loop unwinding activity (Silva et al., 2016; Xue et al., 2016). Fml1 is known to have both pro- and anti-recombinogenic roles at *RTS1* (Sun et al., 2008; Morrow et al., 2017), and Dbl2 may control the balance between them.

Another putative Dbl2 interaction partner is Fbh1. Absence of Dbl2 results in the failure of chromosome segregation during meiosis I, which correlates with persistent Rad51 foci (Polakova et al., 2016). It has also been shown that the formation of CPT- and MMS-induced Fbh1 foci (in cells where YFP-tagged Fbh1 was overexpressed from the *nmt1* promoter in the plasmid pREP1) is impaired in *dbl2*Δ cells (Polakova et al., 2016). In contrast, deletion of *fbh1* had no effect on the formation of Dbl2 foci (Polakova et al., 2016). Altogether these findings suggest that Dbl2 may have a role in directing the Rad51 disruptase activity of Fbh1, albeit a direct physically interaction between the two proteins has not been reported.

My finding (in Chapter 4) that the *dbl2*Δ mutant phenotype resembles that of a *fbh1*Δ mutant in many respects, prompted me to investigate further if Fbh1 and Dbl2 function in the same anti-recombinogenic pathway. At the same time, I was intrigued to discover whether Dbl2 may also act in a pathway involving Fml1. To these ends, I investigated the genetic interaction of *dbl2*Δ with *fbh1*Δ, *fml1*Δ, and other key components of homologous recombination machinery to reveal the functional relationships between these genes and the pathways in which they operate.

5.2 Results

5.2.1 Genetic interactions between *dbl2*Δ and *fml1*Δ

To investigate whether *dbl2* and *fml1* in *S. pombe* exhibit similar genetic interactions as seen for *mte1* and *mph1* in *S. cerevisiae*, I constructed a *dbl2*Δ

*fml1*Δ double mutant and compared its genotoxin sensitivity to the single mutants and wild-type (Fig. 5.1). In budding yeast deletion of *mte1* does not cause an increase in cellular sensitivity to DNA-damaging agents but does partially rescue *mph1*Δ MMS hypersensitivity (Silva et al., 2016). In contrast, a *dbl2*Δ *fml1*Δ double mutant is more sensitive to both CPT and MMS than either *dbl2*Δ or *fml1*Δ single mutant (Fig. 5.1). Moreover, even though neither of the single mutants is hypersensitive to UV, the double mutant is. Importantly, the double mutant exhibits a greater than additive increase in sensitivity to CPT, MMS and UV, and this synergistic interaction suggests that Dbl2 and Fml1 function in alternative/redundant pathways for the repair and/or tolerance of CPT-, MMS- and UV-induced DNA damage.

I also determined what effect the *dbl2*Δ suppressor has on the interaction between *dbl2*Δ and *fml1*Δ. Three *dbl2*Δ *fml1*Δ double mutant isolates, derived from a cross between *fml1*Δ and suppressed *dbl2*Δ strains, were compared for growth and genotoxin sensitivity to their parental strains (Fig. 5.2A). In parallel, equivalent isolates from a cross between *fml1*Δ and non-suppressed *dbl2*Δ strains were also tested (Fig. 5.2B). Consistent with the data in Fig. 5.1, all three *dbl2*Δ *fml1*Δ isolates derived from the non-suppressed *dbl2*Δ strain exhibited heightened genotoxin sensitivity to CPT, MMS and UV. However, in this experiment I also observed a reduction in growth on the control plate compared to the *dbl2*Δ single mutant, which was not evident in the data in Fig. 5.1. In contrast, the *dbl2*Δ *fml1*Δ double mutant isolates derived from suppressed *dbl2*Δ all displayed the same sensitivity as a *fml1*Δ single mutant (Fig. 5.2B).

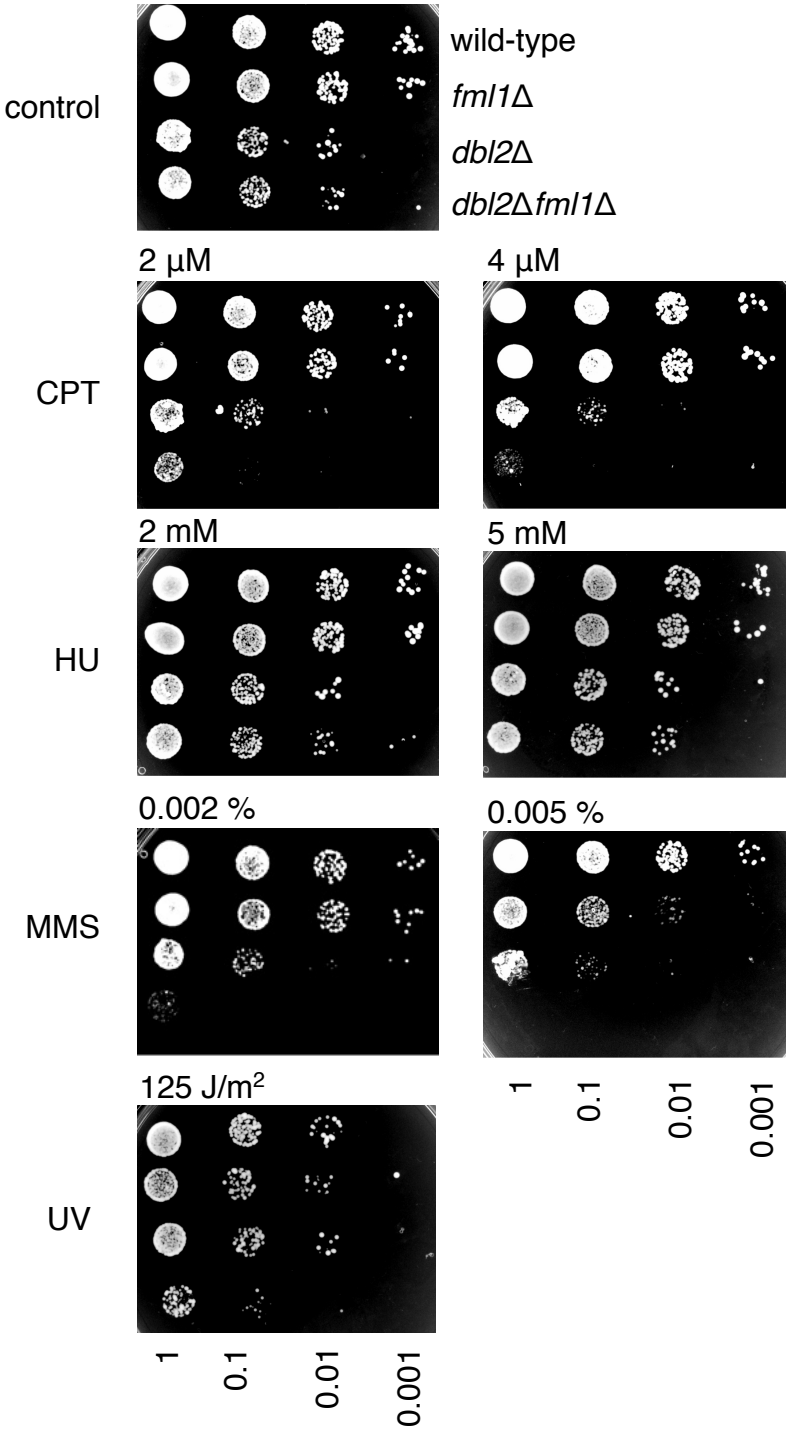


Figure 5.1. Genetic interaction between *dbl2* and *fml1* is not epistatic.

Spot assay comparing the growth and genotoxin sensitivity of wild-type (FO656), *fml1*Δ (MCW2080), *dbl2*Δ (MCW8564), and *dbl2*Δ*fml1*Δ (MCW8747). The plates were photographed after 4 days of incubation at 30 °C.

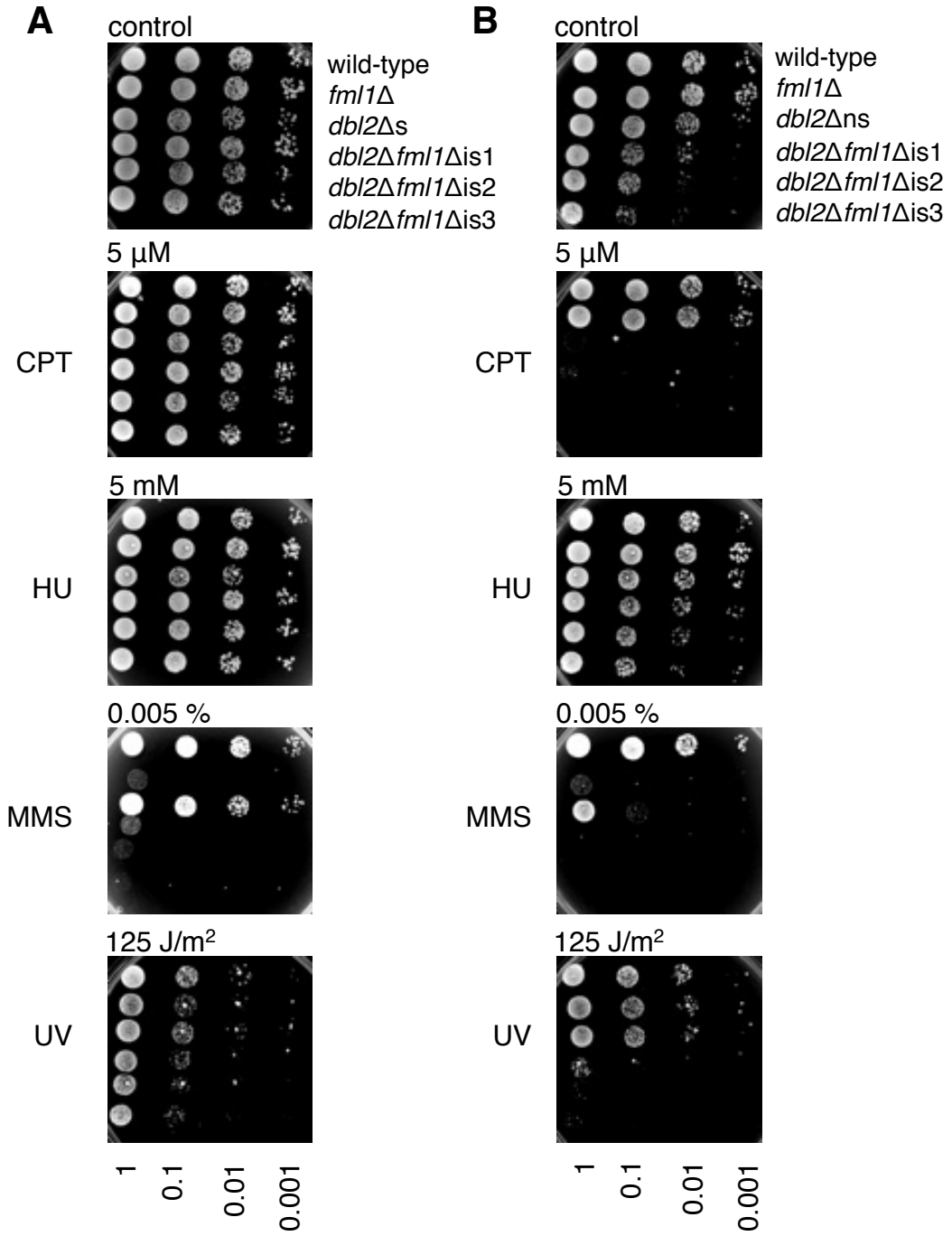


Figure 5.2. Genetic interaction between *dbl2*Δ and *fml1*Δ is affected by *dbl2* suppressor.

Spot assays comparing the growth and genotoxin sensitivities of wild-type (FO652), *fml1*Δ (MCW2080), *dbl2*Δ non-suppressed (MCW8564), *dbl2*Δ suppressed (MCW8563), and different isolates of *dbl2*Δ *fml1*Δ (is1-is3) derived from suppressed *dbl2*Δ (**A**) and from non-suppressed *dbl2*Δ (**B**). The plates were photographed after 4 days of incubation at 30 °C.

This difference in the genetic interactions of suppressed and non-suppressed strains indicates that: 1) the *dbl2*Δ suppressor does not require Fml1 for its suppression of *dbl2*Δ; and 2) the *dbl2*Δ suppressor does not affect the requirement for Fml1 to promote MMS resistance. To gain further insight into the nature of the genetic interaction between *dbl2* and *fml1,* I next assessed the effect that a *dbl2*Δ *fml1*Δ double mutant has on spontaneous (*RTS1-IO*) and *RTS1-AO*-induced direct repeat recombination at the endogenous *ade6* locus on chromosome III (see Fig. 4.9 in Chapter 4 for a description of the assay system) (Fig. 5.3). Consistent with published data, deletion of *fml1* reduces spontaneous conversion-type formation by ~ 3-fold compared to the wild-type ($P < 0.001$) but does not affect the frequency of deletion-types ($P = 0.039$) (Fig. 5.3A). Surprisingly, when *dbl2*Δ is combined with *fml1*Δ, the frequency of spontaneous deletions increases ~ 3-fold, which is significantly higher than in either of the single mutants (both $P < 0.001$). There is also a slight increase ~ 1.8-fold in conversion-types in comparison with wild-type ($P = 0.001$). These data suggest that, unlike in a wild-type background, Fml1 is required to limit the formation of deletion-type recombinants in a *dbl2*Δ mutant. Moreover, the need for Fml1 to promote gene conversions appears to be suppressed in the absence of Dbl2.

Similar to what is observed in the *RTS1*-IO strain, when *fml1* is deleted in the *RTS1*-AO strain, the frequency of conversion-types is significantly reduced by ~ 8-fold compared to wild-type ($P < 0.001$) (Fig. 5.3B).

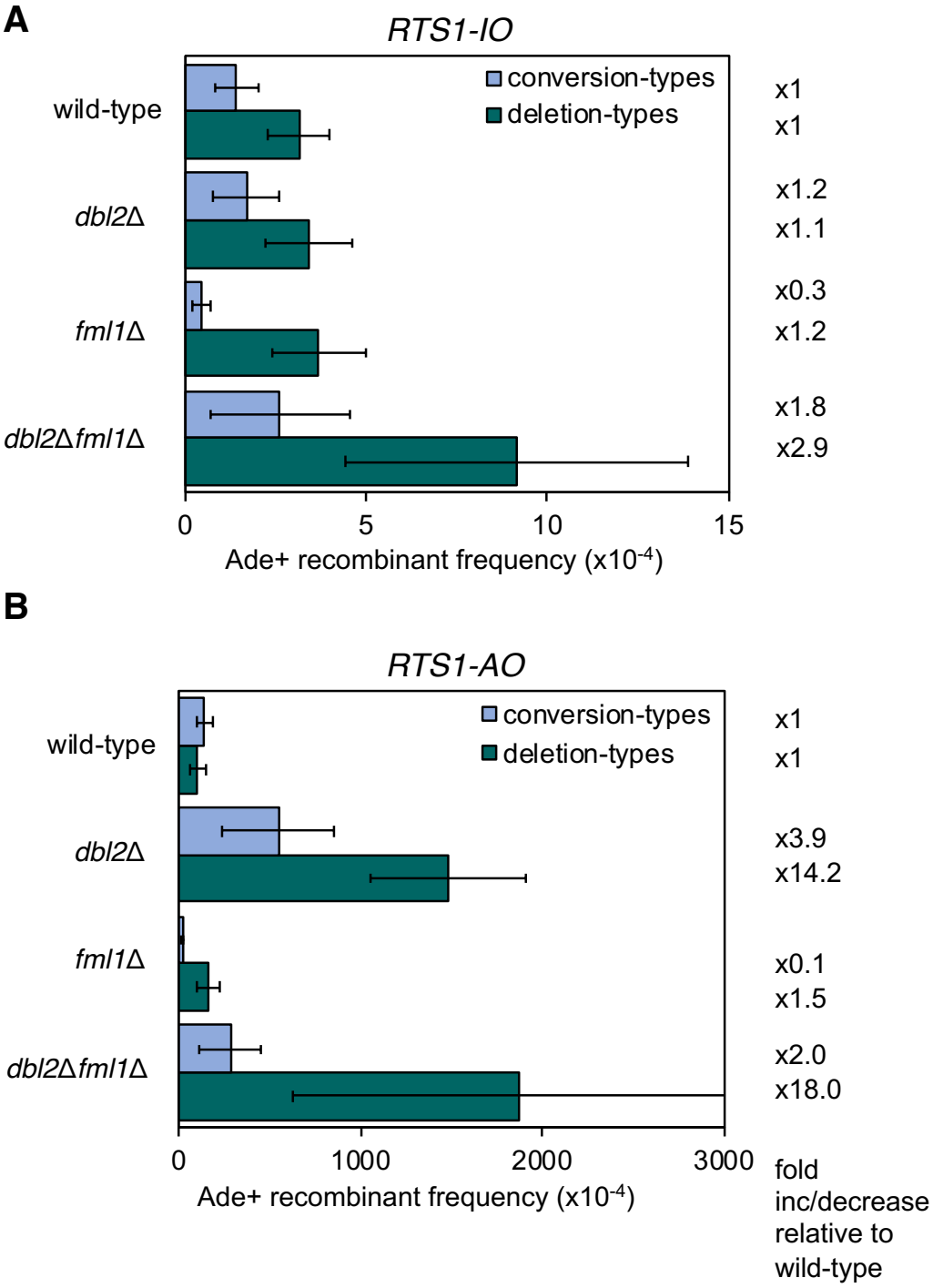


Figure 5.3. Analysis of the genetic interaction between *dbl2*Δ and *fml1*Δ for spontaneous and *RTS1-AO*-induced direct repeat recombination.

Bar chart showing the frequency of conversion- and deletion-type Ade+ recombinants in wild-type, *dbl2*Δ, *fml1*Δ and *dbl2*Δ*fml1*Δ strains with either *RTS1*-IO (**A**) or *RTS1*-AO (**B**). Error bars represent ± one standard deviation. In order of presentation, the strains are MCW4712, MCW8627, MCW3058, MCW8622, MCW4713, MCW8628, MCW3060, and MCW8623.

However, in contrast to the *RTS1*-IO strain, there is also an increase in the frequency of deletion-types (~ 1.5-fold relative to wild-type) ($P < 0.001$). In the double mutant the frequency of both conversions and deletions is increased relative to wild-type and *fml1*Δ single mutant, such that the total recombinants are comparable to that obtained for the *dbl2*Δ single mutant, albeit the frequency of conversions is 2-fold less ($P < 0.001$) (Fig. 5.3B). These data indicate that Fml1 is not required for the high levels of deletions observed in a *dbl2*Δ mutant. However, it does promote some of the gene conversions, albeit its requirement here appears to be less than in a wild-type background. Altogether these data suggest that Dbl2 and Fml1 function in alternative/redundant pathways for the suppression of spontaneous direct repeat recombination but affect *RTS1-AO*-induced recombination by non-overlapping/independent pathways.

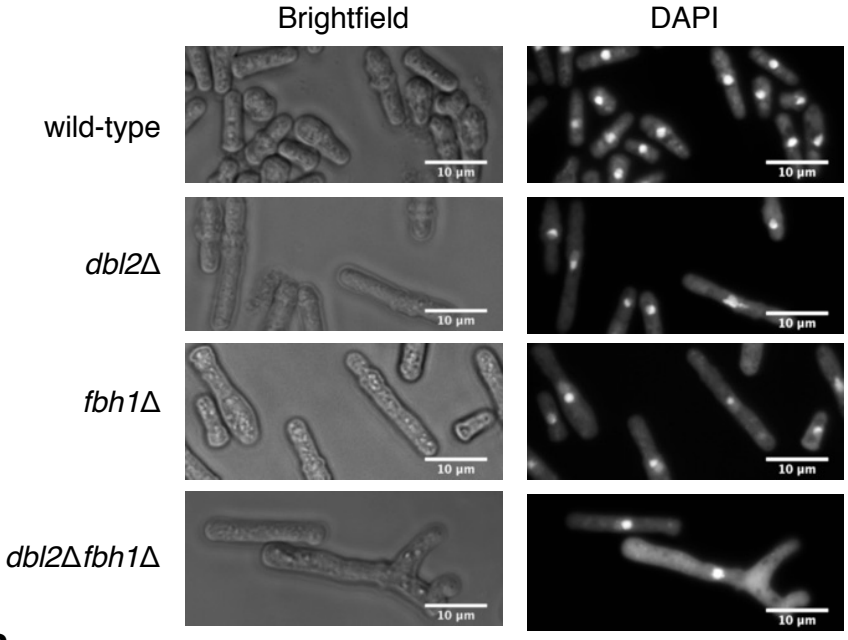
5.2.2 Epistasis analysis between *dbl2*Δ and *fbh1*Δ

To determine whether Dbl2 works in the same pathway as Fbh1 to limit Rad51-dependent recombination, I compared phenotypes of single *dbl2*Δ and *fbh1*Δ mutants to a double *dbl2*Δ*fbh1*Δ mutant. As both single mutants have a quite distinctive cytological phenotype, I first examined morphology and chromosome segregation of DAPI-stained *dbl2*Δ*fbh1*Δ double mutant cells (Fig. 5.4A). This examination revealed similar levels of aberrant cell morphology and chromosome segregation in a *dbl2*Δ*fbh1*Δ mutant as in the single mutants (Fig. 5.4B). There is a slight decrease in the number of long cells in the double mutant compared to wild-type, which may be explained by

the increase of the aberrant shaped cells in the population. It should be noted that, when constructing the *dbl2*Δ*fbh1*Δ double mutant, I obtained isolates that exhibited a less severe morphology phenotype than shown in Fig. 5.4. This is most likely due to the tendency of *dbl2*Δ and *fbh1*Δ mutants to acquire suppressor mutations (Osman et al., 2005) (see Chapter 4).

I next investigated the genetic interaction between *dbl2*Δ and *fbh1*Δ in terms of growth and sensitivity to different genotoxins. During the construction of this double mutant I screened 8 independent double mutant isolates for their genotoxin sensitivity (after a preliminary morphology screen, data not shown). From this analysis I could categorise three main types of double mutant: 1) those that exhibited similar genotoxin sensitivity as a wild-type; 2) those that exhibited sensitivity that was more than wild-type but less than one/both of the single mutants for at least one genotoxin; and 3) those that were at least as sensitive as the most sensitive single mutant to all genotoxins tested. An example from each of the latter two categories is shown in Fig. 5.5. Similar to both *dbl2*Δ and *fbh1*Δ single mutants, the *dbl2*Δ *fbh1*Δ (isolate 1 – a category 3 double mutant) double mutant is hyper-sensitive to CPT and MMS (Fig. 5.5). It also exhibits an increase in HU sensitivity that is similar to a *fbh1*Δ single mutant. However, this double mutant is noticeably more sensitive to CPT and MMS than either of the single mutants. The isolate 2 *dbl2*Δ*fbh1*Δ double mutant (an example of a category 2 mutant) displays similar HU sensitivity as the *fbh1*Δ single mutant and isolate 1 double mutant but is less sensitive to CPT and MMS.

A



B

	wild-type	*dbl2*Δ	*fbh1*Δ	*dbl2*Δ*fbh1*Δ
% long cells	<0.1	24.7	36.7	23.8
% very long cells	<0.1	3	15.4	6.2
% anucleate cells	1	5	21.3	12.1
% not septated binucleate cells	1	5.5	0.5	2.5
% cells with fragmented DNA	0.8	11.2	14.2	16.0
%cells septated cells with aberrant chromosome generation	<0.1	56	55.9	59.0
% cells with figure-of-eight nucleus	0.8	11.5	20.0	11.7

Figure 5.4. The *dbl2*Δ*fbh1*Δ double mutant has a similar cytological phenotype as *dbl2*Δ and *fbh1*Δ single mutants

(**A**) Examples of phase-contrast and fluorescence microscopic images of DAPI stained *dbl2*Δ, *fbh1*Δ, *dbl2*Δ*fbh1*Δ and wild-type. Cells were taken from logarithmically growing cultures. (**B**) Comparison of cell morphology and DNA segregation in wild-type, *dbl2*Δ, *fbh1*Δ, and *dbl2*Δ*fbh1*Δ strains. Long cells are 14 to 28 µm in length, and very long cells are >28 µm. Septated cells were scored as having aberrant chromosome segregation if they displayed an unequal distribution of DNA between the two daughter cells or if the DNA was fragmented or bisected by the septum. For each strain at least 600 cells were assessed.

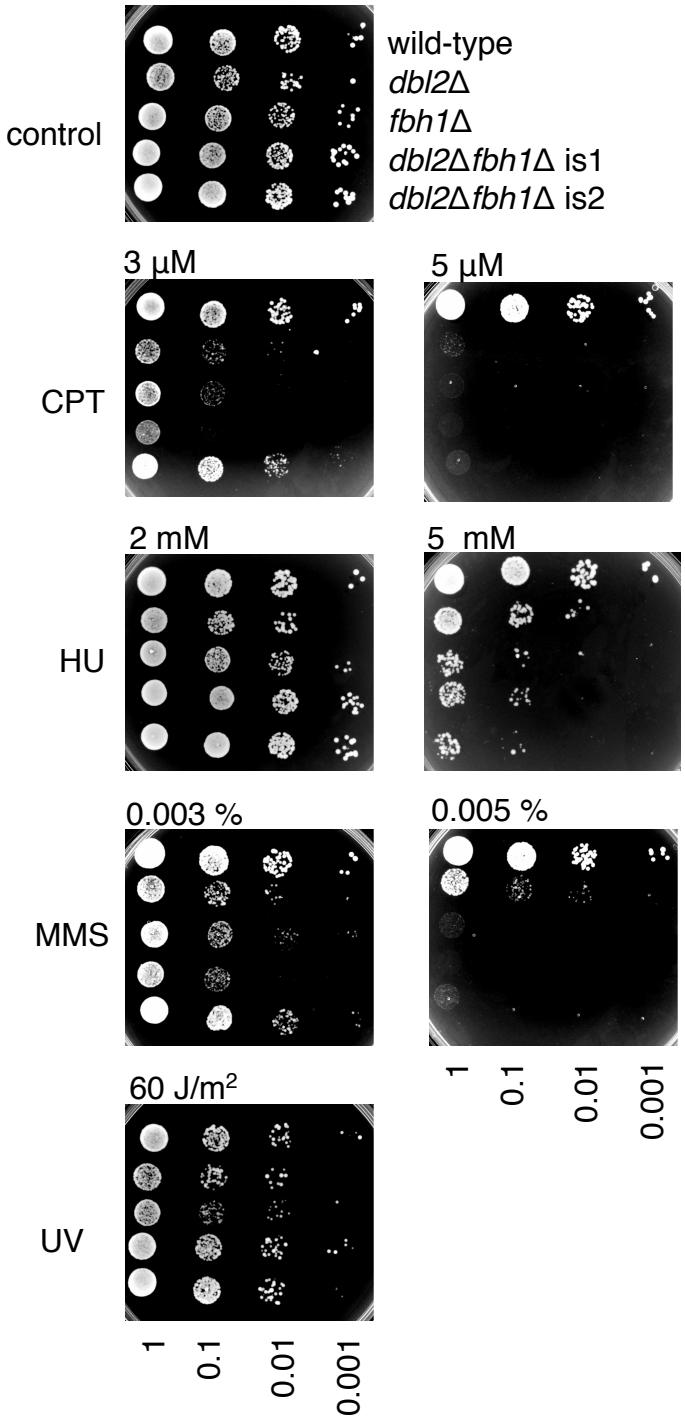


Figure 5.5. Genetic interaction between *dbl2* and *fbh1* is not epistatic.

Spot assay comparing the growth and genotoxin sensitivity of wild-type (FO656), *fbh1*Δ (MCW1884), *dbl2*Δ (MCW8564), and *dbl2*Δ*fbh1*Δ (MCW8748) (isolate 1) and partially suppressed isolate of *dbl2*Δ*fbh1*Δ (isolate 2). The plates were photographed after 5 days of incubation at 30 °C.

The observation that different *fbh1*Δ*dbl2*Δ double mutant isolates exhibit different genotoxin sensitivities suggests that they can acquire different types of suppressor mutation. The category three double mutant appears to be non-suppressed as it displays slightly more sensitivity to MMS and CPT than its component single mutants. Importantly this increase in sensitivity appears to be no more than additive, which suggests that Fbh1 and Dbl2 can function in independent (but non-overlapping) pathways for the repair/tolerance of MMS/CPT-induced DNA damage.

To further dissect the interaction between *dbl2* and *fbh1*, I determined the frequency of direct repeat recombination in single and double mutant strains (Fig. 5.6). When *dbl2*Δ is combined with *fbh1*Δ, the resultant double mutant strain exhibits no change in spontaneous recombination (Fig. 5.6A). In the case of *RTS1-AO*-induced recombination, the frequency of Ade^+ recombinants is slightly higher in a *fbh1*Δ mutant than a *dbl2*Δ mutant (~ 1.4-fold for deletion-types (P = 0.002) and ~ 1.5-fold for conversions (P = 0.004)). The *dbl2Δ fbh1Δ* double mutant, on the other hand, is epistatic to *fbh1*Δ in terms of the frequency of *RTS1-AO*-induced conversions and deletions (P = 0.811 and P = 0.047, respectively) (Fig. 5.6B). These data indicate that Dbl2 and Fbh1 act in the same pathway to suppress direct repeat recombination induced by *RTS1*.

5.2.3 Evidence that Dbl2 has a role in the repair/tolerance of DNA damage that is independent of both Fml1 and Fbh1

My finding that deletion of *dbl2* causes additive or synergistic increases in genotoxin sensitivity in *fml1*Δ and *fbh1*Δ mutants suggests that Dbl2 can work

independently of either Fml1 or Fbh1. However, my data did not exclude the possibility that Dbl2 functions in both Fml1- and Fbh1-dependent pathways. If Dbl2 only functioned in these pathways, then a *dbl2*Δ*fml1*Δ*fbh1*Δ triple mutant should exhibit a similar or lesser genotoxin sensitivity as a *fml1*Δ*fbh1*Δ double mutant. To test this, I generated a *dbl2*Δ*fbh1*Δ*fml1*Δ triple mutant strain and compared it to all possible combinations of double mutants for genotoxin sensitivity (Fig. 5.7). The triple mutant exhibited reduced growth on the control plate compared to the double mutants and, even when allowing for this weaker growth, appeared to be more sensitive to CPT, HU, MMS, UV (Fig. 5.7). These data suggest that Dbl2 has a role in promoting cell viability and resistance to genotoxins that is independent of Fml1 and Fbh1.

5.2.4 Overexpression of Fbh1 improves the growth of a *dbl2*Δ mutant but also sensitizes it to MMS

If the role of Dbl2 were to facilitate Fbh1 activity at blocked RFs, the overexpression of Fbh1 might suppress the *dbl2*Δ mutant phenotype. To test this idea, I compared the growth and genotoxin sensitivity of wild-type and *dbl2*Δ strains harbouring either the pREP41 plasmid or a derivative of it containing *dbl2* or *fbh1*. Expression of these genes in pREP41 is controlled by the *nmt41* promoter, which is repressed by thiamine and, therefore, comparisons were made under both plus and minus thiamine conditions (Fig. 5.8).

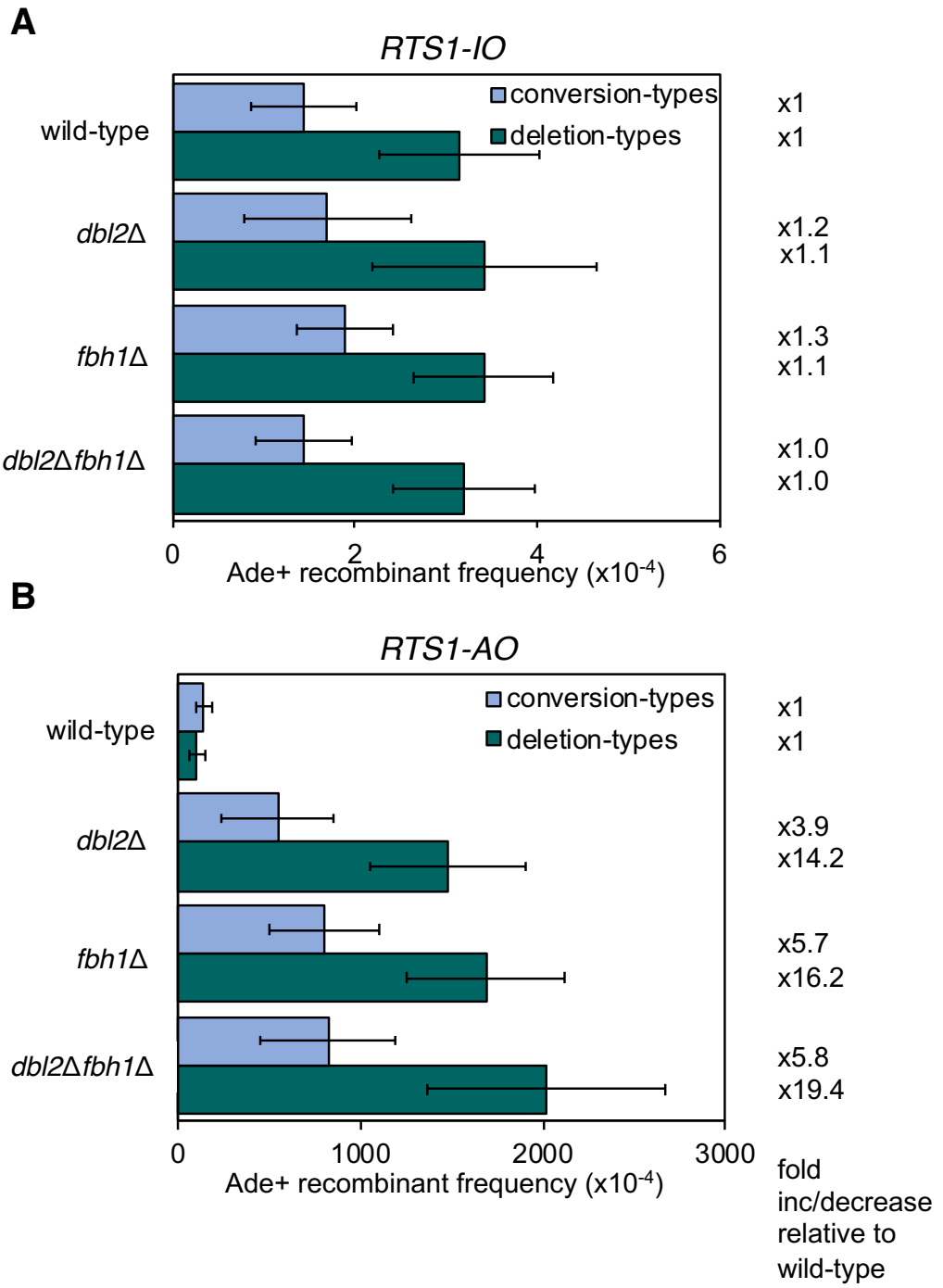


Figure 5.6. Analysis of the genetic interaction between *dbl2* and *fbh1* for spontaneous and *RTS1-AO*-induced direct repeat recombination

Bar chart showing the mean frequency of conversion- and deletion-type Ade$^+$ recombinants in wild-type, *dbl2*Δ, *fbh1*Δ and *dbl2*Δ*fbh1*Δ strains with either *RTS1*-IO (**A**) or *RTS1*-AO (**B**). Error bars represent ± one standard deviation. In order of presentation, the strains are MCW4712, MCW8627, FO1814, MCW8739, MCW4713, MCW8628, FO1816, and MCW8740.

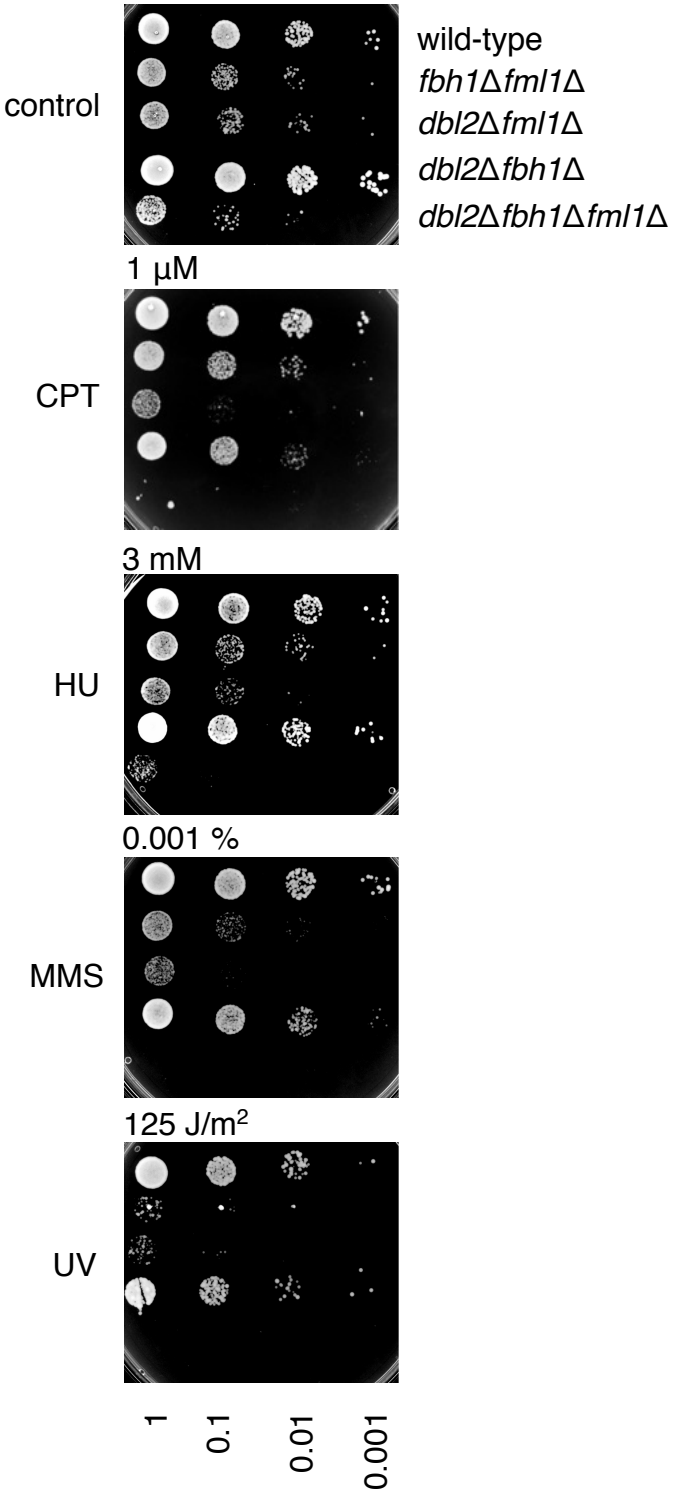


Figure 5.7. Genetic interaction between *dbl2*, *fml1 and fbh1* is not epistatic.

Spot assay comparing the growth and genotoxin sensitivity of wild-type (FO656), *fbh1*Δ*fml1*Δ (MCW2544), *dbl2*Δ*fml1*Δ (MCW8747), *dbl2*Δ*fbh1*Δ (MCW8748) and *dbl2*Δ*fbh1*Δ*fml1*Δ (MCW 8768). The plates were photographed after 5 days of incubation at 30 °C.

Consistent with previous data (Lorenz et al., 2009), overexpression of Fbh1 sensitizes a wild-type to CPT, HU, MMS and UV, especially under conditions of no thiamine when the *nmt41* promoter is fully de-repressed and expression of Fbh1 is maximal. This toxic effect of Fbh1 overexpression is greater than seen with overexpression of Dbl2, which is only evident in the absence of thiamine (Fig. 5.8B). Surprisingly, overexpression of Fbh1 (under both + and – thiamine conditions) improves the growth of a *dbl2*Δ mutant on the control plate to a level that is even better than the wild-type + pREP41 control. If this improved growth on the control plate is taken into account, then Fbh1 overexpression (under both + and – thiamine conditions) does not appear to further sensitize a *dbl2*Δ mutant to CPT or HU and may even partially suppress its CPT sensitivity. In contrast *dbl2*Δ with pREP41-*fbh1* exhibits noticeably greater sensitivity to high doses of MMS and slightly increased sensitivity to UV (Fig. 5.8). It is known that the sensitization of the wild type by Fbh1 overexpression is a consequence of Fbh1 perturbing Rad51 activity (Lorenz et al., 2009). Therefore, my finding that under certain conditions the toxic effects of Fbh1 overexpression can be ameliorated by removing Dbl2, and that *dbl2*Δ growth and resistance to CPT is partially suppressed by Fbh1 overexpression, is consistent with the idea that Dbl2 has a role in promoting the Rad51 disruptase activity of Fbh1. However, the hypersensitivity of *dbl2*Δ to Fbh1 overexpression in the presence of MMS, suggests that under this condition Dbl2 is required to limit/regulate Fbh1 activity.

5.2.5 Overexpression of Dbl2 rescues *fbh1*Δ sensitivity to CPT, MMS and UV

Having discovered that Fbh1 overexpression improves the growth and resistance to CPT of a *dbl2*Δ mutant, I next wanted to see if overexpression of Dbl2 has any effect on *fbh1*Δ growth and genotoxin sensitivity. Amazingly, overexpression of Dbl2 from the *nmt41* promoter in pREP41 partially suppressed *fbh1*Δ mutant hypersensitivity to CPT and MMS (Fig. 5.9). This was most noticeable under the lower levels of Dbl2 overexpression achieved when the *nmt41* promoter is repressed by thiamine (Fig. 5.9A). In the absence of thiamine, the toxic effect of very high levels of Dbl2 appears to partially offset its beneficial effect on *fbh1*Δ (Fig. 5.9B). These data provide further evidence that Dbl2 can function independently of Fbh1. Moreover, it would seem that this independent function can compensate for the loss of Fbh1.

5.2.6 Dbl2 influences both Rad51-dependent and Rad51-independent recombination

Fbh1 is known to negatively regulate Rad51-mediated homologous recombination by both its DNA helicase/translocase activity, which can strip Rad51 from DNA, and by its role as part of an E3 ligase, which ubiquitinates Rad51 to target it for degradation (Simandlova et al., 2013; Tsutsui et al., 2014; Chu et al., 2015). The similarities in *dbl2*Δ and *fbh1*Δ mutant phenotypes suggested that Dbl2 might function in a Rad51-dependent pathway for DNA repair.

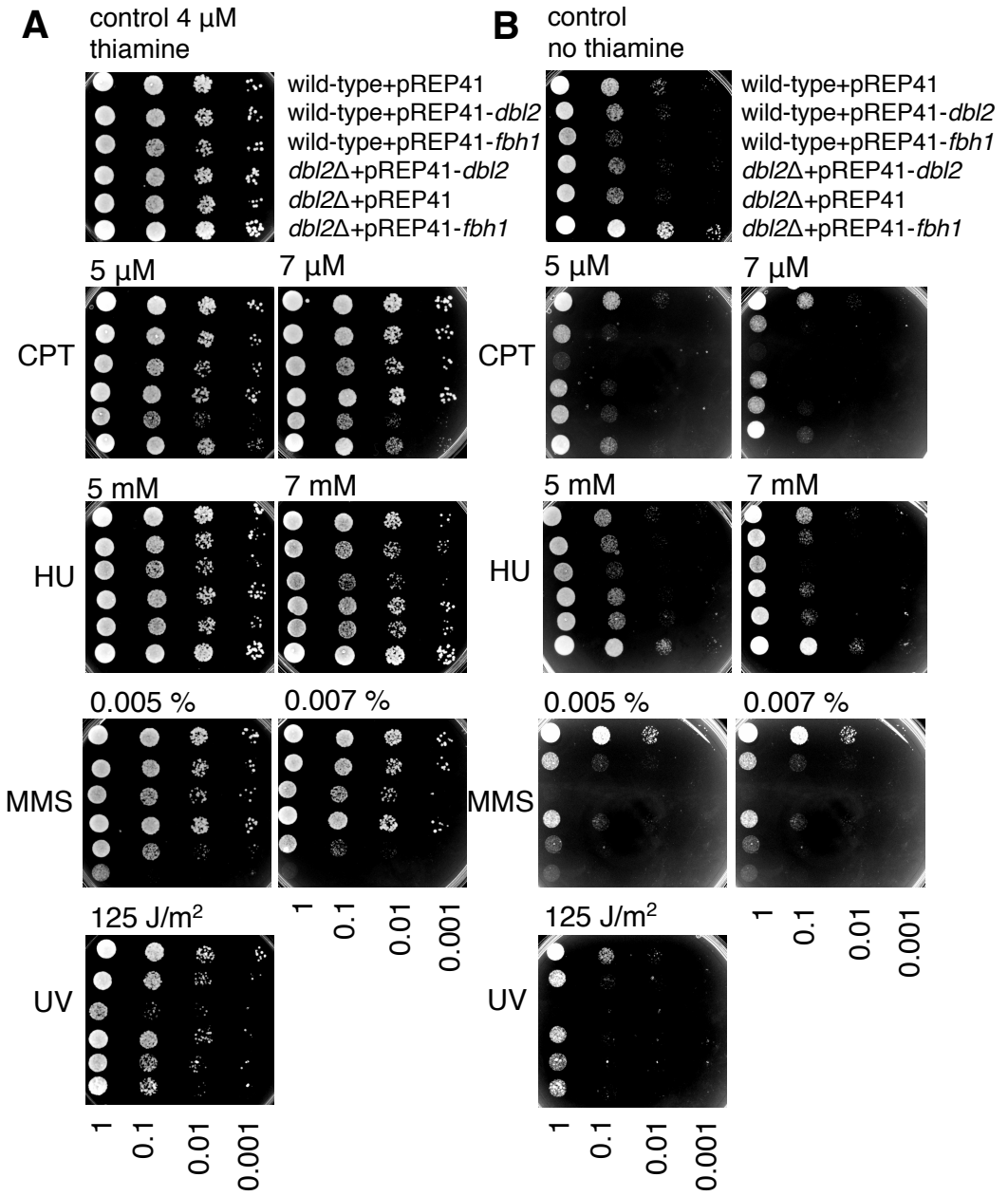


Figure 5.8. Effect of Fbh1 overexpression on *dbl2*Δ growth and sensitivity to genotoxins.

Spot assay comparing the growth and genotoxin sensitivities of wild-type (FO656) and *dbl2*Δ (MCW8564) carrying the indicated plasmids. The plates were photographed after 4 days of incubation at 30 °C.

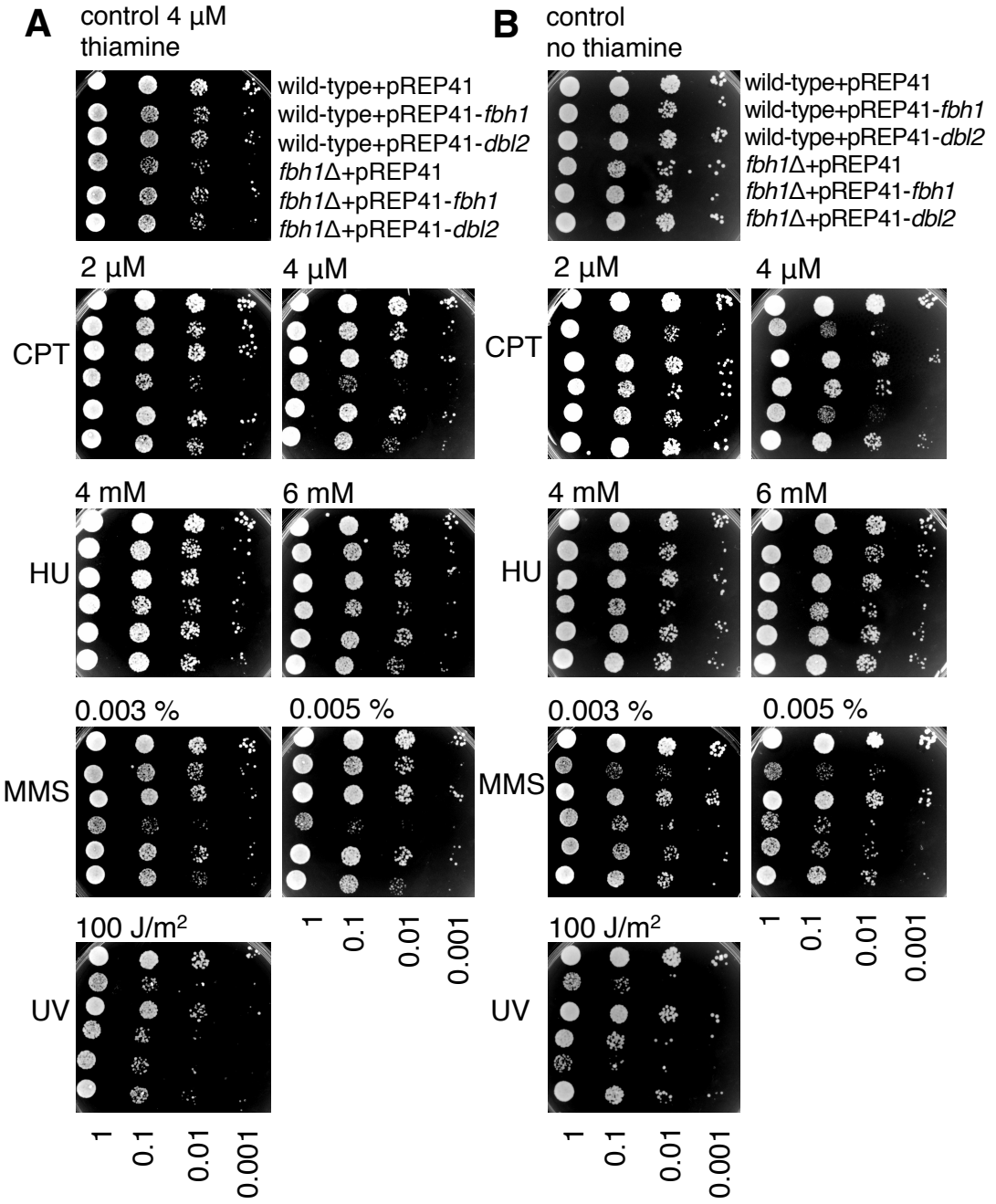


Figure 5.9. The overexpression of Dbl2 partially suppresses *fbh1*Δ sensitivity to CPT, HU, MMS and UV.

Spot assay comparing the growth and genotoxin sensitivities of wild-type (FO656) and *fbh1*Δ (MCW1884) carrying the indicated plasmids. The plates were photographed after 4 days (**A**) and 6 days (**B**) of incubation at 30 °C.

To see if this was indeed the case, I first compared wild-type, *dbl2*Δ, *rad51*Δ and *dbl2*Δ*rad51*Δ strains in a spot assay to assess their relative genotoxin sensitivities (Fig. 5.10). These data show that a *dbl2*Δ *rad51*Δ double mutant has similar sensitivities to CPT, HU and UV as a *rad51*Δ single mutant, indicating an epistatic interaction between *dbl2*Δ and *rad51*Δ. However, the double mutant is also slightly more sensitive to MMS than either single mutant, which suggests that Dbl2 has a role in the repair/tolerance of MMS-induced DNA damage that is independent of Rad51 (Fig. 5.10).

I next wanted to see whether the hyperrecombination in a *dbl2Δ* mutant is dependent on Rad51. To this end I again used the *ade6*$^{-}$ direct repeat recombination reporter on chromosome 3 to assess both spontaneous and *RTS1-AO*-induced Ade^{+} recombinant frequencies in a *dbl2*Δ*rad51*Δ double mutant (Fig. 5.11). As a comparison, I also analysed recombinant formation in a *fbh1*Δ *dbl2*Δ double mutant and in *dbl2*Δ, *fbh1*Δ and *rad51*Δ single mutants (Fig. 5.11). Consistent with published data, the frequency of spontaneous deletions increases (~ 4.9-fold, $P < 0.001$) in a *rad51*Δ single mutant, whereas gene conversions are greatly reduced (~ 4.6-fold, $P < 0.001$) (Fig. 5.11A) (Lorenz et al., 2009). The frequency of recombinants in a *fbh1*Δ*rad51*Δ double mutant is very similar to a *rad51*Δ mutant. In contrast, a *dbl2*Δ*rad51*Δ double mutant exhibits only a modest increase in deletions compared to wild-type (~ 1.5-fold, $P < 0.001$) and no decrease in gene conversions (Fig. 5.11A). These data indicate that Dbl2 constrains spontaneous Rad51-independent gene conversions whilst promoting Rad51-independent deletions.

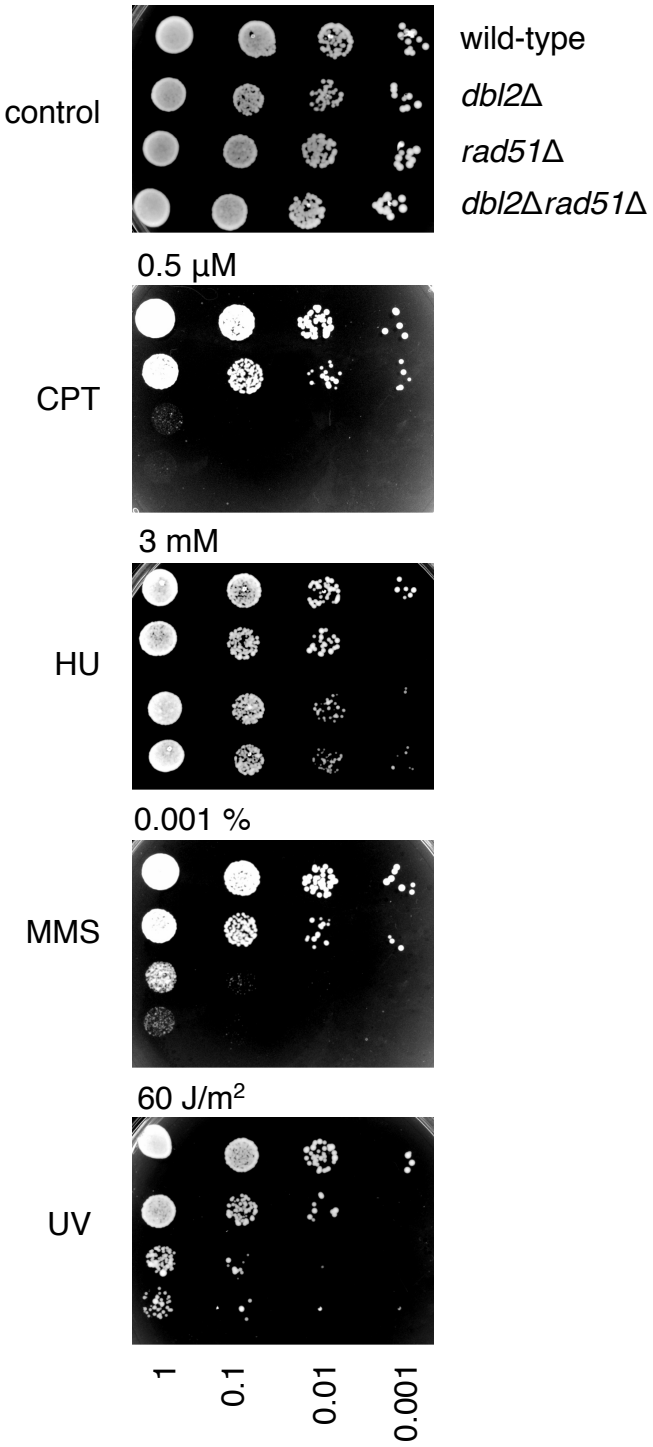


Figure 5.10. Genetic interaction between *dbl2* and *rad51* is epistatic.

Spot assay comparing the growth and genotoxin sensitivity of wild-type (FO656), *dbl2*Δ (MCW8564), *rad51*Δ (MCW1088) and *dbl2*Δ*rad51*Δ (MCW 8756). The plates were photographed after 5 days of incubation at 30 °C.

As expected, in strains carrying *RTS1-AO*, deletion of *rad51* suppresses the hyper-recombination of a *fbh1*Δ mutant to *rad51*Δ single mutant levels (Fig. 5.11B) (Lorenz et al., 2009). Deletion of *rad51* also suppressed the hyper-recombination of a *dbl2*Δ mutant, however in this case the amount of suppression is less, such that the residual levels of deletions and gene conversions are ~ 2-fold ($P < 0.001$) and ~ 2.1-fold ($P = 0.001$) higher in the *dbl2*Δ *rad51*Δ double mutant than in the *rad51*Δ single mutant. Together these data indicate that Dbl2 is required to limit Rad51-dependent direct repeat recombination induced by replication fork collapse at the *RTS1* RFB. However, unlike Fbh1, it also appears to play a role in limiting Rad51-independent recombination at the barrier.

5.2.7 Effect of *rad55* deletion on spontaneous and *RTS1-AO*-induced direct repeat recombination in a *dbl2*Δ mutant.

The formation and function of the Rad51 nucleoprotein filament is assisted by so-called Rad51 mediators, some of which are Rad51 paralogs as they share sequence similarity to Rad51 (Kans and Mortimer, 1991; Khasanov et al., 1999; Tsutsui et al., 2000; Godin et al., 2016). In fission and budding yeast, they include Rad55 and Rad57 (Khasanov et al., 1999). Rad55-Rad57 is believed to stabilise the Rad51 nucleoprotein filament and protect it from dissociation by Fbh1 and/or Srs2 (Fortin et al., 2002; Osman et al., 2005; Akamatsu et al., 2007; Liu et al., 2011). I reasoned that if Dbl2 does indeed have a Rad51-independent role in controlling recombination, then this should also be evident in a *rad55*Δ mutant. Therefore, to provide further evidence of

Dbl2's Rad51-independent role, I compared spontaneous and *RTS1-AO*-induced recombination in *dbl2*Δ, *rad55*Δ and *dbl2*Δ*rad55*Δ mutants (Fig. 5.12). Similar to the interaction between *dbl2*Δ and *rad51*Δ, a *dbl2*Δ*rad55*Δ double mutant exhibits a reduction in the hyper-level of spontaneous deletions seen in a *rad55*Δ single mutant (~ 2.1-fold, $P < 0.001$) (Fig. 5.12A). However, contrary to a *dbl2*Δ*rad51*Δ mutant, the frequency of conversion-types in the *dbl2*Δ*rad55*Δ mutant is as low as in a *rad55*Δ single mutant and reduced significantly relative to wild-type (~ 6.5-fold, $P < 0.001$) (Fig. 5.12A). These data indicate that Dbl2 functions in a Rad55-independent pathway of deletion formation. When *RTS1* is in the active orientation, the *dbl2*Δ*rad55*Δ double mutant displays a significant reduction in the frequency of deletion-type recombinants compared to a *dbl2*Δ single mutant (~ 13.5-fold, $P < 0.001$) (Fig. 5.12B). However, importantly the frequency of deletion-types is not reduced to the level seen in a *rad55*Δ single mutant (the frequency in the double mutant is ~ 4-fold higher than in the *rad55*Δ single mutant, $P < 0.001$). The frequency of conversion-type recombinants is also decreased significantly by ~ 56-fold ($P < 0.001$) in the double mutant compared to the *dbl2*Δ single mutant, but again not to the level of a *rad55*Δ single mutant (the frequency of conversion-type recombinants in the double mutant is ~ 10-fold higher than in the *rad55*Δ single mutant, $P < 0.001$) (Fig. 5.12B). These data provide further evidence that Dbl2 suppresses both Rad51/Rad55-dependent recombination and Rad51/Rad55-independent recombination induced by RF collapse at *RTS1*.

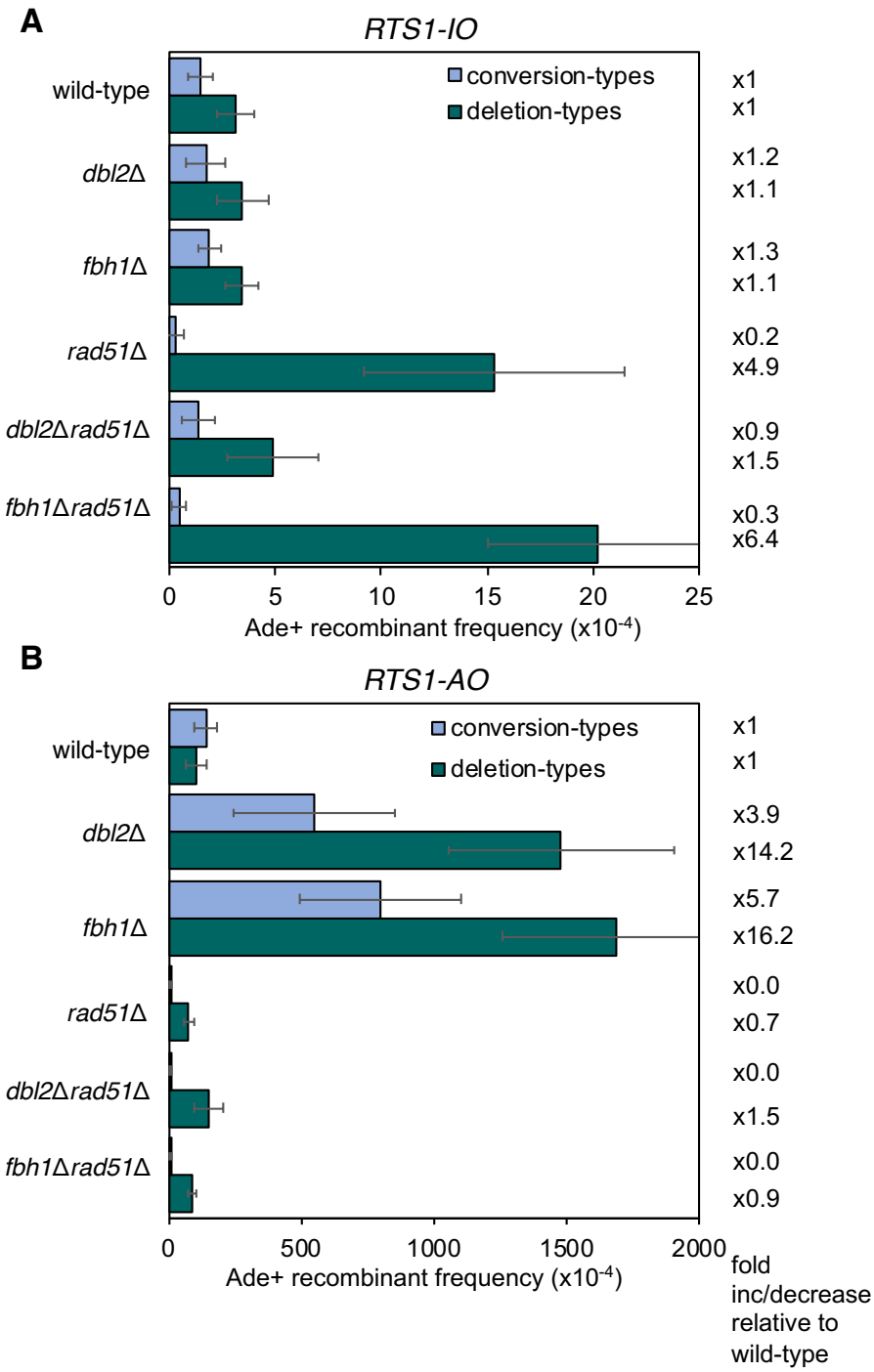


Figure 5.11. Effect of *rad51* deletion on spontaneous and *RTS1-AO*-induced recombination in a *dbl2*Δ mutant.

Bar chart showing the frequency of conversion- and deletion-type Ade$^+$ recombinants in wild-type, *dbl2*Δ, *fbh1*Δ, *rad51*Δ, *dbl2*Δ*rad51*Δ and *fbh1*Δ*rad51*Δ strains with either *RTS1*-IO (**A**) or *RTS1*-AO (**B**). Error bars represent ± one standard deviation about the mean. In order of presentation, the strains are MCW4712, MCW8627, FO1814, MCW1691, MCW9116, MCW2113, MCW4713, MCW8628, FO1816, MCW1692, MCW9117 and MCW2115.

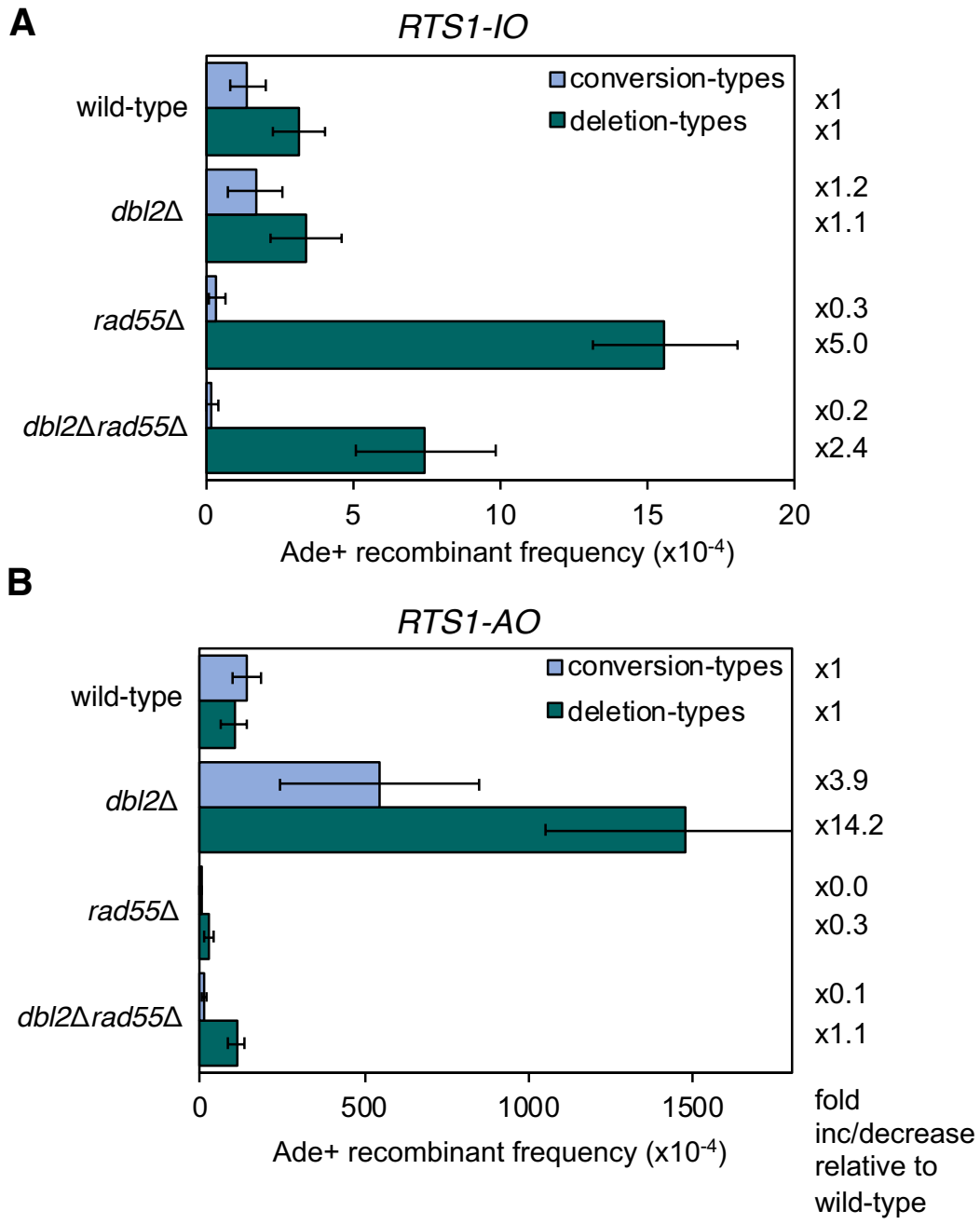


Figure 5.12. Effect of *rad55* deletion on spontaneous and *RTS1-AO*-induced direct repeat recombination in a *dbl2*Δ mutant.

Bar chart showing the frequency of conversion- and deletion-type Ade$^+$ recombinants in wild-type, *dbl2*Δ, *rad55*Δ, and *dbl2*Δ*rad55*Δ strains with either *RTS1*-IO (**A**) or *RTS1*-AO (**B**). Error bars represent ± one standard deviation. In order of presentation, the strains are MCW4712, MCW8627, MCW2649, MCW8645, MCW4713, MCW8628, MCW2654, and MCW8646.

5.2.8 Dbl2 limits both Rad51-dependent and Rad51-independent recombination induced by the *RTS1* RFB in spacer strains

To gain further evidence that Dbl2 has a role in suppressing Rad51-independent recombination, I next turned to a variant of the *ade6*$^{-}$ direct repeat recombination reporter, which contains an extra 5 kb spacer DNA between the repeats. Previous work had shown that addition of this spacer resulted in a ~ 10-fold increase in the frequency of *RTS1-AO*-induced deletions compared to a strain without the spacer (Morrow et al., 2017). Importantly these spacer-dependent deletions depend on Rad52 but are independent of Rad51 (Morrow et al., 2017). To see if Dbl2 suppresses Rad51-independent spacer-dependent deletions, I compared the frequency of Ade^{+} recombinants in wild-type, *dbl2*Δ, *rad51*Δ and *dbl2*Δ *rad51*Δ strains containing the recombination reporter with *RTS1-AO* and 5 kb spacer (Fig. 5.13). As shown in Chapter 4, deletion of *dbl2* results in extremely high levels of both conversion- and deletion-types recombinants. When *dbl2*Δ is combined with *rad51*Δ, the number of gene-conversion recombinants is reduced to the single *rad51*Δ mutant level. However, whilst there is a decrease in deletion-types in the *dbl2*Δ *rad51*Δ double mutant relative to a *dbl2*Δ single mutant (~ 1.4-fold, $P < 0.001$), the frequency remains ~ 2-fold higher than in a *rad51*Δ single mutant (Fig. 5.13). Altogether these data provide further evidence that Dbl2 limits both Rad51-dependent and Rad51-independent recombination induced by the *RTS1* RFB.

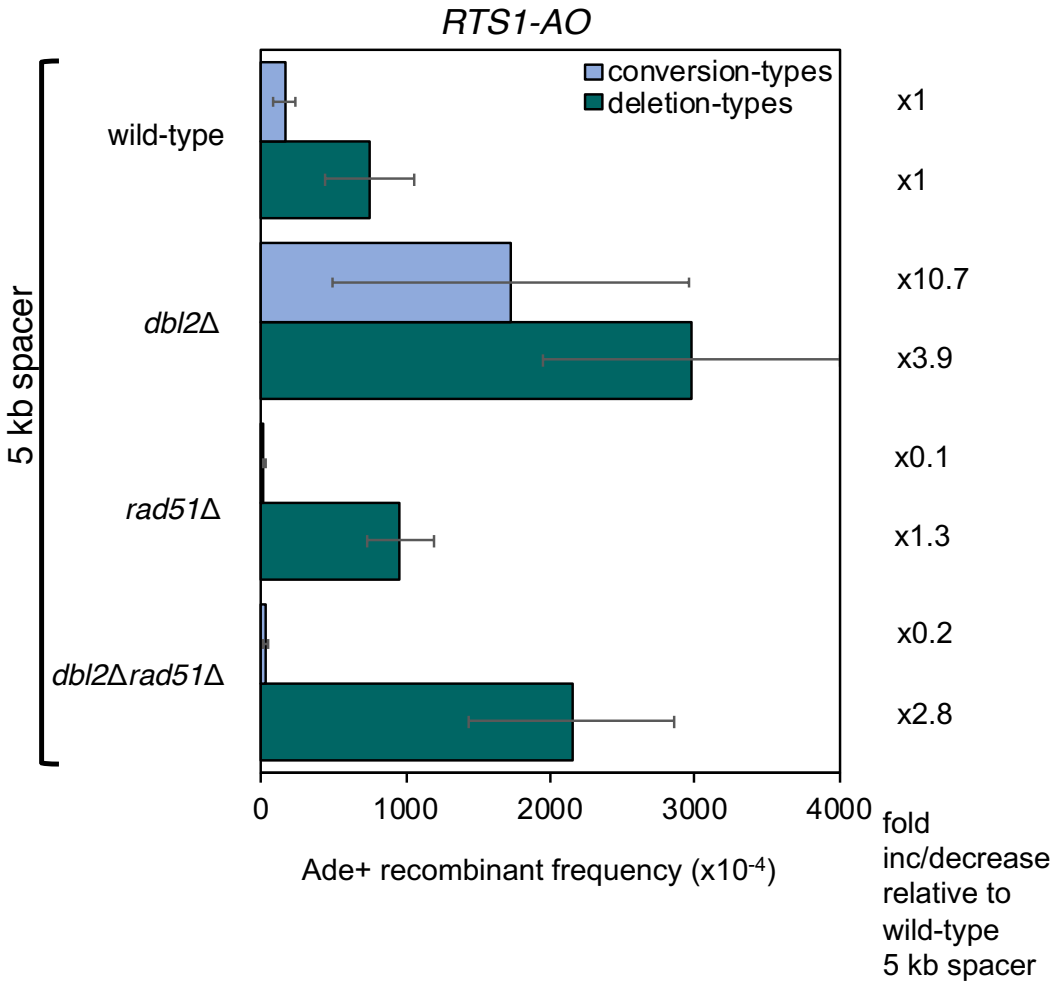


Figure 5.13. Effect of *rad51* deletion on the frequency of spacer-dependent deletions in wild-type and *dbl2*Δ strains

Bar chart showing the frequency of conversion- and deletion-type Ade$^+$ recombinants in wild-type, *dbl2*Δ, *rad51*Δ, and *dbl2*Δ*rad51*Δ strains with 5 kb spacer and *RTS1*-AO. Error bars represent ± one standard deviation. In order of presentation, the strains are MCW8023, MCW9124, MCW8136, and MCW9125.

5.2.9 Dbl2 functions in a Rad52-dependent pathway of DNA repair

My finding that Dbl2 regulates Rad51-independent recombination prompted me to test the genetic interaction between *dbl2*Δ and *rad52*Δ. Having constructed a *dbl2*Δ*rad52*Δ double mutant, I first determined its sensitivity to genotoxins by a spot assay (Fig. 5.14). As comparisons, I included both its component single mutants as well as a *fbh1*Δ single mutant and *fbh1*Δ *rad52*Δ double mutant. The *fbh1*Δ*rad52*Δ double mutant was included because *fbh1*Δ is known to suppress the genotoxin sensitivity of a *rad52*Δ mutant (Osman et al., 2005). As expected, the *rad52*Δ single mutant grew very poorly on the control plate and even more so in the presence of genotoxins. Consistent with published data, the poor growth and genotoxin sensitivity of a *rad52*Δ mutant was suppressed in a *fbh1*Δ*rad52*Δ double mutant. In contrast, no suppression was seen in the *dbl2*Δ*rad52*Δ double mutant, which exhibited very similar growth and sensitivity to genotoxins as a *rad52*Δ single mutant (Fig. 5.14).

I next determined the phenotype of the *dbl2*Δ *rad52*Δ double mutant for spontaneous and *RTS1-AO*-induced direct repeat recombination (Fig. 5.15). Previous work has shown that both spontaneous and *RTS1-AO*-induced direct repeat recombination is largely abolished in a *rad52*Δ mutant with only very low levels of deletions remaining (Doe et al., 2004; Ahn et al., 2005; Nguyen et al., 2015). Consistent with this published work, I observed very few conversion-type recombinants in a *rad52*Δ mutant. However, the mean frequency of deletions was higher than expected in the *rad52*Δ *RTS1-IO* strain (Fig. 5.15A). As indicated by the very large standard deviation, the numbers of

deletions varied greatly for this strain from colony to colony, and it is possible that this is caused by the acquisition of a suppressor mutation in some of the founding cells. Importantly, both *fbh1*Δ and *dbl2*Δ suppressed the loss of spontaneous gene conversions in a *rad52*Δ mutant (Fig. 5.15A). Moreover, the frequency of deletions in both double mutants was comparable to wild-type, which likely also represents a suppression of the true *rad52*Δ phenotype.

In the case of *RTS1-AO*-induced recombination, deletion of *rad52* abolishes almost all of the recombinants in a *dbl2*Δ or *fbh1*Δ mutant (Fig. 5.15B). However, the frequency of both conversions and deletions is noticeably higher in the double mutants (especially in *fbh1*Δ*rad52*Δ) compared to the *rad52*Δ single mutant (Fig. 5.15B). Altogether these data confirm that Dbl2 functions in Rad52-dependent pathways of DNA repair and recombination. Moreover, similar to Fbh1, Dbl2 appears to inhibit Rad51-mediated recombination in the absence of Rad52.

5.2.10 The effect of *dbl2* deletion on Rad51-CFP and Rad52-YFP focus formation at *RTS1*

Having established that Dbl2 limits both Rad51-dependent and Rad51-independent recombination at *RTS1-AO*, I next analysed Rad51 and Rad52 focus formation at the RFB in a *dbl2*Δ mutant background (Fig. 5.16). To monitor recruitment of Rad51 and Rad52 to *RTS1*, and how this is affected by other recombination proteins, our lab created an experimental system in which

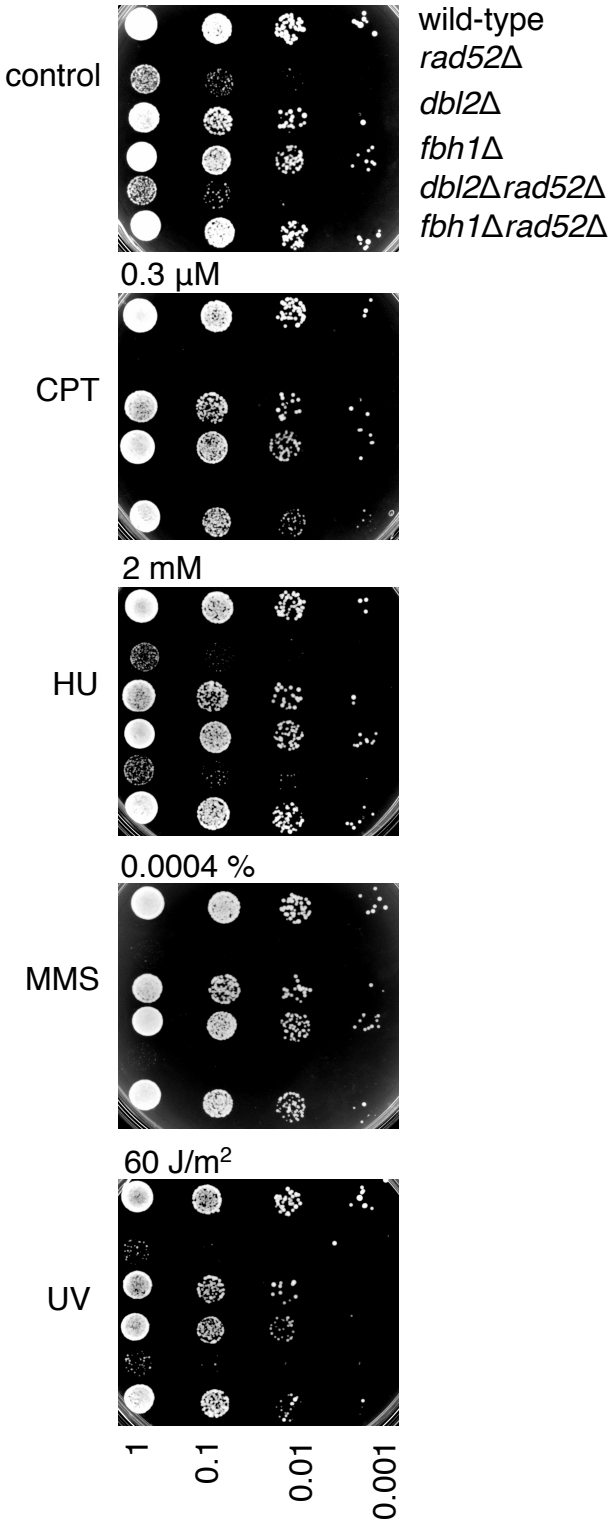


Figure 5.14. Deletion of *dbl2* does not suppress *rad52*Δ genotoxin sensitivity.

Spot assay comparing the growth and genotoxin sensitivity of wild-type (FO656), *rad52*Δ (OMW1285), *dbl2*Δ (MCW8564), *fbh1*Δ (MCW1884), *dbl2*Δ*rad52*Δ (MCW8755) and *fbh1*Δrad52Δ (MCW1586). The plates were photographed after 4 days of incubation at 30 °C.

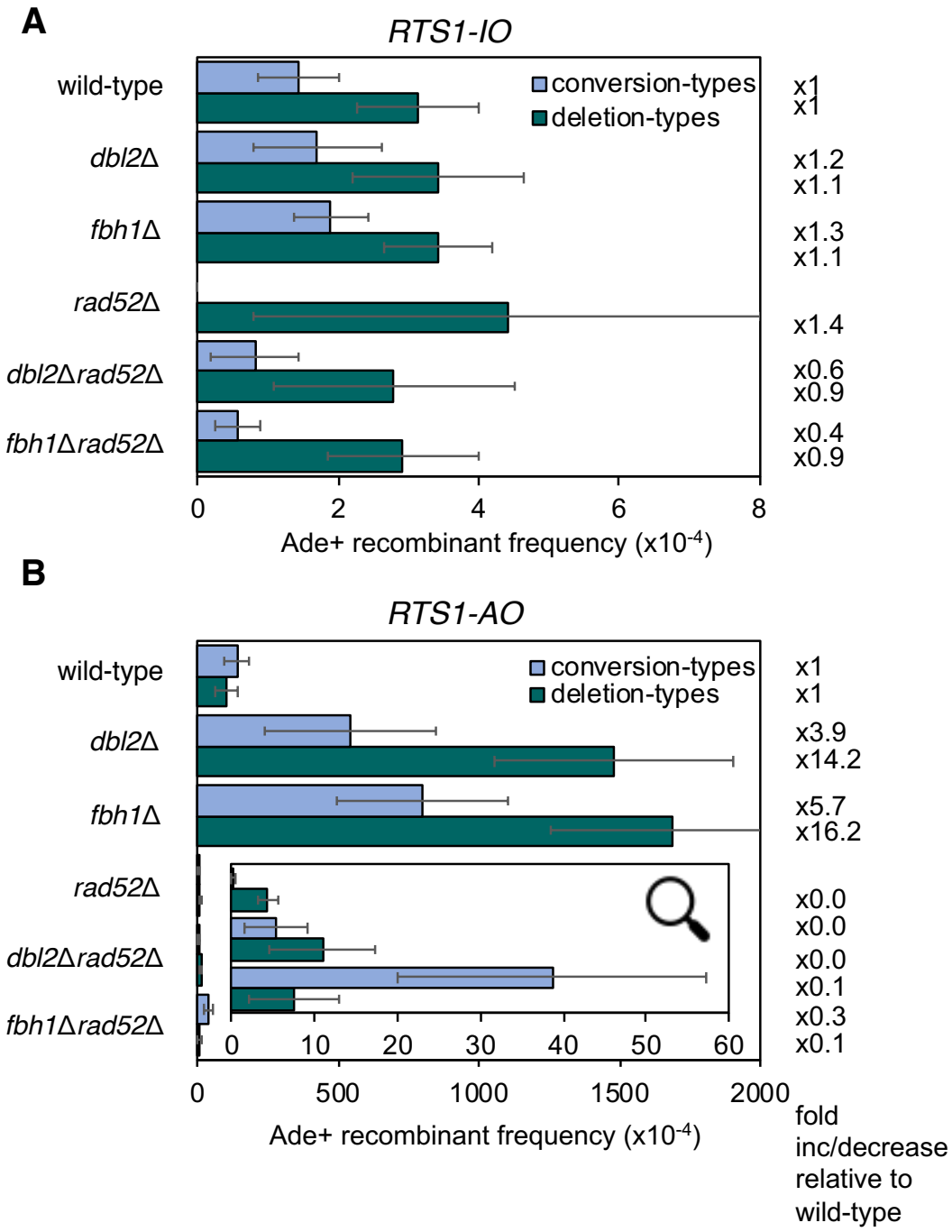
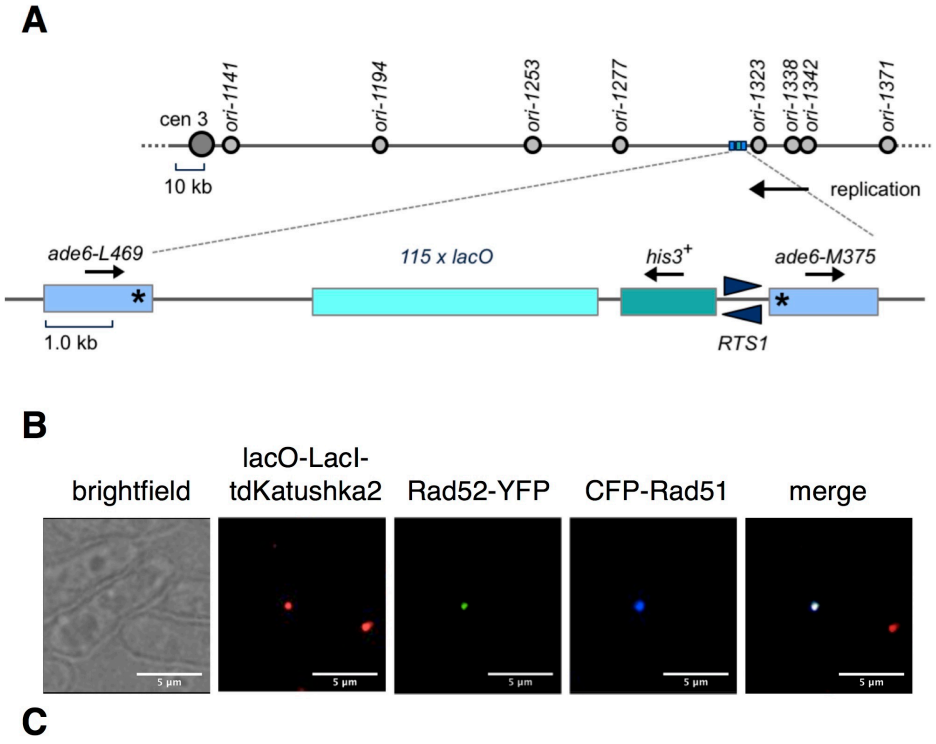


Figure 5.15. Effect of *rad52*Δ on the frequency of spontaneous and *RTS1-AO*-induced direct repeat recombination in wild-type, *dbl2*Δ and *fbh1*Δ genetic backgrounds.

Bar chart showing the mean frequency of conversion- and deletion-type Ade$^+$ recombinants in wild-type, *dbl2*Δ, *fbh1*Δ, *rad52*Δ, *dbl2*Δ*rad52*Δ and *fbh1*Δ*rad52*Δ strains with either *RTS1*-IO (**A**) or *RTS1*-AO (**B**). Error bars represent ± one standard deviation. In order of presentation, the strains are MCW4712, MCW8627, FO1814, MCW1687, MCW8647, FO1831, MCW4713, MCW8628, FO1816, MCW1688, MCW8648 and FO1833.

an array of *lacO* sequences is inserted downstream of *RTS1* so that one can track its location in cells expressing the LacI repressor fused to the far-red fluorescent protein tdKatushka2 using fluorescent microscopy (Fig. 5.16A). Rad52 is tagged at its C-terminus with yellow fluorescent protein (YFP) and Rad51 is fused at its N-terminus with cyan fluorescent protein (CFP)(Nguyen et al., 2015) (Fig. 5.16B). In snapshots of asynchronously growing wild-type cells containing *RTS1*-IO, 8.1 % of cells exhibit a Rad52 focus and 6.6 % a Rad51 focus, with 95 % of the latter co-localizing with a Rad52 focus. Only 2.6 % of Rad52 foci and 3.2 % of Rad51 foci were observed to co-localize with *lacO*-LacI in these cells (Nguyen et al., 2015). In contrast, in *dbl2*Δ cells containing *RTS1*-IO ~ 55 % of cells had Rad51 foci and ~ 88 % had Rad52 foci, and most of the Rad51 foci (~ 82 %) colocalised with a Rad52 focus (Fig. 5.16B, C). Approximately 23 % of Rad51 foci colocalised with *lacO*-LacI and all of these foci also co-localised with Rad52. Only ~ 13 % of Rad52 foci colocalised with *lacO*-LacI (Fig. 5.16C). These data indicate that Dbl2 is required to suppress the appearance of spontaneous Rad51 and Rad52 foci. The increase in frequency of these foci co-localizing with *lacO*-LacI may indicate that either *RTS1-IO* or *lacO*-LacI itself is triggering a recombinational response in the absence of Dbl2.

In wild-type cells with *RTS1*-AO, the population of cells with Rad52 and Rad51 foci increases to 13 % and 12 %, respectively, with the vast majority (97 %) of Rad51 foci again co-localizing with a Rad52 focus (Nguyen et al., 2015).



	wild-type		*dbl2Δ*	
	RTS1-IO	*RTS1-AO*	*RTS1-IO*	*RTS1-AO*
% cells with a Rad51 focus	6.6	12.0	54.9	62.4
% cells with a Rad52 focus	8.1	13.0	87.7	65.8
% Rad51 foci that co-localize with Rad52	95.2	97.0	82.1	89.7
% Rad52 foci that co-localize with Rad51	77.6	88.9	48.6	91.6
% Rad51 foci that co-localize with lacO-LacI	3.2	37.9	22.6	51.6
% Rad52 foci that co-localize with lacO-LacI	2.6	36.5	29.6	60
% Rad51 foci that co-localize with Rad52 at lacO-LacI	3.2	36.2	22.6	51.6
% Rad52 foci that co-localize with Rad51 at lacO-LacI	2.6	33.3	12.7	54.8

Figure 5.16. The effect of *dbl2* deletion on Rad51-CFP and Rad22-YFP focus formation.

(**A**) Schematic showing the modification of the direct repeat recombination reporter for the microscopy. (**B**) Example snapshots of a *RTS1-AO* cell with both a CFP-Rad51 and Rad52-YFP focus co-localizing with a *lacO*-LacI-tdKatushka2 focus. (**C**) Quantification of data like in (**B**)**,** 120 cells were analysed for each *dbl2*Δ strain. Quantification of wild-type strains is done by Dr. Michael Nguyen: 944 and 485 cells were analysed for *RTS1*-IO and *RTS1*-AO, respectively (Nguyen et al., 2015).

36.5 % of Rad52 foci and 37.9 % of Rad51 foci co-localized with *lacO*-LacI, with greater than 90 % of these foci also co-localizing with each other (Nguyen et al., 2015). Similar to the *dbl2*Δ strain with *RTS1-IO*, the majority of *dbl2*Δ cells with *RTS1-AO* contain Rad51 (~ 62 %) and Rad52 (~ 66 %) foci, albeit the percentage of cells with Rad52 foci is smaller than in the strain with *RTS1-IO* (Fig. 5.16C). As with the wild-type strain and *dbl2*Δ strain the vast majority (~ 96 %) of Rad51 foci co-localize with a Rad52 focus. Importantly, the percentage of both Rad51 and Rad52 foci that co-localize with *lacO*-LacI (~ 52 % and 60 %, respectively) is noticeably greater than in the equivalent wild-type strain or the *dbl2*Δ strain with *RTS1-IO* (Fig. 5.16C). These data suggest that Dbl2 limits the recruitment and/or retention of both Rad51 and Rad52 foci to/at the *RTS1* RFB.

5.2.11 Overexpression of Rad52 does not mimic the *dbl2Δ* phenotype

My finding that Dbl2 appears to suppress both Rad51-dependent and Rad51-independent recombination made me wonder whether it might in some way regulate Rad52 activity. If it did then overexpression of Rad52 might mimic some or all of the phenotypes of a *dbl2*Δ mutant. To test this idea, I overexpressed Rad52 from the *nmt41* promoter in pREP41 in a wild-type strain carrying the *ade6*$^{-}$ direct repeat recombination reporter with *RTS1-AO*.

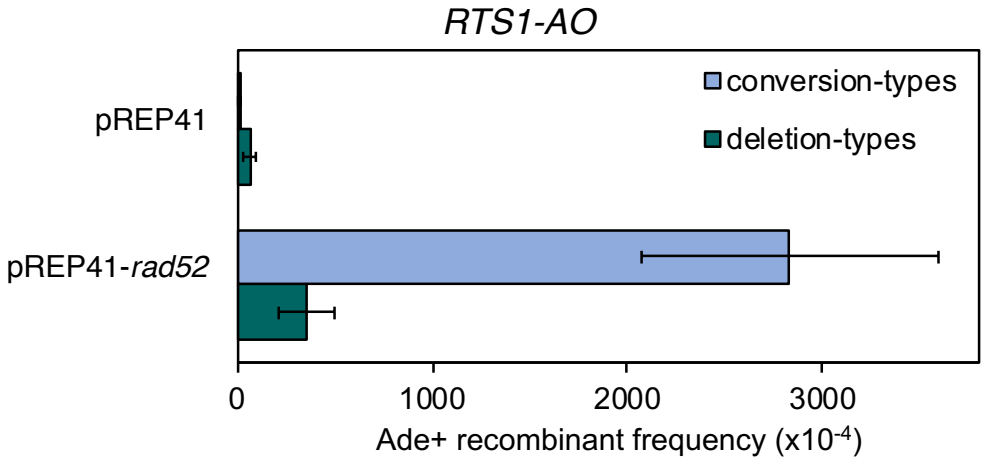


Figure 5.17. Rad52 overexpression promotes *RTS-AO*-induced gene conversions.

Bar chart showing the mean frequency of conversion- and deletion-type Ade$^+$ recombinants in wild-type strain carrying pREP41 and pREP41-*rad52* with *RTS1*-AO Error bars represent ± one standard deviation. In order of presentation, the strains are MCW9156, MCW9155. Note that a general reduction in the frequency of recombinants is typically observed when equivalent strains are grown on EMMG compared to YES. It should be noted that he recombination values for pREP41 appear to be lower than expected even when accounting for the reduced levels seen on EMMG (Lorenz et al., 2009).

The wild-type strain overexpressing Rad52 did not display any additional sensitivity to genotoxins (CPT, HU, MMS, UV) at the range of concentrations tested (data not shown). However, similar to a *dbl2*Δ strain, cells with induced expression of Rad52 were elongated (data not shown) and exhibited hyper-levels of *RTS1-AO*-induced direct repeat recombination (Fig. 5.17). However, unlike *dbl2*Δ, which causes a greater increase in deletions than gene conversions, overexpression of Rad52 results in a greater increase in gene conversions than deletions (Fig. 5.17). Thus, the mutant *dbl2*Δ phenotype cannot be explained only by accumulation of Rad52 at the sites of ongoing DNA repair.

5.2.12 Genetic interactions between *dbl2*/*fbh1* and *Rad51* mediators

My findings linking Dbl2 to both Fbh1-dependent and Fbh1-independent pathways of regulating recombination lead me to investigate the genetic interaction between *dbl2*Δ and mutants of some of the known Rad51 mediators. Since the genetic interaction between *dbl2* and *rad52* is not identical to that between *fbh1* and *rad52*, I also included a comparison with equivalent *fbh1*Δ double mutants to see whether there are further differences between *dbl2* and *fbh1* in terms of their genetic interactions. As mentioned earlier (Chapter 1) each mediator complex (Rad55-Rad57, Swi5-Sfr1, and Rdl1-Rlp1-Sws1) is believed to aid formation and stabilisation of Rad51 nucleoprotein filament via a different mechanism. However, it is currently unclear what distinguishes their functions (Filippo et al., 2008).

5.2.12.1 rad55 and rad57

I first tested the interaction between *dbl2*Δ and *rad55*Δ for genotoxin sensitivity (Fig. 5.18B), making a comparison to a *fbh1*Δ*rad55*Δ double mutant strain that had been made previously by Dr. Fikret Osman (Whitby Lab) (Fig 5.18A). As reported previously, a *fbh1*Δ*rad55*Δ double mutant is less sensitive to MMS, CPT and UV than a *rad55*Δ single mutant, and also less sensitive to MMS and CPT than a *fbh1*Δ single mutant (Osman et al., 2005) (Fig. 5.18A). Similar to *fbh1*Δ, deletion of *dbl2* suppresses the genotoxin hypersensitivity of a *rad55*Δ mutant (Fig. 5.18B). However, although there is suppression for CPT, HU and UV sensitivity, the *dbl2*Δ*rad55*Δ double mutant exhibits slightly more sensitivity to MMS than a *dbl2*Δ single mutant (Fig. 5.18B). Deletion of *dbl2* also suppresses the sensitivity of a *rad57*Δ mutant to CPT, MMS and HU (Fig. 5.19). However, unlike a *dbl2*Δ*rad55*Δ double mutant, the *dbl2*Δ*rad57*Δ double mutant exhibits no reciprocal suppression of CPT or HU sensitivity and is significantly more sensitive to MMS than *rad57*Δ. Altogether these data indicate that Dbl2 has a negative effect on the repair/tolerance of DNA damage in the absence of Rad55-Rad57 consistent with the notion that it functions together with Fbh1 to inhibit Rad51. However, unlike deletion of *fbh1*, which fully suppresses *rad55*Δ hypersensitivity to MMS, deletion of *dbl2* only partially suppresses *rad55*Δ and *rad57*Δ MMS sensitivity. This difference suggests that loss of Dbl2 does not fully disable Fbh1-mediated inhibition of Rad51.

5.2.12.2 swi5 and sfr1

I next analysed the genotoxin sensitivities of *swi5*Δ*dbl2*Δ and *sfr1*Δ*dbl2*Δ double mutants, again comparing to the relevant single mutants and to the

equivalent *fbh1*Δ double mutants (Figs. 5.20 and 5.21). The single *swi5*Δ and *sfr1*Δ single mutants exhibit hypersensitivity to relatively high doses of MMS and UV, which are suppressed back to wild-type levels upon deletion of *fbh1* (Figs. 5.20A and 5.21A). The suppression is reciprocal because *swi5*Δ/*sfr1*Δ also suppresses *fbh1*Δ hypersensitivity to CPT, HU and MMS. Similar reciprocal suppression of genotoxin sensitivities back to wild-type levels are seen with both *swi5*Δ*dbl2*Δ and *sfr1*Δ*dbl2*Δ double mutants (Figs. 5.20B and 5.21B).

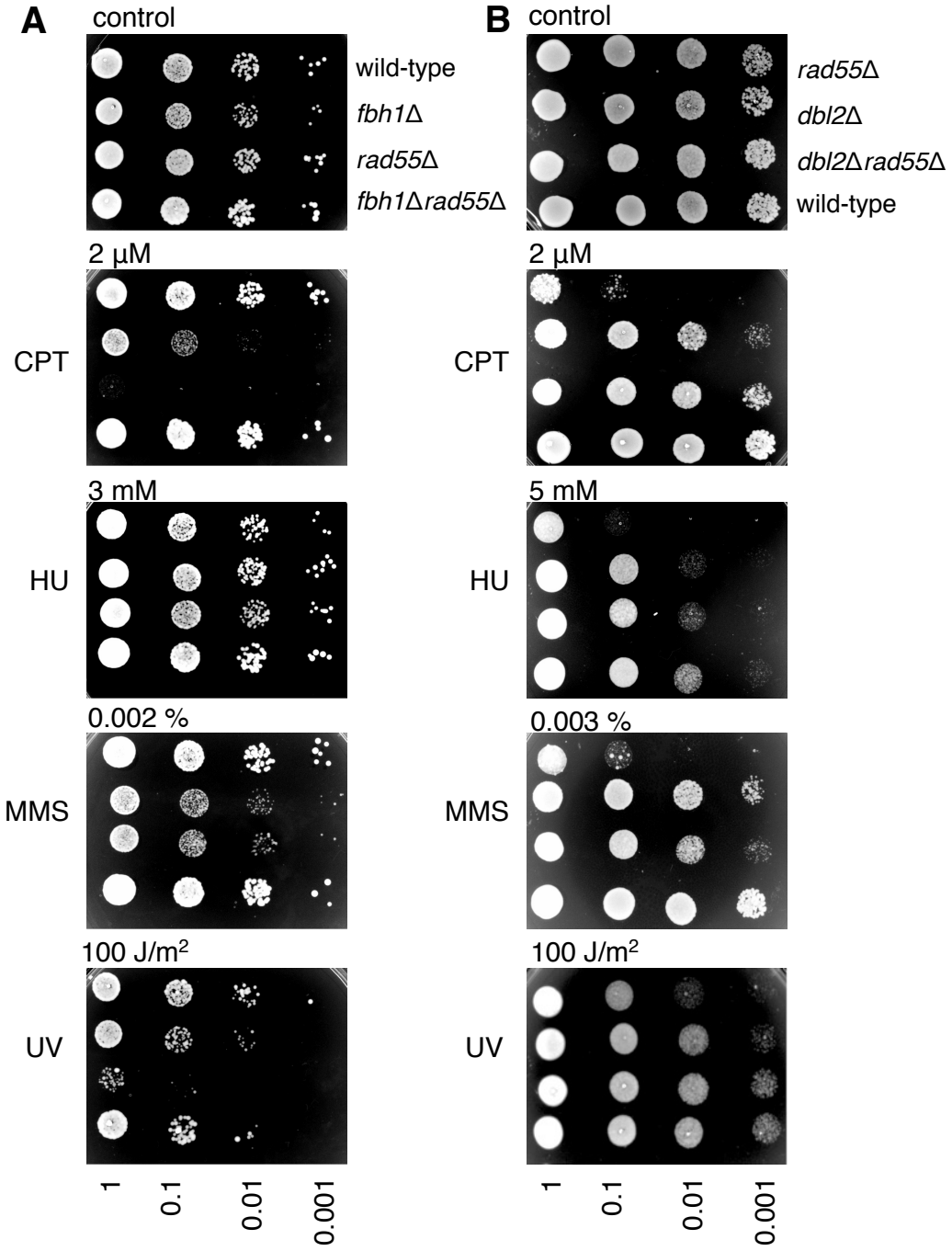


Figure 5.18. Genetic interaction between *fbh1*/*dbl2* and *rad55*.

Spot assay comparing the growth and genotoxin sensitivity of (**A**) wild-type (FO656), *fbh1*Δ (MCW1884), *rad55*Δ (MCW1231) and *fbh1*Δ*rad55*Δ (MCW1566). (**B**) *rad55*Δ (MCW1231), *dbl2*Δ (MCW8564), *dbl2*Δ*rad55*Δ (MCW8760), and wild-type (FO656). The plates were photographed after 5 days of incubation at 30 °C.

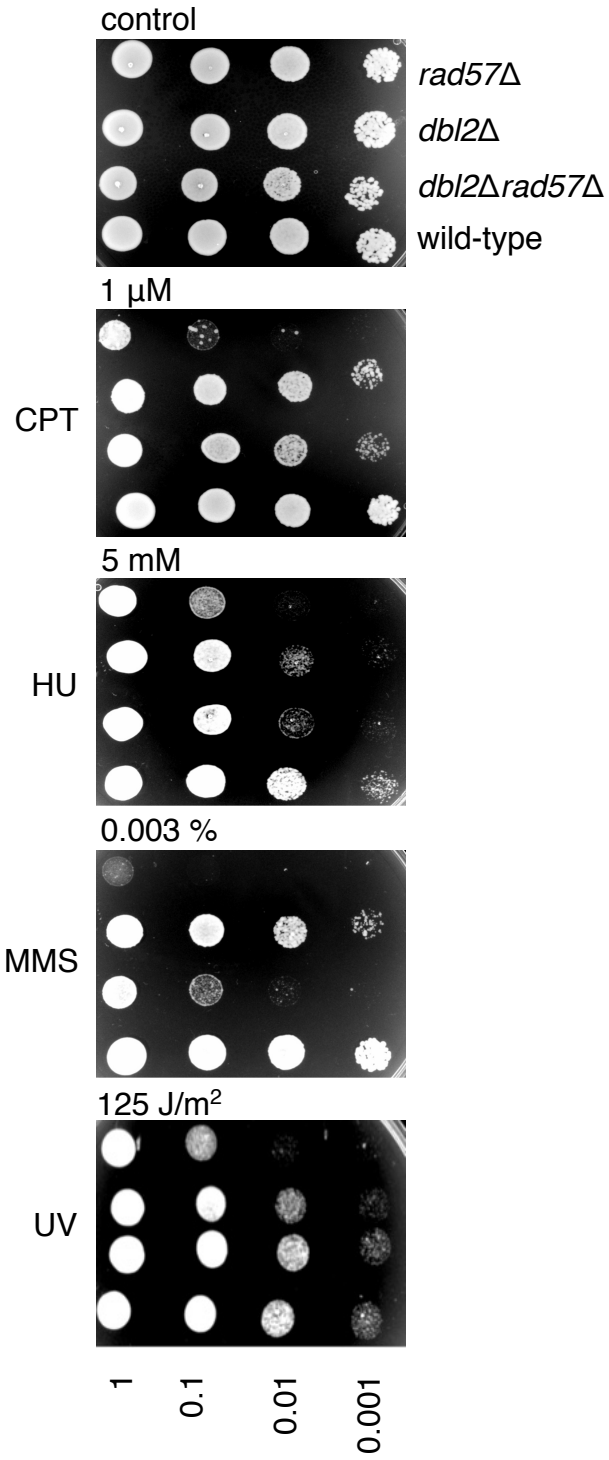


Figure 5.19. Genetic interaction between *dbl2* and *rad57*.

Spot assay comparing the growth and genotoxin sensitivity of *rad57*Δ (MCW1242), *dbl2*Δ (MCW8564), *dbl2*Δ*rad57*Δ (MCW8715), and wild-type (FO656). The plates were photographed after 5 days of incubation at 30 °C.

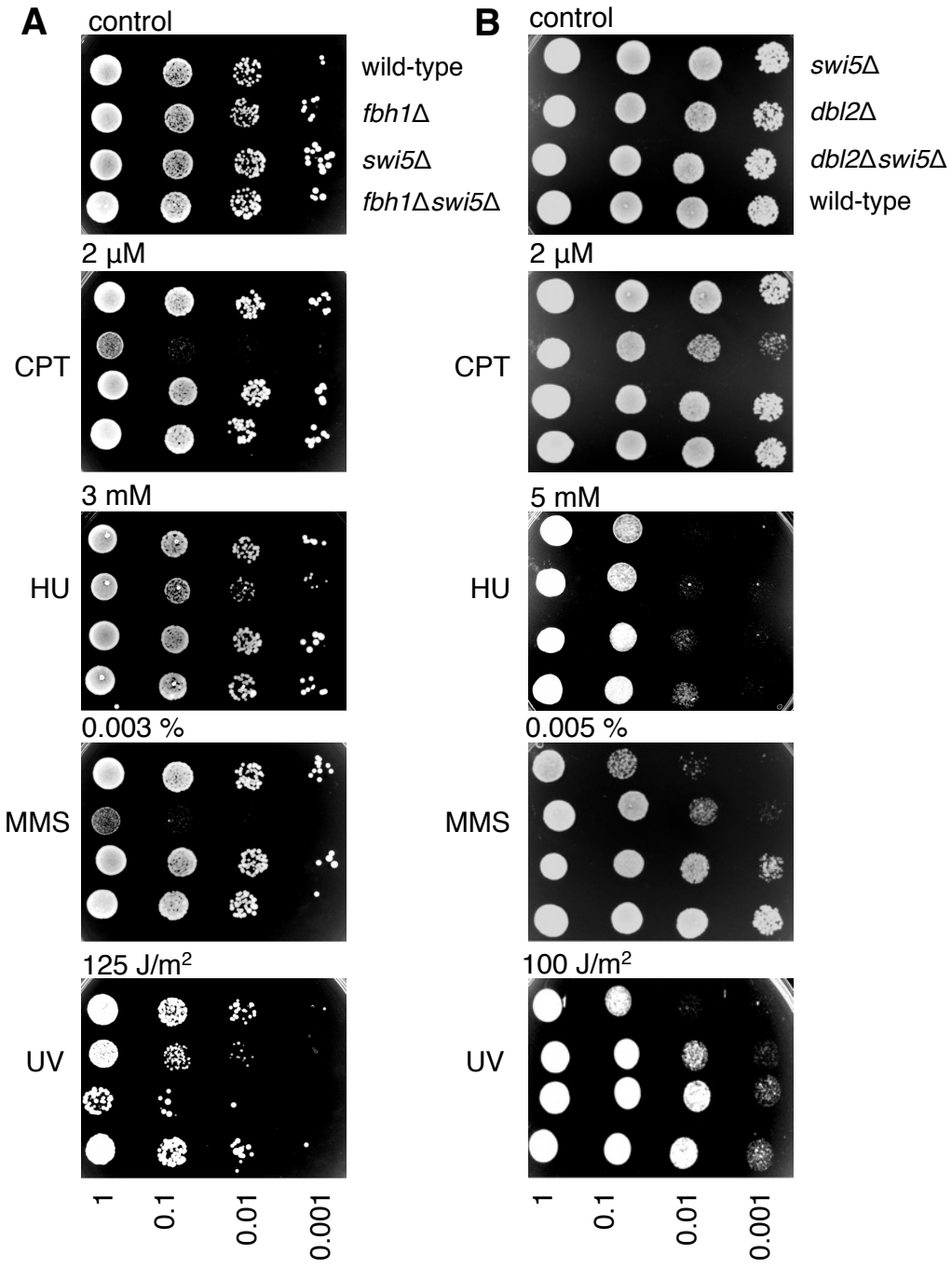


Figure 5.20. Genetic interaction between *fbh1*/*dbl2* and *swi5*.

Spot assay comparing the growth and genotoxin sensitivity of (**A**) wild-type (FO656), *fbh1*Δ (MCW1884), *swi5*Δ (MCW1481) and *fbh1*Δ*swi5*Δ (MCW4985). (**B**) *swi5*Δ (MCW1481), *dbl2*Δ (MCW8564), *dbl2*Δ *swi5*Δ (MCW8717), and wild-type (FO656). The plates were photographed after 5 days of incubation at 30 °C.

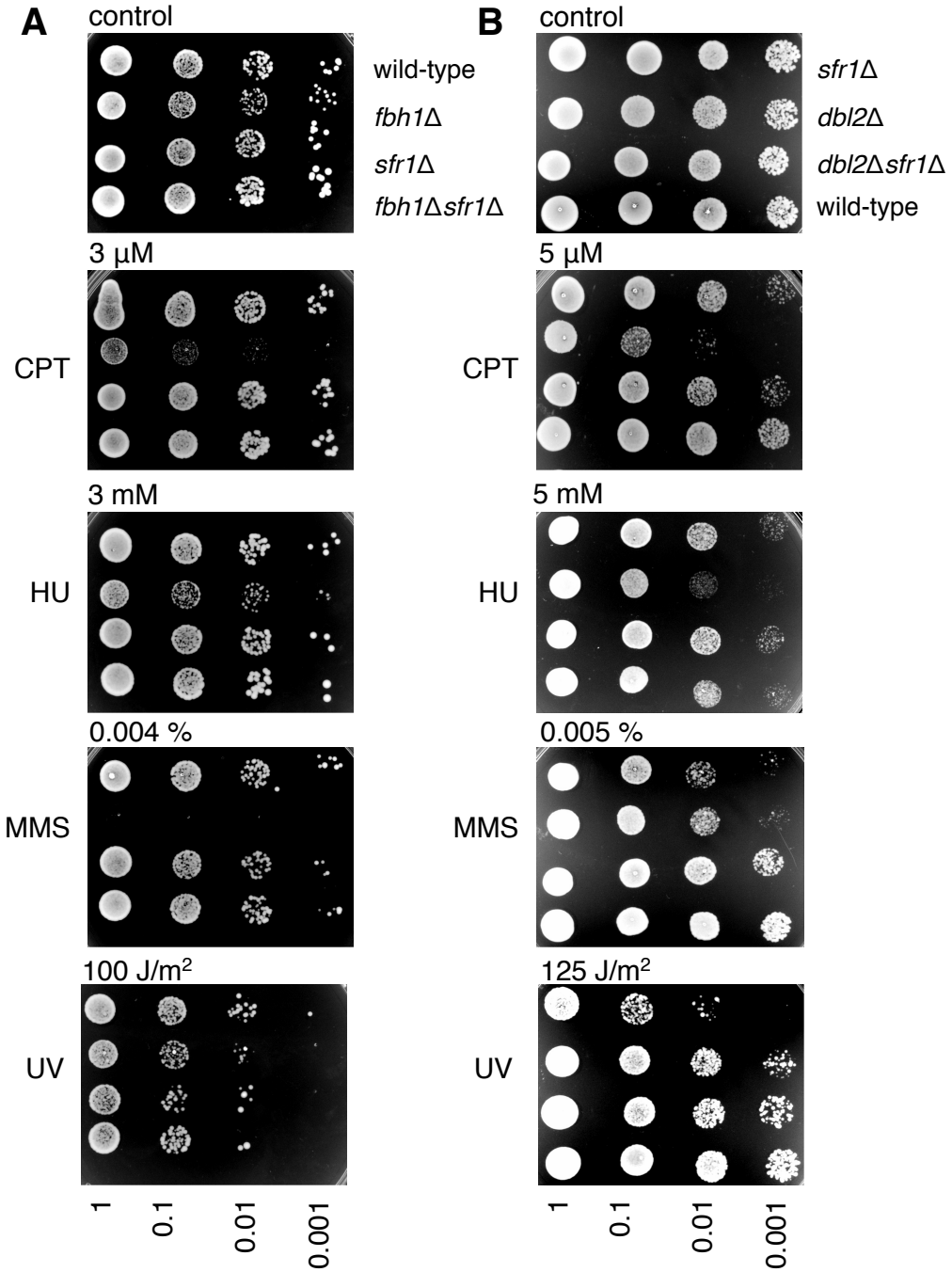


Figure 5.21. Genetic interaction between *fbh1*/*dbl2* and *sfr1*.

Spot assay comparing the growth and genotoxin sensitivity of (**A**) wild-type (FO656), *fbh1*Δ (MCW1884), *sfr1*Δ (MCW3263) and *fbh1*Δ*sfr1*Δ (MCW5864). (**B**) *sfr1*Δ (MCW3263), *dbl2*Δ (MCW8564), *dbl2*Δ *sfr1*Δ (MCW8759), and wild-type (FO656). The plates were photographed after 5 days of incubation at 30 °C.

5.2.12.3 rdl1, rlp1 and sws1

The final set of Rad51 mediator mutants that I tested with *dbl2*Δ and *fbh1*Δ was *rdl1*Δ, *rlp1*Δ and *sws1*Δ (Figs. 5.22, 5.23 and 5.24). The single mutant *rdl1*Δ, *rlp1*Δ and *sws1*Δ strains did not exhibit hypersensitivity to the doses of genotoxins that I used. However, both *rdl1*Δ and *rlp1*Δ suppressed the genotoxin sensitivities of a *fbh1*Δ and *dbl2*Δ mutant back to wild-type levels (Figs. 5.22, 5.23 and 5.24). In contrast, *sws1*Δ does not suppress the hypersensitivity of a *fbh1*Δ mutant to MMS and UV (at the doses tested) and only partially suppresses its sensitivity to CPT (Fig. 5.24A). Similarly, *sws1*Δ only partially suppresses *dbl2*Δ CPT hypersensitivity (Fig. 5.24B). However, unlike with *fbh1*Δ, *sws1*Δ also partially suppresses *dbl2*Δ HU and MMS hypersensitivity (Fig. 5.24B).

Altogether, the data reported above (Section 5.2.9) indicate that the mediator proteins are important for promoting Rad51 action in the presence of Fbh1 and Dbl2. Furthermore, where Rad51 action is attenuated by the removal of a mediator protein, the requirement for Fbh1 and Dbl2 to promote growth and DNA repair is reduced.

5.2.13 Genetic interaction between *dbl2*Δ and *rqh1*Δ

The RecQ family DNA helicase Rqh1, which is known to limit the accumulation of toxic Rad51-dependent recombination intermediates following RF stalling in HU, is essential for viability in the absence of Fbh1 (Laursen et al., 2003; Morishita et al., 2005; Osman et al., 2005). It was also reported that *dbl2*Δ is synthetically lethal with *rqh1*Δ (Polakova et al., 2016).

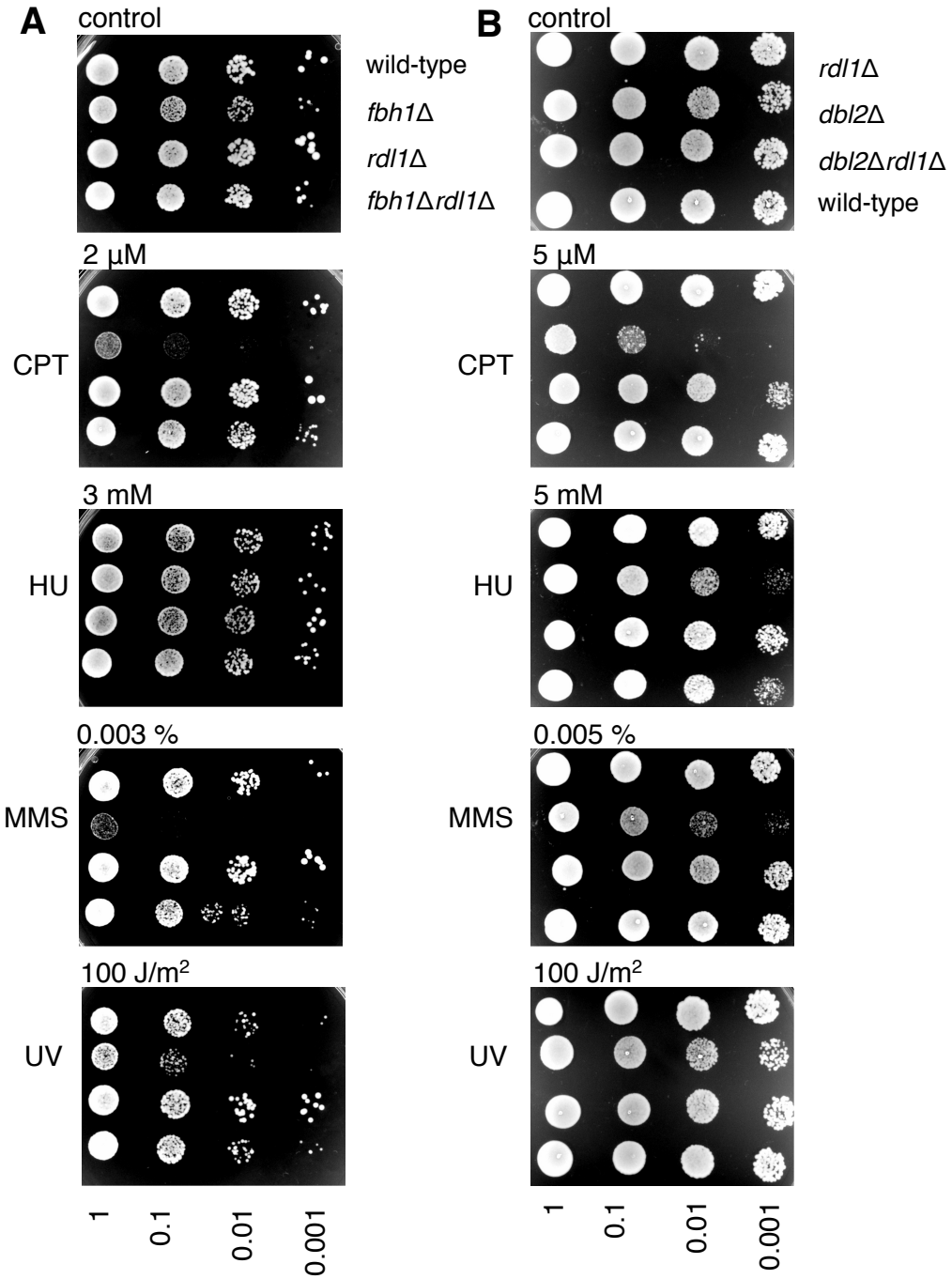


Figure 5.22. Genetic interaction between *fbh1*/*dbl2* and *rdl1*.

Spot assay comparing the growth and genotoxin sensitivity of (**A**) wild-type (FO656), *fbh1*Δ (MCW1884), *rdl1*Δ (MCW6119) and *fbh1*Δ*rdl1*Δ (MCW4971). (**B**) *rdl1*Δ (MCW6119), *dbl2*Δ (MCW8564), *dbl2*Δ *rdl1*Δ (MCW8718), and wild-type (FO656). The plates were photographed after 5 days of incubation at 30 °C.

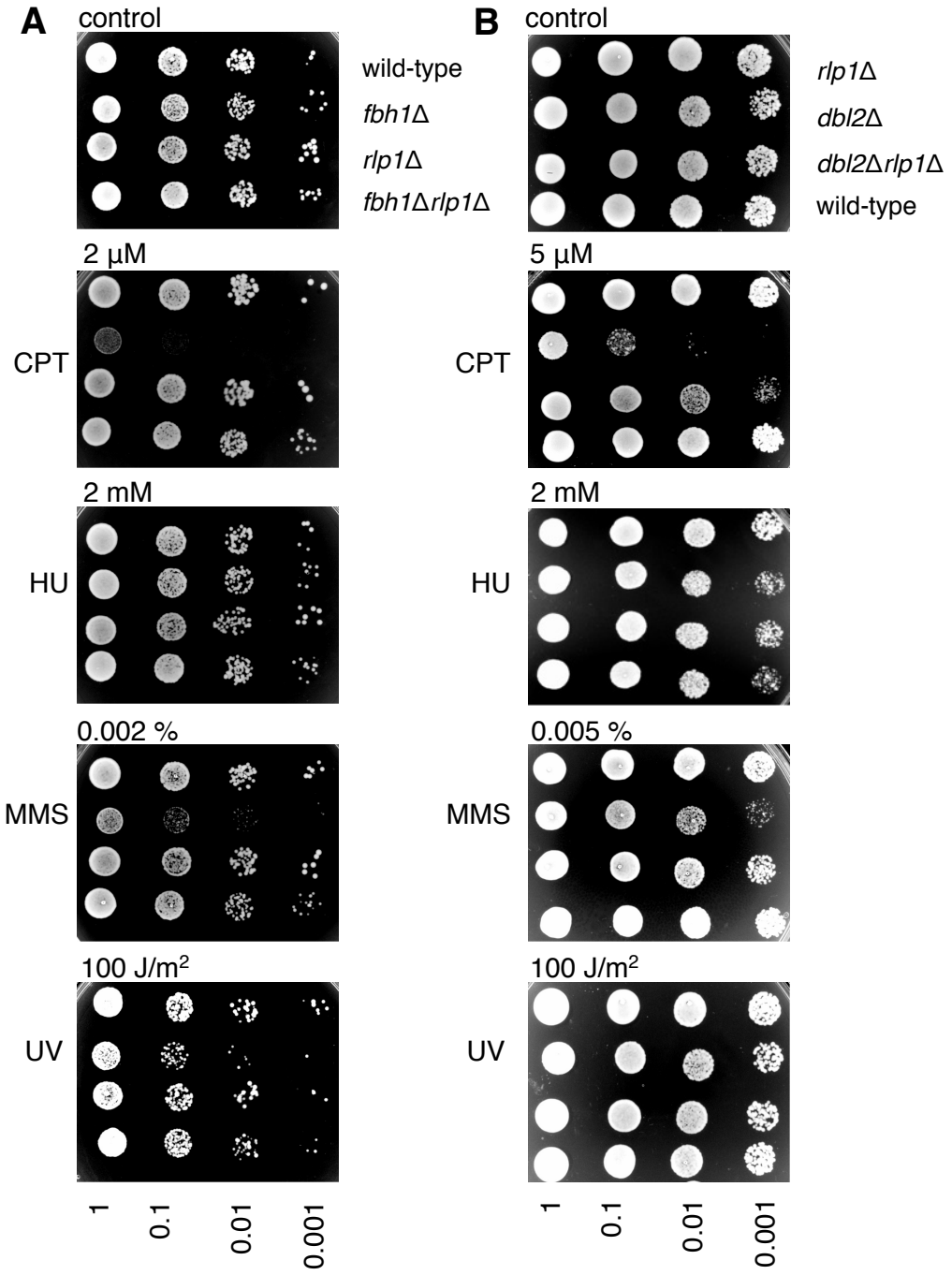


Figure 5.23. Genetic interaction between *fbh1*/*dbl2* and *rlp1*.

Spot assay comparing the growth and genotoxin sensitivity of (**A**) wild-type (FO656), *fbh1*Δ (MCW1884), *rlp1*Δ (MCW6120) and *fbh1*Δ*rlp1*Δ (MCW4982). (**B**) *rlp1*Δ (MCW6120), *dbl2*Δ (MCW8564), *dbl2*Δ *rlp1*Δ (MCW8720), and wild-type (FO656). The plates were photographed after 5 days of incubation at 30 °C.

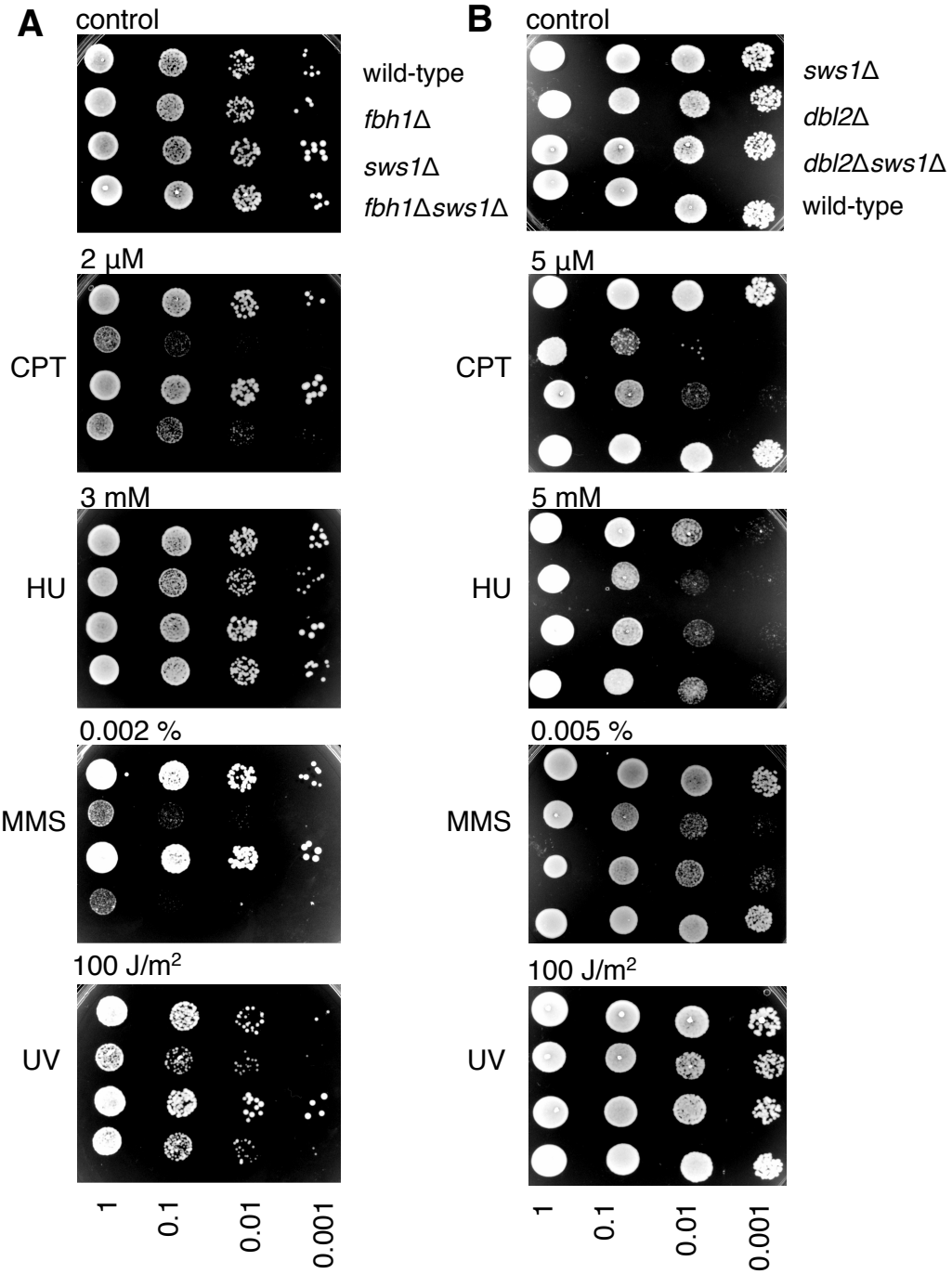


Figure 5.24. Genetic interaction between *fbh1*/*dbl2* and *sws1*.

Spot assay comparing the growth and genotoxin sensitivity of (**A**) wild-type (FO656), *fbh1*Δ (MCW1884), *sws1*Δ (MCW6342) and *fbh1*Δ*sws1*Δ (MCW4979). (**B**) *sws1*Δ (MCW6342), *dbl2*Δ (MCW8564), *dbl2*Δ*sws1*Δ (MCW8719), and wild-type (FO656). The plates were photographed after 5 days of incubation at 30 °C.

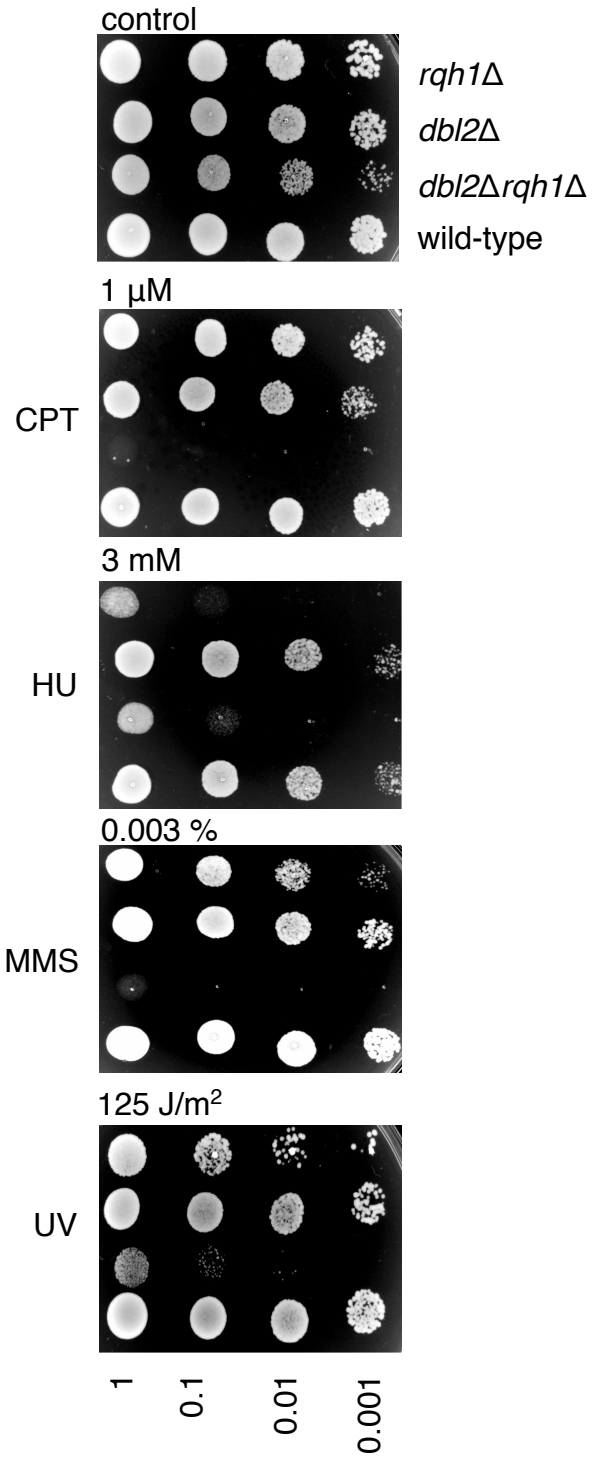


Figure 5.25. Genetic interaction between *dbl2* and *rqh1*.

Spot assay comparing the growth and genotoxin sensitivity of *rqh1*Δ (MCW1818), *dbl2*Δ (MCW8564), *dbl2*Δ*rqh1*Δ (MCW8754), and wild-type (FO656). The plates were photographed after 5 days of incubation at 30 °C.

To confirm this finding, I attempted to make a *dbl2*Δ*rqh1*Δ by a standard genetic cross. To my surprise, I was able to readily isolate a viable *dbl2*Δ*rqh1*Δ double mutant. However, this may be due to the double mutant acquiring a suppressor mutation, which enabled it to survive. Nevertheless, I tested the *dbl2*Δ*rqh1*Δ double mutant for its sensitivity to genotoxins (Fig. 5.25). The double mutant grows more poorly than either of its component single mutants and exhibits a synergistic increase in sensitivity to CPT, MMS and UV (Fig. 5.25). However, surprisingly the double mutant was slightly less sensitive to HU than a *rqh1*Δ single mutant. This partial suppression of *rqh1*Δ HU sensitivity by *dbl2*Δ is reminiscent of the genetic interaction between *fml1*Δ and *rqh1*Δ (Sun et al., 2008). Together these data indicate that Dbl2 and Rqh1 function in distinct but overlapping pathways for the tolerance/repair of CPT, MMS and UV-induced DNA damage. The partial suppression of *rqh1*Δ HU sensitivity suggests that Dbl2 may also promote recombination at certain types of stalled replication fork.

5.3 Discussion

In this chapter, I have shown that the genetic interaction between *dbl2* and *fml1* is not epistatic (Fig. 5.1), however some of the recombination induced at the *RTS1* barrier in the absence of Dbl2 is Fml1-dependent (Fig. 5.3). Fml1 limits formation of both spontaneous gene conversion and deletion types in a *dbl2*Δ mutant. The synergistic interaction between *dbl2*Δ and *fml1*Δ for both genotoxin sensitivity and spontaneous direct repeat recombination is in stark contrast with the epistatic interaction observed for *mte1* and *mph1* in budding

yeast (Yimit et al., 2015; Silva et al., 2016; Xue et al., 2016). This difference may be explained by Dbl2 acquiring a different/additional interaction partner in fission yeast (i.e. Fbh1, which has no homolog in budding yeast).

In contrast to its genetic interaction with *fml1*, I found that there are a lot of similarities of *dbl2*Δ with *fbh1*Δ phenotypes, including aberrant chromosome segregation, genotoxin sensitivity, ability to acquire suppressor, dramatically increased *RTS1* induced but not spontaneous recombination, accumulation of Rad51 foci in deletion mutants, positive genetic interactions of *fbh1*Δ *or dbl2*Δ with most of the Rad51 mediators deletion mutants (Chapter 4 and Chapter 5). These data indicate that Dbl2 and Fbh1 work in the same pathway to regulate Rad51-dependent recombination at collapsed replication forks. How exactly Dbl2 functions together with Fbh1 to regulate recombination remains unknown. The finding that Dbl2 is needed for efficient formation of Fbh1 foci at genotoxin-induced DSB sites (when Fbh1-YFP is overexpressed from the strong *nmt* promoter on a plasmid) indicates that it might play a role in the recruitment or retention of Fbh1 to sites of DNA damage/collapsed replication forks (Polakova et al., 2016). However, the overexpression even from weaker *nmt*41 promoter (~ 10-fold decrease in amount of protein) of Fbh1 or Dbl2 is poisonous to the wild-type cells (Figs. 5.8 – 5.9), it impacts growth and is characterised by hypersensitivity to UV, HU, MMS, and CPT ((Lorenz et al., 2009) and Chapter 4 and 5). Therefore, there is a possibility that observations made by Polakova et al. (2016) are true only in non-physiological conditions due to massive over-expression of Fbh1-YFP, Dbl2-YFP or the presence of

spontaneous suppressor mutations which may occur in *fbh1*Δ and *dbl2*Δ mutant cells (Osman et al., 2005 and this study).

However, such a function would not explain my finding that overexpression of Dbl2 partially rescues the CPT and MMS hypersensitivity of a *fbh1*Δ mutant (Fig. 5.9). This result suggests that Dbl2 is capable of compensating for the absence of Fbh1, presumably by directly or indirectly inhibiting Rad51. As discussed below, Dbl2 appears to inhibit Rad52-dependent/Rad51-independent recombination and, therefore, it is possible that it negatively regulates Rad51 by inhibiting Rad52. Alternatively, it might promote the activity of other antirecombinases, such as Srs2, or interfere with other Rad51 promoting factors such as Rad55-Rad57 or Rad54.

Even though *dbl2*Δ and *fbh1*Δ mutants share many common phenotypes, and an epistatic interaction with respect to aberrant cell morphology, chromosome segregation and *RTS1*-AO induced recombination, a *dbl2*Δ*fbh1*Δ double mutant is more sensitive to MMS and CPT than single mutant (Fig. 5.5). This finding indicates that Dbl2 has a role in repairing/tolerating DNA damage that is independent of Fbh1. Insight into what this role might be coming from my finding that Dbl2, unlike Fbh1, is required for limiting Rad52-dependent recombination (that is independent of Rad51) at the *RTS1* barrier (Fig. 5.11). As discussed in Chapter 1, a major role for Rad52 is to mediate the nucleation of Rad51 onto RPA-coated ssDNA and thereby promote the Rad51-dependent pathway of recombination (Mortensen et al., 1996; Sung, 1997b; Sugiyama et al., 1998; Kurokawa et al., 2008). However, Rad52 can also direct DSB repair by SSA independently of Rad51 through its ability to catalyse DNA strand

annealing between complementary sequences coated with RPA (Bai and Symington, 1996; Sung, 1997b; Petukhova et al., 1999; Davis and Symington, 2001; Pohl and Nickoloff, 2008). Rad52 can also promote Rad51-independent BIR in both yeast and in mammalian cells (Sakofsky and Malkova, 2017). However, recent work in humans suggests that Rad52-promoted DNA synthesis in response to replication stress can be the preferred pathway in some circumstances (Ciccia and Symington, 2016; Mazina et al., 2017). Exactly how it does this is still unknown, but it may depend on its ability to catalyse 'inverse strand exchange' in which a complex of Rad52 bound to dsDNA "invades" a complementary ssDNA (Keskin et al., 2014; Hanamshet et al., 2016; Mazina et al., 2017).

Moreover, unpublished work from the Whitby laboratory has shown that Rad51-independent replication restart at the *RTS1* RFB is more efficient and robust than previously thought. How exactly Rad52 catalyses replication restart without Rad51 is unknown, although it has been shown to catalyse D-loop formation *in vitro* (Mortensen et al., 1996; Reddy et al., 1997; Kagawa et al., 2001; Kumar et al., 2004). Intriguingly, Fml1 has a role in limiting Rad52-dependent/Rad51-independent recombination at the *RTS1* RFB (Sun et al., 2008; Morrow et al., 2017) and, therefore, it is possible that Dbl2 functions together with Fml1 in this regard. Interestingly, Dbl2 is also needed for the elevated frequency of spontaneous deletion-type recombinants in a *rad51*Δ mutant (Fig. 5.11). This implies that Dbl2 potentially can not only limit Rad52-dependent, but also promote Rad52-dependent recombination in the absence of Rad51.

In budding yeast Mte1 was shown to stimulate the helicase and fork regression activities of Mph1 while inhibiting the ability of Mph1 to dissociate recombination intermediates (Silva et al., 2016). If Dbl2 is capable of regulating Fml1 in a similar manner, a potential mechanism by which it could affect Rad52-dependent recombination, in the absence of Rad51, can be envisaged. Fml1 catalyses both fork reversal and fork resetting (Sun et al., 2008; Nandi and Whitby, 2012; and Whitby laboratory unpublished data). If Dbl2 promotes reversal by inhibiting resetting of the fork then, in its absence, the amount of fork resetting would increase, which could lead to the generation of longer ssDNA tails. Rad52 could bind to these tails and more efficiently promote deletion-type formation via its ssDNA annealing activity (Reddy et al., 1997; Petukhova et al., 1999; Davis and Symington, 2001; Kagawa et al., 2001).

Consistent with Fbh1's function in limiting Rad51 accumulation at stalled replication forks, deletion of *fbh1* causes accumulation of Rad51 (Morishita et al., 2005; Lorenz et al., 2009; Tsutsui et al., 2014). I examined whether Dbl2 can similarly restrict Rad51 and/or Rad52 accumulation at the *RTS1* RFB in *S. pombe.* The *dbl2*Δ mutant cells exhibit extremely high levels of Rad51 and Rad52 nuclear foci irrespective of the orientation of the barrier. This accumulation of Rad51 and Rad52 suggest that, although Dbl2 is not required to limit spontaneous recombination at *RTS1* placed at endogenous *ade6* locus, it seems to prevent accumulation of Rad51 and Rad52 at other spots of ongoing HR. Consistent with *dbl2*Δ mutant displaying a dramatic increase in Rad51-dependent recombination at *RTS1*-AO, a significant increase in the percentage of Rad51 and Rad52 foci that colocalize with *RTS1* in active

orientation compared to inactive orientation is observed (Fig. 5.16). These data suggest that Dbl2 limits Rad51 and Rad52 accumulation at blocked replication forks and might facilitate Fbh1 anti-recombinase activity. In addition to this Dbl2 also seems to be required for the regulation of Rad52 activity as in *dbl2*Δ cells there is increase in cells with Rad52 foci.

Another distinction between Dbl2 and Fbh1 is the failure of *dbl2*Δ to suppress the phenotype of a *rad52*Δ mutant (Fig. 5.14). Rad52 promotes the nucleation of Rad51 onto RPA-coated ssDNA. The fact that deletion of *fbh1* suppresses the genotoxin sensitivity of a *rad52*Δ mutant suggests that Rad51 nucleofilament formation can occur without Rad52 mediated nucleation but is not sufficiently robust to resist disruption by Fbh1. However, Rad52-independent recombination, even in the absence of Fbh1, exhibits a much-reduced ability to generate recombinants in the direct repeat assay. This suggests that other anti-recombinases (e.g. Srs2) may disrupt the Rad51 nucleofilament without Rad52, or that Rad52 is required for activities in addition to nucleating Rad51 onto DNA. My finding that deleting *dbl2* does not suppress *rad52*Δ genotoxin sensitivity suggests that Dbl2 is not essential for Fbh1 activity. Indeed, Fbh1 may still function well enough without Dbl2 to disrupt Rad51 nucleofilaments as long as they are weakened by the absence of Rad52. However, the same may not be true for the disruption of Rad51 nucleofilaments in the absence of Rad55-Rad57 as, in this case, deletion of *dbl2* suppresses the genotoxin hypersensitivity of a *rad55*Δ mutant almost as well as deleting *fbh1* (Figs. 5.18 – 5.19). This suggests that Fbh1 has a

stronger requirement for Dbl2 when attempting to disrupt Rad51 nucleofilaments in the presence of Rad52.

Tsutsui et al. (2014) showed that *in vitro*, in the absence of the Swi5-Sfr1 complex, Fbh1 inhibits DNA strand-exchange by disruption of the Rad51 filament, but not when the Rad51 filament has been activated by the Swi5-Sfr1 complex. Furthermore, W. Heyer's group showed that in budding yeast Rad55-Rad57 stabilizes Rad51-ssDNA filaments against disruption by Srs2 (Liu et al., 2011a). This stabilisation also appears to depend on the so-called Shu complex (Shu1-Shu2-Psy3-Csm2), which is the functional equivalent of the fission yeast Rdl1-Rlp1-Sws1 complex (Bernstein et al., 2011). Recently Ma et al. (2018) showed that Rad52 is essential for protecting Rad51 filaments against dissociation activity of Srs2. Thus, the yin and yang between factors promoting Rad51 nucleofilament formation and those trying to de-stabilize appears to be a conserved feature of homologous recombination. The genetic interactions between *dbl2*Δ and the various Rad51 mediator mutants, reported in this Chapter (Figs. 5.18 – 5.24), clearly show that Dbl2 is a key component of this yin and yang system. However, its precise function will only become clear with studies involving the *in vitro* reconstitution of the reactions in which it is thought to act.

Intriguingly, interaction between *fbh1* and *sws1* was the only one that did not result in suppression sensitivity to MMS relative to single mutants, however deletion of Sws1 partially suppresses *dbl2*Δ (Fig. 5.24), *rqh1*Δ and *srs2*Δ (Martín et al., 2006). This might suggest that Fbh1 acts in a different pathway

than Rqh1, Srs2 and Dbl2 and cannot counter the assembly of Rad51 filament modulated by Sws1.

To gain clearer understanding of the molecular mechanisms of the pathways Dbl2 is involved in, future analysis should be focused on the discovery of Dbl2 physical interaction partners. Putative interaction partners can be searched by pull-down of Dbl2 followed by mass-spectrometry and complemented by the immunoprecipitation experiments with putative interaction partners such as Fml1, Fbh1, Rad51, Rad52. I attempted to address both approaches. However, I never was able to detect the tagged protein by western blot in strains with Dbl2 tagged on its C-terminus with 3HA, 13-myc, GST or GFP tags. Dbl2 tagged at its N-terminus with YFP was detectable in alkaline cell lysates, but not reproducibly. Therefore, Dbl2 does seem to be hard to extract from the cell lysate in native conditions necessary for interaction studies, and the potential reason for this will be discussed in Chapter 6.

Chapter 6

6 Purification of Dbl2 and analysis of its N-terminal domain

6.1 Introduction

Dbl2 is a 78.1 kDa 715 amino acid long protein. As mentioned before (Chapter 1) Dbl2 has homologs in *S. cerevisiae* (Mte1) and *H. sapiens* (ZGRF1) (Fig. 6.1) (this study; Polakova et al., 2016). Dbl2 has only one domain of unknown function at its N-terminus termed DUF2439. DUF2439 is also found within the N-terminal region of the meiosis-specific recombination protein Rdh54 in *S. pombe* and its homologues in *S. cerevisiae* (Rdh54) and human (RAD54B), which function in both mitotic and meiotic cells (Catlett and Forsburg, 2003; Raschle et al., 2004; Chi et al., 2006, 2009; Sarai et al., 2008; Santa Maria et al., 2013). These proteins are members of the wider Swi2/Snf2 protein family, which also includes their close relative Rad54. However, Rad54 itself does not contain DUF2439. Although there are reports on the biochemical analysis of the N-terminal regions of RAD54B and budding yeast Rdh54, there is no information about the function or structure of DUF2439 (Chi et al., 2006; Sarai et al., 2008).

Structure-function analysis of Mte1 revealed that the DNA-binding fragment is located in the middle and the Mph1-interacting domain is at the C-terminus of the protein. No function was assigned to the DUF2439 domain (Xue et al., 2016). In this chapter I describe the purification of both full-length Dbl2 protein and its N-terminal domain as well as my attempts to characterise the protein using biophysical and structural techniques.

6.2 Results

6.2.1 Bioinformatic analysis of Dbl2

To identify homologs of Dbl2 and to confirm previously reported homologs (Polakova et al., 2016), I utilized the EMBL-EBI bioinformatics web tools including FASTA, PSI-Search and InterPro. FASTA performs a local heuristic search of a protein database for a query sequence. Contrary to FASTA, PSI-Search (similar to PSI-BLAST) performs an optimal local alignment search using the Smith-Waterman search algorithm (SSEARCH) followed by the PSI-BLAST profile construction strategy to find distantly related protein sequences (Li et al., 2015). InterPro is an online tool that allows functional analysis of protein sequences, it assigns proteins to the families based on signatures from several different databases (including CATH-Gene3D, Pfam, ProDom, PANTHER, etc.) and thus predicts the presence of functional domains and sites (Finn et al., 2017).

Using the Dbl2 sequence as the starting query, hits with the highest significance score are orthologues from other *Schizosaccharomyces* species that are categorized as meiotic chromosome segregation proteins. If DUF2439 is used as the starting query, ZGRF1 from different organisms, including Human ZGRF1, is identified. InterPro does not find homologous super-families or protein family membership for Dbl2, however it does identify proteins with the 7-85 amino acid (aa) DUF2439, and among the proteins that

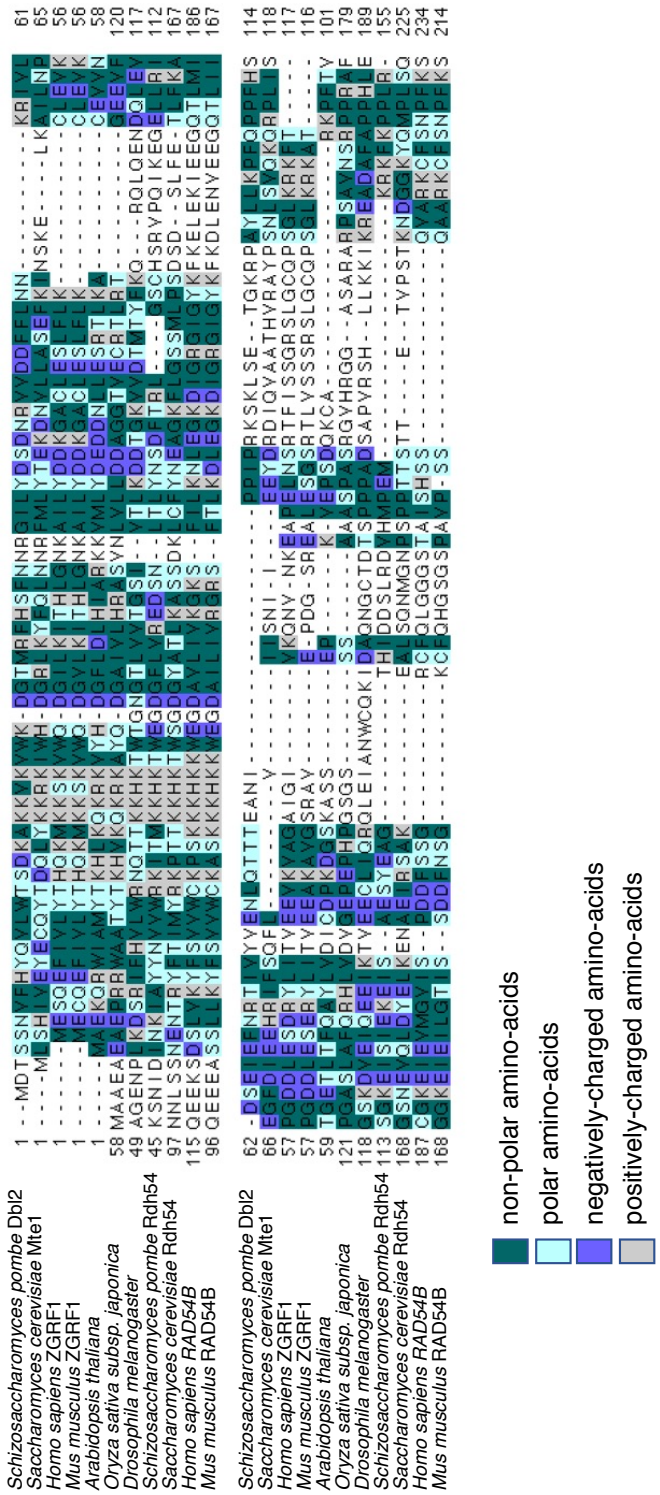


Figure 6.1. N-terminal region of Dbl2 is conserved in plants, fungi and animal. DUF2439 domain is also conserved in Rdh54/RAD54B proteins.

Alignment of the N-terminal domain of Dbl2 and homologous proteins with the DUF2439 domain in Rdh54/RAD54B. Proteins were identified with FASTA, PSI-Search and InterPro (Li et al., 2015; Finn et al., 2017). The alignment was performed using Clustal Omega and visualized in Jalview (Waterhouse et al., 2009).

have this domain are isoforms of human and mouse ZGRF1, Mte1 and Rdh54 from *S. cerevisiae,* Dbl2 and Rdh54 from *S. pombe*, uncharacterized proteins from *Arabidopsis thaliana, Oryza sativa subsp. Japonica* and *Drosophila melanogaster* (Fig. 6.1).

To predict and model the 3D structure of Dbl2, I used a set of web-tools called Phyre2. Phyre2, similar to all other existent protein structure modelling software, performs a search for similar protein sequences from a large database and constructs a model of the protein based on its alignment with sequences with known structure (Kelley et al., 2015). According to analysis by Phyre2 ~ 79 % of Dbl2 is disordered ~ 8 % is comprised of beta-strands, mostly packed into the DUF2439 domain (Fig. 6.2), and 13 % is alpha-helix, located in the middle of the protein (~ 381-392 aa) and at its C-terminus (~ 682-700 aa) (Fig. 6.2). The high amount of disordered structure in Dbl2 is not surprising given its amino acid sequence is rich in polar and charged residues with only a small proportion of hydrophobic amino acids, which makes it unable to form a globular tertiary structure (Radivojac et al., 2007; Dunker et al., 2008). However, it should be noted that the prediction of the scale of disorder in Dbl2 varied depending on which algorithm was applied ranging from 2.1 % disorder (ESpritz-DisProt) to 86.4 % (VSL2b) (Oates et al., 2012; Piovesan et al., 2018) (Fig. 6.3).

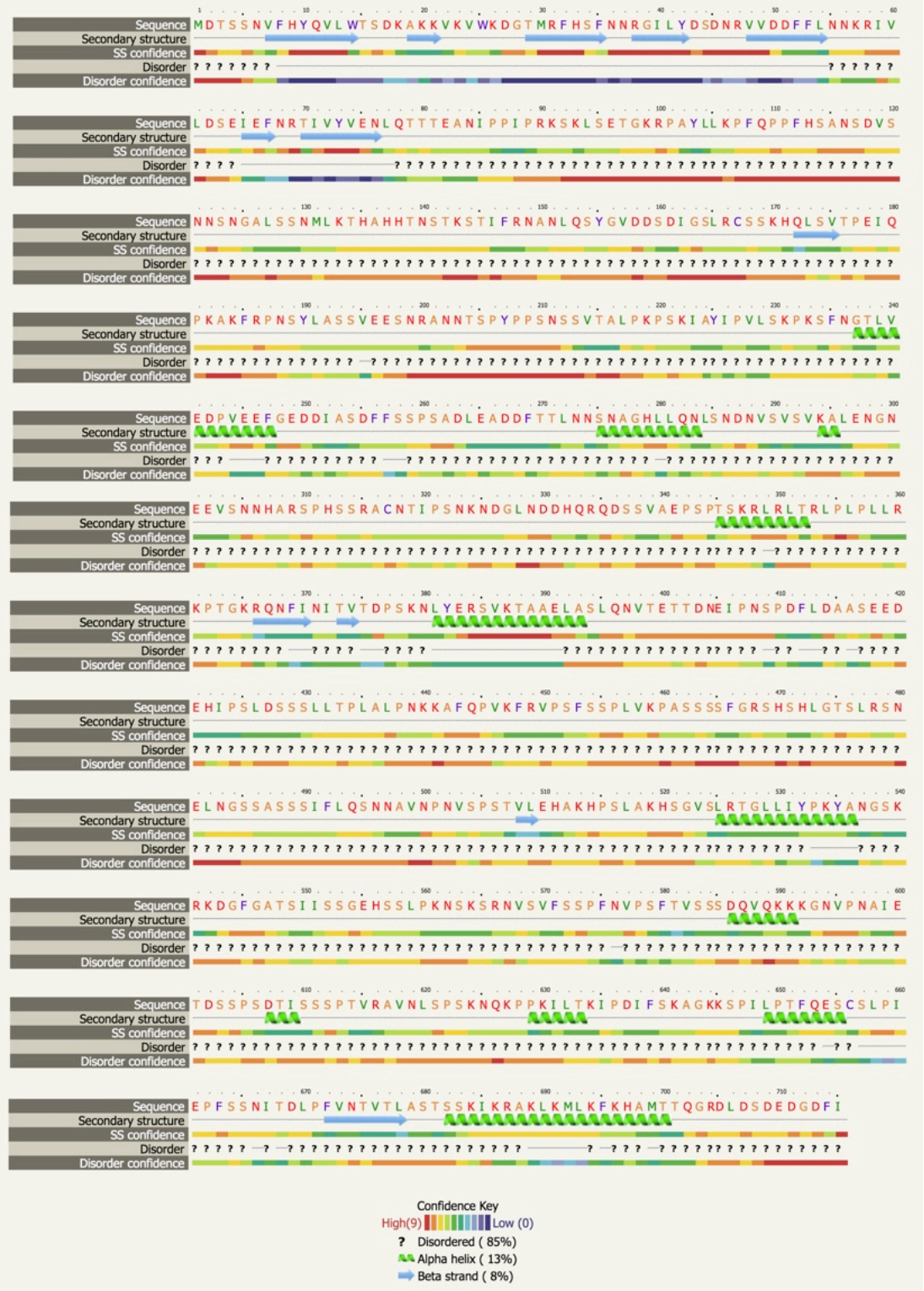


Figure 6.2. Dbl2 secondary structure and disorder prediction.

Dbl2 secondary structure and disorder prediction with Phyre2 (Kelley et al., 2015).

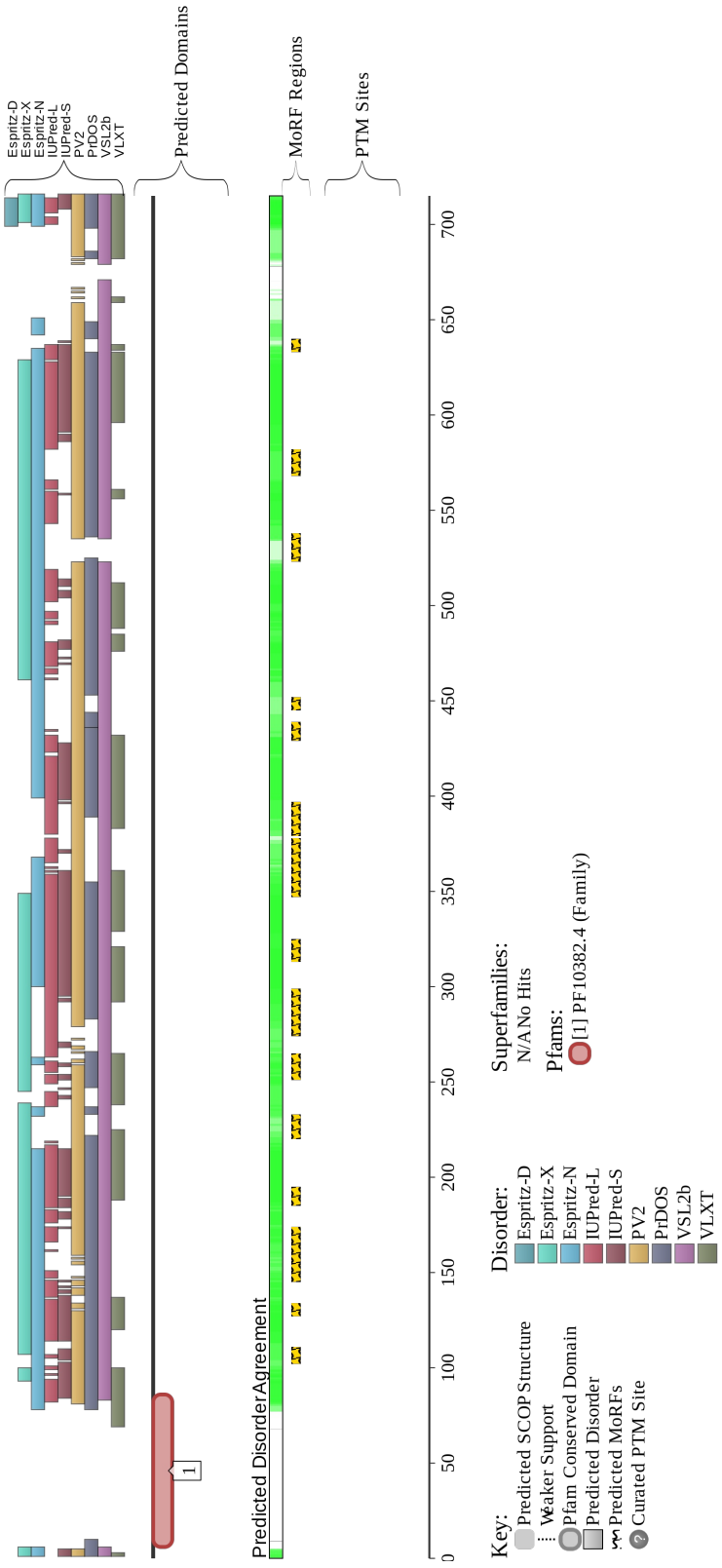


Figure 6.3. Dbl2 is predicted to be a highly disordered protein.

Disorder predictions by different algorithms (Oates et al., 2012): Espritz (Walsh et al., 2012), IUPred-L,-S (Dosztányi et al., 2005), PV2 (Ghalwash et al., 2012), PrDOS (Ishida and Kinoshita, 2007), VSL2b (Peng et al., 2006), and VLXT (Romero et al., 2001).

Overall, based on bioinformatic analysis, Dbl2 appears to be a highly disordered protein, with a domain of unknown function at its N-terminus (DUF2439) which appears to be conserved from yeast to humans. Intriguingly DUF2439 is also found in the DNA repair and recombination protein Rdh54/RAD54B.

6.2.2 Purification of full-length Dbl2 from *E. coli* and *S. cerevisiae*

The expression and purification of full-length Dbl2 was first attempted in the *E. coli* strain BL21(DE3). The *dbl2* gene was cloned into pET14b to express full-length protein (78.1 kDa) tagged at its N-terminus with a 6xHis-tag and thrombin cleavage site in between. However, SDS-PAGE analysis of the expression products from *E. coli* revealed the presence of multiple protein bands, with different intensities ranging from ~ 30 to ~ 55 kDa, instead of the expected product of 79.9 kDa (full-length Dbl2 + tag). Western blotting confirmed that the obtained products were all His-tagged (Fig 6.4A). These truncated products could be the result of protein degradation and/or premature termination of translation. The intrinsically disordered proteins are known to be hard to purify in bacteria as unfolded protein is easily assessed and digested by bacterial proteases resulting in very low yields (Livernois et al., 2009). Moreover, the *dbl2* gene contains a number of rare codons encoding Arginine, Glycine and Proline. To tackle the latter problem expression was attempted in Rosetta (DE3) *E. coli* strain. Rosetta strains carry the genes of the rare codon tRNAs. Change of the host strain improved the expression when expression

was induced at 37 °C, however most of the protein expressed was in the insoluble fraction, no full-length protein was detectable at 25 °C (Fig. 6.4B).

S. cerevisiae has proven to be a useful host organism for the efficient expression of yeast proteins (Frigola et al., 2013; Yeeles et al., 2015). To test its utility for the expression and purification of Dbl2, I constructed a *S. cerevisiae* strain containing an integrated copy of *GST-dbl2* expressed from the galactose inducible *GAL1-10* promoter. Initial small-scale experiments showed that a protein of the correct size was detectable, after purification using GST-resin, on a Coomassie blue stained SDS-PAGE gel (Fig. 6.4C). Initial scaling up of the purification appeared promising, but I then encountered problems with inconsistent efficiency of induction of the protein. Moreover, my attempts to purify the protein by Size Exclusion Chromatography (SEC) were unsuccessful because the protein precipitated under a range of different conditions (including, pH of SEC buffer 7.0, 8.0, 9.0; 150 mM, 300 mM NaCl), probably due to its disordered structure.

6.2.3 Expression and purification of Dbl2's functional domains

To identify important functional regions in Dbl2 I attempted to express and purify four specific segments of the protein that seemed to be the most conserved or structured and, therefore, most probable to have activity (Fig. 6.3).

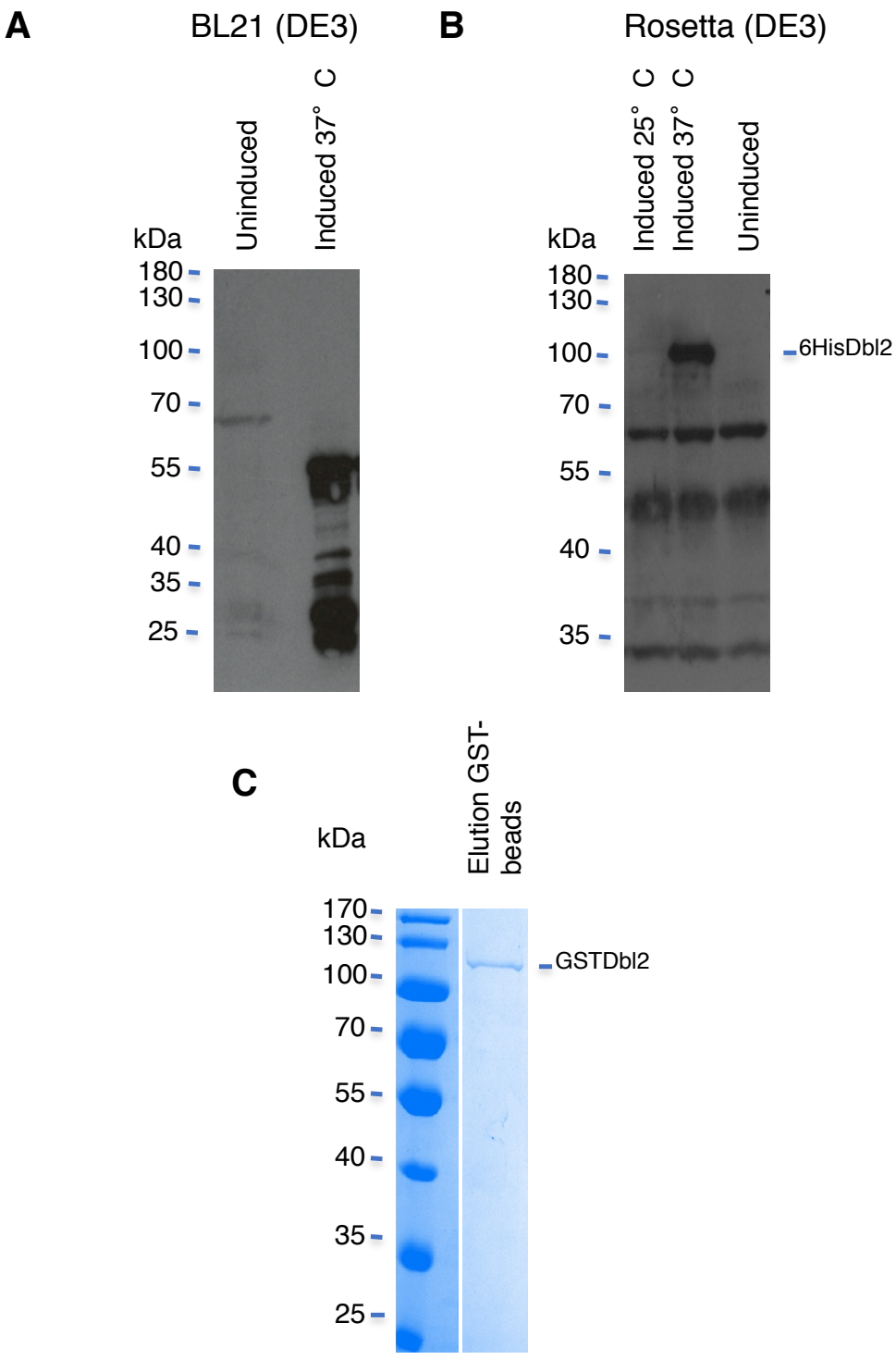


Figure 6.4. Full-length Dbl2 can be expressed and purified using *S. cerevisiae* as the host organism.

(**A**) Western blot showing the truncated Dbl2 variants produced when expressing full-length protein in BL21 (DE3) *E. coli* cells. (**B**) Western blot showing truncated Dbl2 variants and full-length protein expressed in Rosetta (DE3) *E. coli* cells. Blots in (**A**) and (**B**) were probed with anti-His antibody. (**C**) Coomassie blue stained SDS-PAGE gel showing full length GST-Dbl2 that was expressed and purified from *S. cerevisiae.*

Construct 1 is a 13.8 kDa fragment that includes: DUF2439 (amino acids 7-85); the first 6 amino acids, which should act as a natural flexible fusion protein linker to preserve the biological activity of the fragment in the presence of the tag and facilitate thrombin cleavage (Chen et al., 2013); and amino acids 85-100, which are conserved in Dbl2, Mte1 and ZGRF1 and include a significant number of positive charged residue which increases the pI of the protein. This prevents its aggregation at neutral pH and should facilitate purification using Ion Exchange Chromatography. Henceforth, I will refer to this construct as N-terminus Dbl2 (Fig. 6.5A).

Construct 2 (amino acids 621-715) is a 12.8 kDa fragment that includes the C-terminus of the protein, which is predicted to be the most structured part of the protein likely consisting of three alpha-helixes and one beta-strand (Figs. 6.2, 6.3 and 6.5A). Amino acids 688-709 are rich in hydrophobic and positively-charged residues and also conserved in human ZGRF1.

Construct 3 (amino acids 321-426) is a 14.1 kDa fragment in the middle of the protein which, according to most of the structure prediction software used, is highly likely to be structured (Fig. 6.5A). Two alpha helixes and one beta strand are predicted to be located in this region. Interestingly, this region has clusters of positively charged and hydrophobic residues which are usually characteristic of DNA-binding domains.

Construct 4 (amino acids 1-467) is a 54 kDa fragment that was designed to include both DUF2439 and the construct 3 region (Fig. 6.5A).

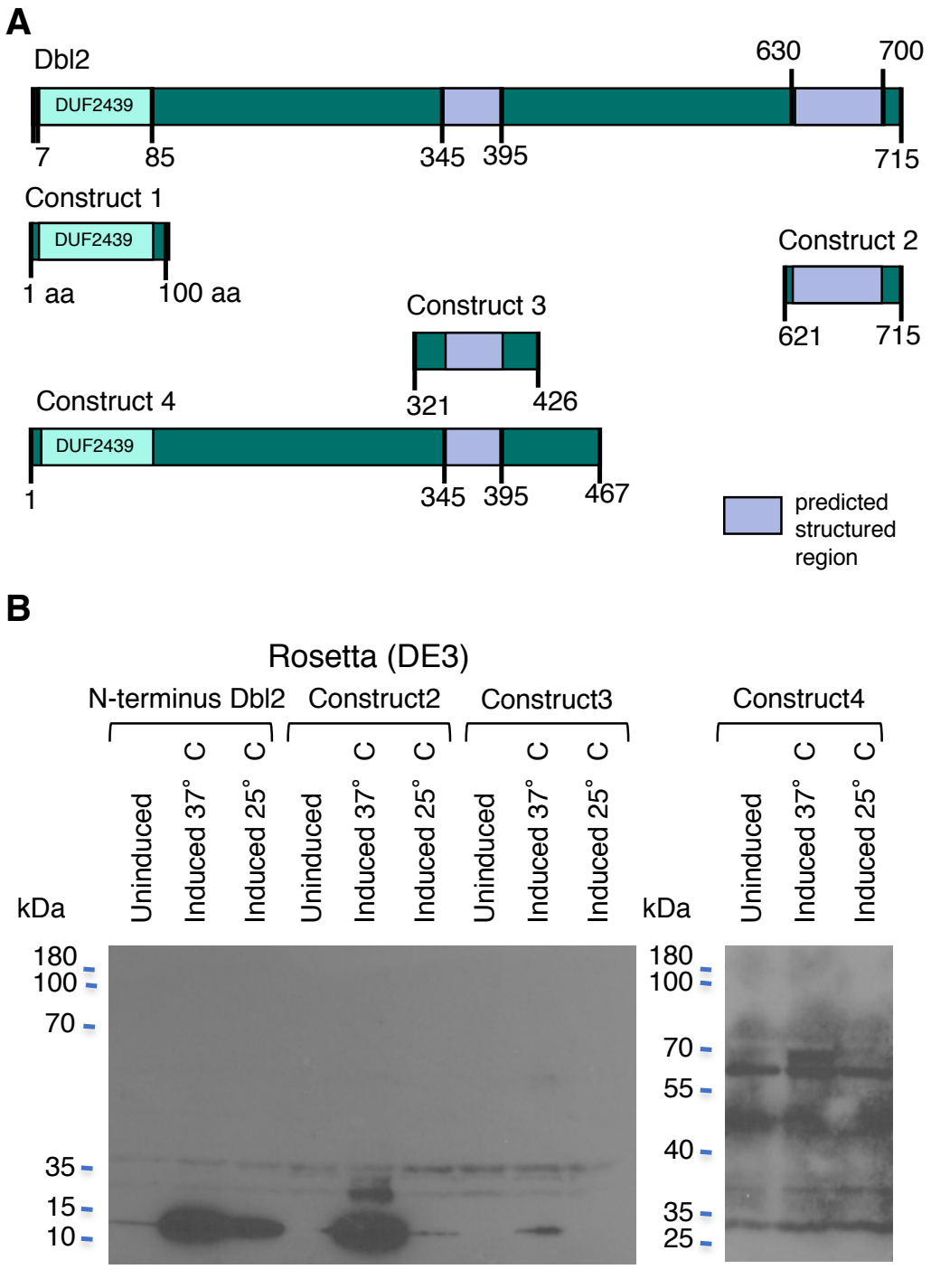


Figure 6.5. Truncated fragments of Dbl2 can be expressed in *E. coli*

(**A**) Schematic showing the four different fragments of Dbl2 that were investigated. (**B**) Western blot showing different truncated Dbl2 proteins expressed at 25 °C and 37 °C in Rosetta (DE3) *E. coli* cells. Western blots were probed with anti-His antibody.

Depending on which algorithm is used to predict protein disorder, the exact length of the structured segment in the middle of the protein varies, but at its most extended it encompasses residues 348-460 (predicted using ESpritzX) (Walsh et al., 2012).

The expression of each construct was tested in the Rosetta (DE3) *E. coli* strain. Proteins of the correct expected sizes were detected with each construct when expression was induced at 37 °C (Fig. 6.5B). However, only N-terminus Dbl2 was expressed at high levels at 25 °C and proved to be liberated into the soluble fraction upon cell lysis (Fig. 6.5B). Due to time constraints, I did not attempt to further optimize the expression of constructs 2-4.

6.2.4 Purification of N-terminus Dbl2 from *E. coli*

To optimize the large-scale expression and purification of N-terminus Dbl2 (construct 1), I tested several different host *E. coli* strains (Rosetta (DE3), RIPL (DE3), BL21 (DE3)), and various induction conditions (induction at 18 °C, 25 °C, 30 °C and 37 °C for 4 hours and overnight) and protein purification methods (SEC, then ion exchange chromatography (IEC), Heparin affinity chromatography, SEC after concentration by IEC). The final protein purification strategy that I settled on allowed me to achieve milligram amounts of highly purified protein and included the following chromatography steps: nickel affinity; ion exchange; gel filtration; and a second ion exchange chromatography step to concentrate the sample (Fig. 6.6). Interestingly, the purified protein runs as two bands on SDS-PAGE gels: one of the expected

size (~ 14 kDa) and another that is ~ 1 kDa lighter (Fig. 6.6C). Size Exclusion Chromatography with Multi-Angle Light Scattering analysis (SEC-MALS) confirmed that the sample was homogeneous and of the correct size (Fig. 6.7A). The size of the protein was also confirmed by positive electrospray ionization time-of-flight mass spectrometry (TOF MS ES+) analysis. The TOF MS ES+ spectrum indicated that the purified protein was predominantly a 13,787 kDa species (Fig. 6.7B, C). The 131.2 Da difference between this detected species and the predicted molecular weight of N-terminus Dbl2 fragment can be explained by the loss of the N-terminal methionine, which commonly occurs during N-terminal sequence analysis (Liao et al., 2004). The minor species detected by TOF MS ES+ is 58 Da larger than the main species and would unlikely to be resolved from the main species by SDS-PAGE (Fig. 6.7). This mass change usually corresponds to the carboxymethyl on cysteine or other residues. However, N-terminus Dbl2 fragment does not contain cysteine and, therefore, the change is mostly like explained by non-enzymatic glycation of lysine resulting in N^{ε}-(carboxymethyl)lysine. Non-enzymatic glycation can occur in proteins at rich Lys/Arg regions when expressed in *E. coli* (Miyata et al., 1997; Mironova et al., 2001, 2003).

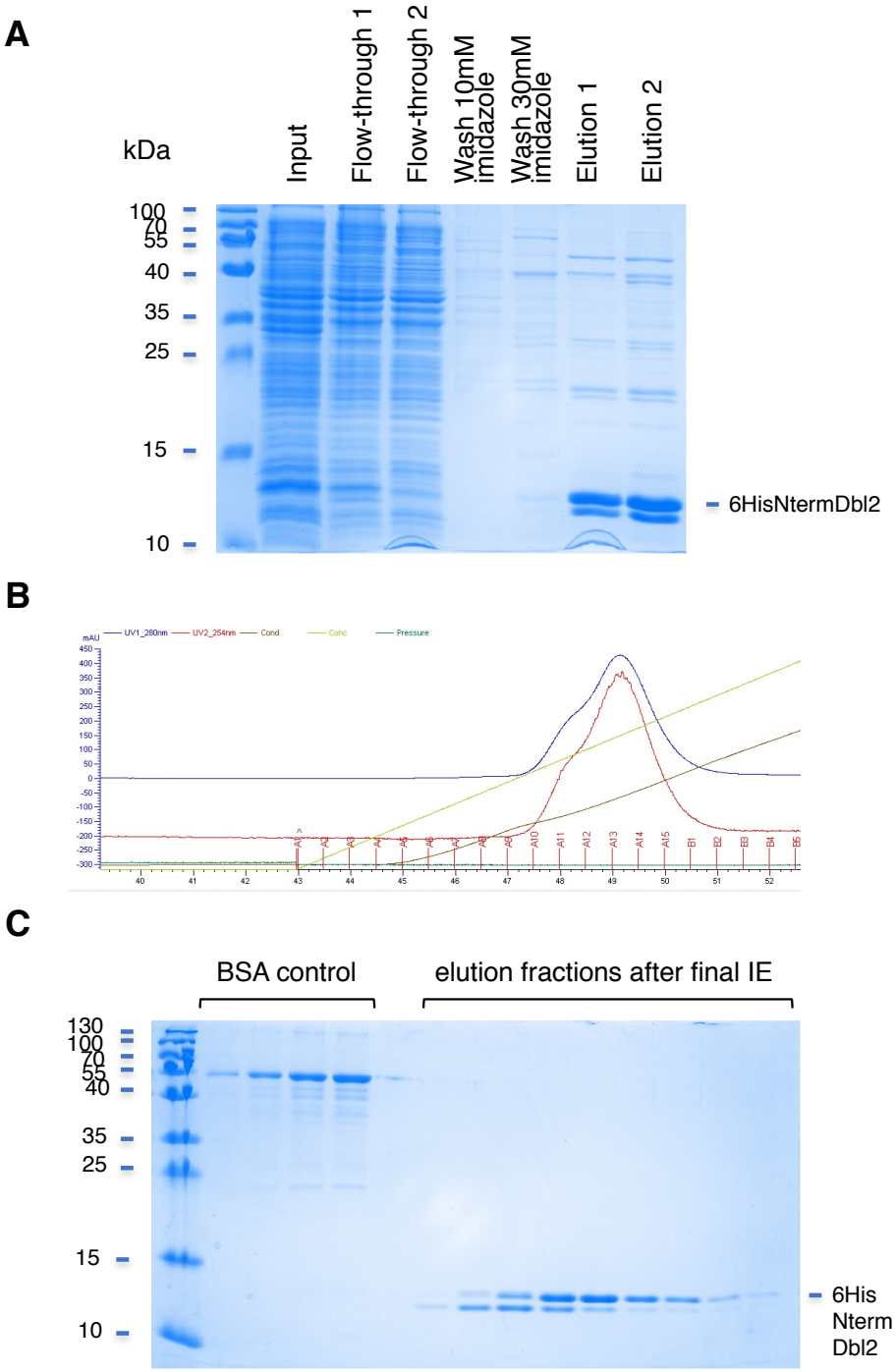


Figure 6.6. Key steps in the purification of N-terminus Dbl2.

(**A**) Coomassie blue stained SDS-PAGE gel showing samples from the Ni-NTA resin purification of N-terminus Dbl2. (**B**) Trace showing the absorbance peak at 280 nm from the final ion exchange chromatography step in the purification N-terminus Dbl2. (**C**) SDS-PAGE gel showing fractions A9-B2 from the final ion exchange column.

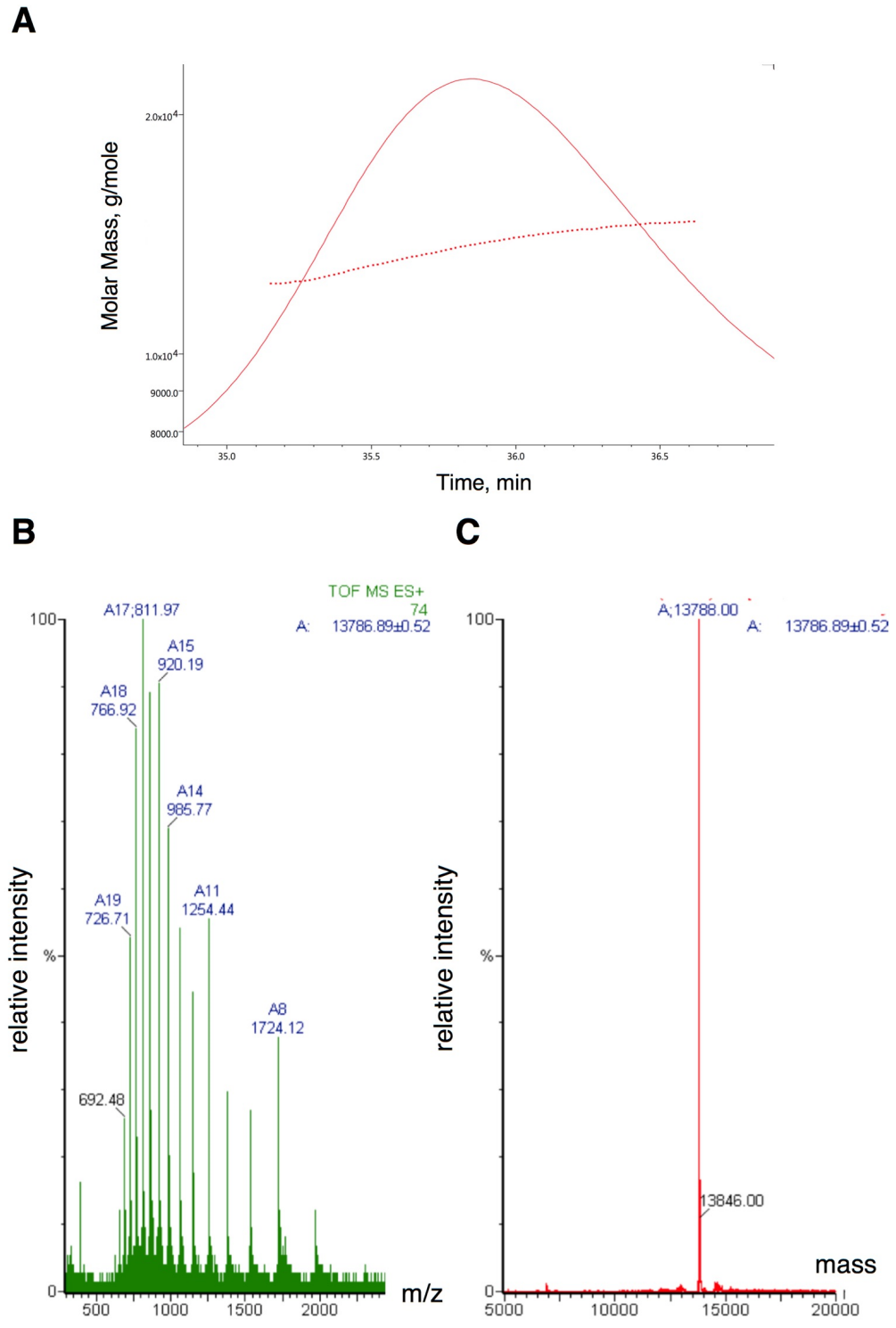


Figure 6.7. SEC-MALS and TOF MS ES+ analysis of the purified N-terminus Dbl2 showing that it is homogeneous and has the expected size.

(**A**) Molar mass versus elution time of N-terminus Dbl2 obtained from SEC and combined with MALS detection. (**B**) Positive ion ES mass spectrum of N-terminus Dbl2 and (**C**) the same spectrum in its deconvoluted form showing the average molecular mass of the N-terminus Dbl2.

6.2.5 Crystallisation trials of N-terminus Dbl2.

Since there is no structural information on the conserved N-terminal domain of Dbl2 or more widely on DUF2439 in any protein, I decided to perform crystallization experiments on N-terminus Dbl2 fragment that I had purified. The protein obtained from the final ion exchange chromatography step was concentrated further using a centrifugal filter device (protein concentrators (ThermoFisher, 5,000 Da molecular weight cut-off, 20 ml)) to ~ 18 mg/ml. This material was then placed into crystallization trials, and after one month of growth at 18 °C, small needle- and triangular-shaped crystals (15-30 µm) were obtained under several different conditions. However, these crystals were not big enough for data collection and were therefore used to seed further crystallization experiments. Seeding experiments are based on the fact that in one of the supersaturation zones where homogeneous nucleation cannot happen spontaneously, crystals can grow from the crystal seeds (Luft and DeTitta, 1999). Indeed, a 268x206x164 µm crystal formed in 0.2 M ammonium nitrate and 20 w/v polyethylene glycol (PEG) 3,350 after 72 days at 18 °C (Fig. 6.8A, B). Other smaller crystals were also obtained that formed mainly in a classical JPEG crystal screen with different PEG and salt conditions, and in the presence of neutralized organic acids (succinate, malonate, malate) (data not shown). Both large and smaller crystals were cryoprotected by increasing the PEG 3,350 concentration to 35 % (w/v) and were analysed at the synchrotron beamline. However, unfortunately none of the tested crystals diffracted and, therefore, no data was collected (Fig. 6.8C).

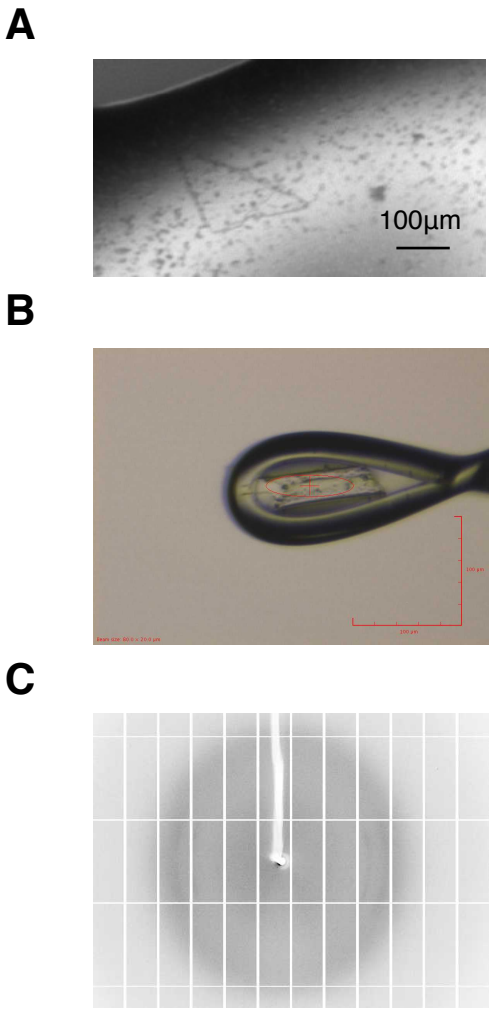


Figure 6.8. N-terminus Dbl2 was crystallized but the lack of diffraction prevented any structural data from being collected.

(**A**) Screenshot of the 96-well crystallization plate containing the biggest obtained crystal. (**B**) Example of the crystal mounted in the cryo-loop in the synchrotron. (**C**) The crystals analysed in the synchrotron did not diffract.

6.2.6 Analysis of N-terminus Dbl2 by NMR

NMR spectroscopy is a powerful technique for determining the structure of small proteins or protein domains. Since NMR is performed on proteins in solution, it has an important advantage over traditional X-ray crystallography because it allows one to follow protein dynamics. As such it can provide complementary data to X-ray crystallography, revealing characteristics of conformational changes and protein behaviour in solution (Feng et al., 2011). However, 1D and 2D NMR spectra, even of small proteins, are very crowded and only provide general information on secondary structure and the stability of the protein under the experimental conditions. This latter information is important because for NMR spectroscopy to be successful the protein needs to stay in its native conformation without precipitating or unfolding at room temperature (or the chosen temperature for the data acquisition) for weeks to acquire all of the necessary information for structure determination. Moreover, the salt concentration of the sample usually should not be higher than 80-100 mM since higher salt concentrations decreases the signal to noise ratio.

To collect preliminary data on protein structure and establish if the protein is suitable for heteronuclear 3D NMR experiments, I performed 1D and homonuclear 2D NMR analysis of the purified N-terminus Dbl2 (Fig. 6.9). A series of ^{1}H mono-dimensional NMR experiments were performed to assess the stability of the sample over time (12 days) (Fig. 6.9A). Aromatic and backbone amides cover wide range of chemical shifts (6.5-10 ppm) which is indicative of a folded globular protein, that was stable under the conditions of

the experiment. Downfield shifted H^{α} is possible evidence for beta strands. Methyl peaks upfield of 0.5 ppm are indicative of a hydrophobic core. The analysis of the well-resolved two-dimensional NMR TOCSY spectrum confirms that protein in the solution is folded (Fig. 6.9A). Off diagonal peaks represent pairs of ^{1}H that are close ($\leq$ 6 Å) in the protein structure. Altogether, these data suggest that the protein is folded and globular with a hydrophobic core. The protein probably has beta sheets in its structure. From the preliminary data I collected, it can be concluded that structure determination by NMR is feasible.

To perform 3D heteronuclear NMR, the protein has to be isotopically labelled with ^{15}N and ^{13}C. This is achieved by growing *E. coli* cells expressing the protein in minimal media with $^{15}NH_4Cl$ as a nitrogen source and $^{13}C_6$ glucose as a carbon source. The isotopic labels are expensive so before performing the labelling I attempted to optimize expression of the protein in minimal media to obtain the amount of protein (tens of milligrams) required for the analysis. Unfortunately, I was unable to obtain any detectable expression of N-terminus Dbl2 from cultures grown in minimal media despite testing various different regimes and conditions.

6.3 Discussion

In this chapter I have described the use of various algorithms to predict the structure of Dbl2. Based on my analysis, Dbl2 appears to be a highly disordered protein with a conserved domain of unknown function (DUF2439) (Figs. 6.1 – 6.3).

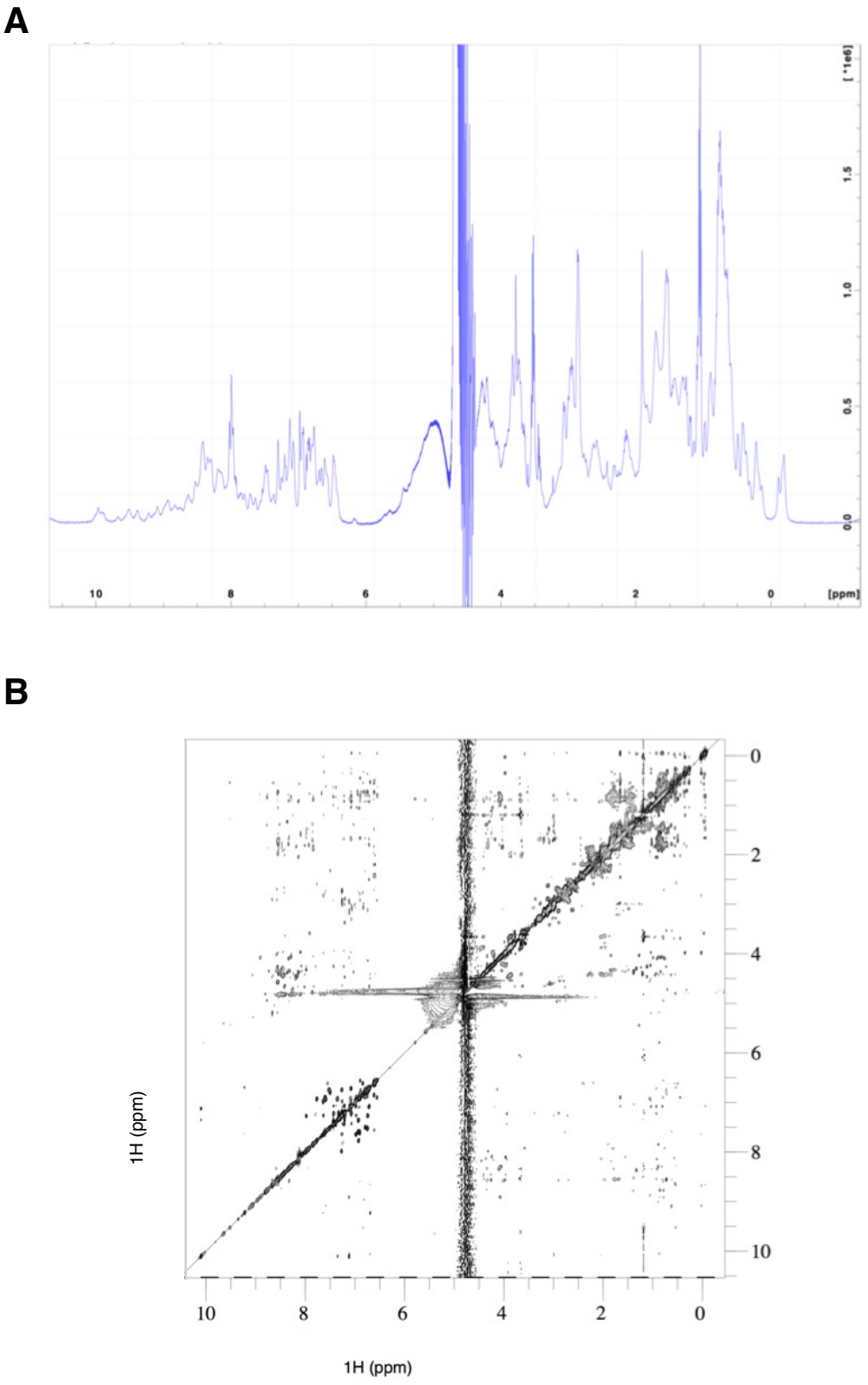


Figure 6.9. NMR-analyses of N-terminus Dbl2.

(**A**) 1D ^{1}H NMR spectrum acquired at pH 7.8, 298 K on 500 MHz spectrometer. (**B**) 2D ^{1}H-^{1}H NOESY spectrum acquired at pH 7.8, 298 K on 500 MHz spectrometer.

Dbl2 is also enriched in Molecular Recognition Features (Sharma et al., 2016). Molecular Recognition Features are short regions (5-25 aa) that are found in many intrinsically disordered proteins. These fragments are functional units and undergo a disorder-to-order transition on binding their partner proteins (Dunker et al., 2008; Das et al., 2012). The ability of disordered proteins to interact with multiple proteins make them suitable as a hub of for protein-protein interaction networks (Ekman et al., 2006; Haynes et al., 2006). In the case of Dbl2, it might be such a hub for the interaction with multiple DNA repair and recombination proteins (such as Fml1, Fbh1, Rad51, and potentially other helicases) promoting efficient coordination of their activity.

In this chapter I showed that expression and purification of full-length Dbl2 protein is possible from *S. cerevisiae* (Fig. 6.4), but the protein purification strategy should be carefully optimized because of the tendency of the protein to precipitate probably due to the lack of a defined three-dimensional structure. Nevertheless, my finding that *S. cerevisiae* is a suitable system for producing full-length Dbl2 protein suggests that it may also be useful for the production of truncated forms of Dbl2, which proved to be insoluble when expressed in *E. coli*.

Even though much of Dbl2 proved to be difficult to purify, I was able to develop a protocol for the successful large-scale purification of N-terminus Dbl2. The pure homogeneous sample of the protein was confirmed by SEC-MALS and MALDI-TOF MS analyses (Fig. 6.7). Despite being a homogeneous sample, the purified protein runs as two bands when analysed by SDS-PAGE, and these two different species are also partially resolved by gel filtration and ion

exchange chromatography (Fig. 6.6C). This might suggest that there are two structural conformations of the N-terminus Dbl2, either fixed in the process of purification or present as an equilibrium in solution. Intriguingly, MALDI-TOF MS revealed a minor product that was 58 Da larger than the main protein species. This might represent the modification of a lysine to N^{ε}-(carboxymethyl)lysine by non-enzymatic glycation. It is conceivable that such a modification could stabilize one of the conformational states of the protein and, therefore, it could explain the presence of two conformations of the same protein with slight mass change that can be resolved. Interestingly, this lysine modification *in vivo* has been shown to be characteristic of pathogenic prion isoforms of proteins and is involved in prion propagation (Choi et al., 2016). Dbl2 is a highly disordered protein and has a glutamine/asparagine rich prion-like domain (266-286 aa) according to analysis by the PrionW server (Sabate et al., 2015; Zambrano et al., 2015). This might suggest that in certain conditions Dbl2 can have prion properties. As discussed in Chapter 4, budding yeast Mph1, which interacts with Mte1, has also been reported to be a prion protein that can undergo a conformational change [$MPH1^{+}$] that results in a gain of function (Byers et al., 2017). Perhaps such gain or alteration in function stem from cooperative changes of DNA repair proteins involved in the same DNA repair pathway (Byers et al., 2017).

Although the initial crystallization experiments of N-terminus Dbl2 were successful, and crystals were grown, my attempt to collect structural data from the crystals failed (Fig. 6.8). The affinity tags can have positive and negative effects on crystallization of the proteins (Kobe et al., 2015). However, there

are no ways to predict such an effect for the particular protein, and it can be established only empirically if the removal of the tag is required for the crystallization and good diffraction quality. Short affinity tags due to the lack of structure can potentially increase the flexibility of the construction therefore negatively affecting the crystallization (Kobe et al., 2015). Since the crystallization of N-terminally His-tagged N-terminus was not successful, I purified, and thrombin cleaved His-tag to set up another series of crystallization experiment. This work is currently in progress. The next step in crystallization experiments would be to shorten flexible part of the existing construct and try more different crystallization screens at 18 °C and 4 °C.

Finally, I used NMR spectroscopy analysis to investigate the secondary structure and stability of the N-terminus Dbl2. I concluded that, consistent with structure predictions, the N-terminus Dbl2 is globular with a hydrophobic core enriched in beta-strands but not alpha helixes (Fig. 6.9). I also concluded that the purified N-terminus Dbl2 is stable for a sufficient time at room temperature to perform 2D and 3D heteronuclear experiments. Unfortunately, the protein is not expressed in the minimal media needed for the isotopic labelling of the protein. This issue could be resolved in the future by using alternatives to minimal media, for example isotopically labelled rich media (Gardiennet et al., 2008; Grimm et al., 2017) or *Pichia pastoris* as the host organism (Yao et al., 2002).

Chapter 7

7 Structure-function analysis of Dbl2

7.1 Introduction

In parallel with attempts to purify the structured domains of Dbl2 and characterise them *in vitro,* I conducted a series of genetic and imaging experiments to investigate the biological importance of the DUF2439 domain and other potential functional units of the protein. Following the discovery of Dbl2 in an imaging-based screen, a series of strains carrying different alleles of *dbl2* with various truncations and internal deletions had been constructed (Yu et al., 2013). In these strains, the *dbl2* gene was replaced by a geneticin resistance marker cassette at its endogenous locus, and the partially deleted/truncated *dbl2* versions, together with a YFP-tag, were inserted together with a *leu*1^{+} gene at the *leu1* locus in a *leu1-32* strain. In these strains, Dbl2 protein could be detected by fluorescence microscopy via its N-terminal YFP-tag. The original series of strains from the study by Yu et al. (2013) were kindly provided by Dr. Li-Lin Du (National Institute of Biological Sciences, Beijing, China). Upon arrival, the strains were verified by colony PCR and the expression of Dbl2 tagged tested by western blotting and fluorescent microscopy. The strains were then back-crossed to wild-type to give them a uniform genetic background with a set of auxotrophic markers that would facilitate subsequent strain constructions. In this chapter I describe my genetic analysis of these strains, which provides insight into the structure-function relationships in Dbl2.

7.2 Results

7.2.1 Genotoxin sensitivity of truncation and internal deletion mutants of Dbl2

To examine which regions of the protein complement *dbl2*Δ sensitivity to genotoxins, I compared the sensitivity of each *dbl2* mutant to a *dbl2*Δ and a wild-type strain (Figs. 7.1 – 7.3). A strain that expresses full-length Dbl2 tagged with YFP (fl-*dbl2*) was also included in this analysis to control for the possibility that the tag might affect the activity and function of the protein. To simplify the presentation, the tag label 'YFP' is omitted from the description of each strain as it is present in all of the truncation and deletion mutants. The range of different mutants analysed include various internal deletion mutants of Dbl2 (missing one of the following sections: N-terminus 6-103 (*dbl2*ΔN); half of DUF2439 domain 6-50 (*dbl2*ΔN1/2); amino acids 104-210; 211-321; 321-430 (*dbl2*(Δmid)); 431-520; 521-620), a truncated form missing the C-terminus (amino acids 621-715, *dbl2*ΔC) and mutants that express only the middle region (amino acids 321-430, *dbl2*(mid)) or C-terminus (amino acids 621-715, *dbl2*C). The control strain expressing fl-*dbl2* did not exhibit any hypersensitivity to the genotoxins that were used suggesting that the DNA repair function of Dbl2 is not impaired by an N-terminal YFP tag. Consistent with published data (Yu et al., 2013), full or partial deletion of the conserved N-terminus did not result in any increase in sensitivity (Fig. 7.1). This was also true for the deletion of the C-terminus and all the internal deletion mutants except *dbl2*(Δmid). (Figs. 7.2, 7.3 and data not shown). Loss of the middle part of the protein leads to hypersensitivity to CPT, MMS and UV, similar to the *dbl2*Δ mutant (Fig. 7.3).

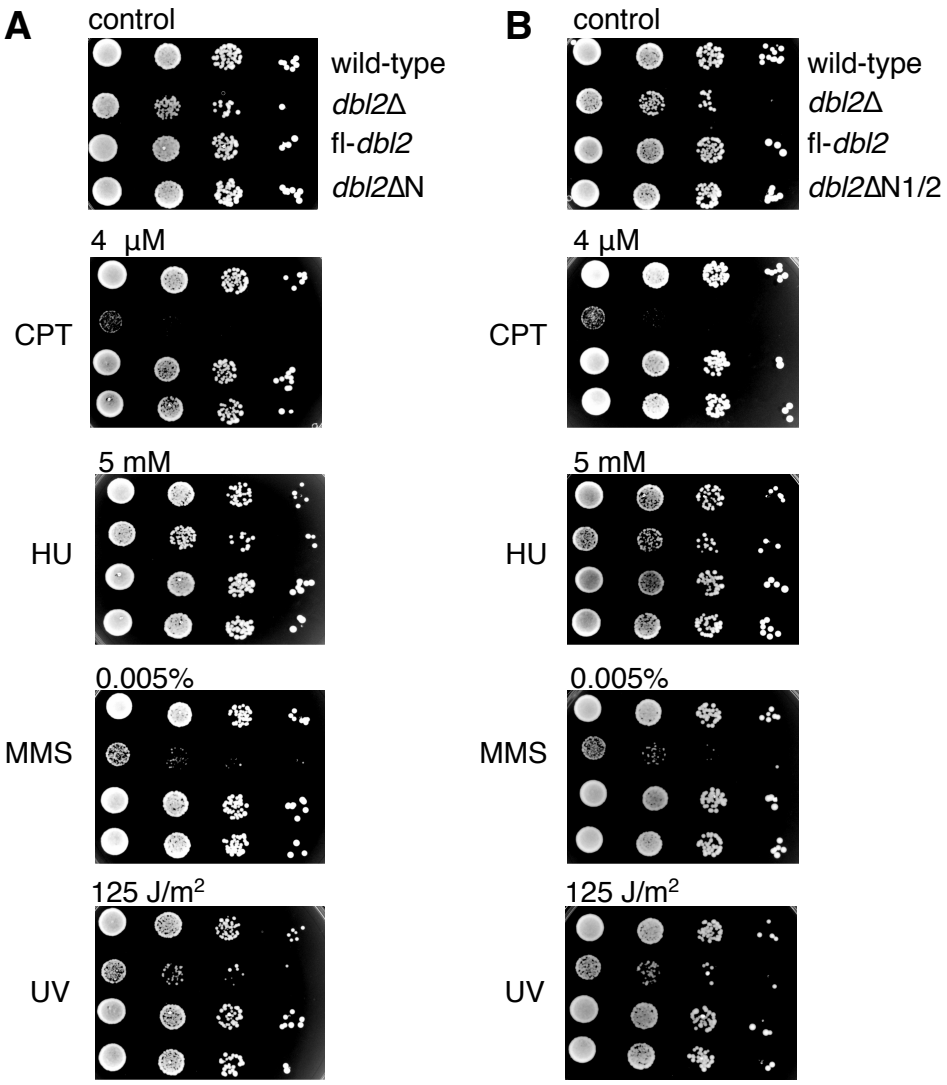


Figure 7.1. Genotoxin sensitivity of *dbl2*ΔN and *dbl2*ΔN1/2 strains.

Spot assay comparing the growth and genotoxin sensitivity of wild-type (FO656), *dbl2*Δ (MCW8564), fl-*dbl2* (MCW8870), *dbl2*ΔN (MCW8869) (**A**), and *dbl2*ΔN1/2 (MCW8874) (**B**). The plates were photographed after 4 days of incubation at 30 °C.

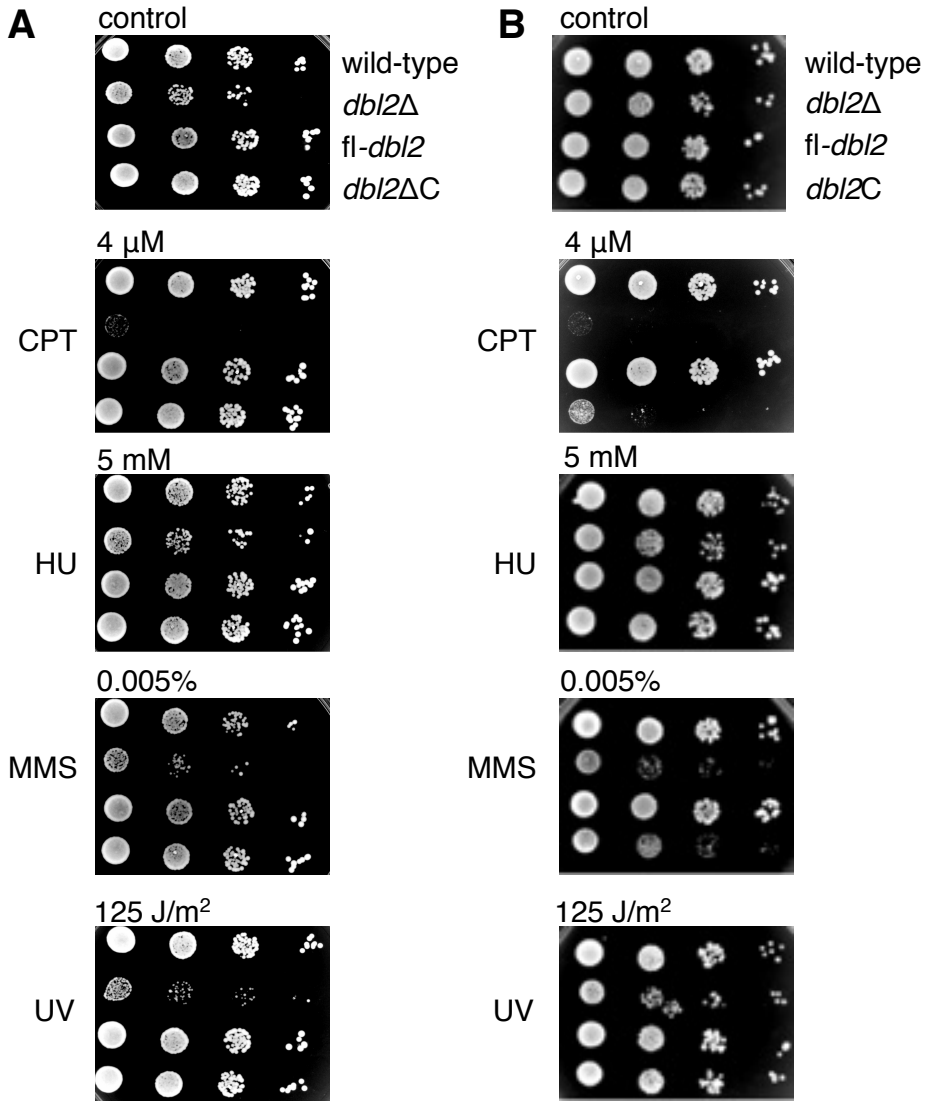


Figure 7.2. Genotoxin sensitivity of *dbl2*ΔC and *dbl2*C strains.

Spot assay comparing the growth and genotoxin sensitivity of wild-type (FO656), *dbl2*Δ (MCW8564), fl-*dbl2* (MCW8870), *dbl2*ΔC (MCW8873) (**A**), and *dbl2*C (MCW8880) (**B**). The plates were photographed after 4 days of incubation at 30 °C.

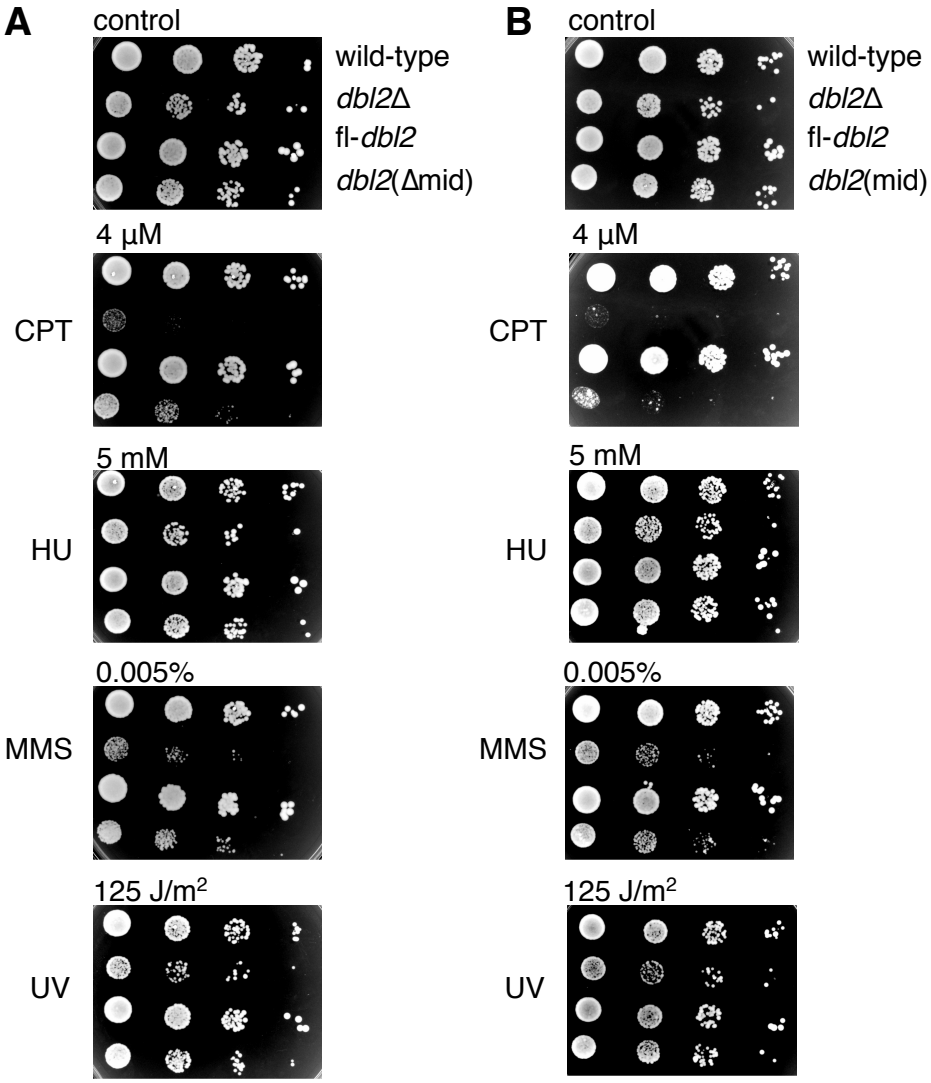


Figure 7.3. Genotoxin sensitivity of *dbl2*(Δmid) and *dbl2*(mid) strains.

Spot assay comparing the growth and genotoxin sensitivity of wild-type (FO656), *dbl2*Δ (MCW8564), fl-*dbl2* (MCW8870), *dbl2*(Δmid) (MCW8871) (**A**), and *dbl2*(mid) (MCW8881) (**B**). The plates were photographed after 4 days of incubation at 30 °C.

7.2.2 The importance of different Dbl2 domains in suppressing spontaneous and *RTS1*-induced direct repeat recombination

Deletion of *dbl2* does not change the frequency of spontaneous recombination (Chapter 4). Similarly, most of the Dbl2 truncation and internal deletion mutants tested had no effect on spontaneous recombination (Fig. 7.4). Intriguingly, the *dbl2*ΔN mutant exhibited ~ 1.5-fold increase in the frequency of deletions ($P = 0.007$) and a 2.6-fold increase in gene conversions ($P < 0.001$) relative to wild-type. Together these data suggest that Dbl2's N-terminal domain, containing DUF2439, may be important for preventing some kind of "toxic effect" of the protein that would lead to an increase in spontaneous recombination. However, even though the differences in recombinant frequency values between the *dbl2*ΔN mutant and wild-type appear to be statistically significant (based on the statistical test that was used), the spread of values obtained for the *dbl2*ΔN strain was especially large leading me to doubt whether they really are biologically relevant.

As was shown in Chapter 4, Dbl2 is required for limiting *RTS1*-induced recombination. To determine which domains within Dbl2 are important for providing this function, I tested a selection of Dbl2 truncation and internal deletion mutants for *RTS1-AO*-induced direct repeat recombination (Fig. 7.5). As expected, the control fl-*dbl2* strain exhibited the same level of recombination as the wild-type strain. There was also no significant change in the frequency of recombinants in mutants lacking all or half of Dbl2's N-terminal domain (Fig. 7.5). The *dbl2*(Δmid) strain showed an increase in the

frequency of both conversion-type (~ 3.7-fold, $P < 0.001$) and deletion-type recombinants (~ 4.3-fold, $P < 0.001$). However, whereas the increase in conversions was comparable to that in a *dbl2*Δ mutant ($P = 0.661$), the increase in deletions was ~ 3-fold less ($P < 0.001$). The frequency of *RTS1*-induced recombination is also increased in the *dbl2*ΔC strain, however in this case the increases in both conversions (~ 2.7-fold) and deletions (~ 10.4-fold are more comparable to those in a *dbl2*Δ mutant, however the difference was still significant ($P < 0.001$ and $P = 0.002$ for conversions and deletions, respectively). The *dbl2*C strain, which expresses only Dbl2's C-terminal domain, exhibits similar high levels of recombination as a *dbl2*Δ mutant (~ 4.7-fold and ~ 12.6-fold increase for conversion- ($P = 0.459$) and deletion-types ($P = 0.297$), respectively). Intriguingly the *dbl2*(mid) strain, whilst exhibiting levels of gene conversions that are as high as a *dbl2*Δ mutant ($P = 0.012$), has a frequency of deletion-type recombinants that is ~ 2-fold less than a *dbl2*Δ mutant ($P < 0.001$). Altogether these data show that the central and C-terminal domains of Dbl2 are both important for limiting *RTS1-AO*-induced direct repeat recombination. However, surprisingly the central domain, whilst being critical for Dbl2's role in limiting gene conversions, is not as important for its ability to suppress deletions.

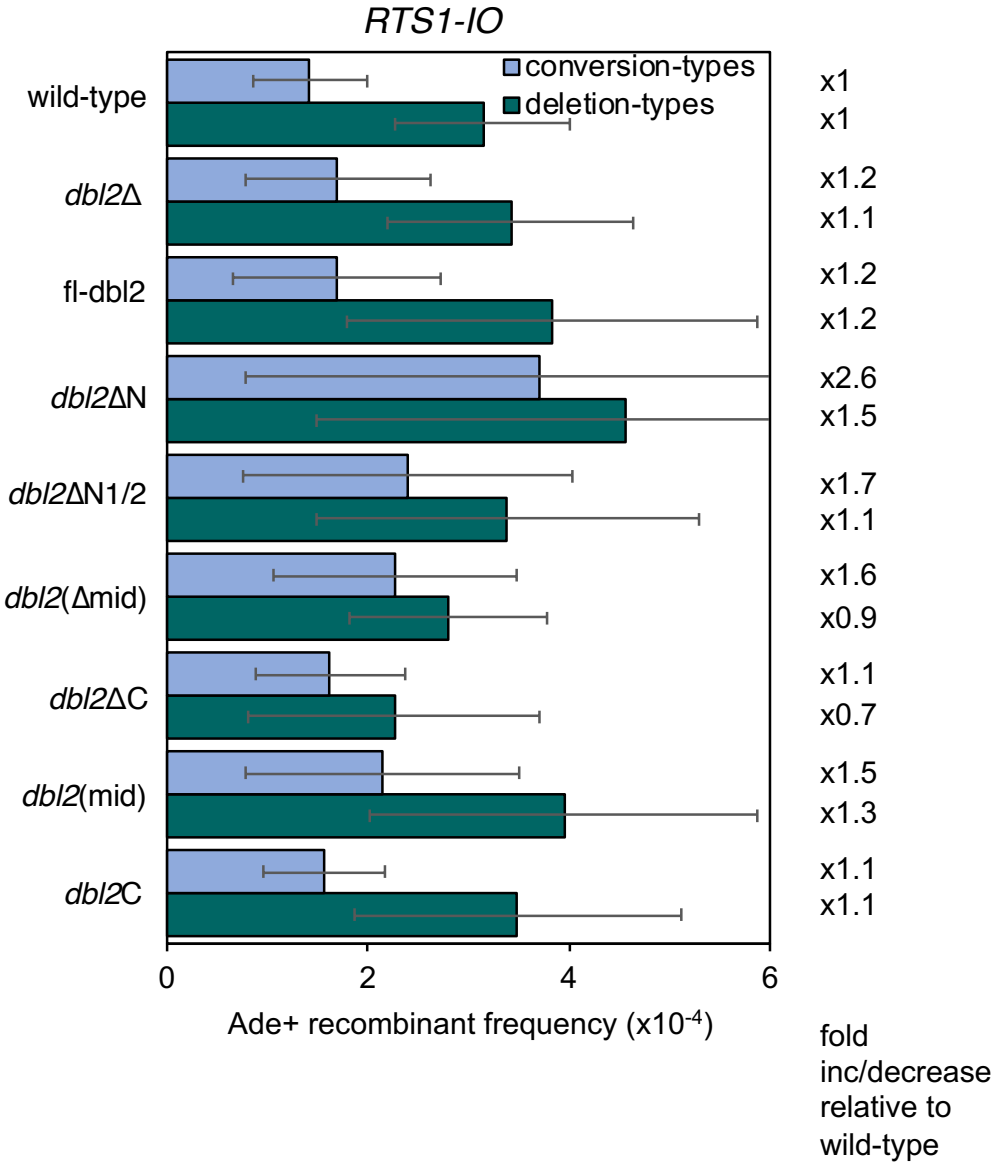


Figure 7.4. The effect of Dbl2 truncations and internal deletions on spontaneous direct repeat recombination.

Bar chart showing the mean frequency of conversion- and deletion-type Ade+ recombinants in wild-type, *dbl2*Δ, fl-*dbl2*, *dbl2*ΔN, *dbl2*ΔN1/2, *dbl2*(Δmid), *dbl2*ΔC, *dbl2*(mid), *dbl2*C strains with *RTS1*-IO. Error bars represent ± one standard deviation. In order of presentation, the strains are MCW4712, MCW8627, MCW8892, MCW8890, MCW8898, MCW8894, MCW8896, MCW8904, MCW8902.

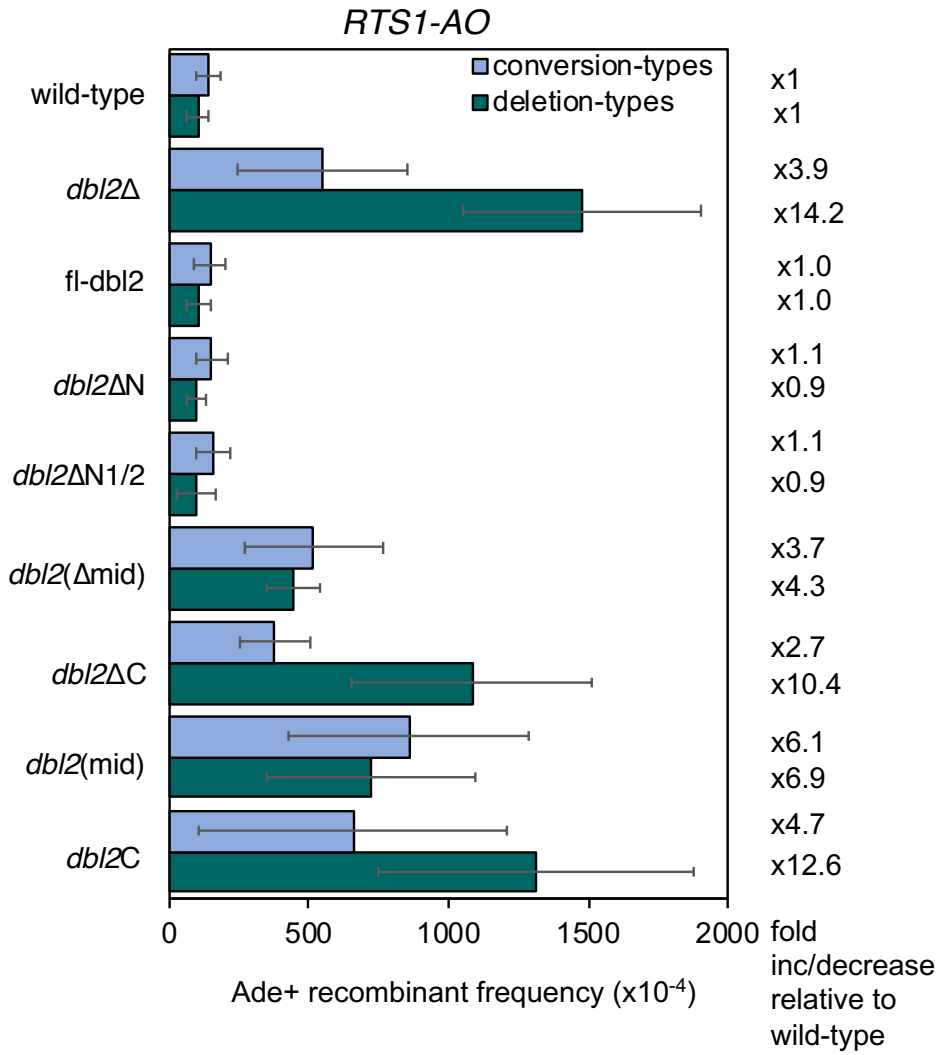


Figure 7.5. The effect of Dbl2 truncations and internal deletions on *RTS1*-induced direct repeat recombination.

Bar chart showing the mean frequency of conversion- and deletion-type Ade$^+$ recombinants in wild-type, *dbl2*Δ, fl-*dbl2*, *dbl2*ΔN, *dbl2*ΔN1/2, *dbl2*(Δmid), *dbl2*ΔC, *dbl2*(mid), *dbl2*C strains with *RTS1*-AO. Error bars represent ± one standard deviation. In order of presentation, the strains are MCW4713, MCW8628, MCW8893, MCW8891, MCW8899, MCW8895, MCW8897, MCW8905, MCW8903.

7.2.3 Genetic interactions between truncation and internal deletion mutants of Dbl2 and key components of the homologous recombination machinery

Dbl2 has positive genetic interactions with components of the Rad51-mediator complexes Rad55-Rad57, Swi5-Sfr1 and Rdl1-Rlp1-Sws1 suggesting that it might act by opposing their activities in forming and maintaining the Rad51 nucleofilament (Chapter 5). To determine if there is a specific functional domain in Dbl2 that is key for this proposed role, I generated a series of double mutants combining *dbl2* truncation and internal deletion mutants with a deletion of either *rad55*, *swi5* or *rdl1*. These double mutant strains were then compared to their component single mutant strains and wild-type control strains for genotoxin sensitivity (Figs. 7.6 – 7.10). As expected, when *fl-dbl2* is combined with either *rad55*Δ or *swi5*Δ, the resulting double mutant exhibits the same sensitivity to genotoxins as its equivalent *rad55*Δ/*swi5*Δ single mutant (Figs. 7.6A and 7.8A). Deletion of *swi5* rescues *dbl2*(Δmid), *dbl2*(mid) and *dbl2*C hypersensitivity to MMS and CPT (Fig. 7.6B and data not shown). However, unlike a *dbl2*Δ*swi5*Δ double mutant, partial deletion and truncation *dbl2* double mutants are as sensitive to UV as a *swi5*Δ single mutant (Fig. 7.6B and data not shown). Deletion of Dbl2's N- or C-terminal domains did not affect the sensitivity of *swi5*Δ to UV (data not shown).

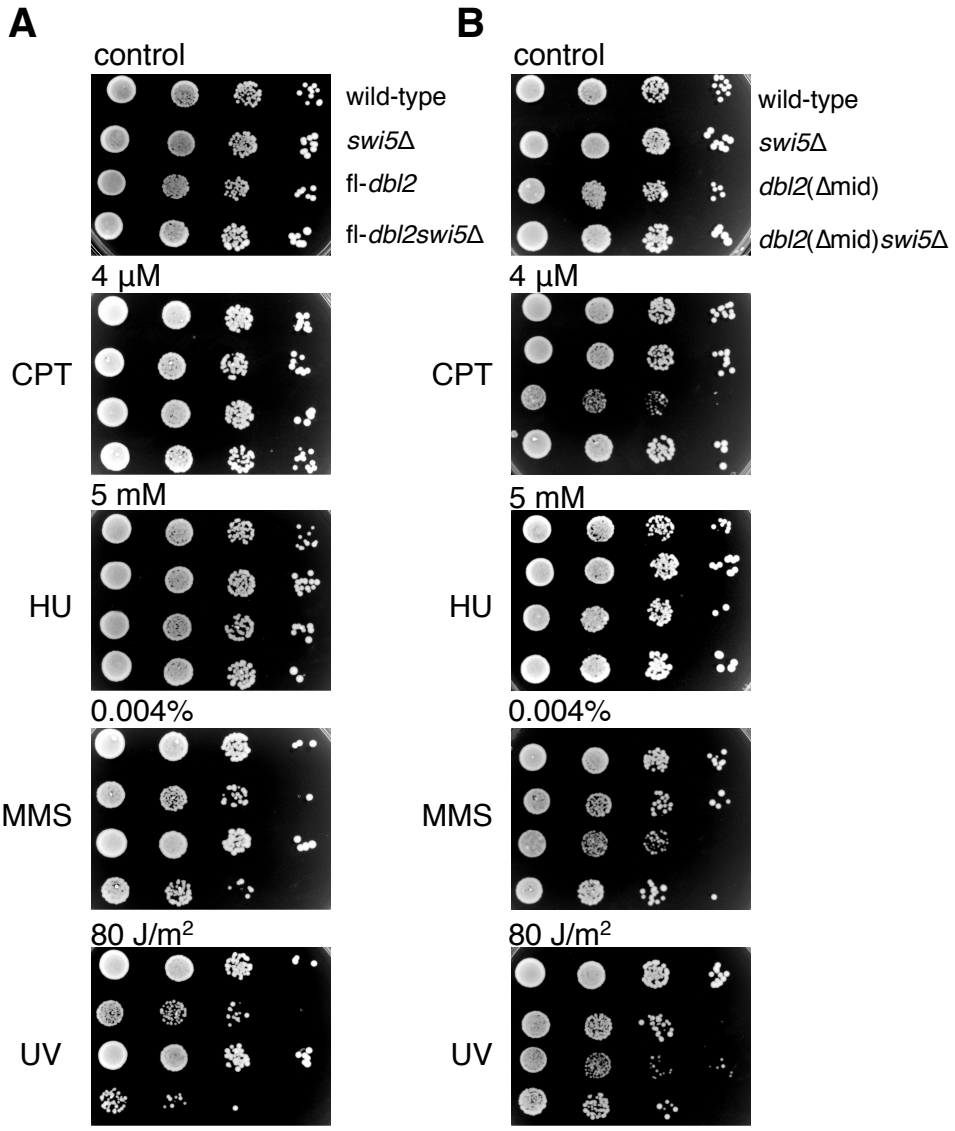


Figure 7.6. Genetic interaction between *dbl2* and *swi5*.

Spot assay comparing the growth and genotoxin sensitivity of wild-type (FO656), *swi5*Δ (MCW1481), fl-*dbl2* (MCW8870), and fl-*dbl2swi5*Δ (MCW8971) (**A**); wild-type (FO656), *swi5*Δ (MCW1481), *dbl2*(Δmid) (MCW8871), and *dbl2*(Δmid)*swi5*Δ (MCW8973) (**B**). The plates were photographed after 5 days of incubation at 30 °C.

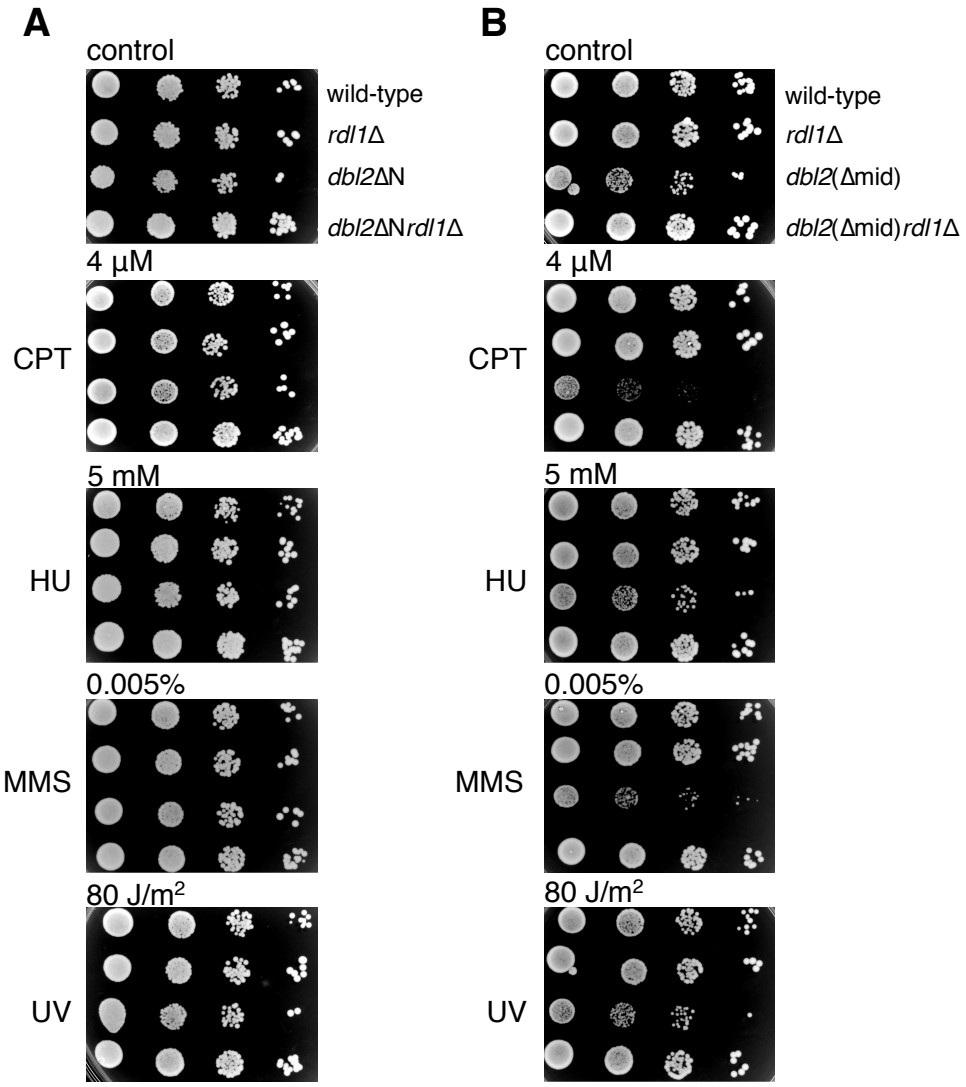


Figure 7.7. Genetic interaction between *dbl2* and *rdl1*.

Spot assay comparing the growth and genotoxin sensitivity of wild-type (FO656), *rdl1*Δ (MCW6119), *dbl2Δ*N (MCW8869) and *dbl2*Δ*N**rdl1*Δ (MCW8982) (**A**); wild-type (FO656), *rdl1*Δ (MCW6119), *dbl2*(Δmid) (MCW8871), and *dbl2*(Δmid)*rdl1*Δ (MCW9012) (**B**). The plates were photographed after 5 days of incubation at 30 °C.

The *rdl1*Δ single mutant exhibits no hypersensitivity to the doses of genotoxins used in my experiment but, similarly to *swi5*Δ*, rdl1*Δ suppresses *dbl2*(Δmid), *dbl2*(mid) and *dbl2*C sensitivity to MMS and CPT back to wild-type levels (Fig. 7.7 and data not shown). Interestingly, deletion of either N- or C-terminal domain of Dbl2 fully suppressed *rad55*Δ hypersensitivity to CPT, MMS and HU (Figs. 7.8 and 7.9A). Reciprocal suppression of genotoxin hypersensitivity is observed in double mutants of *rad55*Δ combined with *dbl2*(Δmid), *dbl2*(mid) or *dbl2*C (Figs. 7.9B and 7.10). Taken together, these data suggest that the central region (amino acids 321-430) of Dbl2 is essential in most cases for the proteins role in limiting Rad51 activity in the presence of mediator proteins. However, the inability of *dbl2*(Δmid) to suppress the UV sensitivity of a *swi5*Δ mutant suggests that Dbl2, lacking its central region, retains sufficient activity to block the repair of UV-induced DNA damage when Swi5 is missing. Although important for Dbl2's role in controlling Rad51, the central region is not sufficient to perform this function. Indeed, both N- and C- terminal domains are required for Dbl2 to counter Rad51 activity in the presence of Rad55.

7.2.4 Identifying which of Dbl2's domains is required for it to form nuclear foci

Dbl2 (fused to a fluorescent protein) has previously been shown to localize within the nucleus at an HO endonuclease-induced DSB (Yu et al., 2013).

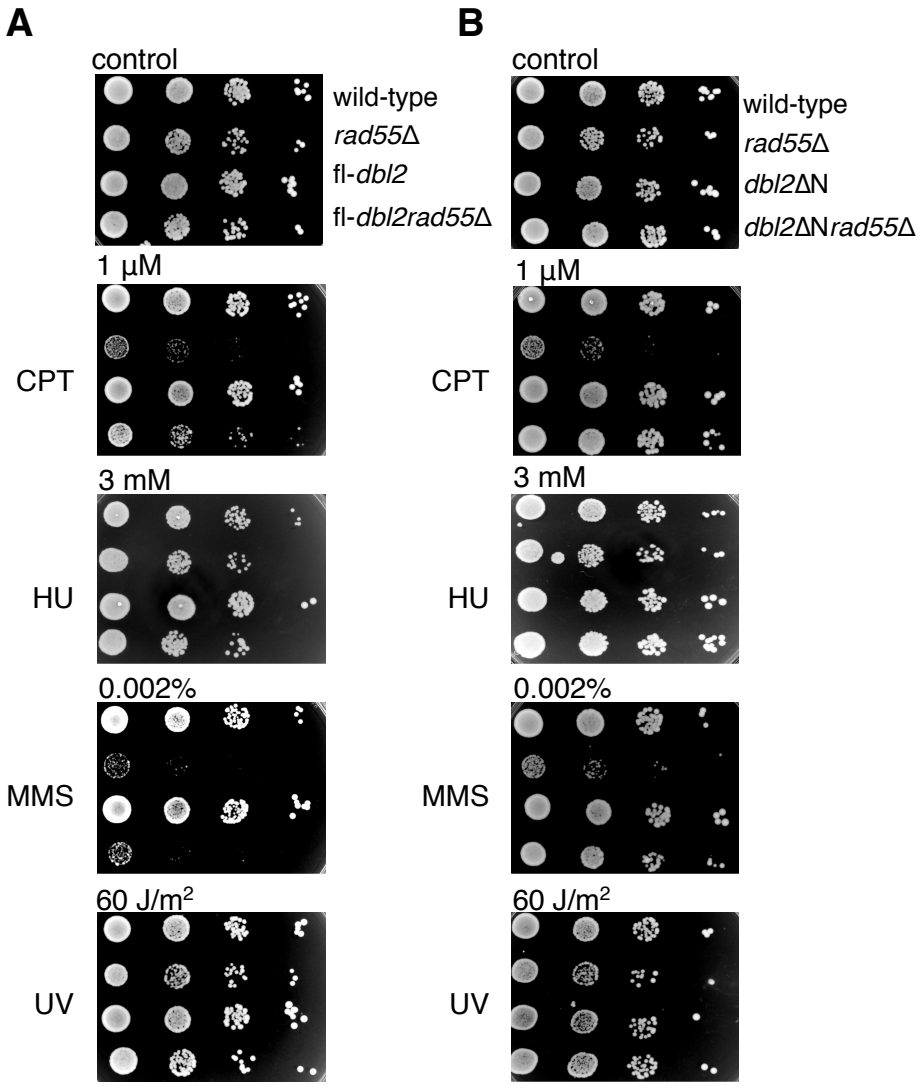


Figure 7.8. Genetic interaction between *dbl2* and *rad55*.

Spot assay comparing the growth and genotoxin sensitivity of wild-type (FO656), *rad55*Δ (MCW1231), fl-*dbl2* (MCW8870), and fl-*dbl2rad55*Δ (MCW8977) (**A**); wild-type (FO656), *rad55*Δ (MCW1231), *dbl2*ΔN (MCW8869) and *dbl2*ΔN*rad55*Δ (MCW8979) (**B**). The plates were photographed after 5 days of incubation at 30 °C.

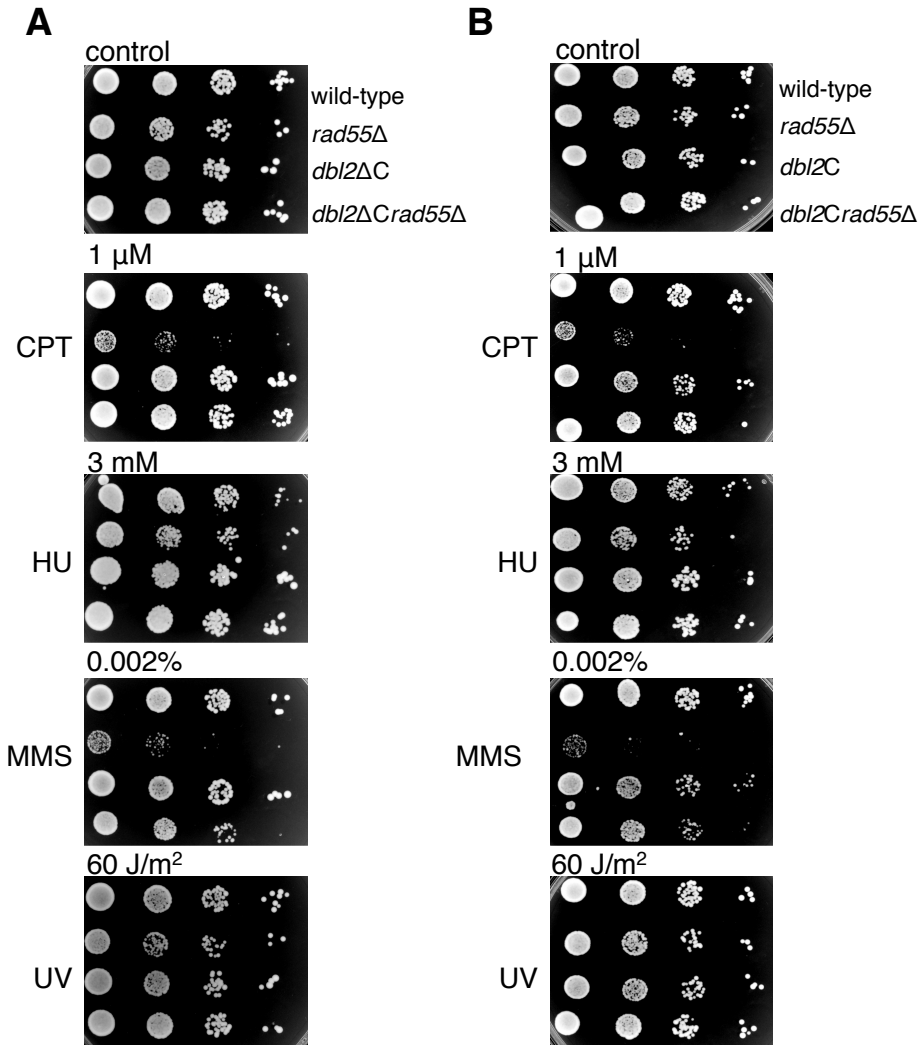


Figure 7.9. Genetic interaction between *dbl2* and *rad55*.

Spot assay comparing the growth and genotoxin sensitivity of wild-type (FO656), *rad55*Δ (MCW1231), *dbl2*ΔC (MCW8873), and *dbl2*Δ*Crad55*Δ (MCW8980) (**A**); wild-type (FO656), *rad55*Δ (MCW1231), *dbl2*C (MCW8880), and *dbl2*C*rad55*Δ (MCW8978) (**B**). The plates were photographed after 5 days of incubation at 30 °C.

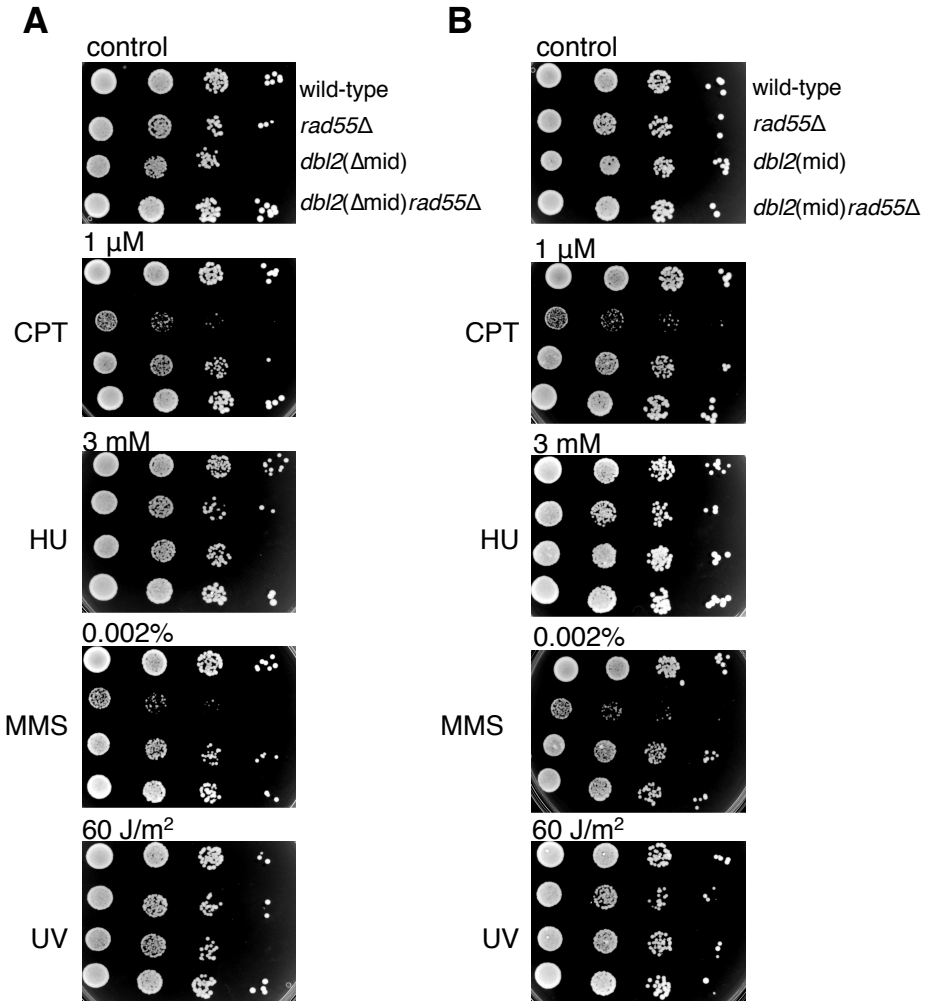


Figure 7.10. Genetic interaction between *dbl2* and *rad55*.

Spot assay comparing the growth and genotoxin sensitivity of wild-type (FO656), *rad55*Δ (MCW1231), *dbl2*(Δmid) (MCW8871), and *dbl2*(Δmid)*rad55*Δ (MCW9010) (**A**); wild-type (FO656), *rad55*Δ (MCW1231), *dbl2*(mid) (MCW8881), and *dbl2*(mid)*rad55*Δ (MCW8974) (**B**). The plates were photographed after 5 days of incubation at 30 °C.

It also forms foci when overexpressed from the strong *nmt* promoter upon treatment with high concentrations of CPT and MMS (Polakova et al., 2016). I wanted to see if Dbl2 forms nuclear foci spontaneously and if the formation of the foci is affected by deletion of its central region, N-terminal domain or C-terminal domain. Epifluorescence microscopy of strains expressing YFP-tagged forms of Dbl2 from its endogenous promoter revealed that full-length Dbl2 expressed forms multiple nuclear foci spontaneously which are usually discerned as a “speckling” of fluorescence throughout the nucleus, with some brighter foci that stand out from the general speckling (Fig. 7.11).

When the N-terminus of Dbl2 is deleted overall nuclear fluorescence appeared to be less compare to cells with full-length protein expressed (Figs. 7.11A and B). Since quantification of the fluorescent speckling by eye can be very subjective, I used ImageJ to quantify the total corrected nuclear fluorescence (described in Chapter 2) (Burgess et al., 2010; McCloy et al., 2014). This analysis showed that the total corrected nuclear fluorescence for *dbl2*ΔN was ~ 1.8-fold less than for full-length Dbl2 ($P < 0.001$) (Table 7.1). A similar reduction was observed for *dbl2*(Δmid) (~ 1.9-fold, $P < 0.001$) and for *dbl2*ΔC (~ 1.6-fold, $P = 0.001$) (Fig. 7.11C and Table 7.1). Interestingly, in a sub-population of *dbl2*(Δmid) mutant cells speckling was noticeably reduced or abolished and was replaced by one or more distinct foci (Fig. 7.11C). My attempts to quantify this phenotype using ImageJ were unsuccessful, but manual counting by eye revealed that ~ 3.5 % of *dbl2*(Δmid) cells in asynchronously growing cultures exhibited distinct foci without any fluorescence in the rest of the nucleus (Table 7.1).

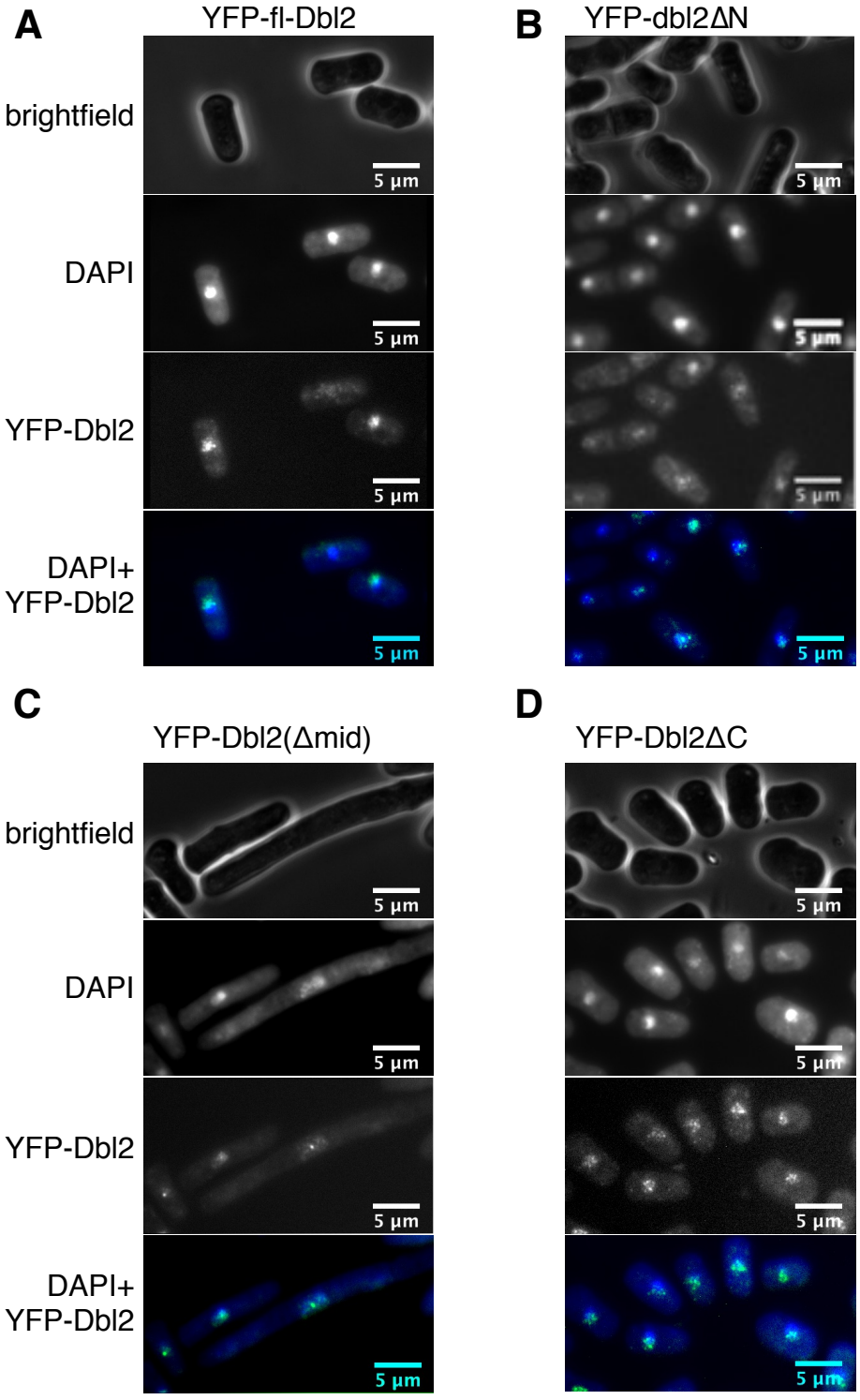


Figure 7.11. Spontaneous focus formation of the full-length Dbl2 and Dbl2 deletion mutants.

Example epifluorescent images of DAPI stained cells presenting the localisation of fl-Dbl2-YFP (MCW8870) (**A**), YFP-Dbl2ΔN (**B**) (MCW8869), YFP-Dbl2(Δmid) (**C**) (MCW8871), and YFP-Dbl2ΔC (MCW8873) (**D**) from an asynchronously growing culture.

Assuming that the fluorescent speckling in the nucleus represents protein that is associated with chromatin, the reduced fluorescence seen in each of the aforementioned mutants suggests that the N-terminal, central and C-terminal domains of Dbl2 are all important for its efficient recruitment to sites across the genome. However, the reduction in fluorescence in each of the mutants could equally stem from reduced protein expression and/or stability. To further investigate the importance of the Dbl2 domains, I next analysed nuclear localization and focus formation in cells treated with CPT or MMS (Figs. 7.12 and 7.13). In cells expressing full-length Dbl2, the fluorescence is reduced following treatment with either CPT (~ 1.4-fold, $P < 0.001$) or MMS (~ 1.7-fold, $P < 0.001$) (Table 7.1). Both genotoxins also increased the number of cells with distinct foci and no background speckling fluorescence from 0.2 % in non-treated cells to 2.1 % and 6.1 % in CPT and MMS treated cultures, respectively (Fig. 7.12A and Table 7.1). Similarly, nuclear fluorescence decreases in *dbl2*ΔN cells in response to CPT (~ 1.7-fold, $P < 0.001$) and MMS (~ 1.5-fold, $P < 0.001$) treatment relative to non-treated cells (Table 7.1). Cells exhibiting distinct foci with no background speckling are also more numerous in cells treated with CPT (2.6 %) or MMS (15.7 %) compared to their non-treated counterparts (0.2 %) (Fig. 7.12B and Table 7.1).

The *dbl2*(Δmid) cells, unlike cells with full-length Dbl2 or *dbl2*ΔN, do not show a significant difference in fluorescence upon CPT or MMS treatment relative to untreated cells (Fig. 7.13A and Table 7.1).

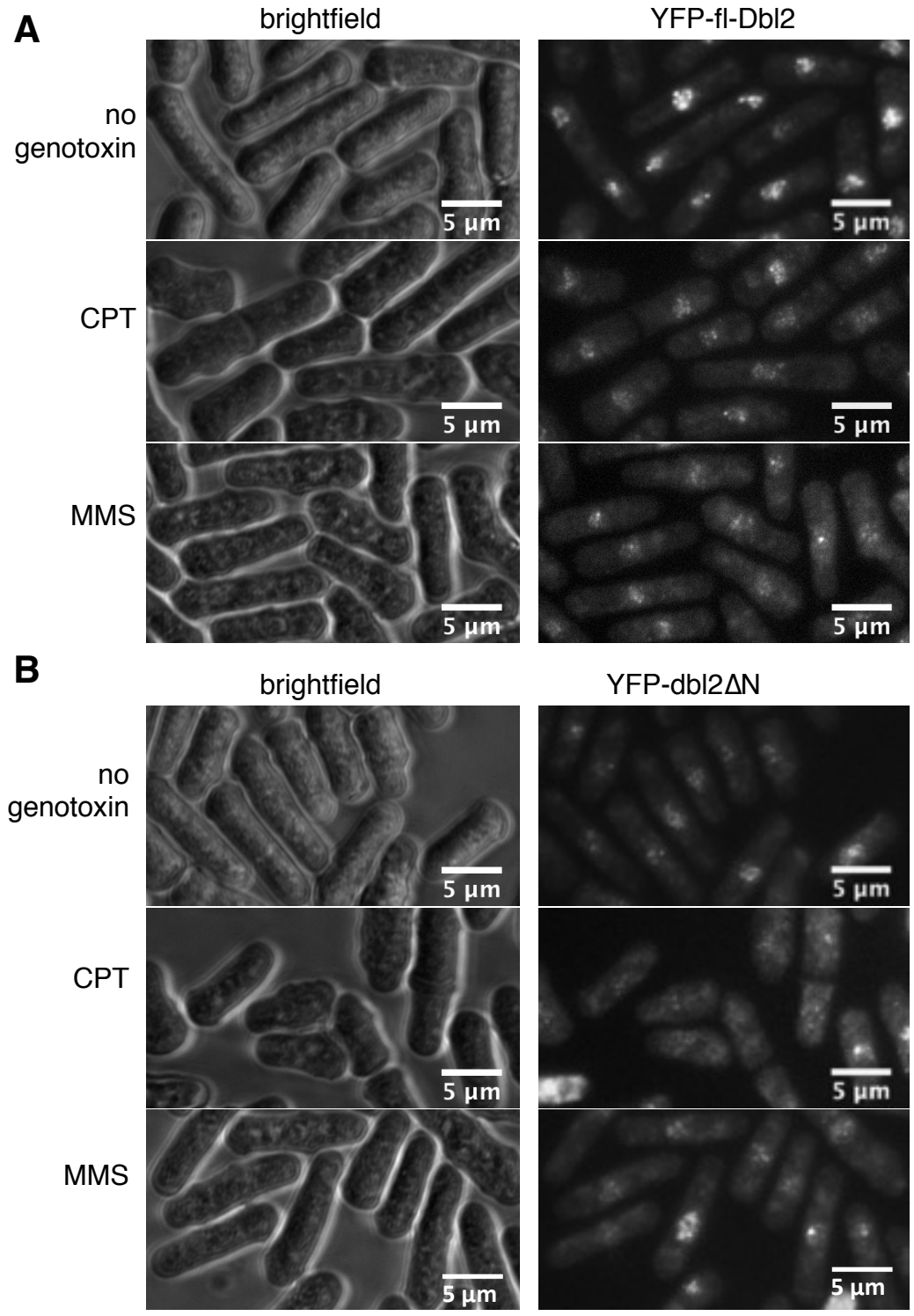


Figure 7.12. CPT- and MMS-induced focus formation of full-length YFP-Dbl2 and YFP-Dbl2ΔN.

Example epifluorescent images of cells comparing the localisation of YFP-fl-Dbl2 (MCW8870) (**A**) and YFP-Dbl2ΔN (MCW8869) (**B**) from an asynchronously growing culture without genotoxins and following treatment with 10 µM CPT or 10 % MMS for 4 hours at 30 °C.

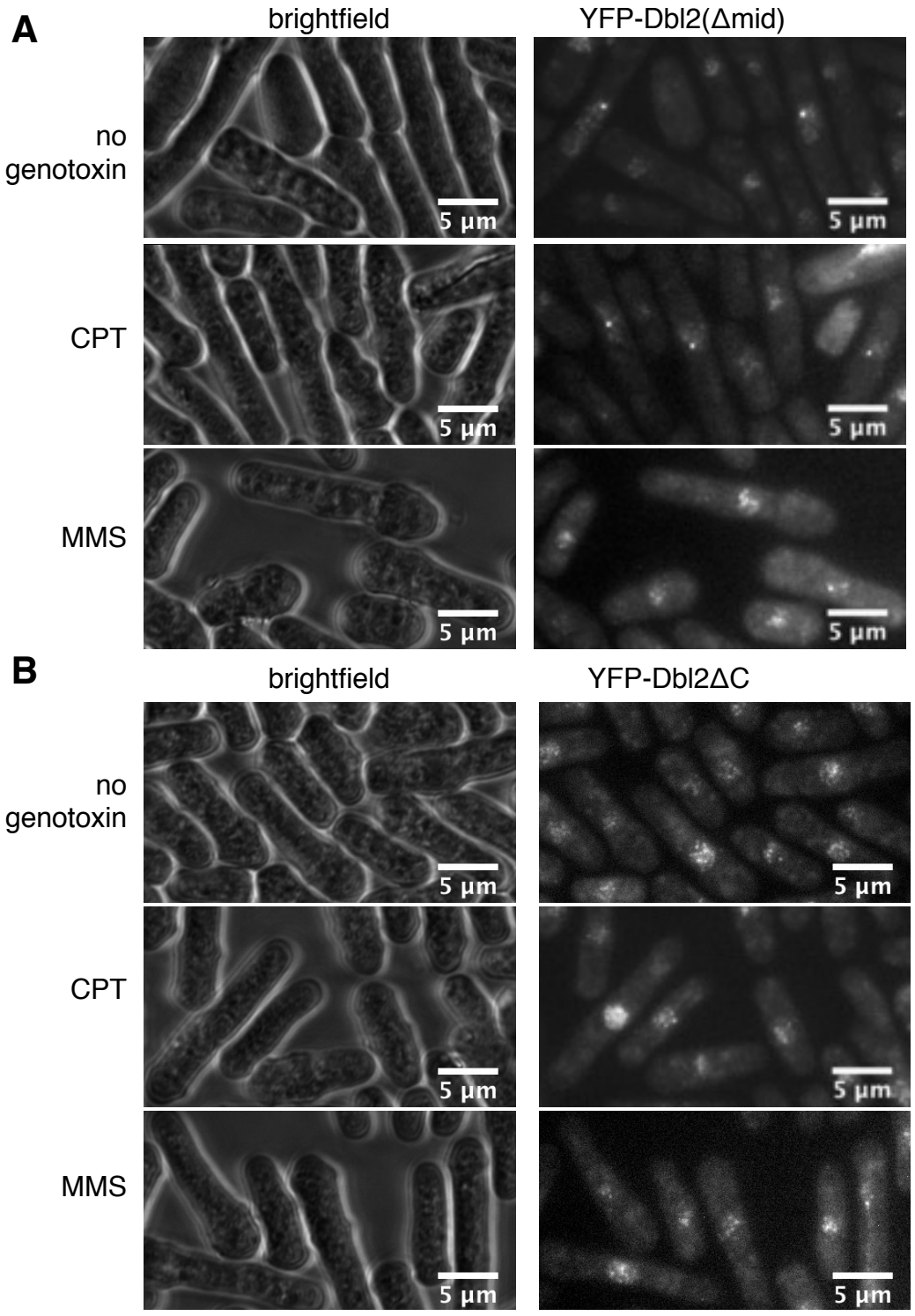


Figure 7.13. CPT- and MMS-induced focus formation of YFP-Dbl2(Δmid) and YFP-Dbl2ΔC.

Example epifluorescent images of cells comparing the localisation YFP-Dbl2(Δmid) (MCW8871) (**A**) and YFP-Dbl2ΔC (MCW8873) (**B**). Cells are from asynchronously growing cultures and are analysed following treatment with 10 µM CPT or 10 % MMS for 4 hours at 30 °C as indicated.

Table 7.1. Comparison of speckling fluorescence intensity and distinct Dbl2 foci in different Dbl2 deletion mutants without genotoxin treatment and following CPT and MMS treatment.

	Geno toxin	Number of cells analysed	Total corrected nuclear fluorescence, arb. unit	Fold decrease relative to fl-*dbl2* non-treated cells	Fold decrease relative to non-treated cells	% of cells with foci
fl-*dbl2*	-	470	79905	1	1	0.2
	CPT	515	58424	-	1.37	2.1
	MMS	507	47747	-	1.68	6.1
*dbl2*ΔN	-	543	43404	1.84	1	0.2
	CPT	508	25804	-	1.68	2.6
	MMS	420	29809	-	1.46	15.7
*dbl2(*Δmid)	-	494	42288	1.89	1	3.5
	CPT	502	48463	-	0.87	12.6
	MMS	483	36964	-	1.14	12.2
*dbl2*ΔC	-	545	49646	1.61	1	0.2
	CPT	577	44569	-	1.12	0.7
	MMS	524	41818	-	1.19	1.2

However, both genotoxins result in a marked increase in the population of cells with discernible bright foci and no background speckling from 3.5 % in untreated cells to 12.6 % and 12.2 % in cells after CPT and MMS treatment, respectively (Fig. 7.13A and Table 7.1).

Lastly *dbl2*ΔC cells do not exhibit any significant change in the fluorescence (Fig. 7.13B) following genotoxins treatment and proportion of the cells with defined foci only slightly increase following MMS treatment from 0.2 % to 1.2%. Together these data suggest that Dbl2 is recruited to sites of DNA damage induced by MMS and CPT, and in some cells, this leads to a concentration of protein into one or a few foci at the expense of its wider distribution across the genome. This behaviour appears to be largely unaffected by loss of either its N-terminal or central domains, albeit loss of the central domain seems to result in the accumulation of protein into fewer and brighter foci. However, the ability of Dbl2 to form DNA damage-induced foci appears to be impaired in *dbl2*ΔC cells suggesting that its C-terminus is needed for its efficient recruitment to sites of DNA damage.

7.2.5 Investigating the recruitment of Dbl2 to *RTS1* by fluorescence microscopy

As Dbl2 plays an important role in limiting *RTS1-AO*-induced direct repeat recombination, I next investigated whether the full-length protein (or its partial deletion variants) forms detectable foci at *RTS1* in living cells. To this end, I constructed strains containing a *lacO* array adjacent to *RTS1*, YFP-tagged Dbl2 (or partial deletion variant) and LacI tagged with the red fluorescent

protein tdKatushka2 (Chapter 5). I took snapshots of cells from these strains growing in asynchronous culture and determined the percentage of cells in which a YFP-tagged fl-Dbl2, Dbl2ΔN or Dbl2(Δmid) focus co-localized with a *lacO*-LacI focus when the *RTS1* RFB is in its active and inactive orientation (Fig. 7.14). As mentioned above, YFP-Dbl2 forms speckling throughout the whole nucleus, which resolves into multiple closely located foci lying in different z-planes. This general nuclear fluorescence complicates analysis of Dbl2 localization at *RTS1*. Nevertheless, I determined that between 38-45 % of cells exhibited YFP-Dbl2 fluorescence that co-localized with a *lacO*-LacI focus, and that this was true irrespective of the barrier orientation and which variant of Dbl2 was analysed.

7.3 Discussion

In this chapter, I have described my attempts to identify functional domains within Dbl2 by analysing the effect of deleting different parts of the protein on: genotoxin sensitivity; spontaneous and *RTS1*-induced recombination; genetic interaction with Rad51-mediator proteins; spontaneous and DNA-damage induced foci formation; and localisation at the *RTS1* RFB.

Previous studies have found no phenotypic effect upon deleting the N-terminal domain (amino acids 6-103) of Dbl2 containing DUF2439 (Yu et al., 2013; Polakova et al., 2016).

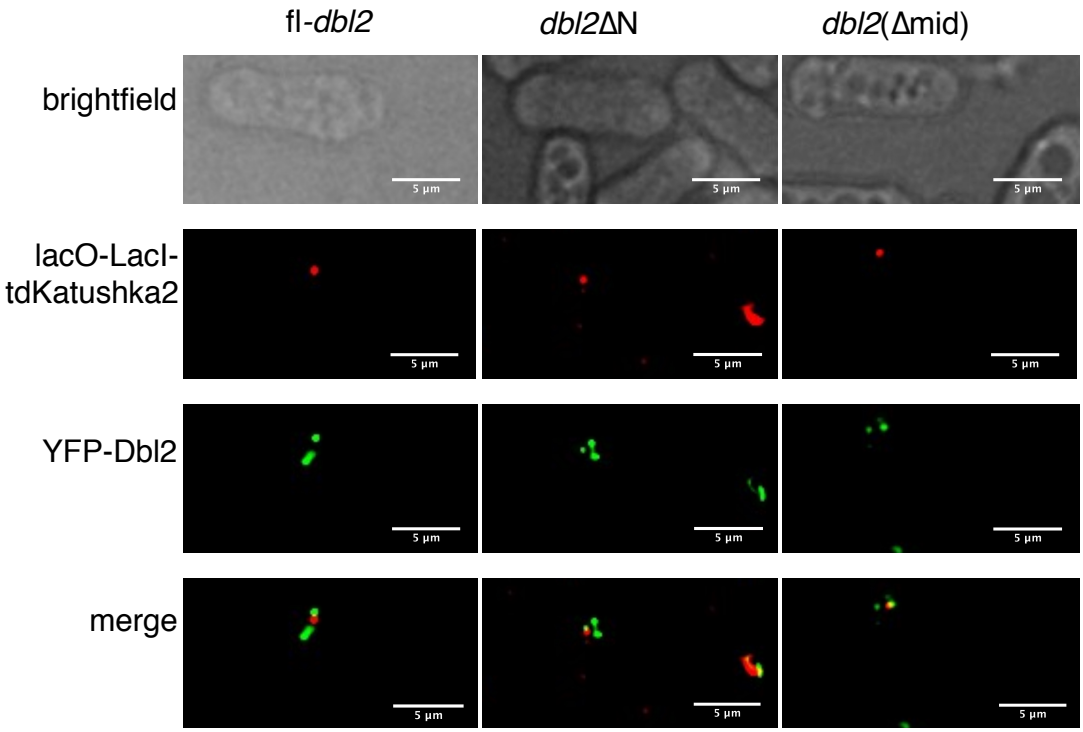


Figure 7.14. The localisation of YFP-fl-Dbl2, YFP-Dbl2ΔN and YFP-Dbl2(Δmid) at *RTS1.*

Example snapshots of *RTS1-IO* containing cells in which YFP-Dbl2 foci are either co-localizing or not co-localizing with a *lacO*-LacI-tdKatushka2 focus. In order of presentation, the strains are MCW9020, MCW9018, MCW9022.

Indeed, I found that *dbl2*ΔN is not sensitive to any of the genotoxins that I used and does not exhibit any increased level of *RTS1*-induced recombination (Figs. 7.1 and 7.5). Deletion of the DUF2439 domain in budding yeast Rdh54 also has no effect on genotoxin sensitivity (Santa Maria et al., 2013). However, I did find that loss of Dbl2's N-terminal region seemed to result in a slight but significant increase in the frequency of spontaneous recombination (Fig. 7.4). This increase is not seen in a *dbl2*Δ mutant and, therefore, my finding suggests that without its N-terminal domain Dbl2 may interfere with a DNA repair/replication/recombination process leading to heightened spontaneous recombination.

Similar to the deletion of other functional domains, loss of the N-terminus of Dbl2 also reduced the nuclear fluorescence relative to full-length protein (Fig. 7.11A, B). One plausible explanation for the reduction in fluorescence in the different deletion mutants is an increased level of protein degradation, which could occur if the protein is misfolded in the absence of its most structured regions. Alternatively, cooperative action between each of its domains is needed for the folding of functional Dbl2 protein that is capable of being recruited to sites across the genome through protein-DNA and/or protein-protein interactions. To investigate the levels of Dbl2 *in vivo* I used western blot analysis of total cell lysates. However, the detection of Dbl2 by this method proved very variable and unreliable seemingly due to a low efficiency of protein extraction that might stem from its binding to DNA or from its disordered structure. Future studies will be needed to address this problem.

Only the *dbl2*ΔN mutant exhibited further reduction in the intensity of speckling of fluorescence following CPT and MMS treatment, suggesting its role in the localisation of the protein to the DNA-repair sites across genome. It is important to note that N-terminally truncated Rdh54 does not bind Rad51 *in vitro* and *in vivo* and exhibits reduced efficiency of Rad51 removal from DNA (Chi et al., 2006; Santa Maria et al., 2013). Dbl2 was shown to interact with Rad51 in yeast two-hybrid assay (Polakova et al., 2016). The impaired interaction of Dbl2 and Rad51 mutant could explain observed mutant phenotype.

The speckling of fluorescence in the nucleus is reminiscent of the phenotype observed in cells with Mhf1-GFP. It is mostly lost in the *fml1*Δ mutant and is believed to represent Mhf1 co-localisation with Fml1 at the sites where the latter is involved in DNA repair and recombination (Bhattacharjee et al., 2013). Dbl2 also weakly interacts with Fml1 in two-hybrid assay (Polakova et al., 2016). Taken together, these observations indicate that Dbl2 might be distributed across the genome partially through interaction of its N-terminus with Rad51 and/or Fml1 and this interaction becomes more important when DNA-damage is induced.

Neither N-terminal or C-terminal domains of Dbl2 were required for resistance to genotoxins (Figs. 7.1 and 7.2A). In contrast, deletion of its central domain (amino acids 321-430) resulted in hypersensitivity to MMS and CPT that was similar to a *dbl2*Δ mutant (Fig. 7.3A), indicating that this region is vital for its DNA damage repair/tolerance function. However, expression of this region (amino acids 321-430) on its own is not sufficient to suppress genotoxin

hypersensitivity of the *dbl2*Δ mutant (Fig. 7.3B), which shows that other regions of the protein are needed.

The partial deletion mutant *dbl2*(Δmid) and truncation mutants *dbl2*(mid) and *dbl2*C have positive interaction with mediator protein deletion mutants *swi5*Δ and *rdl1*Δ (Figs. 7.6 – 7.7), suggesting that interaction provided by the middle segment of the protein is essential for Dbl2 counteractivity toward Swi5 and Rdl1. Contrary to that, deletion of either Dbl2 middle segment or any of the termini leads to the suppression of *rad55*Δ genotoxin sensitivity (Figs. 7.8 – 7.10). This result indicates that role of Dbl2 in opposing Rad55 activity in formation and maintenance of Rad51-filament is potentially implemented in a different way to Swi5 and Rdl1 mechanism and requires N- and C-termini and middle region of the protein.

The frequency of the recombination induced at blocked RF at *RTS1* is increased when N-terminal, central or C-terminal domains are deleted, but to a lesser extent than in a *dbl2*Δ mutant (Fig. 7.5). Interestingly, *dbl2*(Δmid) shows similar to *dbl2*Δ increase in the frequency of the conversion-type recombinants at *RTS1*-AO but more moderate increase in deletions suggesting that even without the middle region Dbl2 is capable to partially limit the *RTS1*-induced recombination. On the other hand, the redistribution of Dbl2(Δmid) from the sites across the genome to form distinct nuclear foci following the CPT and MMS-treatment indicates that 321-430 aa are not essential for the protein recruitment to the sites of DNA repair.

The C-terminus Dbl2 truncation mutant is not sensitive to genotoxins and does not contribute to the countering activity toward Swi5, although similarly to the

N-terminus, is needed for potentially cooperative action of all Dbl2 structural elements to counter activity of Rad55. Interestingly, CPT or MMS treatment of *dbl2*ΔC did not affect the distribution of the protein in the nucleus (Fig. 7.13B), indicating that the C-terminus is needed for the formation of the nuclear foci in the conditions of genotoxic stress, which is consistent with the C-terminus being needed for the localisation to HO-induced DSBs (Yu et al., 2013).

Taken together, these data suggest that the cooperative action of N- and C-terminal domains and middle region of Dbl2 are important for providing all its functions. The middle region 350-431 aa is essential for the genotoxin sensitivity while other parts ensure redundant DNA repair functions. Dbl2 is distributed throughout the genome by co-localising with Rad51, Fml1 or any other interaction partners. Redistribution to form discernible foci following the CPT and MMS treatment depends on the C-terminus of Dbl2.

Chapter 8

8 Concluding remarks

Defects in DNA replication can lead to the genome rearrangements that are considered to result from events at stalled and collapsed DNA replication forks. The Whitby group has successfully employed the *RTS1* in *S. pombe* as a model for studying how cells cope with replication fork collapse and strong programmed replication fork barriers. This specific RF blockage can be resolved either through fork collapse followed by recombination-dependent restart or by passive termination involving forks merging at the barrier (Ahn et al., 2005; Nguyen et al., 2015).

In the first part of this dissertation (Chapter 3) I attempted to establish an unbiased system to interrogate the replisome composition at site-specific pRFB by purification of Rtf1-Halo together with barrier DNA and crosslinked to it proteins which can be further identified by MS-SILAC. The success of this method depended on the ability to efficiently pull-down the *RTS1* binding protein Rtf1. However, despite repeated attempts to optimize this procedure using different epitope tags and pull-down conditions, a sufficiently robust pull-down was not achieved (Fig. 3.4). My data suggest that the Halo-tag cannot be used for the efficient pull-down of Rtf1, most probably due to the partial unfolding of the Halo-tag during the process of protein lysis or inhibition of Halo-tag/Halo-resin interactions by the compounds released during *S. pombe* lysis. Therefore, other tags that covalently bind to their resin should be used for the development of the aforementioned proteomic system, for example SNAP- and CLIP-tag.

Further, I have focused on identification of the putative partners of the Fml1 DNA helicase. I have shown that Fml1 interacts with Elg1 (Fig. 3.5A), which is

consistent with data from budding yeast where Elg1 was shown to interact with Mph1 (Singh et al., 2013). Contrary to the reported results from a budding yeast two-hybrid assay (Singh et al., 2013), Elg1 does not pull down Mhf1 (Fig. 3.5B), although this might be explained by the use of asynchronous cultures. If the interaction between Elg1 and Mhf1 is transient and controlled by the cell cycle or by DNA replication stress, it may be underrepresented in the analysed samples. The interaction between Fml1 and Elg1 might be important for the elucidation of the molecular mechanism of Fml1 recruitment to the sites of stalled and/or collapsed replication forks.

In addition, consistent with a budding yeast study (Chen et al., 2009), Fml1 seems to directly interact with Smc5-Smc6 through Smc5 (Fig. 3.6). Future work in this direction should include the confirmation of the interaction of Fml1 with Elg1 and Smc5 by reciprocal immunoprecipitations. Mapping of the interactions detected by site-directed mutagenesis and biochemical studies of the purified protein will elucidate the biological significance and molecular mechanisms of these interactions.

In the next chapters, I presented a putative Fml1 partner protein Dbl2, which appears to be conserved from yeast to human (Yu et al., 2013; Yimit et al., 2015; Polakova et al., 2016). The *dbl2*Δ mutant strain is hypersensitive to agents that cause DNA lesions that perturb replication forks (Fig. 4.3). However, unlike a *fml1*Δ mutant, it exhibits hyper-recombination at the *RTS1* barrier (Fig. 4.9). These data from fission yeast are in contrast with the studies in budding yeast, where *mph1*Δ and *mte1*Δ are epistatic and Mte1 is believed to be part of the Mph1-dependent machinery involved in mitotic DSB repair by

negatively regulating the D-loop-dissociative activity and promoting its fork reversal and branch-migration activity (Yimit et al., 2015; Silva et al., 2016; Xue et al., 2016). Data from epistasis analysis with *fml1* and other crucial recombination factors reveal further differences between *dbl2*Δ and *fml1*Δ mutants (Fig. 5.1) and suggest that Dbl2 acts as a negative regulator of Rad51 nucleoprotein filament formation and stabilization in the same pathway as Fbh1. Indeed, *dbl2*Δ and *fbh1*Δ have very similar phenotypes and characterized by chromosome missegrargation, sensitivity to CPT and MMS, a tendency to acquire suppressor mutations (although not identified in the case of *dbl2*Δ), increased levels of Rad51-dependent recombination induced by RF blocked at site-specific RFB *RTS1* (Figs. 5.4 – 5.6) (Morishita et al., 2005; Osman et al., 2005; Lorenz et al., 2009). In addition, both mutants exhibit positive interactions with *rad55*Δ, *rad57*Δ, *swi5*Δ, *sfr1*Δ, *rlp1*Δ and *rdl1*Δ (Figs. 5.18 – 5.24). Similar to *fbh1*Δ, deletion of *dbl2* results in accumulation of Rad51 foci (Morishita et al., 2005; Osman et al., 2005; Lorenz et al., 2009). Taken together with findings made by Polakova et al. (2016) that Dbl2 is required for the efficient formation of Fbh1 foci following CPT-treatment, my results suggest the Dbl2 may assist recruitment of Fbh1 to the site of DNA damage. However, the genetic analysis also revealed that Dbl2 has functions that are independent of Fbh1, which may include a role in regulating Fml1. First, I have demonstrated that Dbl2 but not Fbh1 is required for suppression Rad52-dependent (Rad51-independent) recombination induced at the *RTS*1 barrier (Fig. 5.15). Second, Dbl2 seems to be needed for the formation of spontaneous, additional compare to wild-type, Rad52-dependent deletions

observed in *rad51*Δ mutant. These suggest that Dbl2 can positively and negatively regulate Rad52-dependent recombination/restart. Until recently, Rad51-independent replication restart (that depends on Rad52) was thought to be a very minor and inefficient pathway based on studies of BIR in budding yeast (Bai and Symington, 1996; Sung, 1997b; Petukhova et al., 1999; Davis and Symington, 2001; Pohl and Nickoloff, 2008). However, recent work suggests that it can be essential to promote DNA synthesis in response to replication stress via certain pathways (Costantino et al., 2014; Bhowmick et al., 2016; Ciccia et al., 2016; Sotiriou et al., 2016; Mazina et al., 2017; Min et al., 2017). *In vitro* studies demonstrated that Rad52 is capable of D-loop formation (Mortensen et al., 1996; Reddy et al., 1997; Kagawa et al., 2001; Kumar et al., 2004). If Rad52 promotes D-loop formation *in vivo*, and if this intermediate structure is a critical point for further recombination continuation or abrogation, then Dbl2 might regulate Rad51-independent recombination through its interaction and regulation of Fml1 functions (Sun et al., 2008; Nandi and Whitby, 2012).

In contrast to the hypothesis that Dbl2 is simply required for the recruitment of Fbh1, I have also presented data that overexpression of Dbl2 can partially rescue mutant *fbh1* phenotype (Fig. 5.9). One of the potential explanations could be that excess of Dbl2 allows recruitment and/or positive regulation of anti-recombinogenic activities of other DNA helicases/translocases. Dbl2 was shown to be required for the efficient localisation of Fml1 to DSBs (Yu et al., 2013). Since a functional homolog of Fbh1 is absent in budding yeast it would be reasonable to suggest that Dbl2 acquired an additional protein partner,

however a *dbl2*Δ*fbh1*Δ*fml1*Δ triple mutant is more sensitive to genotoxins than any of the double mutants (Fig. 5.7) which suggests that Dbl2 might have functions independent of both Fml1 and Fbh1. Interestingly, a recent proteomic analysis of another DNA helicase Pfh1 interaction partners, revealed physical interaction between Pfh1 and Dbl2 during S phase (McDonald et al., 2016). Data on recombination downstream of the RFB suggest that Dbl2 can act with Pfh1 to promote efficient replication restart (Fig. 4.10). It is also important to note that the human homolog of Dbl2, ZGRF1 has an ATP-ase domain at its C-terminus. Thus, Dbl2 might play a role of a scaffold// adaptor/ sensor for different helicases, thus regulating their pro- and anti-recombinogenic activities.

To gain clearer understanding of the molecular mechanisms of the pathways Dbl2 is involved in, future analysis should be focused on finding its physical interaction partners. The putative interaction partners can be searched by pull-down experiments of Dbl2 followed by mass-spectrometry and complemented by the immunoprecipitation experiments with putative interaction partners such as Fml1, Fbh1, Rad51, Rad52. I attempted to address both approaches. However, I was never able to detect the tagged protein by western blot analysis in strains containing Dbl2 tagged on its C-terminus with either 3HA, 13-myc, GST or GFP tags. Dbl2 tagged at its N-terminus with YFP was detectable in alkaline cell lysates, but this result was not reproducible. Moreover, Dbl2 does seem to be hard to extract from the cell lysate in native conditions necessary for the interaction studies.

Which structural features of Dbl2 could allow its potential interactions with

multiple helicases and key factors of the HR machinery? Structure prediction analysis of Dbl2 revealed that Dbl2 is a largely disordered protein with a conserved N-terminal domain of unknown function (DUF2439) (Polakova et al., 2016; Figs. 6.1 – 6.3). Dbl2 also contains predicted Molecular Recognition Features (Sharma et al., 2016) – short intrinsically disordered peptides that are responsible for mediating protein interaction through a disorder-to-order transition upon binding to partners (Dunker et al., 2008; Das et al., 2012). It has been shown that in eukaryotes hub proteins that are defined as proteins with more than 10 interaction partners are significantly more disordered and enriched in Molecular Recognition Features compare to 'end protein' (with one interaction partner) (Haynes et al., 2006). The high disorder content of hubs aids their ability to adopt to the various structures of binding partners even when using the same or overlapping binding regions. The presence of Molecular Recognition Features that can undergo a disorder-to-order switch provides reversible highly specific interactions, that are especially important in the context of the inducible responses typical to regulation (Ekman et al., 2006; Haynes et al., 2006; Radivojac et al., 2007). Thus, Dbl2 might play a role as such a hub that coordinates a range of various helicases and via these interactions regulates activity of other recombinational proteins in response to fork stalling and/or collapse.

In line with this hypothesis, I found that the deletion of N-terminal, central or C-terminal domains of Dbl2 resulted in the increase of the frequency of the recombination induced at blocked RF at *RTS1,* but to a lesser extent than the deletion of *dbl2* (Fig. 7.5). In addition, the reduction of nuclear fluorescent

speckling that conceivably represents its association with chromatin, was observed in each of the aforementioned mutants suggesting that a cooperative action of N-terminal, central and C-terminal domains of Dbl2 is required for its efficient recruitment to sites across the genome (Table 7.1). It should be noted that this reduction can be a consequence of the reduced stability, but even if this is the case, it still supports the idea that all protein regions should be present to assist the efficient protein folding and functionality.

I have shown that the middle region of Dbl2 is important for conferring CPT resistance (Fig. 7.3A). This is consistent with the finding that it is needed for Dbl2 to limit Rad51 activity in the presence of Rad51 mediator proteins. However, the collaboration of N-terminal, middle and C-terminal regions is essential to oppose Rad51 activity in the presence of Rad55 (Figs. 7.8 – 7.10). It is currently unknown why cells adopted three different mediator complexes and the particular molecular mechanisms of their stabilization actions are yet to be discovered. However, all of them are believed to have a unique non-redundant function. Rad55–Rad57 blocks disruption of presynaptic filament by blocking Srs2 translocation (Liu et al., 2011a). If Dbl2 counteracts the different roles of mediators in filament maintenance via Fbh1-dependent and independent functions, it is conceivable that its middle region is critical for the contribution to Fbh1-dependent functions in the case of Swi5-Sfr1 and Rdl1-Rlp1-Sws1, whereas the full-length protein folding is required for the Fbh1-independent activity in case of Rad55-Rad57 or *vice versa*.

To elucidate further the function of Dbl2 and its functional domains I have begun biochemical and biophysical characterizations of the full-length protein

and its N-terminal DUF2439 domain. I have developed and optimized systems for the efficient expression and purification of full-length Dbl2 protein and its N-terminal region. I also showed that it is possible to express the middle and C-terminal regions of Dbl2. The future work should be focused on *in vitro* biochemical studies to test the interaction of Dbl2 and its domains with putative protein partners and a possible interaction with DNA.

Appendix

Table S1. Effect of different mutants on *RTS1-IO* direct repeat recombination. All means are presented with ± one standard deviation in parenthesis. P-values are derived from independent-sample t-tests comparing the mean values of the respective mutant to the corresponding mean value found in the wild-type.

Genotype	Number of Colonies Analysed	$Ade^+ His^+$ recombinant frequency (x 10^{-4})		$Ade^+ His^-$ recombinant frequency (x 10^{-4})	
		Mean	P-value	Mean	P-value
wild-type	110	1.43 (± 0.58)	-	3.14 (± 0.87)	-
*dbl2*Δns	84	1.70 (± 0.92)	0.019	3.42 (± 1.22)	0.078
*dbl2*Δs	39	1.47 (± 0.80)	0.773	2.71 (± 1.11)	0.031
*dbl2*Δ*fbh1*Δ	20	1.44 (± 0.52)	0.937	3.18 (± 0.78)	0.834
*dbl2*Δ*fml1*Δ	38	2.61 (± 1.92)	0.001	9.17 (± 4.75)	<0.001
*dbl2*Δ*rad51*Δ	30	1.35 (± 0.75)	0.613	4.86 (± 12.13)	<0.001
*dbl2*Δ*rad55*Δ	14	0.22 (± 0.20)	<0.001	7.47 (± 2.36)	<0.001
*dbl2*Δ*rad52*Δ	28	0.82 (± 0.62)	<0.001	2.79 (± 1.72)	0.296
*fbh1*Δ	25	1.89 (± 0.53)	<0.001	3.41 (± 0.77)	0.136
*fbh1*Δ*rad51*Δ	10	0.44 (± 0.37)	<0.001	20.21 (± 5.13)	<0.001
*fbh1*Δ*rad52*Δ	30	0.56 (± 0.33)	<0.001	2.92 (± 1.08)	0.297
*fml1*Δ	28	0.48 (± 0.25)	<0.001	3.70 (± 1.30)	0.039
*rad51*Δ	15	0.31 (± 0.39)	<0.001	15.31 (± 6.17)	<0.001
*rad52*Δ	5	0	-	4.41 (± 3.61)	0.477
*rad55*Δ	15	0.38 (± 0.25)	<0.001	15.49 (± 2.47)	<0.001
YFP-*dbl2*-fl	20	1.70 (± 1.03)	0.264	3.83 (± 2.03)	0.151
YFP-*dbl2*(Δ6-103)	39	3.71 (± 2.93)	<0.001	4.56 (± 3.07)	0.007
YFP-*dbl2*(Δ6-50)	20	2.40 (± 1.64)	0.016	3.39 (± 1.98)	0.574

Genotype	Number of Colonies Analysed	$Ade^+ His^+$ recombinant frequency (x 10^{-4})		$Ade^+ His^-$ recombinant frequency (x 10^{-4})	
		Mean	P-value	Mean	P-value
YFP-*dbl2*(Δ321-430)	17	2.26 (± 1.21)	0.012	2.79 (± 0.98)	0.181
YFP- *dbl2*(321-430)	20	2.14 (± 1.36)	0.033	3.95 (± 1.93)	0.080
YFP-*dbl2*(Δ621-715)	20	1.63 (± 0.74)	0.261	2.26 (± 145)	0.015
YFP-*dbl2*(621-715)	19	1.56 (± 0.60)	0.390	3.48 (± 1.62)	0.381
wild-type, 5 kb spacer	20	1.25 (± 0.50)	0.173	3.75 (± 1.55)	0.101
*dbl2*Δ, 5kb spacer	14	1.22 (± 0.73)	0.328	4.57 (± 2.01)	0.020
wild-type, 12.4 kb downstream	10	1.23 (± 0.64)	0.365	2.59 (± 1.06)	0.139
*dbl2*Δ, *RTS1* 12.4 kb downstream	20	1.62 (± 0.95)	0.394	4.15 (± 1.10)	0.001

Table S2. Effect of different mutants on *RTS1-AO* direct repeat recombination. All means are presented with ± one standard deviation in parenthesis. P-values are derived from independent-sample t-tests comparing the mean values of the respective mutant to the corresponding mean value found in the wild-type.

Genotype	Number of Colonies Analysed	$Ade^+ His^+$ recombinant frequency (x 10^{-4})		$Ade^+ His^-$ recombinant frequency (x 10^{-4})	
		Mean	P-value	Mean	P-value
wild-type	99	140.58 (± 43.84)	-	104.04 (± 39.35)	-
*dbl2*Δns	111	545.85 (±303.47)	<0.001	1478.67 (±426.5)	<0.001
*dbl2*Δs	37	27.75 (± 18.63)	<0.001	50.66 (± 27.33)	<0.001
*dbl2*Δ*fbh1*Δ	20	821.42 (± 369.89)	<0.001	2022.09 (± 650.97)	<0.001
*dbl2*Δ*fml1*Δ	29	281.52 (±173.41)	<0.001	1876.02 (± 1242.95)	<0.001
*dbl2*Δ*rad51*Δ	37	5.04 (± 3.38)	<0.001	154.52 (± 53.93)	<0.001
*dbl2*Δ*rad55*Δ	15	9.67 (± 7.25)	<0.001	109.79 (± 25.31)	0.459
*dbl2*Δ*rad52*Δ	38	5.20 (± 3.83)	<0.001	10.89 (± 6.44)	<0.001
*fbh1*Δ	39	798.32 (±302.66)	<0.001	1687.71 (±431.4)	<0.001
*fbh1*Δ*rad51*Δ	20	2.07 (± 1.26)	<0.001	88.70 (± 14.25)	0.003
*fbh1*Δ*rad52*Δ	39	38.69 (± 18.70)	<0.001	7.49 (± 5.47)	<0.001
*fml1*Δ	25	18.30 (± 9.38)	<0.001	159.53 (± 64.82)	<0.001
*rad51*Δ	14	2.31 (± 0.71)	<0.001	76.99 (± 17.88)	<0.001
*rad52*Δ	4	0.16 (± 0.11)	<0.001	4.35 (± 1.27)	<0.001
*rad55*Δ	15	0.96 (± 1.16)	<0.001	27.23 (± 16.25)	<0.001
YFP-*dbl2*-fl	23	147.21 (± 55.79)	0.598	102.30 (± 43.58)	0.861

Genotype	Number of Colonies Analysed	$Ade^+ His^+$ recombinant frequency (x 10^{-4})		$Ade^+ His^-$ recombinant frequency (x 10^{-4})	
		Mean	P-value	Mean	P-value
YFP-*dbl2*(Δ6-103)	44	152.43 (± 56.91)	0.223	98.81 (± 33.92	0.420
YFP-*dbl2*(Δ6-50)	24	156.77 (± 62.80)	0.242	95.99 (± 66.83)	0.575
YFP-*dbl2*(Δ321-430)	18	517.31 (± 243.87)	<0.001	444.07 (± 99.63)	<0.001
YFP- *dbl2*(321-430)	16	859.22 (± 429.72)	<0.001	721.40 (±474.85)	<0.001
YFP-*dbl2*(Δ621-715)	18	375.40 (± 126.39)	<0.001	1084.58 (±431.72)	<0.001
YFP-*dbl2*(621-715)	15	656.82 (± 554.93)	<0.001	1315.72 (± 1564.05)	<0.001
wild-type, 5 kb spacer	24	161.14 (± 83.85)	0.255	756.14 (±311.04)	<0.001
*dbl2*Δ, 5kb spacer	20	1721.31 (± 1230.93)	<0.001	2.980.15 (± 1029.42)	<0.001
*dbl2*Δ*rad51*Δ, 5 kb spacer	19	24.95 (± 17.87)	<0.001	2146.92 (±715.43)	<0.001
*rad51*Δ, 5 kb spacer	5	22.63 (± 9.40)	<0.001	962.19 (±226.85)	0.001
wild-type, 12.4 kb downstream	10	7.44 (± 5.02)	<0.001	73.02 (± 27.36)	0.006
*dbl2*Δ, *RTS1* 12.4 kb downstream	19	6.84 (± 4.26)	<0.001	118.54 (± 65.80)	0.364
wild-type + pREP41	18	10.05 (±7.75)	<0.001	66.09 (± 34.94)	<0.001
wild-type + pREP41-*rad52*	10	2830.47 (± 762.96)	<0.001	361.69 (±141.59)	<0.001

Bibliography

Ahn, J. S., Osman, F., Whitby, M. C. 2005. Replication fork blockage by RTS1 at an ectopic site promotes recombination in fission yeast. *The EMBO Journal* **24**: 2011–2023.

Ait Saada, A., Lambert, S. A. E., Carr, A. M. 2018. Preserving replication fork integrity and competence via the homologous recombination pathway. *DNA Repair* **71**: 135–147 DOI: 10.1016/j.dnarep.2018.08.017.

Ait Saada A., Teixeira-Silva A., Iraqui I., Costes A., Hardy J., Paoletti G., et al. (2017). Unprotected replication forks are converted into mitotic sister chromatid bridges. Mol. Cell 66 398–410.e4. 10.1016/j.molcel.2017.04.002

Akamatsu, Y., Dziadkowiec, D., Ikeguchi, M., Shinagawa, H., Iwasaki, H. 2003. Two different Swi5-containing protein complexes are involved in mating-type switching and recombination repair in fission yeast. *Proceedings of the National Academy of Sciences* **100**: 15770–15775.

Akamatsu, Y., Tsutsui, Y., Morishita, T., Siddique, M. S. P., Kurokawa, Y., Ikeguchi, M., Yamao, F., Arcangioli, B., Iwasaki, H. 2007. Fission yeast Swi5/Sfr1 and Rhp55/Rhp57 differentially regulate Rhp51-dependent recombination outcomes. *The EMBO journal* **26**: 1352–1362.

Alexeev, A., Mazin, A., Kowalczykowski, S. C. 2003. Rad54 protein possesses chromatin-remodeling activity stimulated by the Rad51–ssDNA nucleoprotein filament. *Nature Structural & Molecular Biology* **10**: 182–186.

Ampatzidou, E., Irmisch, A., O'Connell, M. J., Murray, J. M. 2006. Smc5/6 is required for repair at collapsed replication forks. *Molecular and cellular biology* **26**: 9387–9401.

Anand, R. P., Lovett, S. T., Haber, J. E. 2013. Break-Induced DNA Replication. *Cold Spring Harbor Perspectives in Biology* **5** (12): DOI: 10.1101/cshperspect.a010397.

Andersen, J. S., Lam, Y. W., Leung, A. K. L., Ong, S. E., Lyon, C. E., Lamond, A. I., Mann, M. 2005. Nucleolar proteome dynamics. *Nature* **433**: 77–83.

Antony, E., Tomko, E. J., Xiao, Q., Krejci, L., Lohman, T. M., Ellenberger, T. 2009. Srs2 Disassembles Rad51 Filaments by a Protein-Protein Interaction Triggering ATP Turnover and Dissociation of Rad51 from DNA. *Molecular Cell* **35**: 105–115.

Argunhan, B., Murayama, Y., Iwasaki, H. 2017. The differentiated and conserved roles of Swi5-Sfr1 in homologous recombination. *FEBS Letters* **591** (14): 2035-2047.

Bai, Y., Symington, L. S. 1996. A Rad52 homolog is required for RAD51-independent mitouc recombination in *Saccharomyces cerevisiae*. *Genes and Development* **10** (16): 2025-2037.

Barbour, P., Xiao, W., Barbour, L., Xiao, W. 2006. Mating type regulation of cellular tolerance to DNA damage is specific to the DNA post-replication repair and mutagenesis pathway. *Molecular Microbiology* **59**: 637–650.

Baumann, P., Benson, F. E., West, S. C. 1996. Human Rad51 protein promotes ATP-dependent homologous pairing and strand transfer reactions

in vitro. *Cell* **87**: 757–766.

Bekker-Jensen, S., Lukas, C., Kitagawa, R., Melander, F., Kastan, M. B., Bartek, J., Lukas, J. 2006. Spatial organization of the mammalian genome surveillance machinery in response to DNA strand breaks. *The Journal of cell biology* **173**: 195–206.

Bennett, B. T., Bewersdorf, J., Knight, K. L. 2009. Immunofluorescence imaging of DNA damage response proteins: optimizing protocols for super-resolution microscopy. *Methods (San Diego, Calif.)* **48**: 63–71.

Bergoglio, V., Boyer, A. S., Walsh, E., Naim, V., Legube, G., Lee, M. Y. W. T., Rey, L., Rosselli, F., Cazaux, C., Eckert, K. A., Hoffmann, J. S. 2013. DNA synthesis by Pol η promotes fragile site stability by preventing under-replicated DNA in mitosis. *The Journal of cell biology* **201**: 395–408.

Bernstein, K. A., Reid, R. J. D., Sunjevaric, I., Demuth, K., Burgess, R. C., Rothstein, R. 2011. The Shu complex, which contains Rad51 paralogues, promotes DNA repair through inhibition of the Srs2 anti-recombinase.*Molecular Biology of the Cell* **22**: 1599–1607.

Berti, M., Ray Chaudhuri, A., Thangavel, S., Gomathinayagam, S., Kenig, S., Vujanovic, M., Odreman, F., Glatter, T., Graziano, S., Mendoza-Maldonado, R., Marino, F., Lucic, B., Biasin, V., Gstaiger, M., Aebersold, R., Sidorova, J. M., Monnat Jr, R. J., Lopes, M., Vindigni, A. 2013. Human RECQ1 promotes restart of replication forks reversed by DNA topoisomerase I inhibition. *Nature Structural &Amp; Molecular Biology* **20**: 347.

Berti, M., Vindigni, A. 2016, February 3. Replication stress: Getting back on track. *Nature Structural and Molecular Biology* **23**(2): 103-109.

Bhattacharjee, S., Osman, F., Feeney, L., Lorenz, A., Bryer, C., Whitby, M. C. 2013. MHF1-2/CENP-S-X performs distinct roles in centromere metabolism and genetic recombination. *Open biology* **3**: DOI: 10.1098/rsob.130102.

Bhowmick, R., Minocherhomji, S., Hickson, I. D. 2016. RAD52 Facilitates Mitotic DNA Synthesis Following Replication Stress. *Molecular Cell* **64**: 1117–1126.

Binz, S. K., Sheehan, A. M., Wold, M. S. 2004. Replication Protein A phosphorylation and the cellular response to DNA damage. *DNA Repair* **3**: 1015–1024.

Blyth, J., Makrantoni, V., Barton, R. E., Spanos, C., Rappsilber, J., Marston, A. L. 2018. Genes Important for *Schizosaccharomyces pombe* Meiosis Identified Through a Functional Genomics Screen. *Genetics* **208**: 589–603.

Boyer, A. S., Sørensen, C. S. 2015. FBH1: a new checkpoint factor. *Oncotarget* **6**: 19354–19355.

Branzei, D., Foiani, M. 2010. Maintaining genome stability at the replication fork. *Nature Reviews Molecular Cell Biology* **11**: 208–219.

Branzei, D. 2011. Ubiquitin family modifications and template switching. *FEBS Letters* **585**: 2810–2817.

Branzei, D., Szakal, B. 2016. DNA damage tolerance by recombination: Molecular pathways and DNA structures. *DNA repair* **44**: 68–75.

Brewer, B. J., Fangman, W. L. 1988. A replication fork barrier at the 3' end of yeast ribosomal RNA genes. *Cell* **55**: 637–643.

Brüning, J. G., Howard, J. L., McGlynn, P. 2014. Accessory Replicative Helicases and the Replication of Protein-Bound DNA. *Journal of Molecular Biology* **426**: 3917–3928.

Budworth, H., McMurray, C. T. 2013. A brief history of triplet repeat diseases. *Methods in molecular biology* **1010**: 3–17.

Bugreev, D. V., Rossi, M. J., Mazin, A. V. 2011. Cooperation of RAD51 and RAD54 in regression of a model replication fork. *Nucleic Acids Research* **39**: 2153–2164.

Buis, J., Wu, Y., Deng, Y., Leddon, J., Westfield, G., Eckersdorff, M., Sekiguchi, J. M., Chang, S., Ferguson, D. O. 2008. Mre11 Nuclease Activity Has Essential Roles in DNA Repair and Genomic Stability Distinct from ATM Activation. *Cell* **135**: 85–96.

Burgess, A., Vigneron, S., Brioudes, E., Labbé, J. C., Lorca, T., Castro, A. 2010. Loss of human Greatwall results in G2 arrest and multiple mitotic defects due to deregulation of the cyclin B-Cdc2/PP2A balance. *Proceedings of the National Academy of Sciences of the United States of America* **107**: 12564–12569.

Byers, J. S., Garcia, D. M., Jarosz, D. F. 2017. Epigenetic regulation of genome integrity by a prion-based mechanism. *bioRxiv* 152512.

Byrd, A. K., Raney, K. D. 2017. Structure and function of Pif1 helicase. *Biochemical Society transactions* **45**: 1159–1171.

Bzymek, M., Thayer, N. H., Oh, S. D., Kleckner, N., Hunter, N. 2010. Double Holliday junctions are intermediates of DNA break repair. *Nature* **464**: 937–941.

Caldecott, K. W. 2008. Single-strand break repair and genetic disease. *Nature Reviews Genetics* **9**: 619–631.

Calzada, A., Hodgson, B., Kanemaki, M., Bueno, A., Labib, K. 2005. Molecular anatomy and regulation of a stable replisome at a paused eukaryotic DNA replication fork. *Genes & Development* **19**: 1905–1919.

Catlett, M. G., Forsburg, S. L. 2003. *Schizosaccharomyces pombe* Rdh54 (TID1) acts with Rhp54 (RAD54) to repair meiotic double-strand breaks. *Molecular biology of the cell* **14**: 4707–4720.

Ceballos, S. J., Heyer, W. D. 2011. Functions of the Snf2/Swi2 family Rad54 motor protein in homologous recombination. *Biochimica et Biophysica Acta - Gene Regulatory Mechanisms* **1809**: 509–523.

Cejka, P., Plank, J. L., Bachrati, C. Z., Hickson, I. D., Kowalczykowski, S. C. 2010. Rmi1 stimulates decatenation of double Holliday junctions during dissolution by Sgs1-Top3. *Nature structural & molecular biology* **17**: 1377–

1382.

Chakrabortee, S., Byers, J. S., Jones, S., Garcia, D. M., Bhullar, B., Chang, A., She, R., Lee, L., Fremin, B., Lindquist, S., Jarosz, D. F. 2016. Intrinsically Disordered Proteins Drive Emergence and Inheritance of Biological Traits. *Cell* **167**: 369–381.e12.

Champion, M. D., Hawley, R. S. 2002. Playing for half the deck: the molecular biology of meiosis. *Nature Cell Biology* **4**: S50–S56.

Chen, J. M., Cooper, D. N., Chuzhanova, N., Férec, C., Patrinos, G. P. 2007. Gene conversion: mechanisms, evolution and human disease. *Nature Reviews Genetics* **8**: 762–775.

Chen, J. M., Cooper, D. N., Férec, C., Kehrer-Sawatzki, H., Patrinos, G. P. 2010. Genomic rearrangements in inherited disease and cancer. *Seminars in Cancer Biology* **20**: 222–233.

Chen, X., Zaro, J. L., Shen, W. C. 2013. Fusion protein linkers: property, design and functionality. *Advanced drug delivery reviews* **65**: 1357–1369.

Chen, Y. H., Choi, K., Szakal, B., Arenz, J., Duan, X., Ye, H., Branzei, D., Zhao, X. 2009. Interplay between the Smc5/6 complex and the Mph1 helicase in recombinational repair. *Proceedings of the National Academy of Sciences of the United States of America* **106**: 21252–21257.

Chi, P., Kwon, Y., Seong, C., Epshtein, A., Lam, I., Sung, P., Klein, H. L. 2006. Yeast recombination factor Rdh54 functionally interacts with the Rad51 recombinase and catalyzes Rad51 removal from DNA. *Journal of Biological Chemistry* **281**: 26268–26279.

Chi, P., Kwon, Y., Moses, D. N., Seong, C., Sehorn, M. G., Singh, A. K., Tsubouchi, H., Greene, E. C., Klein, H. L., Sung, P. 2009. Functional interactions of meiotic recombination factors Rdh54 and Dmc1. *DNA repair* **8**: 279–284.

Chiolo, I., Saponaro, M., Baryshnikova, A., Kim, J. H., Seo, Y. S., Liberi, G. 2007. The Human F-Box DNA Helicase FBH1 Faces *Saccharomyces cerevisiae* Srs2 and Postreplication Repair Pathway Roles. *Molecular and Cellular Biology* **27**: 7439–7450.

Choi, Y. G., Shin, H. Y., Kim, J. I., Choi, E. K., Carp, R. I., Kim, Y. S. 2016. N(ε)-Carboxymethyl Modification of Lysine Residues in Pathogenic Prion Isoforms. *Molecular neurobiology* **53**: 3102–3112.

Choudhury, M., Zaman, S., Jiang, J. C., Jazwinski, S. M., Bastia, D. 2015. Mechanism of regulation of 'chromosome kissing' induced by Fob1 and its physiological significance. *Genes & development* **29**: 1188–1201.

Chu, W. K., Payne, M. J., Beli, P., Hanada, K., Choudhary, C., Hickson, I. D. 2015. FBH1 influences DNA replication fork stability and homologous recombination through ubiquitylation of RAD51. *Nature Communications* **6**: 5931.

Ciccia, A., Symington, L. S. 2016. Stressing Out About RAD52. *Molecular Cell* **64**: 1017–1019.

Cobb, J. A., Bjergbaek, L., Shimada, K., Frei, C., Gasser, S. M. 2003. DNA polymerase stabilization at stalled replication forks requires Mec1 and the RecQ helicase Sgs1. *The EMBO journal* **22**: 4325–4336.

Codlin, S., Dalgaard, J. Z. 2003. Complex mechanism of site-specific DNA replication termination in fission yeast. *The EMBO journal* **22**: 3431–3440.

Cortez, D. 2015. Preventing replication fork collapse to maintain genome integrity. *DNA Repair* **32**: 149–157.

Costantino, L., Sotiriou, S. K., Rantala, J. K., Magin, S., Mladenov, E., Helleday, T., Haber, J. E., Iliakis, G., Kallioniemi, O. P., Halazonetis, T. D. 2014. Break-Induced Replication Repair of Damaged Forks Induces Genomic Duplications in Human Cells. *Science* **343**: 88-91.

Costanzo, V. 2011. Brca2, Rad51 and Mre11: Performing balancing acts on replication forks. *DNA Repair* **10**: 1060–1065.

Costes, A., Lambert, S. A. E. 2012. Homologous recombination as a replication fork escort: fork-protection and recovery. *Biomolecules* **3**: 39–71.

Crismani, W., Girard, C., Froger, N., Pradillo, M., Santos, J. L., Chelysheva, L., Copenhaver, G. P., Horlow, C., Mercier, R. 2012. FANCM Limits Meiotic Crossovers. *Science* **336**: 1588–1590.

Cuomo, A., Soldi, M., Bonaldi, T. 2017. SILAC-Based Quantitative Strategies for Accurate Histone Posttranslational Modification Profiling Across Multiple Biological Samples. Humana Press, New York, NY, pp. 97–119.

Daigaku, Y., Davies, A. A., Ulrich, H. D. 2010. Ubiquitin-dependent DNA damage bypass is separable from genome replication. *Nature* **465**: 951–955.

Dalgaard, J. Z., Klar, A. J. S. 1999. Orientation of DNA replication establishes mating-type switching pattern in *S. pombe*. *Nature* **400**: 181–184.

Dalgaard, J. Z., Klar, A. J. 2000. swi1 and swi3 perform imprinting, pausing, and termination of DNA replication in *S. pombe*. *Cell* **102**: 745–751.

Dalgaard, J. Z., Klar, A. J. 2001. A DNA replication-arrest site RTS1 regulates imprinting by determining the direction of replication at mat1 in *S. pombe*. *Genes & development* **15**: 2060–2068.

Das, R. K., Mao, A. H., Pappu, R. V 2012. Unmasking functional motifs within disordered regions of proteins. *Science signaling* **5**: pe17.

Davis, A. P., Symington, L. S. 2001. The yeast recombinational repair protein Rad59 interacts with Rad52 and stimulates single-strand annealing. *Genetics* **159**: 515–525.

De Piccoli, G., Katou, Y., Itoh, T., Nakato, R., Shirahige, K., Labib, K. 2012. Replisome Stability at Defective DNA Replication Forks Is Independent of S Phase Checkpoint Kinases. *Molecular Cell* **45**: 696–704.

Deem, A., Keszthelyi, A., Blackgrove, T., Vayl, A., Coffey, B., Mathur, R., Chabes, A., Malkova, A. 2011. Break-Induced Replication Is Highly Inaccurate. *PLoS Biology* **9**: e1000594.

Dehé, P. M., Coulon, S., Scaglione, S., Shanahan, P., Takedachi, A., Wohlschlegel, J. A., Yates, J. R., Llorente, B., Russell, P., Gaillard, P. H. L. 2013. Regulation of Mus81–Eme1 Holliday junction resolvase in response to DNA damage. *Nature Structural & Molecular Biology* **20**: 598–603.

Dehé, P. M., Gaillard, P. H. L. 2017. Control of structure-specific endonucleases to maintain genome stability. *Nature Reviews Molecular Cell Biology* **18**: 315–330.

Dewar, J. M., Budzowska, M., Walter, J. C. 2015. The mechanism of DNA replication termination in vertebrates. *Nature* **525**: 345–350.

Dewar, J. M., Walter, J. C. 2017. Mechanisms of DNA replication termination. *Nature Reviews Molecular Cell Biology* **18**: 507–516.

Dewar, J. M., Low, E., Mann, M., Räschle, M., Walter, J. C. 2017. CRL2Lrr1promotes unloading of the vertebrate replisome from chromatin during replication termination. *Genes and Development* **31**: 275–290.

Dilley, R. L., Verma, P., Cho, N. W., Winters, H. D., Wondisford, A. R., Greenberg, R. A. 2016. Break-induced telomere synthesis underlies alternative telomere maintenance. *Nature* **539**: 54–58.

Dimude, J. U., Midgley-Smith, S. L., Stein, M., Rudolph, C. J. 2016. Replication Termination: Containing Fork Fusion-Mediated Pathologies in *Escherichia coli*. *Genes* **7** (8): DOI:10.3390/genes7080040.

Doe, C. L., Ahn, J. S., Dixon, J., Whitby, M. C. 2002. Mus81-Eme1 and Rqh1 involvement in processing stalled and collapsed replication forks. *The Journal of biological chemistry* **277**: 32753–32759.

Doe, C. L., Osman, F., Dixon, J., Whitby, M. C. 2004. DNA repair by a Rad22-Mus81-dependent pathway that is independent of Rhp51. *Nucleic acids research* **32**: 5570–5581.

Donnianni, R. A., Symington, L. S. 2013. Break-induced replication occurs by conservative DNA synthesis. *Proceedings of the National Academy of Sciences* **110**: 13475–13480.

Dosztányi, Z., Csizmók, V., Tompa, P., Simon, I. 2005. The Pairwise Energy Content Estimated from Amino Acid Composition Discriminates between Folded and Intrinsically Unstructured Proteins. *Journal of Molecular Biology* **347**: 827–839.

Duda, H., Arter, M., Gloggnitzer, J., Teloni, F., Wild, P., Blanco, M. G., Altmeyer, M., Matos, J. 2016. A Mechanism for Controlled Breakage of Under-replicated Chromosomes during Mitosis. *Developmental Cell* **39**: 740–755.

Dunderdale, H. J., Benson, F. E., Parsons, C. A., Sharpies, G. J., Lloyd, R. G., West, S. C. 1991. Formation and resolution of recombination intermediates by *E. coli* RecA and RuvC proteins. *Nature* **354**: 506–510.

Dunker, A. K., Silman, I., Uversky, V. N., Sussman, J. L. 2008. Function and structure of inherently disordered proteins. *Current Opinion in Structural Biology* **18**: 756–764.

Egel, R. 2004. DNA Replication: Stalling a Fork for Imprinting and Switching. *Current Biology* **14**: R915–R917.

Ekman, D., Light, S., Björklund, A. K., Elofsson, A. 2006. What properties characterize the hub proteins of the protein-protein interaction network of *Saccharomyces cerevisiae*? *Genome biology* **7**: DOI: 10.1186/gb-2006-7-6-r45.

Elango, R., Sheng, Z., Jackson, J., DeCata, J., Ibrahim, Y., Pham, N. T., Liang, D. H., Sakofsky, C. J., Vindigni, A., Lobachev, K. S., Ira, G., Malkova, A. 2017. Break-induced replication promotes formation of lethal joint molecules dissolved by Srs2. *Nature communications* **8**: DOI: 10.1038/s41467-017-01987-2.

Elbing, K., Brent, R. 2002. Media Preparation and Bacteriological Tools. *Current Protocols in Molecular Biology*. John Wiley & Sons, Inc., Hoboken, NJ, USA, Vol. 59p. 1.1.1-1.1.7.

Errico, A., Costanzo, V. 2012. Mechanisms of replication fork protection: A safeguard for genome stability. *Critical Reviews in Biochemistry and Molecular Biology* **47** (3): 222-235.

Eydmann, T., Sommariva, E., Inagawa, T., Mian, S., Klar, A. J. S., Dalgaard, J. Z. 2008. Rtf1-mediated eukaryotic site-specific replication termination. *Genetics* **180**: 27–39.

Fairhead, M., Howarth, M. 2015. Site-Specific biotinylation of purified proteins using BirA. *Site-Specific Protein Labeling: Methods and Protocols*. Europe PMC Funders, **1266**: 171–184.

Feng, W., Pan, L., Zhang, M. 2011. Combination of NMR spectroscopy and X-ray crystallography offers unique advantages for elucidation of the structural basis of protein complex assembly. *Science China Life Sciences* **54**: 101–111.

Filippo, J. S., Sung, P., Klein, H. 2008. Mechanism of Eukaryotic Homologous Recombination. *Annual Review of Biochemistry* **77** (1): 229-257.

Finn, R. D., Attwood, T. K., Babbitt, P. C., Bateman, A., Bork, P., Bridge, A. J., Chang, H. Y., Dosztányi, Z., El-Gebali, S., Fraser, M., Gough, J., Haft, D., Holliday, G. L., Huang, H., Huang, X., Letunic, I., Lopez, R., Lu, S., Marchler-Bauer, A. et al. 2017. InterPro in 2017-beyond protein family and domain annotations. *Nucleic acids research* **45**: D190–D199.

Forment, J. V., Blasius, M., Guerini, I., Jackson, S. P. 2011. Structure-Specific DNA Endonuclease Mus81/Eme1 Generates DNA Damage Caused by Chk1 Inactivation. *PLoS ONE* **6**: DOI: 10.1371/journal.pone.0023517.

Fornander, L. H., Renodon-Cornière, A., Kuwabara, N., Ito, K., Tsutsui, Y., Shimizu, T., Iwasaki, H., Nordén, B., Takahashi, M. 2014. Swi5-Sfr1 protein stimulates Rad51-mediated DNA strand exchange reaction through organization of DNA bases in the presynaptic filament. *Nucleic Acids Research* **42**: 2358–2365.

Forsburg, S. L. 1993. Comparison of *Schizosaccharomyces pombe*

expression systems. *Nucleic acids research* **21**: 2955–2956.

Fortin, G. S., Symington, L. S. 2002. Mutations in yeast Rad51 that partially bypass the requirement for Rad55 and Rad57 in DNA repair by increasing the stability of Rad51-DNA complexes. *The EMBO journal* **21**: 3160–3170.

Fox, D., 3rd, Yan, Z., Ling, C., Zhao, Y., Lee, D. Y., Fukagawa, T., Yang, W., Wang, W. 2014. The histone-fold complex MHF is remodeled by FANCM to recognize branched DNA and protect genome stability. *Cell Research* **24**: 560-575.

Frigola, J., Remus, D., Mehanna, A., Diffley, J. F. X. 2013. ATPase-dependent quality control of DNA replication origin licensing. *Nature* **495**: 339–343.

Froget, B., Blaisonneau, J., Lambert, S., Baldacci, G. 2008. Cleavage of Stalled Forks by Fission Yeast Mus81/Eme1 in Absence of DNA Replication Checkpoint. *Molecular Biology of the Cell* **19**: 445–456.

Fugger, K., Mistrik, M., Danielsen, J. R., Dinant, C., Falck, J., Bartek, J., Lukas, J., Mailand, N. 2009. Human Fbh1 helicase contributes to genome maintenance via pro- and anti-recombinase activities. *The Journal of cell biology* **186**: 655–663.

Fugger, K., Mistrik, M., Neelsen, K. J., Yao, Q., Zellweger, R., Kousholt, A. N., Haahr, P., Chu, W. K., Bartek, J., Lopes, M., Hickson, I. D., Sørensen, C. S. 2015. FBH1 Catalyzes Regression of Stalled Replication Forks. *Cell Reports* **10**: 1749–1757.

Fusco, F., Paciolla, M., Napolitano, F., Pescatore, A., D'Addario, I., Bal, E., Lioi, M. B., Smahi, A., Miano, M. G., Ursini, M. V. 2012. Genomic architecture at the Incontinentia Pigmenti locus favours de novo pathological alleles through different mechanisms. *Human Molecular Genetics* **21**: 1260–1271.

Gadaleta, M. C., Noguchi, E. 2017, March 7. Regulation of DNA replication through natural impediments in the eukaryotic genome. *Genes* DOI: 10.3390/genes8030098.

Gaillard, H., Herrera-Moyano, E., Aguilera, A. 2013. Transcription-Associated Genome Instability. *Chemical Reviews* **113**: 8638–8661.

Gaillard, P. H. L., Noguchi, E., Shanahan, P., Russell, P. 2003. The Endogenous Mus81-Eme1 Complex Resolves Holliday Junctions by a Nick and Counternick Mechanism. *Molecular Cell* **12**: 747–759.

Gaines, W. A., Godin, S. K., Kabbinavar, F. F., Rao, T., VanDemark, A. P., Sung, P., Bernstein, K. A. 2015. Promotion of presynaptic filament assembly by the ensemble of *S. cerevisiae* Rad51 paralogues with Rad52. *Nature Communications* **6**: 7834 DOI: 10.1038/ncomms8834.

Gambus, A., Jones, R. C., Sanchez-Diaz, A., Kanemaki, M., van Deursen, F., Edmondson, R. D., Labib, K. 2006. GINS maintains association of Cdc45 with MCM in replisome progression complexes at eukaryotic DNA replication forks. *Nature Cell Biology* **8**: 358–366.

Gambus, A., Van Deursen, F., Polychronopoulos, D., Foltman, M., Jones, R.

C., Edmondson, R. D., Calzada, A., Labib, K. 2009. A key role for Ctf4 in coupling the MCM2-7 helicase to DNA polymerase α within the eukaryotic replisome. *EMBO Journal* **28**: 2992–3004.

Gangloff, S., Soustelle, C., Fabre, F. 2000. Homologous recombination is responsible for cell death in the absence of the Sgs1 and Srs2 helicases. *Nature Genetics* **25**: 192–194.

Gao, F., Zhang, C. T. 2007. DoriC: a database of oriC regions in bacterial genomes. *Bioinformatics* **23**: 1866–1867.

Garbacz, M. A., Lujan, S. A., Burkholder, A. B., Cox, P. B., Wu, Q., Zhou, Z. X., Haber, J. E., Kunkel, T. A. 2018. Evidence that DNA polymerase δ contributes to initiating leading strand DNA replication in *Saccharomyces cerevisiae*. *Nature Communications* **9**: DOI: 10.1038/s41467-018-03270-4.

Gardiennet, C., Loquet, A., Etzkorn, M., Heise, H., Baldus, M., Böckmann, A. 2008. Structural constraints for the Crh protein from solid-state NMR experiments. *Journal of biomolecular NMR* **40**: 239–250.

Gari, K., Décaillet, C., Stasiak, A. Z., Stasiak, A., Constantinou, A. 2008a. The Fanconi Anemia Protein FANCM Can Promote Branch Migration of Holliday Junctions and Replication Forks. *Molecular Cell* **29**: 141–148.

Gari, K., Decaillet, C., Delannoy, M., Wu, L., Constantinou, A. 2008b. Remodeling of DNA replication structures by the branch point translocase FANCM. *Proceedings of the National Academy of Sciences* **105**: 16107–16112.

Ge, X. Q., Jackson, D. A., Blow, J. J. 2007. Dormant origins licensed by excess Mcm2-7 are required for human cells to survive replicative stress. *Genes & development* **21**: 3331–3341.

Gerhardt, J., Bhalla, A. D., Butler, J. S., Puckett, J. W., Dervan, P. B., Rosenwaks, Z., Napierala, M. 2016. Stalled DNA Replication Forks at the Endogenous GAA Repeats Drive Repeat Expansion in Friedreich's Ataxia Cells. *Cell Reports* **16**: 1218–1227.

Geronimo, C. L., Zakian, V. A. 2016. Getting it done at the ends: Pif1 family DNA helicases and telomeres. *DNA Repair* **44**: 151–158.

Ghalwash, M. F., Dunker, A. K., Obradović, Z. 2012. Uncertainty analysis in protein disorder prediction. *Mol. BioSyst.* **8**: 381–391.

Godin, S., Wier, A., Kabbinavar, F., Bratton-Palmer, D. S., Ghodke, H., Van Houten, B., VanDemark, A. P., Bernstein, K. A. 2013. The Shu complex interacts with Rad51 through the Rad51 paralogues Rad55–Rad57 to mediate error-free recombination. *Nucleic Acids Research* **41**: 4525–4534.

Godin, S. K., Sullivan, M. R., Bernstein, K. A. 2016. Novel insights into RAD51 activity and regulation during homologous recombination and DNA replication. *Biochemistry and cell biology = Biochimie et biologie cellulaire* **94**: 407–418.

Gomez-Escobar, N., Almobadel, N., Alzahrani, O., Feichtinger, J., Planells-Palop, V., Alshehri, Z., Thallinger, G. G., Wakeman, J. A., McFarlane, R. J.

2016. Translin and Trax differentially regulate telomere-associated transcript homeostasis. *Oncotarget* **7**: 33809–33820.

Goodman, M. F., Woodgate, R. 2013. Translesion DNA Polymerases. *Cold Spring Harbor Perspectives in Biology* **5**: a010363.

Gregan, J., Rabitsch, P. K., Sakem, B., Csutak, O., Latypov, V., Lehmann, E., Kohli, J., Nasmyth, K. 2005. Novel Genes Required for Meiotic Chromosome Segregation Are Identified by a High-Throughput Knockout Screen in Fission Yeast. *Current Biology* **15**: 1663–1669.

Grimm, L. L., Weissbach, S., Flügge, F., Begemann, N., Palcic, M. M., Peters, T. 2017. Protein NMR Studies of Substrate Binding to Human Blood Group A and B Glycosyltransferases. *ChemBioChem* **18**: 1260–1269.

Grimme, J. M., Honda, M., Wright, R., Okuno, Y., Rothenberg, E., Mazin, A. V., Ha, T., Spies, M. 2010. Human Rad52 binds and wraps single-stranded DNA and mediates annealing via two hRad52–ssDNA complexes. *Nucleic Acids Research* **38**: 2917–2930.

Guirouilh-Barbat, J., Lambert, S., Bertrand, P., Lopez, B. S. 2014. Is homologous recombination really an error-free process? *Frontiers in genetics* **5**: 175 DOI: 10.3389/fgene.2014.00175.

Gupta, M. K., Guy, C. P., Yeeles, J. T. P., Atkinson, J., Bell, H., Lloyd, R. G., Marians, K. J., McGlynn, P. 2013. Protein-DNA complexes are the primary sources of replication fork pausing in *Escherichia coli*. *Proceedings of the National Academy of Sciences of the United States of America* **110**: 7252–7257.

Guy, C. P., Atkinson, J., Gupta, M. K., Mahdi, A. A., Gwynn, E. J., Rudolph, C. J., Moon, P. B., van Knippenberg, I. C., Cadman, C. J., Dillingham, M. S., Lloyd, R. G., McGlynn, P. 2009. Rep Provides a Second Motor at the Replisome to Promote Duplication of Protein-Bound DNA. *Molecular Cell* **36**: 654–666.

Haber, J. E. 2000. Partners and pathways: repairing a double-strand break. *Trends in Genetics* **16**: 259–264.

Haber, J. E. 2012. Mating-Type Genes and MAT Switching in *Saccharomyces cerevisiae*. *Genetics* **191**: 33–64.

Hamperl, S., Cimprich, K. A. 2016. Conflict Resolution in the Genome: How Transcription and Replication Make It Work. *Cell* **167**: 1455–1467.

Han, T. X., Xu, X. Y., Zhang, M. J., Peng, X., Du, L. L. 2010. Global fitness profiling of fission yeast deletion strains by barcode sequencing. *Genome biology* **11**: DOI: 10.1186/gb-2010-11-6-r60.

Hanamshet, K., Mazina, O. M., Mazin, A. V 2016. Reappearance from Obscurity: Mammalian Rad52 in Homologous Recombination. *Genes* **7**: Genes 2016, 7, 63; doi:10.3390/genes7090063.

Harper, J. V., Anderson, J. A., O'Neill, P. 2010. Radiation induced DNA DSBs: Contribution from stalled replication forks? *DNA Repair* **9**: 907–913.

Haruta, N., Kurokawa, Y., Murayama, Y., Akamatsu, Y., Unzai, S., Tsutsui, Y., Iwasaki, H. 2006. The Swi5–Sfr1 complex stimulates Rhp51/Rad51 - and Dmc1-mediated DNA strand exchange *in vitro*. *Nature Structural & Molecular Biology* **13**: 823–830.

Haruta, N., Akamatsu, Y., Tsutsui, Y., Kurokawa, Y., Murayama, Y., Arcangioli, B., Iwasaki, H. 2008. Fission yeast Swi5 protein, a novel DNA recombination mediator. *DNA Repair* **7**: 1–9.

Hashimoto, Y., Ray Chaudhuri, A., Lopes, M., Costanzo, V. 2010. Rad51 protects nascent DNA from Mre11-dependent degradation and promotes continuous DNA synthesis. *Nature Structural & Molecular Biology* **17**: 1305–1311.

Hashimoto, Y., Costanzo, V. 2011. Studying DNA Replication Fork Stability in Xenopus Egg Extract. *Methods in molecular biology (Clifton, N.J.)*, Vol. 745pp. 437–445.

Hawthorne, D. C., Leupold, U. 1974. Suppressors in yeast. *Current topics in microbiology and immunology* **64**: 1–47.

Hayase, A., Takagi, M., Miyazaki, T., Oshiumi, H., Shinohara, M., Shinohara, A. 2004. A Protein Complex Containing Mei5 and Sae3 Promotes the Assembly of the Meiosis-Specific RecA Homolog Dmc1. *Cell* **119**: 927–940.

Hayles, J., Wood, V., Jeffery, L., Hoe, K. L., Kim, D. U., Park, H. O., Salas-Pino, S., Heichinger, C., Nurse, P. 2013. A genome-wide resource of cell cycle and cell shape genes of fission yeast. *Open biology* **3**: 130053.

Haynes, C., Oldfield, C. J., Ji, F., Klitgord, N., Cusick, M. E., Radivojac, P., Uversky, V. N., Vidal, M., Iakoucheva, L. M. 2006. Intrinsic disorder is a common feature of hub proteins from four eukaryotic interactomes. *PLoS computational biology* **2**: DOI: 10.1371/journal.pcbi.0020100.

Hays, S. L., Firmenich, A. A., Berg, P. 1995. Complex formation in yeast double-strand break repair: participation of Rad51, Rad52, Rad55, and Rad57 proteins. *Proceedings of the National Academy of Sciences of the United States of America* **92**: 6925–6929.

Heichinger, C., Penkett, C. J., Bähler, J., Nurse, P. 2006. Genome-wide characterization of fission yeast DNA replication origins. *The EMBO journal* **25**: 5171–5179.

Helmrich, A., Ballarino, M., Nudler, E., Tora, L. 2013. Transcription-replication encounters, consequences and genomic instability. *Nature Structural & Molecular Biology* **20**: 412–418.

Hiasa, H., Marians, K. J. 1994. Tus prevents overreplication of oriC plasmid DNA. *The Journal of biological chemistry* **269**: 26959–26968.

Hicks, W. M., Kim, M., Haber, J. E. 2010. Increased Mutagenesis and Unique Mutation Signature Associated with Mitotic Gene Conversion. *Science* **329**: 82–85.

Hoege, C., Pfander, B., Moldovan, G. L., Pyrowolakis, G., Jentsch, S. 2002. RAD6-dependent DNA repair is linked to modification of PCNA by ubiquitin

and SUMO. *Nature* **419**: 135–141.

Holmes, A. M., Kaykov, A., Arcangioli, B. 2005. Molecular and cellular dissection of mating-type switching steps in *Schizosaccharomyces pombe*. *Molecular and cellular biology* **25**: 303–311.

Hsiang, Y. H., Hertzberg, R., Hecht, S., Liu, L. F. 1985. Camptothecin induces protein-linked DNA breaks via mammalian DNA topoisomerase I. *The Journal of biological chemistry* **260**: 14873–14878.

Hu, J., Sun, L., Shen, F., Chen, Y., Hua, Y., Liu, Y., Zhang, M., Hu, Y., Wang, Q., Xu, W., Sun, F., Ji, J., Murray, J. M., Carr, A. M., Kong, D. 2012. The intra-S phase checkpoint targets Dna2 to prevent stalled replication forks from reversing. *Cell* **149**: 1221–1232.

Hunter, N., Kleckner, N. 2001. The single-end invasion: an asymmetric intermediate at the double-strand break to double-holliday junction transition of meiotic recombination. *Cell* **106**: 59–70.

Ibarra, A., Schwob, E., Méndez, J. 2008. Excess MCM proteins protect human cells from replicative stress by licensing backup origins of replication. *Proceedings of the National Academy of Sciences of the United States of America* **105**: 8956–8961.

Ilves, I., Petojevic, T., Pesavento, J. J., Botchan, M. R. 2010. Activation of the MCM2-7 Helicase by Association with Cdc45 and GINS Proteins. *Molecular Cell* **37**: 247–258.

Inagawa, T., Yamada-Inagawa, T., Eydmann, T., Mian, I. S., Wang, T. S., Dalgaard, J. Z. 2009. *Schizosaccharomyces pombe* Rtf2 mediates site-specific replication termination by inhibiting replication restart. *Proceedings of the National Academy of Sciences of the United States of America* **106**: 7927–7932.

Ip, S. C. Y., Rass, U., Blanco, M. G., Flynn, H. R., Skehel, J. M., West, S. C. 2008. Identification of Holliday junction resolvases from humans and yeast. *Nature* **456**: 357–361.

Ira, G., Malkova, A., Liberi, G., Foiani, M., Haber, J. E. 2003. Srs2 and Sgs1-Top3 suppress crossovers during double-strand break repair in yeast. *Cell* **115**: 401–411.

Iraqui, I., Chekkal, Y., Jmari, N., Pietrobon, V., Fréon, K., Costes, A., Lambert, S. A. E. 2012a. Recovery of Arrested Replication Forks by Homologous Recombination Is Error-Prone. *PLoS Genetics* **8**: e1002976.

Iraqui, I., Chekkal, Y., Jmari, N., Pietrobon, V., Fréon, K., Costes, A., Lambert, S. A. E. 2012b. Recovery of arrested replication forks by homologous recombination is error-prone. *PLoS genetics* **8**: e1002976.

Irmisch, A., Ampatzidou, E., Mizuno, K., O'Connell, M. J., Murray, J. M. 2009. Smc5/6 maintains stalled replication forks in a recombination-competent conformation. *The EMBO journal* **28**: 144–155.

Ishida, T., Kinoshita, K. 2007. PrDOS: prediction of disordered protein regions from amino acid sequence. *Nucleic Acids Research* **35**: W460–W464.

Ishimi, Y., Sugasawa, K., Hanaoka, F., Eki, T., Hurwitz, J. 1992. Topoisomerase II plays an essential role as a swivelase in the late stage of SV40 chromosome replication *in vitro*. *The Journal of biological chemistry* **267**: 462–466.

Ito, H., Fukuda, Y., Murata, K., Kimura, A. 1983. Transformation of intact yeast cells treated with alkali cations. *Journal of bacteriology* **153**: 163–168.

Ivessa, A. S., Lenzmeier, B. A., Bessler, J. B., Goudsouzian, L. K., Schnakenberg, S. L., Zakian, V. A. 2003. The *Saccharomyces cerevisiae* Helicase Rrm3p Facilitates Replication Past Nonhistone Protein-DNA Complexes. *Molecular Cell* **12**: 1525–1536.

Jackson, S. P., Bartek, J. 2009. The DNA-damage response in human biology and disease. *Nature* **461**: 1071–1078.

Jarosz, D. F., Brown, J. C. S., Walker, G. A., Datta, M. S., Ung, W. L., Lancaster, A. K., Rotem, A., Chang, A., Newby, G. A., Weitz, D. A., Bisson, L. F., Lindquist, S. 2014. Cross-Kingdom Chemical Communication Drives a Heritable, Mutually Beneficial Prion-Based Transformation of Metabolism. *Cell* **158**: 1083–1093.

Johnson, R. D., Symington, L. S. 1995. Functional differences and interactions among the putative RecA homologs Rad51, Rad55, and Rad57. *Molecular and cellular biology* **15**: 4843–4850.

Johnson, R. E., Prakash, S., Prakash, L. 1994. Yeast DNA repair protein RAD5 that promotes instability of simple repetitive sequences is a DNA-dependent ATPase. *Journal of Biological Chemistry* **269**: 28259–28262.

Johnson, R. E., Klassen, R., Prakash, L., Prakash, S. 2015. A Major Role of DNA Polymerase δ in Replication of Both the Leading and Lagging DNA Strands. *Molecular Cell* **59**: 163–175.

Jones, D. T., Cozzetto, D. 2015. DISOPRED3: precise disordered region predictions with annotated protein-binding activity. *Bioinformatics* **31**: 857–863.

Jones, R. M., Petermann, E. 2012. Replication fork dynamics and the DNA damage response. *Biochemical Journal* **443**: 13–26.

Kagawa, W., Kurumizaka, H., Ikawa, S., Yokoyama, S., Shibata, T. 2001. Homologous Pairing Promoted by the Human Rad52 Protein. *Journal of Biological Chemistry* **276**: 35201–35208.

Kagawa, W., Kurumizaka, H., Ishitani, R., Fukai, S., Nureki, O., Shibata, T., Yokoyama, S. 2002. Crystal structure of the homologous-pairing domain from the human Rad52 recombinase in the undecameric form. *Molecular cell* **10**: 359–371.

Kans, J. A., Mortimer, R. K. 1991. Nucleotide sequence of the RAD57 gene of *Saccharomyces cerevisiae*. *Gene* **105**: 139–140.

Katou, Y., Kanoh, Y., Bando, M., Noguchi, H., Tanaka, H., Ashikari, T., Sugimoto, K., Shirahige, K. 2003. S-phase checkpoint proteins Tof1 and Mrc1 form a stable replication-pausing complex. *Nature* **424**: 1078–1083.

Kawai, S., Hashimoto, W., Murata, K. 2010. Transformation of *Saccharomyces cerevisiae* and other fungi: methods and possible underlying mechanism. *Bioengineered bugs* **1**: 395–403.

Keeble, A. H., Banerjee, A., Ferla, M. P., Reddington, S. C., Anuar, I. N. A. K., Howarth, M. 2017. Evolving Accelerated Amidation by SpyTag/SpyCatcher to Analyze Membrane Dynamics. *Angewandte Chemie International Edition* **56**: 16521–16525.

Kelley, L. A., Mezulis, S., Yates, C. M., Wass, M. N., Sternberg, M. J. E. 2015. The Phyre2 web portal for protein modeling, prediction and analysis. *Nature Protocols* **10**: 845–858.

Kelly, T. 2017. Historical Perspective of Eukaryotic DNA Replication. *Advances in experimental medicine and biology*, Vol. 1042pp. 1–41.

Keskin, H., Shen, Y., Huang, F., Patel, M., Yang, T., Ashley, K., Mazin, A. V., Storici, F. 2014. Transcript-RNA-templated DNA recombination and repair. *Nature* **515**: 436–439.

Khasanov, F. K., Savchenko, G. V., Bashkirova, E. V., Korolev, V. G., Heyer, W. D., Bashkirov, V. I. 1999. A new recombinational DNA repair gene from *Schizosaccharomyces pombe* with homology to *Escherichia col*i RecA. *Genetics*, Vol. **152** (4): 1557-1572.

Khasanov, F. K., Salakhova, A. F., Chepurnaja, O. V., Korolev, V. G., Bashkirov, V. I. 2004. Identification and characterization of the rlp1+, the novel Rad51 paralog in the fission yeast Schizosaccharomyces pombe. *DNA Repair* **3**: 1363–1374.

Kitamura, K., Taki, M., Tanaka, N., Yamashita, I. 2011. Fission yeast Ubr1 ubiquitin ligase influences the oxidative stress response via degradation of active Pap1 bZIP transcription factor in the nucleus. *Molecular Microbiology* **80**: 739–755.

Kobe, B., Ve, T., Williams, S. J. 2015. Fusion-protein-assisted protein crystallization. *Acta Cryst* **71**: 861–869.

Kolinjivadi, A. M., Sannino, V., De Antoni, A., Zadorozhny, K., Kilkenny, M., Técher, H., Baldi, G., Shen, R., Ciccia, A., Pellegrini, L., Krejci, L., Costanzo, V. 2017. Smarcal1-Mediated Fork Reversal Triggers Mre11-Dependent Degradation of Nascent DNA in the Absence of Brca2 and Stable Rad51 Nucleofilaments. *Molecular Cell* **67**: 867–881.

Korolev, S. 2017. Advances in structural studies of recombination mediator proteins. *Biophysical Chemistry* **225**: 27–37.

Kotsantis, P., Silva, L. M., Irmscher, S., Jones, R. M., Folkes, L., Gromak, N., Petermann, E. 2016. Increased global transcription activity as a mechanism of replication stress in cancer. *Nature Communications* **7**: DOI: 10.1038/ncomms13087.

Krejci, L., Van Komen, S., Li, Y., Villemain, J., Reddy, M. S., Klein, H., Ellenberger, T., Sung, P. 2003. DNA helicase Srs2 disrupts the Rad51 presynaptic filament. *Nature* **423**: 305–309.

Krejci, L., Altmannova, V., Spirek, M., Zhao, X. 2012. Homologous recombination and its regulation. *Nucleic Acids Research* **40**: 5795–5818.

Kremer, E. J., Pritchard, M., Lynch, M., Yu, S., Holman, K., Baker, E., Warren, S. T., Schlessinger, D., Sutherland, G. R., Richards, R. I. 1991. Mapping of DNA instability at the fragile X to a trinucleotide repeat sequence p(CCG)n. *Science (New York, N.Y.)* **252**: 1711–1714.

Kumar, J. K., Gupta, R. C. 2004. Strand exchange activity of human recombination protein Rad52. *Proceedings of the National Academy of Sciences* **101**: 9562–9567.

Kupiec, M. 2016. Alternative clamp loaders/unloaders. *FEMS Yeast Research* **16**: DOI: 10.1093/femsyr/fow084.

Kurokawa, Y., Murayama, Y., Haruta-Takahashi, N., Urabe, I., Iwasaki, H. 2008. Reconstitution of DNA Strand Exchange Mediated by Rhp51 Recombinase and Two Mediators. *PLoS Biology* **6**: doi:10.1371/journal.pbio.0060088.

Kuzminov, A. 2001. Single-strand interruptions in replicating chromosomes cause double-strand breaks. *Proceedings of the National Academy of Sciences of the United States of America* **98**: 8241–8246.

Kwon, Y., Sung, P. 2017. Molecular Cell Previews Rad52, Maestro of Inverse Strand Exchange. *Molecular Cell* **67**: 1–3.

Labib, K., Hodgson, B. 2007. Replication fork barriers: pausing for a break or stalling for time? *EMBO reports* **8**: 346–353.

Lafuente-Barquero, J., Luke-Glaser, S., Graf, M., Silva, S., Gómez-González, B., Lockhart, A., Lisby, M., Aguilera, A., Luke, B. 2017. The Smc5/6 complex regulates the yeast Mph1 helicase at RNA-DNA hybrid-mediated DNA damage. *PLoS genetics* **13**: e1007136.

Lambert, S., Watson, A., Sheedy, D. M., Martin, B., Carr, A. M. 2005. Gross Chromosomal Rearrangements and Elevated Recombination at an Inducible Site-Specific Replication Fork Barrier. *Cell* **121**: 689–702.

Lambert, S., Mizuno, K., Blaisonneau, J., Martineau, S., Chanet, R., Fréon, K., Murray, J. M., Carr, A. M., Baldacci, G. 2010. Homologous Recombination Restarts Blocked Replication Forks at the Expense of Genome Rearrangements by Template Exchange. *Molecular Cell* **39**: 346–359.

Lambert, S., Carr, A. M. 2013. Impediments to replication fork movement: Stabilisation, reactivation and genome instability. *Chromosoma* **122**: 33-45.

Laursen, L. V, Ampatzidou, E., Andersen, A. H., Murray, J. M. 2003. Role for the fission yeast RecQ helicase in DNA repair in G2. *Molecular and cellular biology* **23**: 3692–3705.

Le, H. P., Masuda, Y., Tsurimoto, T., Maki, S., Katayama, T., Furukohri, A., Maki, H. 2015. Short CCG repeat in huntingtin gene is an obstacle for replicative DNA polymerases, potentially hampering progression of replication fork. *Genes to Cells* **20**: 817–833.

Lemaçon, D., Jackson, J., Quinet, A., Brickner, J. R., Li, S., Yazinski, S., You, Z., Ira, G., Zou, L., Mosammaparast, N., Vindigni, A. 2017. MRE11 and EXO1 nucleases degrade reversed forks and elicit MUS81-dependent fork rescue in BRCA2-deficient cells. *Nature Communications* **8**: 860.

Leman, A., Noguchi, E. 2013. The Replication Fork: Understanding the Eukaryotic Replication Machinery and the Challenges to Genome Duplication. *Genes* **4**: 1–32.

Leman, A. R., Noguchi, E. 2012. Local and global functions of Timeless and Tipin in replication fork protection. *Cell Cycle* **11**: 3945–3955.

Leonard, A. C., Mechali, M. 2013. DNA Replication Origins. *Cold Spring Harbor Perspectives in Biology* **5**: a010116.

Li, W., Cowley, A., Uludag, M., Gur, T., McWilliam, H., Squizzato, S., Park, Y. M., Buso, N., Lopez, R. 2015. The EMBL-EBI bioinformatics web and programmatic tools framework. *Nucleic acids research* **43**: W580-4.

Liao, Y. D., Jeng, J. C., Wang, C. F., Wang, S. C., Chang, S. T. 2004. Removal of N-terminal methionine from recombinant proteins by engineered *E. coli* methionine aminopeptidase. *Protein Science* **13**: 1802–1810.

Lindsay, H. D., Griffiths, D. J., Edwards, R. J., Christensen, P. U., Murray, J. M., Osman, F., Walworth, N., Carr, A. M. 1998. S-phase-specific activation of Cds1 kinase defines a subpathway of the checkpoint response in *Schizosaccharomyces pombe*. *Genes & development* **12**: 382–395.

Liu, J., Heyer, W. D. 2011. Who's who in human recombination: BRCA2 and RAD52. *Proceedings of the National Academy of Sciences of the United States of America* **108**: 441–442.

Liu, J., Renault, L., Veaute, X., Fabre, F., Stahlberg, H., Heyer, W. D. 2011a. Rad51 paralogues Rad55-Rad57 balance the antirecombinase Srs2 in Rad51 filament formation. *Nature* **479**: 245–248.

Liu, T., Wan, L., Wu, Y., Chen, J., Huang, J. 2011b. hSWS1·SWSAP1 is an evolutionarily conserved complex required for efficient homologous recombination repair. *The Journal of biological chemistry* **286**: 41758–41766.

Livernois, A. M., Hnatchuk, D. J., Findlater, E. E., Graether, S. P. 2009. Obtaining highly purified intrinsically disordered protein by boiling lysis and single step ion exchange. *Analytical Biochemistry* **392**: 70–76.

Lopes, M., Cotta-Ramusino, C., Pellicioli, A., Liberi, G., Plevani, P., Muzi-Falconi, M., Newlon, C. S., Foiani, M. 2001. The DNA replication checkpoint response stabilizes stalled replication forks. *Nature* **412**: 557–561.

Lorenz, A., Osman, F., Folkyte, V., Sofueva, S., Whitby, M. C. 2009. Fbh1 limits Rad51-dependent recombination at blocked replication forks. *Molecular and cellular biology* **29**: 4742–4756.

Lorenz, A., Osman, F., Sun, W., Nandi, S., Steinacher, R., Whitby, M. C. 2012. The fission yeast FANCM ortholog directs non-crossover recombination during meiosis. *Science (New York, N.Y.)* **336**: 1585–1588.

Los, G. V., Encell, L. P., McDougall, M. G., Hartzell, D. D., Karassina, N., Zimprich, C., Wood, M. G., Learish, R., Ohana, R. F., Urh, M., Simpson, D., Mendez, J., Zimmerman, K., Otto, P., Vidugiris, G., Zhu, J., Darzins, A., Klaubert, D. H., Bulleit, R. F. et al. 2008. HaloTag: A Novel Protein Labeling Technology for Cell Imaging and Protein Analysis. *ACS Chemical Biology* **3**: 373–382.

Louis, E. J. 2016. Historical evolution of laboratory strains of *Saccharomyces cerevisiae*. *Cold Spring Harbor Protocols* **2016**: 585–593.

Lucca, C., Vanoli, F., Cotta-Ramusino, C., Pellicioli, A., Liberi, G., Haber, J., Foiani, M. 2004. Checkpoint-mediated control of replisome–fork association and signalling in response to replication pausing. *Oncogene* **23**: 1206–1213.

Luft, J. R., DeTitta, G. T. 1999. A method to produce microseed stock for use in the crystallization of biological macromolecules. *Acta Crystallographica Section D Biological Crystallography* **55**: 988–993.

Lydeard, J. R., Lipkin-Moore, Z., Sheu, Y. J., Stillman, B., Burgers, P. M., Haber, J. E. 2010. Break-induced replication requires all essential DNA replication factors except those specific for pre-RC assembly. *Genes & Development* **24**: 1133–1144.

Ma, C. J., Gibb, B., Kwon, Y., Sung, P., Greene, E. C. 2017. Protein dynamics of human RPA and RAD51 on ssDNA during assembly and disassembly of the RAD51 filament. *Nucleic acids research* **45**: 749–761.

Ma, E., Dupaigne, P., Maloisel, L., Guerois, R., Le Cam, E., Coïc, E. 2018. Rad52-Rad51 association is essential to protect Rad51 filaments against Srs2, but facultative for filament formation. *eLife* **7**: DOI: 10.7554/eLife.32744.

Maculins, T., Nkosi, P. J., Nishikawa, H., Labib, K. 2015. Tethering of SCFDia2 to the Replisome Promotes Efficient Ubiquitylation and Disassembly of the CMG Helicase. *Current Biology* **25**: 2254–2259.

Magdalou, I., Lopez, B. S., Pasero, P., Lambert, S. A. E. 2014. The causes of replication stress and their consequences on genome stability and cell fate. *Seminars in Cell & Developmental Biology* **30**: 154–164.

Majka, J., Burgers, P. M. . 2004. The PCNA–RFC Families of DNA Clamps and Clamp Loaders. *Progress in nucleic acid research and molecular biology*, Vol. 78pp. 227–260.

Maric, M., Maculins, T., De Piccoli, G., Labib, K. 2014. Cdc48 and a ubiquitin ligase drive disassembly of the CMG helicase at the end of DNA replication. *Science* **346**: DOI: 10.1126/science.1253596.

Marteijn, J. A., Lans, H., Vermeulen, W., Hoeijmakers, J. H. J. 2014. Understanding nucleotide excision repair and its roles in cancer and ageing. *Nature Reviews Molecular Cell Biology* **15**: 465–481.

Martín, V., Chahwan, C., Gao, H., Blais, V., Wohlschlegel, J., Yates, J. R., McGowan, C. H., Russell, P. 2006. Sws1 is a conserved regulator of

homologous recombination in eukaryotic cells. *The EMBO journal* **25**: 2564–2574.

Masson, J. Y., Tarsounas, M. C., Stasiak, A. Z., Stasiak, A., Shah, R., McIlwraith, M. J., Benson, F. E., West, S. C. 2001. Identification and purification of two distinct complexes containing the five RAD51 paralogs. *Genes & Development* **15**: 3296–3307.

Matos, J., Blanco, M. G., Maslen, S., Skehel, J. M., West, S. C. 2011. Regulatory Control of the Resolution of DNA Recombination Intermediates during Meiosis and Mitosis. *Cell* **147**: 158–172.

Matsuo, Y., Asakawa, K., Toda, T., Katayama, S. 2006. A Rapid Method for Protein Extraction from Fission Yeast. *Bioscience, Biotechnology, and Biochemistry* **70**: 1992–1994.

Mayle, R., Campbell, I. M., Beck, C. R., Yu, Y., Wilson, M., Shaw, C. A., Bjergbaek, L., Lupski, J. R., Ira, G. 2015. Mus81 and converging forks limit the mutagenicity of replication fork breakage. *Science* **349**: 742 LP-747.

Mazina, O. M., Keskin, H., Hanamshet, K., Storici, F., Mazin, A. V 2017. Rad52 Inverse Strand Exchange Drives RNA-Templated DNA Double-Strand Break Repair. *Molecular Cell* **67**: 19–29.e3.

McCloy, R. A., Rogers, S., Caldon, C. E., Lorca, T., Castro, A., Burgess, A. 2014. Partial inhibition of Cdk1 in G2phase overrides the SAC and decouples mitotic events. *Cell Cycle* **13**: 1400–1412.

McDonald, K. R., Guise, A. J., Pourbozorgi-Langroudi, P., Cristea, I. M., Zakian, V. A., Capra, J. A., Sabouri, N. 2016. Pfh1 Is an Accessory Replicative Helicase that Interacts with the Replisome to Facilitate Fork Progression and Preserve Genome Integrity. *PLOS Genetics* **12**: e1006238.

McGlinchey, R. P., Kryndushkin, D., Wickner, R. B. 2011. Suicidal [PSI+] is a lethal yeast prion. *Proceedings of the National Academy of Sciences of the United States of America* **108**: 5337–5341.

McGlynn, P., Lloyd, R. G. 2002a. Genome stability and the processing of damaged replication forks by RecG. *Trends in genetics : TIG* **18**: 413–419.

McGlynn, P., Lloyd, R. G. 2002b. Recombinational repair and restart of damaged replication forks. *Nature Reviews Molecular Cell Biology* **3**: 859–870.

McIlwraith, M. J., West, S. C. 2008. DNA Repair Synthesis Facilitates RAD52-Mediated Second-End Capture during DSB Repair. *Molecular Cell* **29**: 510–516.

Mcvey, M., Khodaverdian, V. Y., Meyer, D., Gonc, P. 2016. Eukaryotic DNA Polymerases in Homologous Recombination. *Annu. Rev. Genet.* **50**: 393–421.

Mehta, A., Haber, J. E. 2014. Sources of DNA double-strand breaks and models of recombinational DNA repair. *Cold Spring Harbor perspectives in biology* **6**: a016428.

Menck, C. F., Munford, V. 2014. DNA repair diseases: What do they tell us about cancer and aging? *Genetics and molecular biology* **37**: 220–233.

Mendoza, O., Bourdoncle, A., Boulé, J. B., Brosh, R. M., Mergny, J. L. 2016. G-quadruplexes and helicases. *Nucleic Acids Research* **44**: 1989–2006.

Michel, B., Sandler, S. J. 2017. Replication restart in bacteria. *Journal of Bacteriology* **199**: 1–13.

Mijic, S., Zellweger, R., Chappidi, N., Berti, M., Jacobs, K., Mutreja, K., Ursich, S., Ray Chaudhuri, A., Nussenzweig, A., Janscak, P., Lopes, M. 2017. Replication fork reversal triggers fork degradation in BRCA2-defective cells. *Nature Communications* **8**: 859.

Mimitou, E. P., Symington, L. S. 2008. Sae2, Exo1 and Sgs1 collaborate in DNA double-strand break processing. *Nature* **455**: 770–774.

Min, J., Wright, W. E., Shay, J. W. 2017. Alternative Lengthening of Telomeres Mediated by Mitotic DNA Synthesis Engages Break-Induced Replication Processes. *Molecular and cellular biology* **37**: DOI: 10.1128/MCB.00226-17.

Minocherhomji, S., Ying, S., Bjerregaard, V. A., Bursomanno, S., Aleliunaite, A., Wu, W., Mankouri, H. W., Shen, H., Liu, Y., Hickson, I. D. 2015. Replication stress activates DNA repair synthesis in mitosis. *Nature* **528**: 286–290.

Mirkin, E. V, Mirkin, S. M. 2007. Replication fork stalling at natural impediments. *Microbiology and molecular biology reviews : MMBR* **71**: 13–35.

Mironova, R., Niwa, T., Hayashi, H., Dimitrova, R., Ivanov, I. 2001. Evidence for non-enzymatic glycosylation in *Escherichia coli*. *Molecular Microbiology* **39**: 1061–1068.

Mironova, R., Niwa, T., Dimitrova, R., Boyanova, M., Ivanov, I. 2003. Glycation and post-translational processing of human interferon-gamma expressed in *Escherichia coli*. *The Journal of biological chemistry* **278**: 51068–51074.

Miyabe, I., Morishita, T., Hishida, T., Yonei, S., Shinagawa, H. 2006. Rhp51-dependent recombination intermediates that do not generate checkpoint signal are accumulated in *Schizosaccharomyces pombe* rad60 and smc5/6 mutants after release from replication arrest. *Molecular and cellular biology* **26**: 343–353.

Miyabe, I., Kunkel, T. A., Carr, A. M. 2011. The Major Roles of DNA Polymerases Epsilon and Delta at the Eukaryotic Replication Fork Are Evolutionarily Conserved. *PLoS Genetics* **7**: e1002407.

Miyabe, I., Mizuno, K., Keszthelyi, A., Daigaku, Y., Skouteri, M., Mohebi, S., Kunkel, T. A., Murray, J. M., Carr, A. M. 2015. Polymerase δ replicates both strands after homologous recombination–dependent fork restart. *Nature Structural & Molecular Biology* **22**: 932–938.

Miyata, T., Wada, Y., Cal, Z., Iida, Y., Horie, K., Yasuda, Y., Maeda, K., Kurokawa, K., Van, C., De Strihou, Y. 1997. *Implication of an increased*

oxidative stress in the formation of advanced glycation end products in patients with end-stage renal failure. *Kidney international*, Vol. 51.

Mizuno, K., Lambert, S., Baldacci, G., Murray, J. M., Carr, A. M. 2009. Nearby inverted repeats fuse to generate acentric and dicentric palindromic chromosomes by a replication template exchange mechanism. *Genes & Development* **23**: 2876–2886.

Mizuno, K., Miyabe, I., Schalbetter, S. A., Carr, A. M., Murray, J. M. 2012. Recombination-restarted replication makes inverted chromosome fusions at inverted repeats. *Nature* **493**: 246–249.

Mizuno, K., Miyabe, I., Schalbetter, S. A., Carr, A. M., Murray, J. M. 2013. Recombination-restarted replication makes inverted chromosome fusions at inverted repeats. *Nature* **493**: 246–249.

Morishita, T., Furukawa, F., Sakaguchi, C., Toda, T., Carr, A. M., Iwasaki, H., Shinagawa, H. 2005. Role of the *Schizosaccharomyces pombe* F-Box DNA helicase in processing recombination intermediates. *Molecular and cellular biology* **25**: 8074–8083.

Morrow, C. A., Nguyen, M. O., Fower, A., Wong, I. N., Osman, F., Bryer, C., Whitby, M. C. 2017. Inter-Fork Strand Annealing causes genomic deletions during the termination of DNA replication. *eLife* **6**: DOI: 10.7554/eLife.25490.001

Morrow, D. M., Connelly, C., Hieter, P. 1997. "Break copy" duplication: a model for chromosome fragment formation in *Saccharomyces cerevisiae*. *Genetics* **147**: 371–382.

Mortensen, U. H., Bendixen, C., Sunjevaric, I., Rothstein, R. 1996. DNA strand annealing is promoted by the yeast Rad52 protein. *Proceedings of the National Academy of Sciences of the United States of America* **93**: 10729–10734.

Mosedale, G., Niedzwiedz, W., Alpi, A., Perrina, F., Pereira-Leal, J. B., Johnson, M., Langevin, F., Pace, P., Patel, K. J. 2005. The vertebrate Hef ortholog is a component of the Fanconi anemia tumor-suppressor pathway. *Nature Structural & Molecular Biology* **12**: 763–771.

Mourón, S., Rodriguez-Acebes, S., Martínez-Jiménez, M. I., García-Gómez, S., Chocrón, S., Blanco, L., Méndez, J. 2013. Repriming of DNA synthesis at stalled replication forks by human PrimPol. *Nature Structural & Molecular Biology* **20**: 1383–1389.

Mundbjerg, K., Jørgensen, S. W., Fredsøe, J., Nielsen, I., Pedersen, J. M., Bentsen, I. B., Lisby, M., Bjergbaek, L., Andersen, A. H. 2015. Top2 and Sgs1-Top3 Act Redundantly to Ensure rDNA Replication Termination. *PLoS genetics* **11**: e1005697.

Nandi, S., Whitby, M. C. 2012. The ATPase activity of Fml1 is essential for its roles in homologous recombination and DNA repair. *Nucleic acids research* **40**: 9584–9595.

New, J. H., Sugiyama, T., Zaitseva, E., Kowalczykowski, S. C. 1998. Rad52

protein stimulates DNA strand exchange by Rad51 and replicationprotein A. *Nature* **391**: 407–410.

Nguyen, M. O., Jalan, M., Morrow, C. A., Osman, F., Whitby, M. C. 2015. Recombination occurs within minutes of replication blockage by RTS1 producing restarted forks that are prone to collapse. *eLife* **4**: e04539.

Noguchi, C., Rapp, J. B., Skorobogatko, Y. V., Bailey, L. D., Noguchi, E. 2012. Swi1 Associates with Chromatin through the DDT Domain and Recruits Swi3 to Preserve Genomic Integrity. *PLoS ONE* **7**: 1–10.

Noguchi, E., Noguchi, C., Du, L. L., Russell, P. 2003. Swi1 prevents replication fork collapse and controls checkpoint kinase Cds1. *Molecular and cellular biology* **23**: 7861–7874.

Noguchi, E., Noguchi, C., McDonald, W. H., Yates, J. R., Russell, P. 2004. Swi1 and Swi3 Are Components of a Replication Fork Protection Complex in Fission Yeast. *Molecular and Cellular Biology* **24**: 8342–8355.

O'Callaghan, C. A., Byford, M. F., Wyer, J. R., Willcox, B. E., Jakobsen, B. K., McMichael, A. J., Bell, J. I. 1999. BirA Enzyme: Production and Application in the Study of Membrane Receptor–Ligand Interactions by Site-Specific Biotinylation. *Analytical Biochemistry* **266**: 9–15.

Oates, M. E., Romero, P., Ishida, T., Ghalwash, M., Mizianty, M. J., Xue, B., Dosztányi, Z., Uversky, V. N., Obradovic, Z., Kurgan, L., Dunker, A. K., Gough, J. 2012. D2P2: database of disordered protein predictions. *Nucleic Acids Research* **41**: D508–D516.

Okazaki, K., Okazaki, N., Kume, K., Jinno, S., Tanaka, K., Okayama, H. 1990. High-frequency transformation method and library transducing vectors for cloning mammalian cDNAs by trans-complementation of *Schizosaccharomyces pombe. Nucleic acids research* **18**: 6485–6489.

Osman, F., Dixon, J., Barr, A. R., Whitby, M. C. 2005. The F-Box DNA helicase Fbh1 prevents Rhp51-dependent recombination without mediator proteins. *Molecular and cellular biology* **25**: 8084–8096.

Osman, F., Whitby, M. C. 2009. Monitoring homologous recombination following replication fork perturbation in the fission yeast *Schizosaccharomyces pombe*. *Methods in Molecular Biology* **521**: 535–552.

Pages, V., Fuchs, R. P. 2003. Uncoupling of leading- and lagging-strand DNA replication during lesion bypass *in vivo*. *Science* **300**: 1300–1303.

Pancaldi, V., Saraç, Ö. S., Rallis, C., McLean, J. R., Převorovský, M., Gould, K., Beyer, A., Bähler, J. 2012. Predicting the Fission Yeast Protein Interaction Network. *G3: Genes|Genomes|Genetics* **2**: 453–467.

Parker, M. W., Botchan, M. R., Berger, J. M. 2017. Mechanisms and regulation of DNA replication initiation in eukaryotes. *Critical Reviews in Biochemistry and Molecular Biology* **52**: 107–144.

Parnas, O., Zipin-Roitman, A., Pfander, B., Liefshitz, B., Mazor, Y., Ben-Aroya, S., Jentsch, S., Kupiec, M. 2010. Elg1, an alternative subunit of the RFC

clamp loader, preferentially interacts with SUMOylated PCNA. *The EMBO Journal* **29**: 2611–2622.

Paull, T. T., Gellert, M. 1998. The 3' to 5' exonuclease activity of Mre 11 facilitates repair of DNA double-strand breaks. *Molecular cell* **1**: 969–979.

Peng, K., Radivojac, P., Vucetic, S., Dunker, A. K., Obradovic, Z. 2006. Length-dependent prediction of protein intrinsic disorder. *BMC Bioinformatics* **7**: 208.

Petrova, V., Chen, S. H., Molzberger, E. T., Tomko, E., Chitteni-Pattu, S., Jia, H., Ordabayev, Y., Lohman, T. M., Cox, M. M. 2015. Active displacement of RecA filaments by UvrD translocase activity. *Nucleic Acids Research* **43**: 4133–4149.

Petukhova, G., Stratton, S. A., Sung, P. 1999. Single strand DNA binding and annealing activities in the yeast recombination factor Rad59. *The Journal of biological chemistry* **274**: 33839–33842.

Piovesan, D., Tabaro, F., Paladin, L., Necci, M., Micetic, I., Camilloni, C., Davey, N., Dosztányi, Z., Mészáros, B., Monzon, A. M., Parisi, G., Schad, E., Sormanni, P., Tompa, P., Vendruscolo, M., Vranken, W. F., Tosatto, S. C. E. 2018. MobiDB 3.0: more annotations for intrinsic disorder, conformational diversity and interactions in proteins. *Nucleic acids research* **46**: D471–D476.

Pohl, T. J., Nickoloff, J. A. 2008. Rad51-independent interchromosomal double-strand break repair by gene conversion requires Rad52 but not Rad55, Rad57, or Dmc1. *Molecular and cellular biology* **28**: 897–906.

Polakova, S., Molnarova, L., Hyppa, R. W., Benko, Z., Misova, I., Schleiffer, A., Smith, G. R., Gregan, J. 2016. Dbl2 Regulates Rad51 and DNA Joint Molecule Metabolism to Ensure Proper Meiotic Chromosome Segregation. *PLoS Genetics* **12**: e1006102.

Prakash, R., Satory, D., Dray, E., Papusha, A., Scheller, J., Kramer, W., Krejci, L., Klein, H., Haber, J. E., Sung, P., Ira, G. 2009. Yeast Mph1 helicase dissociates Rad51-made D-loops: implications for crossover control in mitotic recombination. *Genes & Development* **23**: 67–79.

Převorovský, M., Oravcová, M., Tvarůžková, J., Zach, R., Folk, P., Půta, F., Bähler, J. 2015. Fission Yeast CSL Transcription Factors: Mapping Their Target Genes and Biological Roles. *PloS one* **10**: e0137820.

Priego Moreno, S., Bailey, R., Campion, N., Herron, S., Gambus, A. 2014. Polyubiquitylation drives replisome disassembly at the termination of DNA replication. *Science* **346**: 477–481.

Promega Corporation 2015. HaloTag ® Protein Purification System Instructions 608–277.

Puig, O., Caspary, F., Rigaut, G., Rutz, B., Bouveret, E., Bragado-Nilsson, E., Wilm, M., Séraphin, B. 2001. The Tandem Affinity Purification (TAP) Method: A General Procedure of Protein Complex Purification. *Methods* **24**: 218–229.

Qi, Z., Redding, S., Lee, J. Y., Gibb, B., Kwon, Y., Niu, H., Gaines, W. A., Sung, P., Greene, E. C. 2015. DNA Sequence Alignment by Microhomology Sampling during Homologous Recombination. *Cell* **160**: 856–869.

Quinet, A., Lemaçon, D., Vindigni, A. 2017. Replication Fork Reversal: Players and Guardians. *Molecular Cell* **68**: 830–833.

Radivojac, P., Iakoucheva, L. M., Oldfield, C. J., Obradovic, Z., Uversky, V. N., Dunker, A. K. 2007. Intrinsic disorder and functional proteomics. *Biophysical journal* **92**: 1439–1456.

Ranjha, L., Howard, S. M., Cejka, P. 2018. Main steps in DNA double-strand break repair: an introduction to homologous recombination and related processes. *Chromosoma* **127**: 187–214.

Raschle, M., Van Komen, S., Chi, P., Ellenberger, T., Sung, P. 2004. Multiple Interactions with the Rad51 Recombinase Govern the Homologous Recombination Function of Rad54. *Journal of Biological Chemistry* **279**: 51973–51980.

Rass, U., Compton, S. A., Matos, J., Singleton, M. R., Ip, S. C. Y., Blanco, M. G., Griffith, J. D., West, S. C. 2010. Mechanism of Holliday junction resolution by the human GEN1 protein. *Genes & Development* **24**: 1559–1569.

Reddy, G., Golub, E. I., Radding, C. M. 1997. Human Rad52 protein promotes single-strand DNA annealing followed by branch migration. *Mutation research* **377**: 53–59.

Renkawitz, J., Lademann, C. A., Jentsch, S. 2014. Mechanisms and principles of homology search during recombination. *Nature Reviews Molecular Cell Biology* **15**: 369–383.

Rijkers, T., Van Den Ouweland, J., Morolli, B., Rolink, A. G., Baarends, W. M., Van Sloun, P. P., Lohman, P. H., Pastink, A. 1998. Targeted inactivation of mouse RAD52 reduces homologous recombination but not resistance to ionizing radiation. *Molecular and cellular biology* **18**: 6423–6429.

Robert, T., Dervins, D., Fabre, F., Gangloff, S. 2006. Mrc1 and Srs2 are major actors in the regulation of spontaneous crossover. *The EMBO Journal* **25**: 2837–2846.

Robertson, B. D., Meyer, T. F. 1992. Genetic variation in pathogenic bacteria. *Trends in genetics : TIG* **8**: 422–427.

Romero, P., Obradovic, Z., Li, X., Garner, E. C., Brown, C. J., Dunker, A. K. 2001. Sequence complexity of disordered protein. *Proteins: Structure, Function, and Genetics* **42**: 38–48.

Roseaulin, L. C., Noguchi, C., Martinez, E., Ziegler, M. A., Toda, T., Noguchi, E. 2013. Coordinated Degradation of Replisome Components Ensures Genome Stability upon Replication Stress in the Absence of the Replication Fork Protection Complex. *PLoS Genetics* **9**: e1003213.

Rudolph, C. J., Upton, A. L., Stockum, A., Nieduszynski, C. A., Lloyd, R. G. 2013. Avoiding chromosome pathology when replication forks collide.

Nature **500**: 608–611.

Rueden, C. T., Schindelin, J., Hiner, M. C., DeZonia, B. E., Walter, A. E., Arena, E. T., Eliceiri, K. W. 2017. ImageJ2: ImageJ for the next generation of scientific image data. *BMC Bioinformatics* **18**: 529.

Ruiz-Maso, J. A., Anand, S. P., Espinosa, M., Khan, S. A., del Solar, G. 2006. Genetic and Biochemical Characterization of the Streptococcus pneumoniae PcrA Helicase and Its Role in Plasmid Rolling Circle Replication. *Journal of Bacteriology* **188**: 7416–7425.

Ryan, C. J., Roguev, A., Patrick, K., Xu, J., Jahari, H., Tong, Z., Beltrao, P., Shales, M., Qu, H., Collins, S. R., Kliegman, J. I., Jiang, L., Kuo, D., Tosti, E., Kim, H. S., Edelmann, W., Keogh, M. C., Greene, D., Tang, C. et al. 2012. Hierarchical modularity and the evolution of genetic interactomes across species. *Molecular cell* **46**: 691–704.

Sabate, R., Rousseau, F., Schymkowitz, J., Ventura, S. 2015. What Makes a Protein Sequence a Prion? *PLoS Computational Biology* **11**: e1004013.

Sabatinos, S. A., Forsburg, S. L. 2010. Molecular genetics of *Schizosaccharomyces pombe*. *Methods in Enzymology* **470**: 759–795.

Sabouri, N., McDonald, K. R., Webb, C. J., Cristea, I. M., Zakian, V. A. 2012. DNA replication through hard-to-replicate sites, including both highly transcribed RNA Pol II and Pol III genes, requires the *S. pombe* Pfh1 helicase. *Genes & Development* **26**: 581–593.

Sabouri, N. 2017. The functions of the multi-tasking Pfh1Pif1 helicase. *Current Genetics* **63**: 621–626.

Saini, N., Ramakrishnan, S., Elango, R., Ayyar, S., Zhang, Y., Deem, A., Ira, G., Haber, J. E., Lobachev, K. S., Malkova, A. 2013. Migrating bubble during break-induced replication drives conservative DNA synthesis. *Nature* **502**: 389.

Sakofsky, C. J., Ayyar, S., Deem, A. K., Chung, W. H., Ira, G., Malkova, A. 2015. Translesion Polymerases Drive Microhomology-Mediated Break-Induced Replication Leading to Complex Chromosomal Rearrangements. *Molecular Cell* **60**: 860–872.

Sakofsky, C. J., Malkova, A. 2017. Break induced replication in eukaryotes: mechanisms, functions, and consequences. *Critical Reviews in Biochemistry and Molecular Biology* **52**: 395–413.

Samadashwily, G. M., Raca, G., Mirkin, S. M. 1997. Trinucleotide repeats affect DNA replication *in vivo*. *Nature Genetics* **17**: 298–304.

Sambrook, J. 2001. *Molecular cloning: a laboratory manual / Joseph Sambrook, David W. Russell*. Cold Spring Harbor Laboratory Press: 82-86.

Santa Maria, S. R., Kwon, Y., Sung, P., Klein, H. L. 2013. Characterization of the interaction between the *Saccharomyces cerevisiae* Rad51 recombinase and the DNA translocase Rdh54. *The Journal of biological chemistry* **288**: 21999–22005.

Sarai, N., Kagawa, W., Fujikawa, N., Saito, K., Hikiba, J., Tanaka, K., Miyagawa, K., Kurumizaka, H., Yokoyama, S. 2008. Biochemical analysis of the N-terminal domain of human RAD54B. *Nucleic acids research* **36**: 5441–5450.

Sartori, A. A., Lukas, C., Coates, J., Mistrik, M., Fu, S., Bartek, J., Baer, R., Lukas, J., Jackson, S. P. 2007. Human CtIP promotes DNA end resection. *Nature* **450**: 509–514.

Sasanuma, H., Furihata, Y., Shinohara, M., Shinohara, A. 2013. Remodeling of the Rad51 DNA Strand-Exchange Protein by the Srs2 Helicase. *Genetics* **194**: 859–872.

Schindelin, J., Arganda-Carreras, I., Frise, E., Kaynig, V., Longair, M., Pietzsch, T., Preibisch, S., Rueden, C., Saalfeld, S., Schmid, B., Tinevez, J. Y., White, D. J., Hartenstein, V., Eliceiri, K., Tomancak, P., Cardona, A. 2012. Fiji: an open-source platform for biological-image analysis. *Nature Methods* **9**: 676–682.

Seong, C., Colavito, S., Kwon, Y., Sung, P., Krejci, L. 2009. Regulation of Rad51 Recombinase Presynaptic Filament Assembly via Interactions with the Rad52 Mediator and the Srs2 Anti-recombinase. *Journal of Biological Chemistry* **284**: 24363–24371.

Shah Punatar, R., Martin, M. J., Wyatt, H. D. M., Chan, Y. W., West, S. C. 2017. Resolution of single and double Holliday junction recombination intermediates by GEN1. *Proceedings of the National Academy of Sciences* **114**: 443–450.

Sharma, R., Kumar, S., Tsunoda, T., Patil, A., Sharma, A. 2016. Predicting MoRFs in protein sequences using HMM profiles. *BMC bioinformatics* **17**: 504.

Shinohara, A., Ogawa, T. 1998. Stimulation by Rad52 of yeast Rad51-mediated recombination. *Nature* **391**: 404–407.

Silva, S., Altmannova, V., Luke-glaser, S., Henriksen, P., Gallina, I., Yang, X., Choudhary, C., Luke, B., Krejci, L., Lisby, M. 2016. Mte1 interacts with Mph1 and promotes crossover recombination and telomere maintenance 1–18.

Simandlova, J., Zagelbaum, J., Payne, M. J., Chu, W. K., Shevelev, I., Hanada, K., Chatterjee, S., Reid, D. A., Liu, Y., Janscak, P., Rothenberg, E., Hickson, I. D. 2013. FBH1 helicase disrupts RAD51 filaments *in vitro* and modulates homologous recombination in mammalian cells. *The Journal of biological chemistry* **288**: 34168–34180.

Sinden, R. R., Pearson, C. E., Potaman, V. N., Ussery, D. W. 1998. DNA: structure and function. *Advances in Genome Biology* **5**: 1–141.

Singh, S., Shemesh, K., Liefshitz, B., Kupiec, M. 2013. Genetic and physical interactions between the yeast ELG1 gene and orthologs of the Fanconi anemia pathway. *Cell cycle (Georgetown, Tex.)* **12**: 1625–1636.

Singh, T. R., Ali, A. M., Busygina, V., Raynard, S., Fan, Q., Du, C. h.,

Andreassen, P. R., Sung, P., Meetei, A. R. 2008. BLAP18/RMI2, a novel OB-fold-containing protein, is an essential component of the Bloom helicase-double Holliday junction dissolvasome. *Genes & Development* **22**: 2856–2868.

Singh, T. R., Saro, D., Ali, A. M., Zheng, X. feng, Du, C. hu, Killen, M. W., Sachpatzidis, A., Wahengbam, K., Pierce, A. J., Xiong, Y., Sung, P., Meetei, A. R. 2010. MHF1-MHF2, a Histone-Fold-Containing Protein Complex, Participates in the Fanconi Anemia Pathway via FANCM. *Molecular cell* **37**: 879.

Sirbu, B. M., Couch, F. B., Feigerle, J. T., Bhaskara, S., Hiebert, S. W., Cortez, D. 2011. Analysis of protein dynamics at active, stalled, and collapsed replication forks. *Genes & Development* **25**: 1320–1327.

Sirbu, B. M., Couch, F. B., Cortez, D. 2012. Monitoring the spatiotemporal dynamics of proteins at replication forks and in assembled chromatin using isolation of proteins on nascent DNA. *Nature Protocols* **7**: 594–605.

Smith, C. E., Llorente, B., Symington, L. S. 2007. Template switching during break-induced replication. *Nature* **447**: 102–105.

Smith, C. E., Lam, A. F., Symington, L. S. 2009. Aberrant double-strand break repair resulting in half crossovers in mutants defective for Rad51 or the DNA polymerase delta complex. *Molecular and cellular biology* **29**: 1432–1441.

Smith, J., Rothstein, R. 1995. A mutation in the gene encoding the *Saccharomyces cerevisiae* single-stranded DNA-binding protein Rfa1 stimulates a RAD52-independent pathway for direct-repeat recombination. *Molecular and Cellular Biology* **15**: 1632–1641.

Solinger, J. A., Kiianitsa, K., Heyer, W. D. 2002. Rad54, a Swi2/Snf2-like recombinational repair protein, disassembles Rad51:dsDNA filaments. *Molecular cell* **10**: 1175–1188.

Song, B., Sung, P. 2000. Functional Interactions among Yeast Rad51 Recombinase, Rad52 Mediator, and Replication Protein A in DNA Strand Exchange. *Journal of Biological Chemistry* **275**: 15895–15904.

Sonneville, R., Moreno, S. P., Knebel, A., Johnson, C., Hastie, C. J., Gartner, A., Gambus, A., Labib, K. 2017. CUL-2LRR-1 and UBXN-3 drive replisome disassembly during DNA replication termination and mitosis. *Nature Cell Biology* **19**: 468–479.

Sotiriou, S. K., Kamileri, I., Lugli, N., Evangelou, K., Da-Ré, C., Huber, F., Padayachy, L., Tardy, S., Nicati, N. L., Barriot, S., Ochs, F., Lukas, C., Lukas, J., Gorgoulis, V. G., Scapozza, L., Halazonetis, T. D. 2016. Mammalian RAD52 Functions in Break-Induced Replication Repair of Collapsed DNA Replication Forks. *Molecular Cell* **64**: 1127–1134.

Stagge, F., Mitronova, G. Y., Belov, V. N., Wurm, C. A., Jakobs, S. 2013. SNAP-, CLIP- and Halo-tag labelling of budding yeast cells. *PloS one* **8**: e78745.

Steinacher, R., Osman, F., Dalgaard, J. Z., Lorenz, A., Whitby, M. C. 2012.

The DNA helicase Pfh1 promotes fork merging at replication termination sites to ensure genome stability. *Genes & development* **26**: 594–602.

Stewart, J. A., Miller, A. S., Campbell, J. L., Bambara, R. A. 2008. Dynamic removal of replication protein A by Dna2 facilitates primer cleavage during Okazaki fragment processing in *Saccharomyces cerevisiae*. *The Journal of biological chemistry* **283**: 31356–31365.

Stewart, J. A., Campbell, J. L., Bambara, R. A. 2009. Significance of the dissociation of Dna2 by flap endonuclease 1 to Okazaki fragment processing in *Saccharomyces cerevisiae*. *The Journal of biological chemistry* **284**: 8283–8291.

Sugiyama, T., New, J. H., Kowalczykowski, S. C. 1998. DNA annealing by RAD52 protein is stimulated by specific interaction with the complex of replication protein A and single-stranded DNA. *Proceedings of the National Academy of Sciences of the United States of America* **95**: 6049–6054.

Sun, W., Nandi, S., Osman, F., Ahn, J. S., Jakovleska, J., Lorenz, A., Whitby, M. C. 2008. The FANCM Ortholog Fml1 Promotes Recombination at Stalled Replication Forks and Limits Crossing Over during DNA Double-Strand Break Repair. *Molecular Cell* **32**: 118–128.

Sung, P. 1997a. Yeast Rad55 and Rad57 proteins form a heterodimer that functions with replication protein A to promote DNA strand exchange by Rad51 recombinase. *Genes & development* **11**: 1111–1121.

Sung, P. 1997b. Function of yeast Rad52 protein as a mediator between replication protein A and the Rad51 recombinase. *The Journal of biological chemistry* **272**: 28194–28197.

Suzuki, G., Shimazu, N., Tanaka, M. 2012. A yeast prion, Mod5, promotes acquired drug resistance and cell survival under environmental stress. *Science* **336**: 355–359.

Szostak, J. W., Orr-Weaver, T. L., Rothstein, R. J., Stahl, F. W. 1983. The double-strand-break repair model for recombination. *Cell* **33**: 25–35.

Taglialatela, A., Alvarez, S., Leuzzi, G., Sannino, V., Ranjha, L., Huang, J. W., Madubata, C., Anand, R., Levy, B., Rabadan, R., Cejka, P., Costanzo, V., Ciccia, A. 2017. Restoration of Replication Fork Stability in BRCA1- and BRCA2-Deficient Cells by Inactivation of SNF2-Family Fork Remodelers. *Molecular Cell* **68**: 414–430.

Teixeira-Silva, A., Ait Saada, A., Hardy, J., Iraqui, I., Nocente, M. C., Fréon, K., Lambert, S. A. E. 2017. The end-joining factor Ku acts in the end-resection of double strand break-free arrested replication forks. *Nature Communications* **8**: DOI: 10.1038/s41467-017-02144-5.

Tercero, J. A., Diffley, J. F. X. 2001. Regulation of DNA replication fork progression through damaged DNA by the Mec1/Rad53 checkpoint. *Nature* **412**: 553–557.

Thangavel, S., Berti, M., Levikova, M., Pinto, C., Gomathinayagam, S., Vujanovic, M., Zellweger, R., Moore, H., Lee, E. H., Hendrickson, E. A.,

Cejka, P., Stewart, S., Lopes, M., Vindigni, A. 2015. DNA2 drives processing and restart of reversed replication forks in human cells. *The Journal of cell biology* **208**: 545–562.

Trujillo, K. M., Roh, D. H., Chen, L., Van Komen, S., Tomkinson, A., Sung, P. 2003. Yeast xrs2 binds DNA and helps target rad50 and mre11 to DNA ends. *The Journal of biological chemistry* **278**: 48957–48964.

Tsai, S. P., Su, G. C., Lin, S. W., Chung, C. I., Xue, X., Dunlop, M. H., Akamatsu, Y., Jasin, M., Sung, P., Chi, P. 2012. Rad51 presynaptic filament stabilization function of the mouse Swi5–Sfr1 heterodimeric complex. *Nucleic Acids Research* **40**: 6558–6569.

Tsang, E., Miyabe, I., Iraqui, I., Zheng, J., Lambert, S. A. E., Carr, A. M. 2014. The extent of error-prone replication restart by homologous recombination is controlled by Exo1 and checkpoint proteins. *Journal of cell science* **127**: 2983–2994.

Tsutsui, Y., Morishita, T., Iwasaki, H., Toh, H., Shinagawa, H. 2000. A recombination repair gene of *Schizosaccharomyces pombe*, rhp57, is a functional homolog of the *Saccharomyces cerevisiae* RAD57 gene and is phylogenetically related to the human XRCC3 gene. *Genetics* **154**: 1451–1461.

Tsutsui, Y., Kurokawa, Y., Ito, K., Siddique, M. S. P., Kawano, Y., Yamao, F., Iwasaki, H. 2014. Multiple regulation of Rad51-mediated homologous recombination by fission yeast Fbh1. *PLoS genetics* **10**: e1004542.

Unsal-Kaçmaz, K., Chastain, P. D., Qu, P. P., Minoo, P., Cordeiro-Stone, M., Sancar, A., Kaufmann, W. K. 2007. The human Tim/Tipin complex coordinates an Intra-S checkpoint response to UV that slows replication fork displacement. *Molecular and cellular biology* **27**: 3131–3142.

Vasianovich, Y., Harrington, L. A., Makovets, S. 2014. Break-Induced Replication Requires DNA Damage-Induced Phosphorylation of Pif1 and Leads to Telomere Lengthening.*PLoS Genetics* **10**: e1004679.

Veaute, X., Jeusset, J., Soustelle, C., Kowalczykowski, S. C., Le Cam, E., Fabre, F. 2003. The Srs2 helicase prevents recombination by disrupting Rad51 nucleoprotein filaments. *Nature* **423**: 309–312.

Veggiani, G., Nakamura, T., Brenner, M. D., Gayet, R. V., Yan, J., Robinson, C. V., Howarth, M. 2016. Programmable polyproteams built using twin peptide superglues. *Proceedings of the National Academy of Sciences* **113**: 1202–1207.

Vengrova, S., Dalgaard, J. Z. 2006. The wild-type *Schizosaccharomyces pombe* mat1 imprint consists of two ribonucleotides. *EMBO reports* **7**: 59–65.

Verma, P., Greenberg, R. A. 2016. Noncanonical views of homology-directed DNA repair. *Genes and Development* **30** (10): 1138-1154.

Vujanovic, M., Krietsch, J., Raso, M. C., Terraneo, N., Zellweger, R., Schmid, J. A., Taglialatela, A., Huang, J. W., Holland, C. L., Zwicky, K., Herrador,

R., Jacobs, H., Cortez, D., Ciccia, A., Penengo, L., Lopes, M. 2017. Replication Fork Slowing and Reversal upon DNA Damage Require PCNA Polyubiquitination and ZRANB3 DNA Translocase Activity. *Molecular Cell* **67**: 882–890.

Waga, S., Stillman, B. 1998. The DNA replication fork in eukariotic cells. *Annual Review of Biochemistry* **67**: 721–751.

Walsh, I., Martin, A. J. M., Di Domenico, T., Tosatto, S. C. E. 2012. ESpritz: accurate and fast prediction of protein disorder. *Bioinformatics* **28**: 503–509.

Wang, J. Y., Chen, S. Y., Sun, C. N., Chien, T., Chern, Y. 2016. A central role of TRAX in the ATM-mediated DNA repair. *Oncogene* **35**: 1657–1670.

Wang, S. W., Goodwin, A., Hickson, I. D., Norbury, C. J. 2001. Involvement of *Schizosaccharomyces pombe* Srs2 in cellular responses to DNA damage. *Nucleic acids research* **29**: 2963–2972.

Wang, X., Ira, G., Tercero, J. A., Holmes, A. M., Diffley, J. F. X., Haber, J. E. 2004. Role of DNA Replication Proteins in Double-Strand Break-Induced Recombination in *Saccharomyces cerevisiae*. *Molecular and Cellular Biology* **24**: 6891–6899.

Waterhouse, A. M., Procter, J. B., Martin, D. M. A., Clamp, M., Barton, G. J. 2009. Jalview Version 2--a multiple sequence alignment editor and analysis workbench. *Bioinformatics* **25**: 1189–1191.

Waters, L. S., Minesinger, B. K., Wiltrout, M. E., D'Souza, S., Woodruff, R. V, Walker, G. C. 2009. Eukaryotic Translesion Polymerases and Their Roles and Regulation in DNA Damage Tolerance. *Microbiology and Molecular Biology Reviews* **73**: 134–154.

Wendel, B. M., Courcelle, C. T., Courcelle, J. 2014. Completion of DNA replication in *Escherichia coli*. *Proceedings of the National Academy of Sciences of the United States of America* **111**: 16454–16459.

Whitby, M. C. 2010. The FANCM family of DNA helicases/translocases. *DNA Repair* **9**: 224–236.

Wilhelm, T., Ragu, S., Magdalou, I., Machon, C., Dardillac, E., Técher, H., Guitton, J., Debatisse, M., Lopez, B. S. 2016. Slow Replication Fork Velocity of Homologous Recombination-Defective Cells Results from Endogenous Oxidative Stress. *PLOS Genetics* **12**: e1006007.

Wilson, M. A., Kwon, Y., Xu, Y., Chung, W. H., Chi, P., Niu, H., Mayle, R., Chen, X., Malkova, A., Sung, P., Ira, G. 2013. Pif1 helicase and Polδ promote recombination-coupled DNA synthesis via bubble migration. *Nature* **502**: 393–396.

Windgassen, T. A., Wessel, S. R., Bhattacharyya, B., Keck, J. L. 2018, January 25. Mechanisms of bacterial DNA replication restart. *Nucleic Acids Research* **46** (2): 504-519.

Wright, W. D., Heyer, W. D. 2014. Rad54 Functions as a Heteroduplex DNA Pump Modulated by Its DNA Substrates and Rad51 during D Loop Formation. *Molecular Cell* **53**: 420–432.

Wu, L., Hickson, I. D. 2003. The Bloom's syndrome helicase suppresses crossing over during homologous recombination. *Nature* **426**: 870–874.

Wyatt, H. D. M., Sarbajna, S., Matos, J., West, S. C. 2013. Coordinated Actions of SLX1-SLX4 and MUS81-EME1 for Holliday Junction Resolution in Human Cells. *Molecular Cell* **52**: 234–247.

Wyatt, M. D., Pittman, D. L. 2006. Methylating Agents and DNA Repair Responses: Methylated Bases and Sources of Strand Breaks. *Chemical Research in Toxicology* **19**: 1580–1594.

Xue, X., Raynard, S., Busygina, V., Singh, A. K., Sung, P. 2013. Role of Replication Protein A in Double Holliday Junction Dissolution Mediated by the BLM-Topo IIIα-RMI1-RMI2 Protein Complex. *Journal of Biological Chemistry* **288**: 14221–14227.

Xue, X., Choi, K., Bonner, J., Chiba, T., Kwon, Y., Xu, Y., Sanchez, H., Wyman, C., Niu, H., Zhao, X., Sung, P. 2014. Restriction of replication fork regression activities by a conserved SMC complex. *Molecular Cell* **56**: 436–445.

Xue, X., Sung, P., Zhao, X. 2015a. Functions and regulation of the multitasking FANCM family of DNA motor proteins. *Genes & development* **29**: 1777–1788.

Xue, X., Choi, K., Bonner, J. N., Szakal, B., Chen, Y. H., Papusha, A., Saro, D., Niu, H., Ira, G., Branzei, D., Sung, P., Zhao, X. 2015b. Selective modulation of the functions of a conserved DNA motor by a histone fold complex. *Genes & development* **29**: 1000–1005.

Xue, X., Papusha, A., Choi, K., Bonner, J. N., Kumar, S., Niu, H., Kaur, H., Zheng, X. F., Donnianni, R. A., Lu, L., Lichten, M., Zhao, X., Ira, G., Sung, P. 2016. Differential regulation of the anti-crossover and replication fork regression activities of mph1 by mte1. *Genes and Development* **30**: 687–699.

Yamada-Inagawa, T., Klar, A. J. S., Dalgaard, J. Z. 2007. *Schizosaccharomyces pombe* switches mating type by the synthesis-dependent strand-annealing mechanism. *Genetics* **177**: 255–265.

Yamanishi, A., Yusa, K., Horie, K., Tokunaga, M., Kusano, K., Kokubu, C., Takeda, J. 2013. Enhancement of microhomology-mediated genomic rearrangements by transient loss of mouse Bloom syndrome helicase. *Genome Research* **23**: 1462–1473.

Yan, Z., Delannoy, M., Ling, C., Daee, D., Osman, F., Muniandy, P. A., Shen, X., Oostra, A. B., Du, H., Steltenpool, J., Lin, T., Schuster, B., Decaillet, C., Stasiak, A., Stasiak, A. Z., Stone, S., Hoatlin, M. E., Schindler, D., Woodcock, C. et al. 2010. A histone-fold complex and FANCM form a conserved DNA remodeling complex to maintain genome stability. *Molecular cell* **37**: 865-878.

Yao, Y., Wang, J., Viroonchatapan, N., Samson, A., Chill, J., Rothe, E., Anglister, J., Wang, Z. Z. 2002. Yeast expression and NMR analysis of the

extracellular domain of muscle nicotinic acetylcholine receptor α subunit. *Journal of Biological Chemistry* **277**: 12613–12621.

Yeeles, J. T. P., Deegan, T. D., Janska, A., Early, A., Diffley, J. F. X. 2015. Regulated eukaryotic DNA replication origin firing with purified proteins. *Nature* **519**: 431–435.

Yimit, A., Kim, T., Anand, R. P., Meister, S., Ou, J., Haber, J. E., Zhang, Z., Grant, W. 2015. YGR042W / MTE1 Functions in Double-Strand Break Repair with MPH1 **4741**: 1–9.

Yu, Y., Ren, J. Y., Zhang, J. M., Suo, F., Fang, X. F., Wu, F., Du, L. L. 2013. A proteome-wide visual screen identifies fission yeast proteins localizing to DNA double-strand breaks. *DNA Repair* **12**: 433–443.

Yuan, J., Chen, J. 2011. The Role of the Human SWI5-MEI5 Complex in Homologous Recombination Repair. *Journal of Biological Chemistry* **286**: 9888–9893.

Zakeri, B., Fierer, J. O., Celik, E., Chittock, E. C., Schwarz-Linek, U., Moy, V. T., Howarth, M. 2012. Peptide tag forming a rapid covalent bond to a protein, through engineering a bacterial adhesin. *Proceedings of the National Academy of Sciences of the United States of America* **109**: 690-697.

Zambrano, R., Conchillo-Sole, O., Iglesias, V., Illa, R., Rousseau, F., Schymkowitz, J., Sabate, R., Daura, X., Ventura, S. 2015. PrionW: a server to identify proteins containing glutamine/asparagine rich prion-like domains and their amyloid cores. *Nucleic Acids Research* **43**: W331–W337.

Zeman, M. K., Cimprich, K. A. 2014. Causes and consequences of replication stress. *Nature Cell Biology* **16**: 2–9.

Zhang, H., Lawrence, C. W. 2005. The error-free component of the RAD6/RAD18 DNA damage tolerance pathway of budding yeast employs sister-strand recombination. *Proceedings of the National Academy of Sciences* **102**: 15954–15959.

Zhao, Q., Saro, D., Sachpatzidis, A., Singh, T. R., Schlingman, D., Zheng, X. F., Mack, A., Tsai, M. S., Mochrie, S., Regan, L., Meetei, A. R., Sung, P., Xiong, Y. 2014. The MHF complex senses branched DNA by binding a pair of crossover DNA duplexes. *Nature communications* **5**: 1-12.

Zheng, X. F., Prakash, R., Saro, D., Longerich, S., Niu, H., Sung, P. 2011. Processing of DNA structures via DNA unwinding and branch migration by the *S. cerevisiae* Mph1 protein. *DNA Repair* **10**: 1034–1043.

Zhu, Z., Chung, W. H., Shim, E. Y., Lee, S. E., Ira, G. 2008. Sgs1 Helicase and Two Nucleases Dna2 and Exo1 Resect DNA Double-Strand Break Ends. *Cell* **134**: 981–994.

Zou, L., Elledge, S. J. 2003. Sensing DNA Damage Through ATRIP Recognition of RPA-ssDNA Complexes. *Science* **300**: 1542 LP-1548.